

**Sedimentology and geochemistry of the Jurassic system in
northern Iraq: Implications for paleoenvironmental
reconstruction, provenance and tectonic setting**

Dissertation

zur

Erlangung des Doktorgrades (Dr. rer. nat.)

der

Mathematisch-Naturwissenschaftlichen Fakultät

der

Rheinischen Friedrich-Wilhelms-Universität Bonn

vorgelegt von

Nagham Omar

aus

Niniveh, Irak

Bonn 2023

Angefertigt mit Genehmigung der Mathematisch-Naturwissenschaftlichen Fakultät
der Rheinischen Friedrich-Wilhelms-Universität Bonn

Gutachter / Betreuer: Prof. Dr. Tom McCann

Gutachter: Prof. Dr. Ali Ismail Al-Juboury

Tag der Promotion: 08/07/2024

Erscheinungsjahr: 2024

Table of Contents

Abstract	1
Chapter 1	4
1. Introduction	5
1.1 Aim of the Work	8
1.2 Regional geology of the Zagros region	13
1.3 Tectonic Framework in North Iraq	15
1.4 Jurassic and Early Cretaceous depositional history of North Iraq	17
Chapter 2: Summary of the published article in Geosciences (DOI:	
10.3390/geosciences12020094)	20
Chapter 3: Summary of the published article in Marine and Petroleum Geology	
(DOI: 10.1016/j.marpetgeo.2023.106430)	24
Chapter 4: Summary of the published article in Neues Jahrbuch für Geologie und	
Paläontologie (DOI: 10.1127/njgpa/2020/0916)	28
Chapter 5: Summary of the published article in Arabian Journal of Geosciences	
(10.1007/s12517-021-07048-9)	32
Chapter 6: Provenance and Tectonic Setting of the Jurassic Shales from	
Northeastern Iraq: Mineralogical and Geochemical Approaches	
(Manuscript)	36
Chapter 7: Conclusions	62
References	66
Appendices	82

Appendix A: Early Jurassic-Early Cretaceous Calcareous Nannofossil Biostratigraphy and Geochemistry, Northeastern Iraqi Kurdistan: Implications for Paleoclimate and Paleoecological Conditions	84
Appendix B: A Comparative Study of the Paleoclimate, Paleosalinity and Paleoredox Conditions of Lower Jurassic-Lower Cretaceous Sediments in Northeastern Iraq	106
Appendix C: Petrography and geochemistry of the Middle-Upper Jurassic Banik section, northernmost Iraq – Implications for Palaeoredox, Evaporitic and Diagenetic Conditions	128
Appendix D: Solid Bitumen in Shales from the Middle to Upper Jurassic Sargelu and Naokelekan Formations of northernmost Iraq: Implication for Reservoir Characterization	158
Supplementary Materials	179

Abstract

This cumulative thesis presents pioneering studies on the paleoclimate, paleosalinity and paleoredox conditions, prevailing during the Jurassic period in northern Iraq, based on a variety of proxies. To this end, several research studies were performed, divided into five individual chapters, four of which were already published in international peer-reviewed journals, while a fifth manuscript will be submitted for publication in due course.

The areas of study were located in northern Iraq and involved detailed examination and analysis of six formations in total. From base to top, these are the Early Jurassic-age Sarki and Sehkaniyan formations, the Middle Jurassic-age Sargelu Formation, the Late Jurassic-age Naokelekan and Barsarin formations, and the Late Jurassic-Early Cretaceous-age Chia Gara Formation. The lithologies present are mainly carbonate rocks (limestones, dolomitic limestones and dolomites), sporadic shale units, in addition to some solid bitumens which were observed from the Sargelu and Naokelekan formations in the Banik area. The formations were examined in three different locations (i.e., the Banik, Warte and Ranya areas) within the three governorates of the Kurdistan region (i.e., Duhok, Erbil and Sulaimaniyah).

Chapter 1 provides an introduction to the areas of study as well as the individual formations. It also outlines the regional geology of northern Iraq. This is followed by Chapter 2 which focusses on a more detailed description of the Early Jurassic- to Early Cretaceous-age formations of northern Iraq. The calcareous nannofossils of the entire Jurassic system from the Warte area in northern Iraq were recorded and analyzed for the first time. The results were used to determine the stratigraphic position of the lower and upper boundaries of the Middle Jurassic in the Warte succession. In addition, calcareous nannofossil data were integrated with

geochemical analyses to reconstruct the paleoecological and paleoclimatic conditions of the Jurassic-Lower Cretaceous succession of the region. Chapter 2 was published in the peer-reviewed journal *Geosciences* in 2022.

Chapter 3 presents the first broad comparative study of the mineralogical and geochemical features of the Early Jurassic-Early Cretaceous-age Sarki, Sehkanyian, Sargelu, Naokelekan, Barsarin and Chia Gara formations from the Ranya section with the same formations from the Warte section (both sections are located in northeastern Iraq). The aim of this study was to reconstruct the paleoclimate, paleosalinity and paleoredox conditions which were active during the deposition of the Early Jurassic-Early Cretaceous-age sedimentary successions in the area. In addition, the results were used to evaluate the variations and/or similarities in the paleoenvironmental conditions that prevailed during the Early Jurassic-Early Cretaceous times across the region of northern Iraq. Chapter 3 was published in the peer-reviewed journal *Marine and Petroleum Geology* in 2023.

Chapter 4 presents a comprehensive examination of the petrography and microfacies of the carbonates from the Middle to Upper Jurassic succession (i.e., Sargelu and Naokelekan formations) from the Banik area in northernmost Iraq. The results were subsequently compared with data on the geochemistry of the shale rocks from the same formations, with the aim of providing important information regarding evaporation proxies, paleoredox and diagenetic conditions, that can be integrated into new depositional paleoenvironments for the area. Chapter 4 was published in the peer-reviewed journal *Neues Jahrbuch für Geologie und Paläontologie* in 2020.

A detailed study of the solid bitumens present in the Middle Jurassic-Late Jurassic-age Sargelu and Naokelekan formations in the Banik area and which, to date, have never been studied,

formed the basis of Chapter 5. This study aimed to propose possible depositional paleoenvironments of the solid bitumens and their host rocks by examining a range of paleoredox proxies and isotopic geochemistry. Furthermore, the results from the geochemical data were integrated with the vitrinite reflectance results in order to reconstruct the accumulation process of the solid bitumens and to interpret their origin. Chapter 5 was published in the peer-reviewed journal *Arabian Journal of Geosciences* in 2021.

Chapter 6 comprises a detailed mineralogical and geochemical examination of the shales from the Early Jurassic-Early Cretaceous-age formations of the Warte and Ranya sections in northern Iraq. The aim of this study was to determine the provenance of the mud-size sediments as well as the tectonic setting. Chapter 6 is currently being prepared as a manuscript for submission.

The final chapter – Chapter 7 – presents a summary of the various aspects of the thesis. In summary, these studies provide important information which is highly relevant for any future hydrocarbon exploration in the region of northern Iraq; they will pave the way for future work in this respect, since the Jurassic system in Iraq is – as noted - highly promising and harbors great potential.

Chapter 1

Introduction

1. Introduction

The Early Jurassic-Early Cretaceous-age successions in Iraq are considered to be of great importance (e.g., Daoud and Karim, 2010; Al-Ameri and Zumberge, 2012; Al-Juboury and McCann, 2013; Jasim, 2013; Abdula, 2017) given the fact that most of the petroleum that has been discovered in Iraq is reported to have been sourced from the Jurassic rocks and trapped in the Cretaceous and Tertiary reservoirs of the Mesopotamian Basin and the Zagros Basin (Pitman et al., 2004) (Figure 1). Therefore, understanding the paleoenvironmental conditions, under which the Early Jurassic-Early Cretaceous-age successions of Iraq were deposited, will provide significant information for future studies in terms of hydrocarbon exploration, given that the Jurassic system is highly promising in this regard. Iraq is a major petroleum-producing country in the Middle East, with current proven reserves of 115 billion barrels of oil (BBO) and 110 trillion cubic feet (TCF) of gas in three total petroleum systems, namely the Paleozoic, Jurassic and Cretaceous-Tertiary systems (see inset map in Figure 1 for names and locations) (United States Geological Survey USGS, 2000; Ahlbrandt et al., 2000; Verma et al., 2004).

The present work focused on northern Iraq, which is estimated to contain about 45 billion barrels (bbls) of Iraq's 115 billion barrels of oil reserves, making Iraq the country with the sixth largest oil reserves in the world (Al-Zubaidi and Al-Zebari, 1998; Jassim and Al-Gailani, 2006; Hill and Shane, 2009). Due to their geological and economic importance, the Jurassic successions of Iraq have been described in a number of academic theses and research papers, the majority of which focused on the lithology and depositional environments, in addition to their economic significance (Salae, 2001; Balaky, 2004, Al-Ahmed, 2006; Abdula, 2010; Daoud and Karim, 2010; Al-Ameri and Zumberge, 2012; Al-Juboury and McCann, 2013;

Jasim, 2013; Sharezwri, 2015; Abdula, 2017). However, detailed studies integrating a comprehensive examination of the sedimentology, petrography, mineralogy and geochemistry of all of the Jurassic-age formations in northern Iraq have, to date, not been attempted.

Initial work in the present study involved a review of all the previously published studies in order to establish a basis for a more detailed examination of the Jurassic successions in northern Iraq, involving the application of advanced analytical methods. The main methods employed included sedimentological and petrographical investigations examining the main characteristics of the various Jurassic units, in addition to geochemical characterization of the major, trace and rare earth elements, carbon and oxygen isotopes, as well as clay mineralogy.

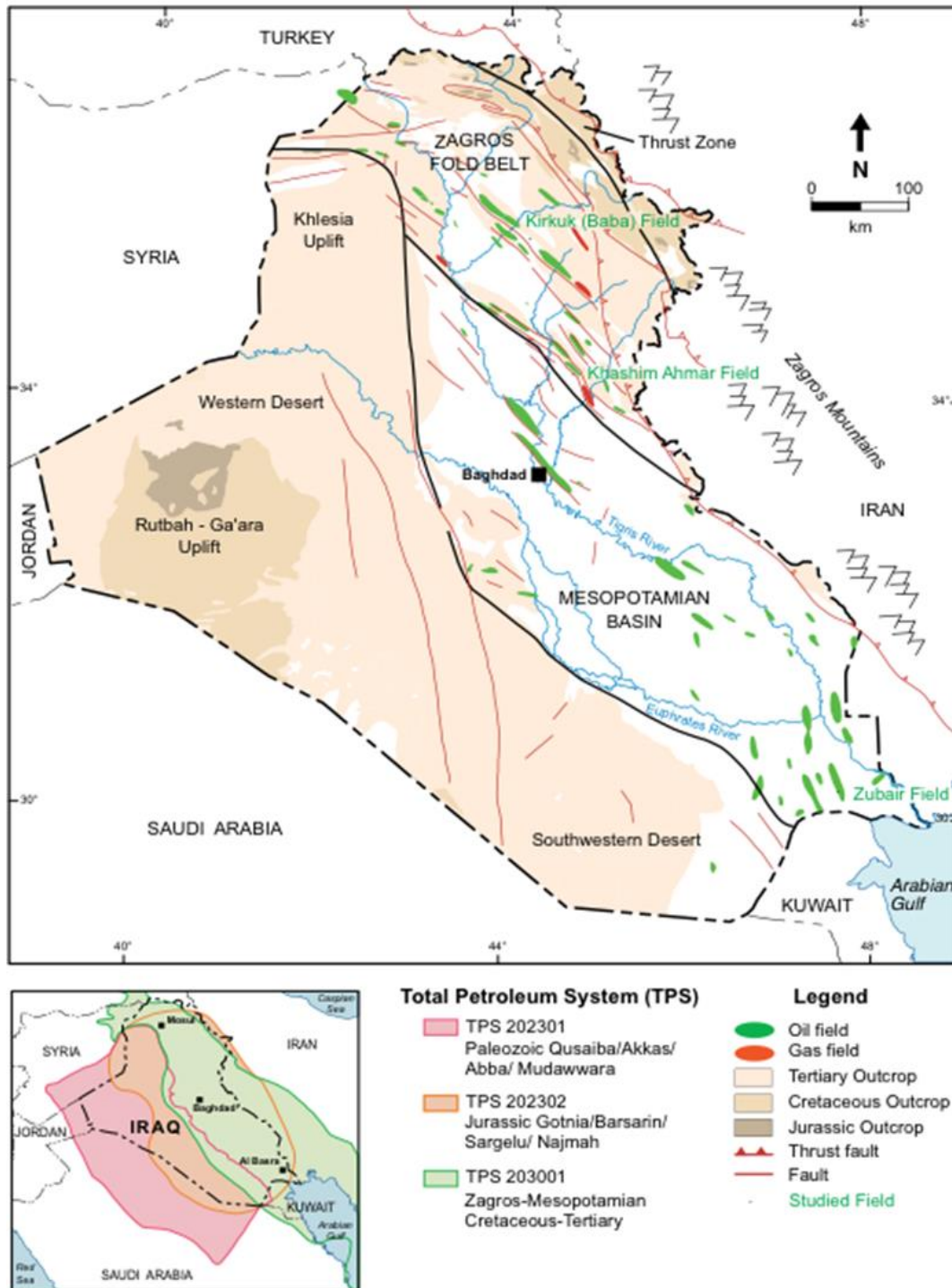


Figure 1. Map showing the major oil and gas fields in the regions of the Mesopotamian Basin and the Zagros Fold Belt, modified from Aqrawi, 1998. Inset map depicts three Total Petroleum Systems (TPS) that have contributed to the petroleum accumulations in Iraq (Ahlbrandt et al., 2000).

1.1 Aim of the Work

This work focused on detailed studies of the paleoenvironmental conditions (i.e., paleoclimate, paleosalinity and paleoredox conditions), provenance and tectonic setting of the Jurassic system in northern Iraq where six formations, namely (from base to top) the Sarki, Sehkanian (both Lower Jurassic), Sargelu (Middle Jurassic), Naokelekan, Barsarin (both Upper Jurassic) and Chia Gara (Upper Jurassic-Lower Cretaceous) formations, are exposed. Three locations in three different areas of northern Iraq (i.e., the Banik, Warte and Ranya areas) were chosen in each of the three Kurdistan Governorates, Duhok, Erbil and Sulaimaniyah (Figure 2). Carbonate rocks including limestones, dolomitic limestones and dolomites in addition to sporadic shale units form the main lithological components of the studied formations (Figures 3 and 4). Some solid bitumens from the Sargelu and Naokelekan formations in the Banik area (Figure 5) were additionally identified which have, to date, not been studied at all, according to our knowledge.

The current work aimed to examine, at high resolution, and by using modern instrumentation and techniques for analyses, the petrography, mineralogy and geochemistry of the Jurassic system in northern Iraq in order to reconstruct the paleoenvironmental conditions, including paleoclimate, paleosalinity and paleoredox conditions, and to provide much-needed new information with regard to the reservoir characteristics of the Jurassic successions. By comparing the Jurassic successions in three different areas in northern Iraq (i.e., the Banik, Warte and Ranya areas), this study integrated sedimentological and petrographical features of the various Jurassic units, together with the mineralogy and geochemistry, in order to provide a broad paleoenvironmental reconstruction of the region during the Jurassic times.

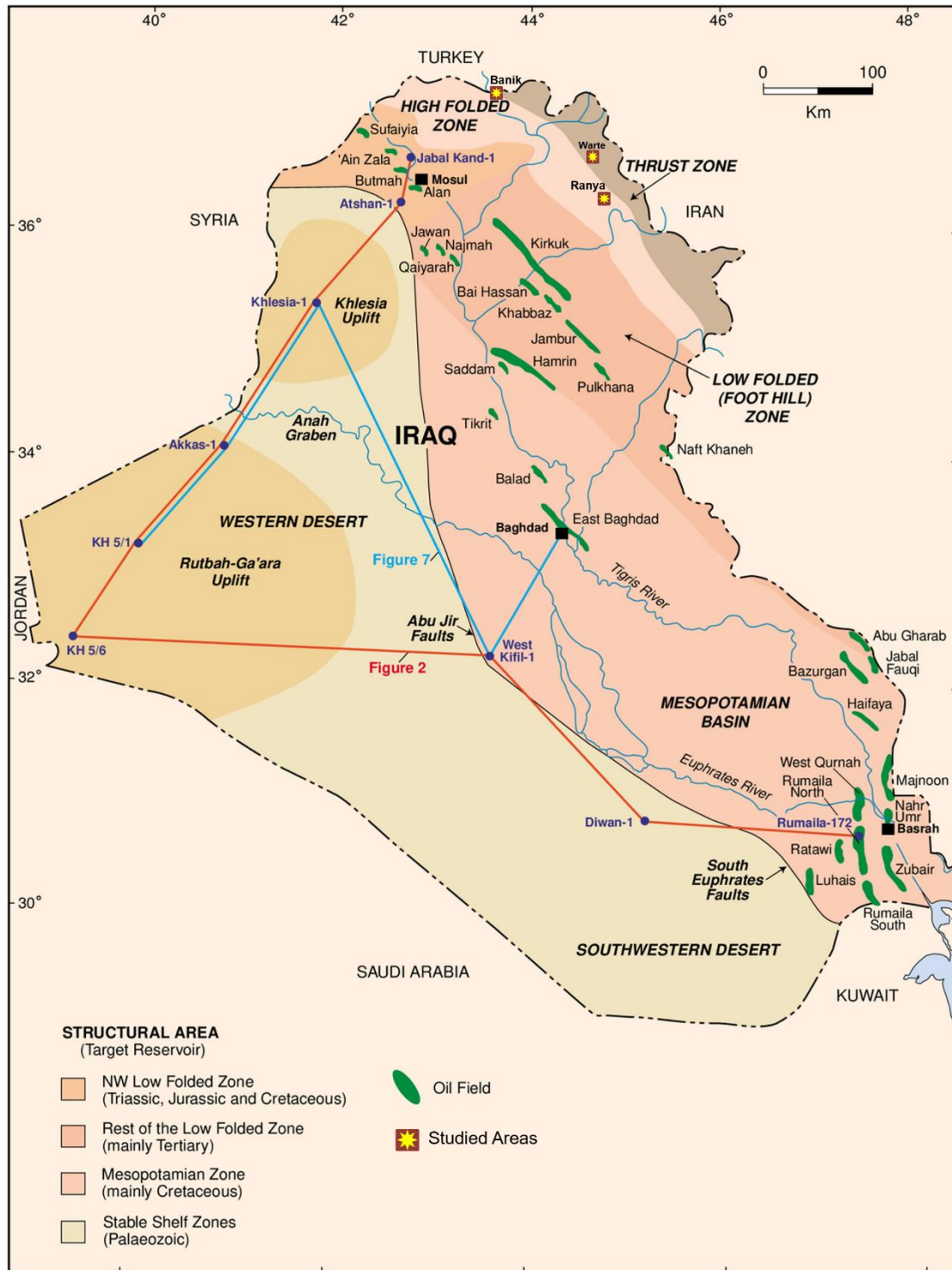


Figure 2. Geological map showing the location of the areas of study in three different sections (the Banik, Warte and Ranya), northern Iraq, where the Jurassic formations have been sampled (modified after Aqrawi, 1998).



Figure 3. Carbonate rocks interbedded with sporadic shales (yellow arrow) in the Warte section (hammer for scale).



Figure 4. Limestones, dolomitic limestones and dolomites in the Ranya section (tree for scale).



Figure 5. Solid bitumen in the Banik section (tree for scale).

Moreover, the combination of the mineralogy and geochemistry of the Jurassic shales from northern Iraq provided an excellent approach leading to a highly precise characterization of the provenance history and tectonic setting.

1.2 Regional geology of the Zagros region

The Zagros Basin, with its massive oil and gas reserves, is one of the most important petroleum provinces in the Middle East (Liu et al., 2018), and it is considered to be the second largest basin in the Middle East (Alsharhan and Nairn, 1997), with an area of about $500 \times 10^3 \text{ km}^2$ (Liu et al., 2018). This basin forms a narrow belt that extends from Turkey, NE Syria and NE Iraq through NW Iran, and into SE Iran (Hempton, 1987). In Iraq, the basin is bounded to the west by the Mesozoic stable shelf (Khlesia Uplift) and by the Mesopotamian Basin to the south. To the NW, the Zagros Basin converges with the Zagros Fold-and-Thrust Belt, with folding along the basin margins. This region, i.e., the deformed margins of the basin, represent almost all our areas of study (Jassim and Goff, 2006) (Figure 1).

The Zagros Basin is a classic foreland basin which developed adjacent and parallel to the Zagros mountain range formed as a result of the collision of the Arabian Plate and the Eurasian Plate, thus forming the Zagros Fold-and-Thrust Belt (Liu et al., 2018). The fold-and-thrust belt is a structurally complex area, approximately 200-300 km wide (Zainy et al., 2017) which forms part of the Alpine-Himalaya mountain chain (Talbot and Alavi, 1996; Lalami et al., 2020), and extends for over 2000 km from Turkey to the Strait of Hormuz (Berberian and King, 1981, Talbot and Alavi, 1996) covering the entire area of N Iraq.

The Zagros Fold-and-Thrust Belt formed as a result of thin-skinned, detachment folding of the sedimentary cover and thick-skinned thrusting in the basement (Pfiffner, 2017), resulting in

the development of a c. 7-12 km thick heterogeneous sedimentary succession (Zainy et al., 2017). Shortening within the zone of deformation tends to be more intense in the region of the suture between the two plates, becoming less intense towards the Zagros Basin (Sepehr and Cosgrove, 2004). The combination of thin- and thick-skinned deformation can be related to the role of detachment fault tectonics in the region of N Iraq (i.e., Kurdistan; Sarkarinejad and Goftari, 2019). Here, the presence of multiple mechanically-weak detachment horizons played an important role in the evolution of the fold-and-thrust belt (Koyi and Mansurbeg, 2021).

The exposed Jurassic formations in the region of N Iraq crop out in isolated locations within the eroded cores and limbs of anticlines in the structural zones of the Zagros Basin (Numan, 2000). Initial subdivisions of the Zagros region (e.g., Falcon 1969, 1974) recognised the existence of extensive and parallel NW-SE-trending structural belts. Subsequent classifications have modified and expanded the original subdivisions, with a total of three (or four) structural zones now defined. Jassim and Goff (2006) suggested that there are three zones, namely, the Low Folded Zone (or Foothills), the High Folded Zone and the Thrust Zone. However, Zainy et al. (2017, see also discussion therein) have suggested that the region can be subdivided into four zones, namely, the Low Folded Zone, the High Folded Zone, the Imbricate Zone and the Zagros Suture Zone. According to the latter authors, the Imbricated Zone can be subdivided into two subzones, including the Balambo-Tanjero Subzone and the northern (Ora) Thrust Subzone (i.e., the Thrust Zone), and thus the Thrust Zone of Jassim and Goff (2006) falls within their Imbricated Zone.

The stratigraphical sections, which were examined as part of this study, are located within the High Folded Zone and the Imbricated Zone (Figure 2). According to Zainy et al. (2017), the High Folded Zone covers an area of c. 15,827 km² and extends from the Iraq-Iran border where

the folds are oriented NW-SE, to the Iraq-Turkey border where the folds show an E-W orientation. The anticlines within the zone show high amplitudes and short wavelengths thus forming rugged anticlinal mountains separated by narrow synclinal valleys (Zainy et al., 2017). The Imbricated Zone, in contrast, is a narrow and high zone comprising mainly SW-directed thrusts and tight folds (Zainy et al., 2017).

1.3 Tectonic Framework in North Iraq

The areas of study in northern Iraq are situated within the Zagros Basin, an area which is, as noted above, rich in hydrocarbons, and forms part of the broader oil-rich Arabian Plate (Jassim and Goff, 2006; Abdula, 2010; Le Garzic et al., 2019). Indeed, the Middle East contains c. 65% of the world's remaining oil reserves as well as 35% of the remaining gas reserves (Sharland et al., 2001). The Arabian Plate was located, in Jurassic times, within the equatorial zone, and it was an area of relative tectonic stability. Across the plate region, organic-rich sediments (as source units) were intercalated with highly porous and permeable shallow-marine carbonate and siliciclastic sediments, which function as excellent reservoir units within the Jurassic and overlying Cretaceous units (Aqrawi et al., 2010). These successions were subsequently overlain by evaporites or non-permeable sediments, forming an ideal seal and thus leading to the formation of closed petroleum systems (Sadooni, 1995; Aqrawi et al., 2010). For this reason, the most petroleum-rich and productive Jurassic- and Cretaceous-age formations exist in Iraq, Saudi Arabia and the other Arabian Gulf countries (Murris, 1980; Beydoun, 1991; Sharland et al., 2001).

Sharland et al. (2001), working with a British independent oil company - LASMO plc - examined the sequence stratigraphy of the Arabian Plate region. Their sequence stratigraphic

and chronostratigraphic interpretations are supported by a detailed tectonostratigraphic review as well as the identification, dating and correlation of 63 Maximum Flooding Surfaces, although the authors note that these should best be considered as "maximum flooding intervals" since a more detailed interpretation would require full integration of the seismic, outcrop and well data, which was beyond the realm of their study (Sharland et al., 2001). Based on a comprehensive review of the literature as well as the experience and observations of the authors, Sharland et al. (2001) identified eleven tectonostratigraphic sequences (AP1-AP11) separated by major unconformities which reflect the evolution from an intracratonic setting, through back arc, to passive margin and finally the active margin setting of today. Five main tectonic phases were considered to be responsible for the evolution of the Arabian Plate, with sedimentary successions being deposited during each tectonic phase, with each megasequence reflecting the tectonic conditions which were active during deposition. The megasequences (AP1-11) can be summarised as follows:

AP1. Precambrian plate accretion and compression.

AP2 to AP3. Late Precambrian-Late Devonian, intracratonic and extensional phase.

AP4 and AP5. Late Devonian-Mid-Permian, back-arc setting with minor extension, separated by a period of compression.

AP6 to AP8. Mid-Permian-Mid-Cretaceous passive margin phase. This period includes the studied Early Jurassic-Early Cretaceous successions.

AP9 to AP11. Late Mesozoic-Present active margin phase (Sharland et al., 2001).

As noted above, the sedimentary successions of northern Iraq, which formed the basis of this thesis, were deposited during AP6-AP8. This period was mostly characterized by a passive margin setting, interrupted by periods of extensional tectonics (Sharland et al., 2001).

In detail, during the Lower Jurassic-Lower Cretaceous period the Arabian plate was dominated by post-rift thermal sagging which generated a passive margin towards the northwest and the northeast. The ongoing evolution of the Neo-Tethys Ocean saw continued spreading to the northeast, while the Mediterranean Sea in the north began to open during the Late Jurassic. The rifting associated with the formation of the Mediterranean Sea is thought to have created local basins in the areas which is now northeastern Iraq, including the areas of the present study (Fadhel and Al Rahim, 2019).

1.4 Jurassic and Early Cretaceous depositional history of North Iraq

The Jurassic and Cretaceous history of deposition of the region did not occur in isolation, but rather is a reflection of the broader regional tectonic and paleogeographic controls (see also above). In detail, six formations including the Sarki, Sehkanyian, Sargelu, Naokelekan, Barsarin and Chia Gara formations were deposited during the Early Jurassic-Early Cretaceous period. However, the controls on their deposition were broadly similar, although the situation in N Iraq would have been subjected to specific tectonic and other conditions. As noted earlier, the Sarki, Sehkanyian, Sargelu, Naokelekan, Barsarin and Chia Gara formations are located within the Zagros Basin of Iraq.

The areas of study from northern Iraq were situated on the wide carbonate shelf of Gondwana in the Upper Triassic-Lower Jurassic (Jassim and Goff, 2006). Some local basins formed in the Middle and Upper Jurassic on the shelf as a result of extensional tectonics, although, as

noted above, the region was predominantly a passive margin one (Sharland et al., 2001). These small basins occasionally became restricted or confined when the sea-level fell (Csató et al., 2014). A major sea-level fall occurred across much of the Arabian Plate in the Lower Jurassic, with a subsequent sea-level rise in the Middle Jurassic (Simmons and Davies, 2018). Several smaller scale regional sea-level fluctuations also occurred during the Jurassic and thus complicated the depositional history. In the Upper Jurassic, there was a large scale fall in sea-level (Sharland et al., 2001) coincident with the deposition of the Barsarin Formation. In the Late Tithonian-Early Cretaceous, the sea level rose once more and this rise coincided with the deposition of the Chia Gara Formation (Jassim and Goff, 2006; Csató et al., 2014).

Chapter 2

Chapter 2

Published in: *Geosciences* 2022, 12(2), 94;

<https://doi.org/10.3390/geosciences12020094>

Title: Early Jurassic-Early Cretaceous Calcareous Nannofossil Biostratigraphy and Geochemistry, Northeastern Iraqi Kurdistan: Implications for Paleoclimate and Paleoeological Conditions

Authors: Nagham Omar, Tom McCann, Ali I. Al-Juboury, Maria A. Ustinova, and Arkan O. Sharezwri

Author contributions: The doctoral student conceived, designed and prepared the study and wrote the main text under the supervision of Prof. Dr. Tom McCann. Maria A. Ustinova investigated the calcareous nannofossils. The final text was edited by all co-authors. All authors have read and agreed to the published version of the manuscript. The doctoral candidate submitted the manuscript acting as the sole corresponding author.

Summary

The correlation between analytical data of calcareous nannofossils and inorganic geochemical results can be used for interpreting paleoenvironmental and paleoclimatic conditions (Reolid et al., 2014; Al-Lhaebi et al., 2020; Al-Miamary et al., 2020). Oxygen isotope geochemistry may additionally be used as an indicator of climatic conditions (Bartolini et al., 2003; Weissert and Erba, 2004; Ruf et al., 2005; Mahanipour et al., 2019). However, detailed studies integrating the calcareous nannofossil biostratigraphy with related isotopic and inorganic geochemistry of the Early Jurassic-Early Cretaceous-age formations (i.e., Sarki, Sehkanyian, Sargelu, Naokelekan, Barsarin and Chia Gara) from northern Iraq have not been attempted to date, even though a few articles on calcareous nannofossils from the Naokelekan and Chia Gara formations in the Kurdistan region of Iraq have been published (Abdula, 2016; Wimbledon et al., 2016).

The Early Jurassic-Early Cretaceous-age Warte succession comprises interbedded shales and carbonates (dolomites and limestones) and rare chert beds. A total of sixty-five samples, covering the entire succession at this location, were selected. The calcareous nannofossils were

investigated using optical methods. The species diversity of the nannofossils was studied throughout each of the examined slides. In addition, the same samples were analyzed using X-ray fluorescence in order to determine the major and trace elements. Measurements were completed in the Institut für Geowissenschaften-Geologie, Bonn University, whilst the oxygen isotope analysis was performed at the Ruhr-University Bochum, using a mass spectrometer.

Of particular importance is the fact that this is the first study that focused on recording and analyzing calcareous nannofossils from the Early Jurassic-Early Cretaceous-age succession in northern Iraq. Investigation of the calcareous nannoplankton revealed that the Sarki and Sehkanyian formations of the Warte section are barren, while the Sargelu, Naokelekan, Barsarin and Chia Gara formations of the same section contain a range of nannofossils, including, *Watznaueria barnesiae*, *W. fossacincta*, *W. britannica*, *W. manivitiae* and *Cyclagelosphaera margerelii*. The first occurrences of *Cyclagelosphaera margerelii*, *Watznaueria britannica*, *W. fossacincta*, *W. manivitiae*, *W. barnesiae* and *W. ovata* would suggest a Bajocian-Callovian age for the Sargelu Formation.

A range of isotopic and inorganic geochemical analyses were carried out with the aim of reconstructing the paleoecological and paleoclimatic conditions predominant during the Early Jurassic-Early Cretaceous period. Based on prominent paleoclimate and paleoecological proxies (Sr, Ca, Al, Rb/Sr, Sr/Cu and Sr/Ba), as well as the results from the oxygen isotope data, it is suggested that warm and arid conditions were predominant during the period of deposition of the Early Jurassic-Early Cretaceous-age formations.

Chapter 3

Chapter 3

Published in: *Marine and Petroleum Geology*, 2023, 156, 106430

<https://doi.org/10.1016/j.marpetgeo.2023.106430>

Title: A comparative study of the paleoclimate, paleosalinity and paleoredox conditions of Lower Jurassic-Lower Cretaceous sediments in northeastern Iraq

Authors: Nagham Omar, Tom McCann, Ali I. Al-Juboury, Sven Oliver Franz, Giovanni Zanoni, and Harry Rowe

Author contributions: The doctoral student conceived, designed and prepared the study and wrote the main text under supervision of Prof. Dr. Tom McCann. Giovanni Zanoni, and Harry Rowe carried out the measurements using the scanning electron microscope. The final text was edited by all co-authors. All authors have read and agreed to the published version of the manuscript. The doctoral candidate submitted the manuscript acting as the sole corresponding author.

Summary

The major aim of paleoenvironmental reconstructions is to reconstruct paleoclimates, paleosalinities and paleoredox conditions (Jones and Manning, 1994; Tribovillard et al., 2006; Wang et al., 2020; Men et al., 2022; Li et al., 2023). Thus, understanding the paleoenvironmental conditions is essential for reconstructing and comprehending how oxygenation, climate and paleosalinity on the surface of the Earth have changed through time (Severmann and Anbar, 2009). A number of researchers (e.g., Cullers, 1995; Canet et al., 2004; Gao et al., 2017; Ivanić et al., 2017; Qin et al., 2018; Hussain et al., 2021; Fathy et al., 2023) have utilized the geochemical features of particular major and trace elements and/or elemental ratios to provide important information about the paleoenvironmental conditions during deposition. Other scientists have used ratios of specific rare earth and trace elements to understand the variations in paleoredox conditions in both modern and ancient marine successions (Calvert and Pedersen, 1993; Kimura and Watanabe, 2001; Algeo and Maynard, 2004; Rimmer, 2004; Fu et al., 2010; Madhavaraju et al., 2015). Mineralogical studies (XRD, SEM and EDX analyses) of clay minerals have also been employed to track changing climate

conditions, providing evidence based on the effects of weather conditions and the paleoclimate on particular minerals present in the source area (e.g., Chamley, 1989; Ruffell et al., 2002; Cao et al., 2012; Madhavaraju et al., 2016; Liu et al., 2021; Hussain et al., 2021).

Certain isotopes (e.g., carbon and oxygen isotopes) can also be studied to provide insights into paleoenvironmental conditions (e.g., Bartolini et al., 2003; Weissert and Erba, 2004; Ruf et al., 2005; Fisher et al., 2005; Li et al., 2016; Hennhofer et al., 2018; Afrozi et al., 2021). However, to date, such broader comparative geochemical studies of the Lower Jurassic-Lower Cretaceous successions of Iraq have not been attempted. The aim of this particular study was, therefore, to focus on a variety of paleoenvironmental proxies, including paleoclimate, paleosalinity and paleoredox proxies in the Early Jurassic-Early Cretaceous period in NE Iraq. To this end, a comparative study of the mineralogical and geochemical features of the Early Jurassic-Early Cretaceous-age Ranya section was carried out, together with a study of the Warte section (also Early Jurassic-Early Cretaceous in age). The Warte and Ranya successions (NE Iraq) are adjacent to the towns of the same name. Both of the sections comprise six formations (Sarki, Sehkanyian, Sargelu, Naokelekan, Barsarin and Chia Gara).

A total of one hundred and forty-one carbonate and shale samples were collected, covering the entire Jurassic-Lower Cretaceous succession of NE Iraq. Their mineralogical composition was examined using X-ray diffraction (XRD) at the Institute for Geosciences-Geology of Bonn University, Germany. Scanning electron microscopy (SEM) with energy-dispersive X-ray microanalysis (EDX) was conducted at the Premier Corex Group, Houston, Texas, USA. In addition, geochemical analyses were performed using X-ray fluorescence (XRF) analysis for major, trace and rare earth elements at the Bureau Veritas Laboratory, Canada. Stable carbon and oxygen isotopes were analyzed using a mass spectrometer MAT253 at the Ruhr University Bochum, Germany. Moreover, petrographic determinations for the main components and diagenetic processes of the carbonate rocks from the two sections were conducted at the Institute for Geosciences-Geology of Bonn University, Germany.

The findings of this work are considered to be of great importance given their singularity as the first comparative mineralogical and geochemical study of the Early Jurassic-Early Cretaceous-age successions in northern Iraq. The results from the paleoclimate proxies (Ca, Al, Sr/Ba, Rb/Sr and Sr/Cu), paleosalinity proxies (Sr, Ca, Al and Sr/Ba) and oxygen isotopes

would suggest that the predominant climate at the time was hot and arid. A mineralogical change from dominance of illite to increasing amounts of kaolinite during the Late Jurassic-Early Cretaceous period, revealed a climatic shift to more humid conditions during this period. Paleoredox proxies, including U/Th, V/Cr, Ni/Co, V/Sc and V/(V+Ni), indicated anoxic (or reduced oxygen) conditions during the depositional time in the examined areas. The changes in paleoclimate, paleosalinity and paleoredox conditions were most likely controlled by the tectonic activity in northern Iraq, where probably small silled subbasins developed within the tectonically-active Zagros Basin.

The final aspect of this particular study focussed on the petrographic and microfacies analyses of the carbonate units. This work revealed that the depositional environments of the Early Jurassic-Early Cretaceous-age formations in both the Warte and Ranya sections were tidal flat (supratidal), restricted lagoons and shallow marine to bathyal.

Chapter 4

Chapter 4

Published in *Neues Jahrbuch für Geologie und Paläontologie*, 2020, 297/2, 125-152

DOI: 10.1127/njgpa/2020/0916

Title: Petrography and geochemistry of the Middle-Upper Jurassic Banik section, northernmost Iraq – Implications for palaeoredox, evaporitic and diagenetic conditions

Authors: Nagham Omar, Tom McCann, Ali I. Al- Juboury, and Sven Oliver Franz

Author contributions: The doctoral student conceived, designed and prepared the study and wrote the main text under supervision of Prof. Dr. Tom McCann. Sven Oliver Franz contributed to the X-ray diffraction and X-ray fluorescence analyses. The final text was edited by all co-authors. All authors have read and agreed to the published version of the manuscript. The doctoral candidate submitted the manuscript acting as the corresponding author.

Summary

The Middle-Late Jurassic-age successions in northern Iraq comprise very significant carbonate source units interbedded within highly porous and permeable siliciclastic reservoir units (Omar et al., 2021). Due to the high contents of total organic carbon (TOC) recorded in the Middle Jurassic-age Sargelu Formation and the Late Jurassic-age Naokelekan Formation these rocks represent an excellent source for further studies (Omar et al., 2021). The current work focused on the Middle to Upper Jurassic succession (i.e., the Sargelu and Naokelekan formations) from the Banik section of northernmost Iraq. These formations have been studied with work focussing on the petrology and organic geochemistry (e.g., Al-Ahmed, 2006; Abdula, 2010; Al-Ameri and Zumberge, 2012; Al-Ameri et al., 2013; Abdula, 2017), sedimentology (e.g., Salae, 2001; Sharezwari, 2015; Abdula et al., 2015) and shale geochemistry (e.g., Tobia et al., 2019). However, a comprehensive examination of the petrography and microfacies of the carbonate units, integrated with the geochemistry of the shale units, has not, to date, been attempted. A total of 34 carbonate and shale samples from the Sargelu and Naokelekan formations were collected for detailed analysis (sedimentological, petrographical, microfacies and geochemical analyses). Thin sections were prepared at the Institut für Geowissenschaften-Geologie, Bonn University. Microfacies analysis was used to interpret the depositional

environments, based on the Dunham (1962) classification. Mineralogical and geochemical analyses were performed at the Institute for Geosciences-Geology of Bonn University, Germany, to obtain supporting information regarding the depositional environments. Scanning electron microscopy (SEM) with energy-dispersive X-ray microanalysis (EDX) were both carried out at the Nees Institute, Bonn University.

The aim of this work was to provide original data as a basis for an updated discussion on the sedimentary and diagenetic history, and, in addition, to examine the evaporation and paleoredox proxies under which the carbonate and clastic sediments were deposited. Lithological analysis of the Sargelu Formation showed the presence of massive dolomites, interbedded with shales, rare cherts and one single limestone bed, while the samples from the Naokelekan Formation comprised mainly shales overlain by limestones and one single dolomite bed. The petrographic analysis of the carbonates showed the presence of rare ostracods, bioclastic fragments as well as calcispheres. Five main microfacies were identified, including bioclastic wackestone, mudstone, dolorudite, dolarenite and dolomicrite. Analysis of the shales revealed the presence of clay mineral assemblages (illite/muscovite and kaolinite) with some quartz, alkali feldspar and rare pyrite.

The detailed study of the microfacies and the fossil content in the area of deposition and related/adjacent areas suggests that the depositional environment was shallow-marine for the Sargelu Formation and a restricted shallow lagoon environment for the Naokelekan Formation. In contrast, anoxic conditions were concluded to have been dominant during the sedimentation of both formations, based on the paleoredox proxies. This observation of marked differences has been explained as a result of the ongoing tectonic activity in the region of northern Iraq. Tectonic activity might have resulted in the formation of small subbasins where water circulation was restricted, thus, resulting in oxygen depletion. Additionally, evaporation processes (controlled by an arid climate) support an interpretation of basin compartmentalization across the region. Such basin subdivision would also have facilitated the development of anoxic periods within small silled basins.

Chapter 5

Chapter 5

Published in *Arabian Journal of Geosciences*, 2021, 14, 755

<https://doi.org/10.1007/s12517-021-07048-9>

Title: Solid bitumen in shales from the Middle to Upper Jurassic Sargelu and Naokelekan Formations of northernmost Iraq: implication for reservoir characterization

Authors: Nagham Omar, Tom McCann, Ali I. Al- Juboury, and Isabel Suárez-Ruiz

Author contributions: The doctoral student conceived, designed and prepared the study and wrote the main text under supervision of Prof. Dr. Tom McCann. Isabel Suárez-Ruiz carried out the petrographic investigation of the solid bitumens. The final text was edited by all co-authors. All authors have read and agreed to the published version of the manuscript. The doctoral candidate submitted the manuscript acting as the sole corresponding author.

Summary

The hydrocarbon reserves of Iraq are the sixth largest in the world (Al-Zubaidi and Al-Zebari, 1998; Jassim and Al-Gailani, 2006) with current proven reserves of 115 billion barrels of oil (BBO) and 110 trillion cubic feet (TCF) of gas. These reserves are contained within three different stratigraphic petroleum systems, namely the Palaeozoic, Jurassic, and Cretaceous-Tertiary (Ahlbrandt et al., 2000; Verma et al., 2004).

This particular study was carried out in the Banik area within the Kurdistan Region of Iraq. This latter area contains, according to current estimates, c. 39% of Iraq's total barrels of oil reserves. Recent studies have shown that most of the discovered oil in the Kurdistan Region of Iraq is sourced from the Sargelu (Middle Jurassic), Naokelekan (Upper Jurassic), and Chia Gara (Late Jurassic-Early Cretaceous) formations (Al-Ameri and Zumberge, 2012; Mohialdeen et al., 2013; Tobia et al., 2019).

Studies on the organic geochemistry of the Sargelu and Naokelekan formations have previously been published (Al-Ahmed, 2006; Aqrawi and Badics, 2015; El Diasty et al., 2018; Abdula et al., 2020). However, detailed studies of the solid bitumens from the Middle-Late Jurassic-age Sargelu and Naokelekan formations in the Banik succession have not, to date,

been conducted. Bellen et al. (1959) studied the presence of solid bitumens in the Naokelekan Formation, but misinterpreted them as coal horizons. To fill this gap, we performed a detailed study comprising petrographic, organic, and inorganic geochemistry of the solid bitumens and the host sediments (i.e., the shales) from the Sargelu and Naokelekan formations from the Banik section.

A total of eight shale samples hosting the solid bitumens were collected from the two formations. The petrographic identification of the solid bitumens was performed using optical microscopy at the Instituto de Ciencia y Tecnología del Carbono (INCAR-CSIC), Oviedo, Spain. Organic petrographical characterization was conducted using reflected white light and blue light excitation (fluorescence mode). The solid bitumens and host shale samples from the Sargelu and Naokelekan formations were additionally studied using scanning electron microscopy with energy-dispersive X-ray microanalysis (EDX) at the Nees Institute, Bonn University.

Mineralogical and geochemical analyses of the host shales were performed using XRD, and XRF measurements, respectively, at the Institut für Geowissenschaften-Geologie, Bonn University. Similarly, the total organic carbon (TOC) measurement of the solid bitumens and host shales was conducted in the Institut für Geowissenschaften-Geologie, Bonn University. Furthermore, carbon and oxygen stable isotopes were examined at the Ruhr University Bochum.

Determining the derivation, and preservation, of the solid bitumens within the shales of the Banik section, was one of the main aims of this particular study. In addition, the conditions under which the solid bitumens and shales were deposited were examined – with these aspects being elucidated using the carbon and oxygen isotopes and paleoredox indicators.

The attained results from the petrographic examination of the Sargelu and Naokelekan formations revealed the presence of two phases of solid bitumen, namely, solid bitumen with high reflectance (first phase) and solid bitumen with low reflectance (second phase). The accumulation process of the solid bitumens was interpreted to have occurred within the shale reservoirs, based on the equivalent vitrinite reflectance, probably as a result of oil migration from other source rocks located within the same (i.e. Sargelu and Naokelekan) formations.

Mineralogical studies (i.e., XRD and SEM-EDX) revealed that the shales hosting the solid bitumens also comprised clay minerals (illite, rectorite, chlorite, montmorillonite, and kaolinite), in addition to carbonate minerals, quartz, alkali feldspar, and pyrite. The carbon and oxygen isotope analysis results, together with the paleoredox proxies, suggested that deposition of the solid bitumen sources and host shales occurred within a shallow-marine setting, and under anoxic conditions, where water circulation was restricted.

Chapter 6

Chapter 6

This manuscript is being prepared for submission

**Title: Provenance and tectonic setting of the Jurassic shales from northeastern Iraq:
Mineralogical and geochemical approaches**

Authors: Nagham Omar, Tom McCann, Ali I. Al- Juboury, Mohammed A. Al-Haj, and
Arkan O. Sharazwri

Provenance and tectonic setting of the Jurassic shales from northeastern Iraq: Mineralogical and geochemical approaches

Nagham Omar^{1, *}, Tom McCann¹, Ali I. Al-Juboury², Mohammed A. Al-Haj³, Arkan O. Sharazwri⁴

¹*Institut für Geowissenschaften, Geologie, University of Bonn, Nussallee 8, 53115 Bonn, Germany; email: s6naomar@uni-bonn.de*

²*Petroleum Engineering Department, College of Engineering, Al-Kitab University, Kirkuk, Iraq*

³*Geology Department, College of Science, Mosul University, Iraq*

⁴*Department of Petroleum Geosciences, Faculty of Science, Soran University, Soran, Erbil, Iraq*

*Corresponding author: N. Omar, Institut für Geowissenschaften, Geologie, University of Bonn, Nussallee 8, 53115 Bonn, Germany; E-mail address: s6naomar@uni-bonn.de

Abstract

Mineralogical and geochemical features of the shales of the Lower Jurassic-Lower Cretaceous successions from the Warte and Ranya areas in northeastern Iraq were investigated, with the aim to determine the provenance and tectonic setting of their source region. X-ray diffraction analysis revealed that the shales' mineral composition was dominated by calcite, dolomite and quartz, with traces of feldspar, illite/mica, kaolinite and chlorite. The geochemical proxies, namely La/Th vs Hf, Th/U, TiO₂ vs Zr, Al₂O₃/TiO₂, TiO₂ vs Al₂O₃, light rare earth elements (LREE)/heavy rare earth elements (HREE), and Eu/Eu*, revealed that felsic and intermediate igneous rocks constituted the predominant source rocks. These results suggest that the sediments were derived from the Zagros ophiolites and related igneous rocks in northeastern Iraq. In addition, the tectonic setting proxies discriminating function-based major element diagrams, K₂O/Na₂O vs SiO₂, and Th-Sc-La ternary diagram, suggest a passive margin setting for the Early Jurassic-Early Cretaceous shale successions, which is consistent with the geological history of the studied areas.

Keywords: Iraq, Jurassic, Shale, Provenance, Tectonic setting

1. Introduction

The chemical composition of shales provides important clues to assess the paleotectonic setting and provenance of these rocks (McLennan et al., 1993; Lee, 2009; Moradi et al., 2016; Al-Juboury et al., 2021). A variety of factors, including the composition of the source rocks, the degree of weathering in the source area, the depositional setting and post-depositional modifications, all influence the chemical and mineralogical composition of siliciclastic rocks (Nesbitt et al., 1980; Dickinson et al., 1983; Roser and Korsch, 1988; McLennan et al., 1993; Nesbitt et al., 1996; Eko Bessa et al., 2021; Mahdi et al., 2021). Many elements, such as transition trace elements (Th, Sc, Hf, and Ti) and rare earth elements (La and Y), are transferred to the sedimentary basin without significant fractionation, thereby preserving the signature of the source materials (Floyd et al., 1989; Mondal et al., 2012). These immobile elements are widely used in provenance studies (Dickinson and Suczek, 1979; Bhatia, 1983; McLennan et al., 1983; Bhatia and Crook, 1986; Roser and Korsch, 1986; McLennan and Taylor, 1991; Wani and Mondal, 2011; Mehrabi et al., 2021), and to assess the relative contribution of felsic and basic sources (Wronkiewicz and Condie, 1987; Armstrong-Altrin et al., 2013; Mudoi et al., 2022). The fine-grained nature and impermeability of shales helps to retain the original geochemical signatures of source rocks (Sochava et al., 1994; Cullers, 1995; Wani and Mondal, 2011; López et al., 2019) thus allowing researchers to decipher the paleotectonic setting of a sedimentary basin based on the geochemical signature of shales (Bhatia, 1983; Bhatia and Crook, 1986; Roser and Korsch, 1986; Wani and Mondal, 2011; Verma and Armstrong-Altrin, 2013; Moradi et al., 2016; Al-Juboury et al., 2021; Tobia and Mustafa, 2022).

In the current study, the shales of the Early Jurassic-Early Cretaceous successions in two outcrop sections from northeastern Iraq namely the Warte and Ranya sections, which comprise six formations (i.e., Sarki, Sehkanyian, Sargelu, Naokelekan, Barsarin and Chia Gara), have been subjected to detailed mineralogical investigations using X-ray diffraction (XRD) and scanning electron microscopy (SEM), as well as geochemical (major, trace and rare earth elemental) analyses by X-ray fluorescence (XRF) spectroscopy. The Jurassic successions of Iraq were previously studied in terms of their depositional environments, hydrocarbon potential, paleoclimate, paleosalinity, paleoweathering, and paleoredox conditions in various formations, while little attention has been paid to investigating their source areas and tectonic

setting (Mohialdeen et al., 2013; Abdula, 2016; Mustafa and Tobia, 2020; Omar et al., 2020, 2022; Tobia and Mustafa, 2022). The present work constitutes a pioneering study that combines the analysis of mineralogical and geochemical data of the Jurassic shales from northeastern Iraq with the aim to determine their provenance history and tectonic setting.

2. General Geology

The studied areas (i.e., Warte and Ranya areas) are located in northeastern Iraq and within the Zagros Basin (see Figure 1), at the northeastern boundary of the Arabian Plate, marking the collision between the continental Arabian Plate and the continental segments of the Eurasian margin (Beydoun et al., 1992; Stampfli and Borel, 2002; Liu et al., 2018). The two studied areas, which are about 70 km apart, are located in different structural zones of the Zagros Basin, namely, the High Folded Zone, and the Imbricated Zone (Figure 1). The Zagros Basin comprises three structural zones, from southwest (SW) to northeast (NE), the Low Folded Zone (or Foothills), the High Folded Zone and the Thrust Zone (Jassim and Goff, 2006). The latter Zone of Jassim and Goff (2006) falls within the Imbricated Zone of Zainy et al. (2017). According to Zainy et al. (2017), the Imbricated Zone can be subdivided into two subzones, including the Balambo-Tanjero Subzone and the northern (Ora) Thrust Subzone (i.e., the Thrust Zone). The Early Jurassic-Early Cretaceous-age succession of the Warte area is exposed within the Imbricated Zone, whilst the Early Jurassic-Early Cretaceous-age succession of the Ranya area is located within the High Folded Zone (Figure 1).

The relative stability of the area during the Early Jurassic was reflected by the deposition of several carbonate and evaporite successions as represented by the Alan, Mus and Adaiyah formations in the Mesopotamian Basin of central Iraq and their correlative Sarki and Sehkaniyan formations in the Zagros Basin of northern Iraq. In the Middle Jurassic, deposition of the organic-rich shales of the Sargelu Formation and their equivalents on the Arabian Plate occurred (Murris, 1980; Beydoun, 1991; Sadooni, 1997).

In the Late Jurassic, the Naokelekan and Barsarin formations were deposited on the eastern margin of the Zagros foreland basin (Murris, 1980; Numan, 2000), while the Najmah Formation was deposited on the western basin margin. The Chia Gara Formation was deposited in the Late Jurassic-Early Cretaceous as a result of global separation and expansion within the deep outer shelf of the Arabian Plate margins (Numan, 1997).

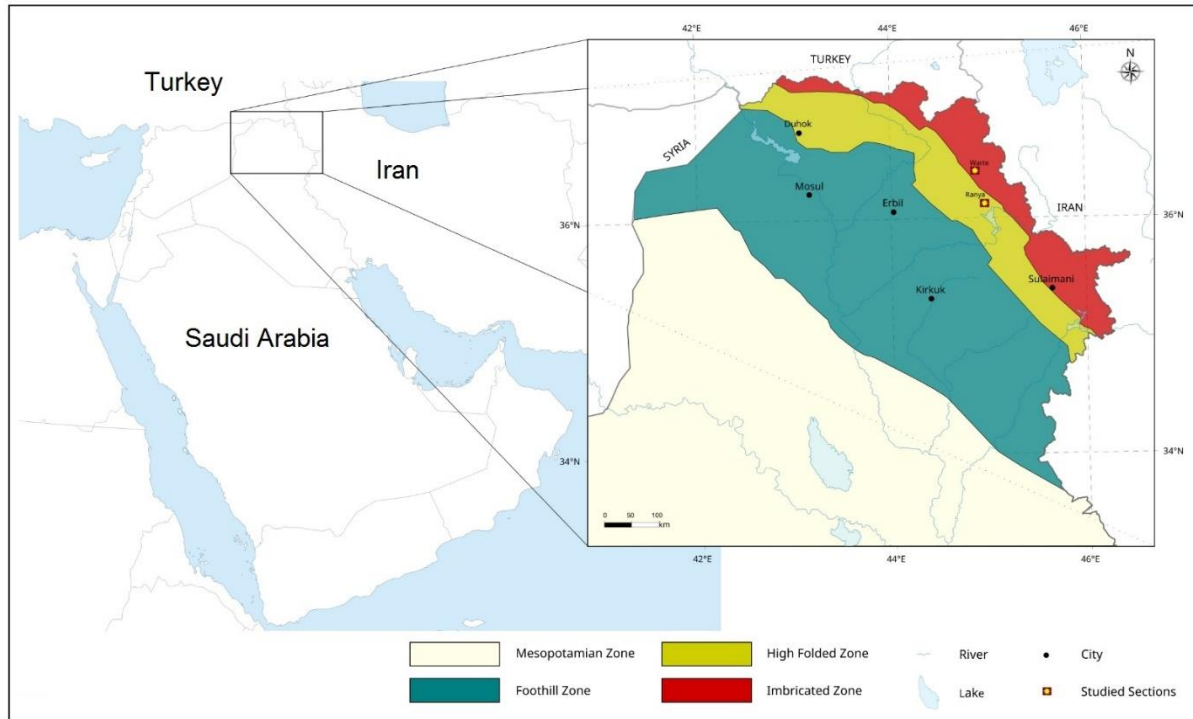


Figure 1. Geological map of northern Iraq showing the study areas and the structural zones of the Zagros Basin.

In the Zagros Thrust Zone of northeastern Iraq, ophiolite complexes are abundant along the Iraq-Iran border that resulted from the opening and subduction of the Neo-Tethys Ocean and subsequent oblique collision of the African-Arabian plate with the Iranian microcontinent in the Late Cretaceous-Early Tertiary (Ismail and Carr, 2008).

The Jurassic rocks are commonly exposed as isolated outcrops in eroded cores and limbs of anticlines within the structural zones of the Zagros Basin (Numan, 2000). This exposure pattern can be related to plate tectonic activity in northern Iraq (Bellen et al., 1959).

The Lower Jurassic-Lower Cretaceous successions of both the Warte and Ranya areas comprise six formations, namely, the Sarki, Sehkanyian, Sargelu, Naokelekan, Barsarin and Chia Gara formations. Some of these formations are considered to be part of the recognized megasequences in the region. Sharland et al. (2001) classified a series of megasequences, namely eleven megasequences, based on the tectonic evolution of the Arabian Plate through its five evolutionary phases. These phases range from the plate accretion and compressional

phase during the Precambrian (AP1), through the intracratonic and extensional phase (AP2 to AP3) in the Late Precambrian to the Late Devonian, the back-arc setting with minor extension separated by a period of compression during the Late Devonian to Mid-Permian (AP4 and AP5), and the passive margin setting during the Mid-Permian to the Mid-Cretaceous (AP6 to AP8), interrupted by periods of extensional tectonics, to the active margin setting of the Late Mesozoic to the present time (AP9 to AP11).

Tectonically, the studied Early Jurassic-Early Cretaceous successions are included within the period of (AP6 to AP8). The Sarki and Sehkanyian formations can be regarded as a part of the sedimentary Megasequence AP6, whilst the Sargelu, Naokelekan and Barsarin formations form part of the Megasequence AP7 (Jassim and Goff, 2006). According to the latter authors, the Chia Gara Formation forms part of the Megasequence AP8.

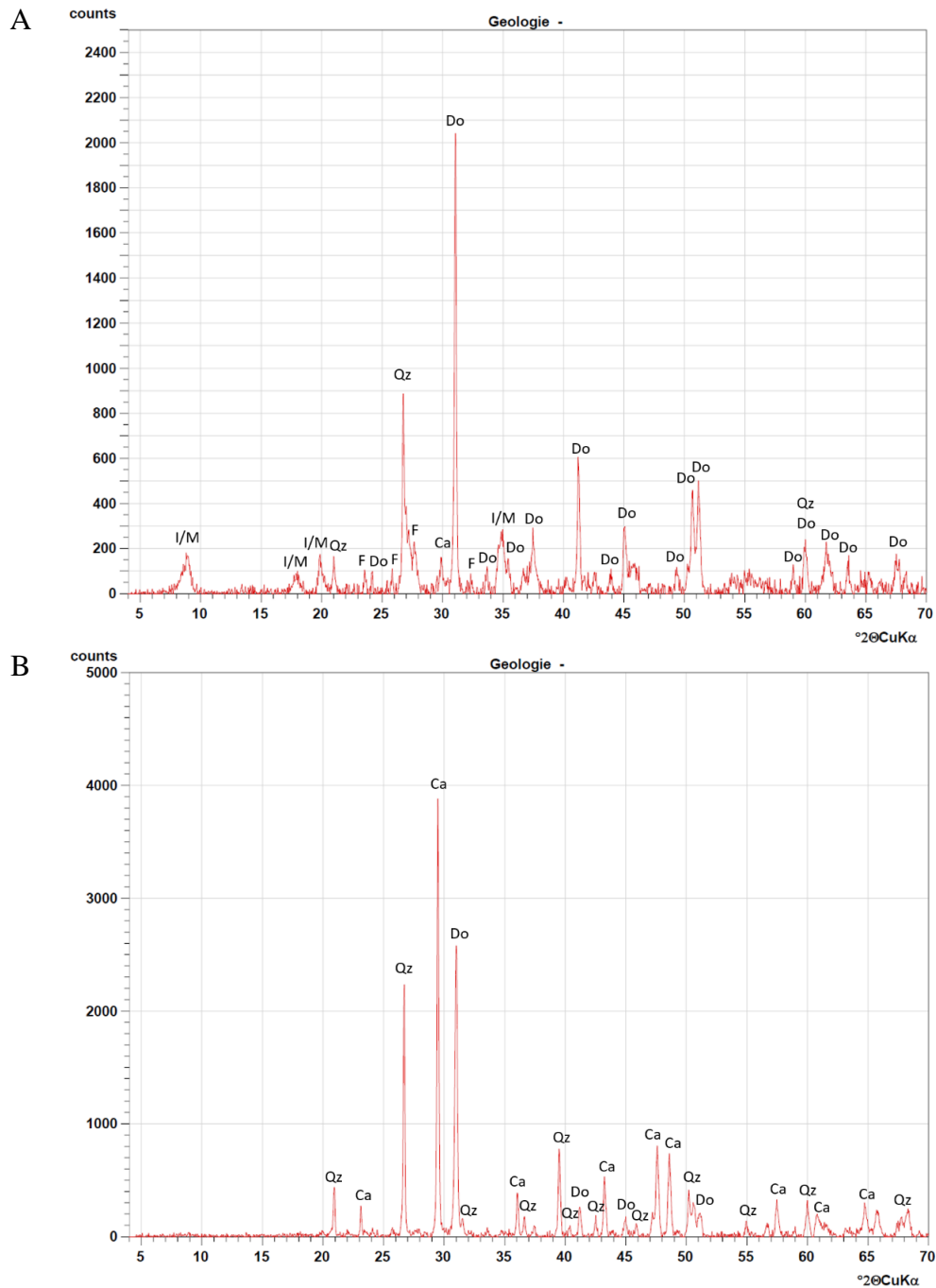
3. Samples and Analytical Methods

Fifty-seven samples from the Lower Jurassic-Lower Cretaceous shale successions of the Sarki, Sehkanian, Sargelu, Naokelekan, Barsarin and Chia Gara formations from the Warte and Ranya sections were collected for detailed mineralogical and geochemical analyses. Mineralogically, the same samples were examined using X-ray diffraction (XRD, using a D8 Advance from the company Bruker AXS GmbH) at the Institut für Geowissenschaften-Geologie of Bonn University, Germany. Geochemical analyses of the shale samples were analyzed using X-ray fluorescence (XRF) spectroscopic analysis for major, trace and rare earth elements) at the Bureau Veritas Laboratory, Canada. Scanning electron microscopy (SEM) analyses were completed on selected samples at the Premier Corex Group Laboratory in Houston, Texas, U.S.A, using a FEI Quanta FEG 650 FE-SEM instrument equipped with two Bruker EDS XFlash 5030 energy dispersive X-ray spectroscopy (EDS) detectors, and a FEI R580 Everhart-Thornley (ETD) electron detector. Freshly broken surfaces were created by breaking a rock segment as close to perpendicular to bedding as possible, and used for the study. All samples were mounted on aluminum stubs using a conductive high viscosity glue. They were then sputter-coated with 10 nm of iridium using a Leica EM ACE600 sputter coater prior to being placed in the SEM. The measurements were performed under high vacuum, with an accelerating voltage of 10 kV.

4. Results

4.1 Mineralogy

The main minerals contained by the shale samples, as indicated by X-ray diffraction analysis, are calcite and quartz. Dolomite was also distinguished, in addition to traces of feldspar and some clay minerals including illite/mica, kaolinite and chlorite (Figure 2).



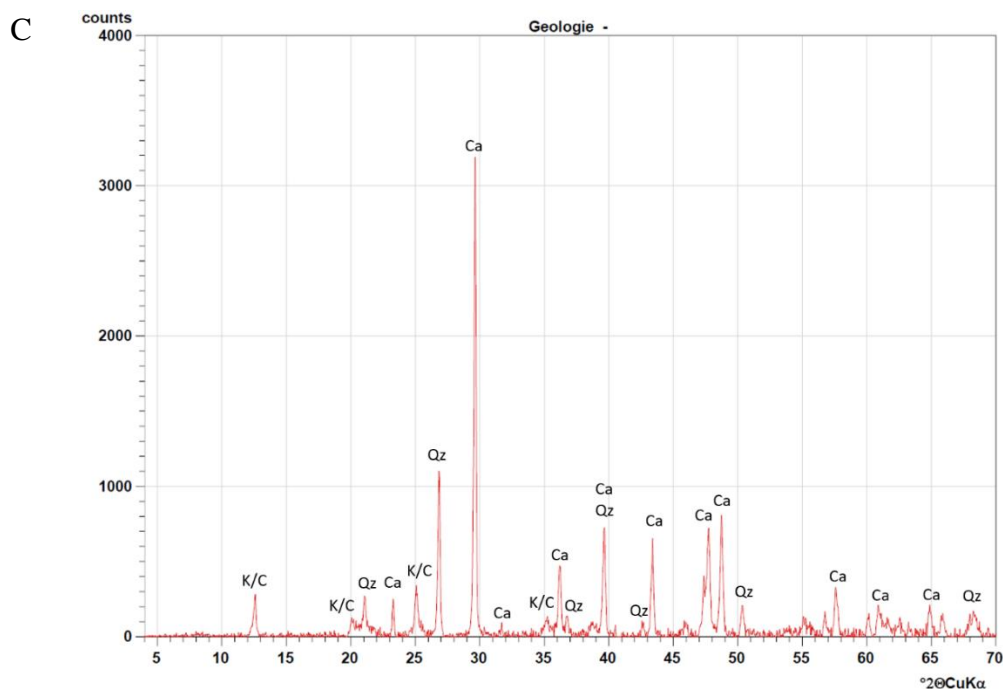


Figure 2. Representative X-ray diffractograms showing the main components in the studied shales. **A.** Sample 8 from the Sarki Formation of the Warte section. **B.** Sample 13 from the Sargelu Formation of the Warte section. **C.** Sample 6 from the Chia Gara Formation of the Ranya section. C, Calcite; Qz, Quartz; I/M, Illite/mica; F, Feldspar; Do, Dolomite; K/C, Kaolinite/Chlorite.

In addition, scanning electron microscopy (SEM) confirmed the presence of illite, of illite/mica- and illite/smectite-mixed layers, and of kaolinite (Figure 3).

Calcite was found to be present in a number of forms, including, euhedral (hexagonal) crystals, star-shaped Mg-calcite microcrystals and columnar calcite crystals (Figure 3). Quartz was found mainly in a subhedral form with overgrowth. Feldspar was detected mainly as euhedral crystals while pyrite framboids were also recognized. The framboidal forms of pyrite were previously reported to reflect anoxic-euxinic conditions in ancient marine (Liao et al., 2010; Tian et al., 2014). A variety of clay minerals were also recognised, including kaolinite as degraded hexagonal plates (Figure 3), illite/mica in the form of fibers and laths or as platelets, with illite/smectite mixed layers present as matted crenulated flakes (Figure 3).

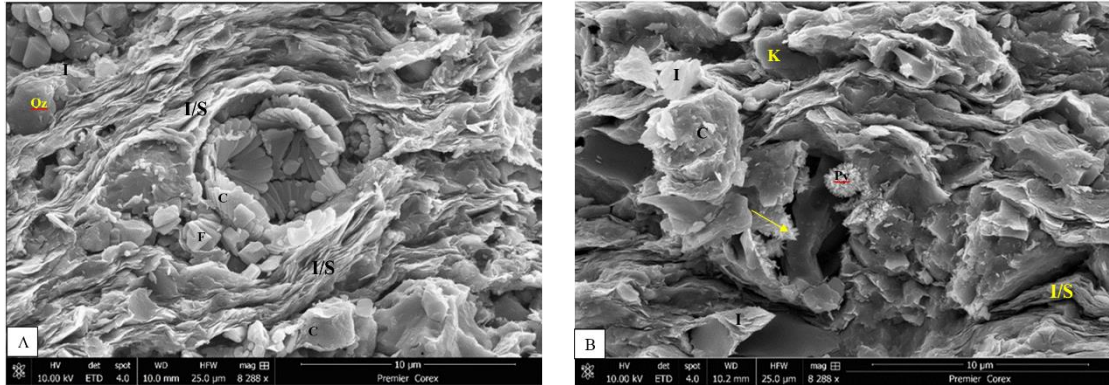


Figure 3. Representative SEM microimages showing the main components in the studied shales. **A.** Shale from Chia Gara Formation. **B.** Shale from Sarki Formation. C, Calcite; Qz, Quartz; I, Illite/mica; I/S, Illite/smectite mixed layers; K, Kaolinite; F, Feldspar; Py, Pyrite; Mg, calcite (arrow).

4.2 Geochemistry

XRF analysis of the major oxides, trace and rare earth elements of the shale samples from the six formations (i.e., Sarki, Sehkanyian, Sargelu, Naokelekan, Barsarin and Chia Gara) of the Warte and Ranya sections, NE Iraq, was carried out (Tables 1, 2). In Table 1, the major elemental data for the studied shales are collected. The Early Jurassic-age formations Sarki and Sehkaniyan shales reflect a higher content of SiO_2 and Al_2O_3 as compared to other middle and Late Jurassic-age formations (Table 1). The average $\text{K}_2\text{O}/\text{Al}_2\text{O}_3$ ratios for the Early Jurassic-age formations are also higher than those of other Jurassic formations. This ratio can be employed for predicting the original composition of ancient sediments. The clay minerals and feldspars have different ratios (0.0 to 0.3, and 0.3 to 0.9, respectively; Cox and Lowe, 1995). The ratios of the Early Jurassic shales are close to the upper limit of the clay mineral range, which reflects the dominance of illite/mica in the clay minerals as indicated by the XRD studies (Figure 2). The $\text{Al}_2\text{O}_3/\text{TiO}_2$ ratios of the studied shale samples are as follows: 14.8 (Lower Jurassic, Sarki and Sehkaniyan), 19.8 (Middle Jurassic Sargelu), and 8.6 (Late Jurassic-age Naokelekan and Barsarin formations). The $\text{Al}_2\text{O}_3/\text{TiO}_2$ ratios of the investigated shales are very similar to that of the Post Archean Australian Shale (PAAS) (19.0; Taylor and

McLennan, 1985) in the Middle Jurassic shales, whereas the lowest values were found in the Late Jurassic shales. Titanium is mainly concentrated in phyllosilicates (Condie et al., 1992); it is immobile in relation to other elements during several sedimentary processes, and may truly represent the source rocks (McLennan et al., 1993). The concentrations of some of the trace elements and ratios used in the current study, along with rare-earth elements, are indicated in Table 2.

Table 1. Major oxide concentrations (%) of the studied samples from various Jurassic formations.

Formation	Section /No.	SiO ₂	Al ₂ O ₃	Fe ₂ O ₃	MnO	MgO	CaO	Na ₂ O	K ₂ O	TiO ₂	P ₂ O ₅	SO ₃
Sarki	w / s2	7.79	2.24	1.65	0.06	19	26.13	0.09	1.1	0.11	0.04	0.21
Sarki	w / s6	36.02	13.03	3.9	0.07	9.9	10.52	0.15	5.16	0.64	0.12	0.1
Sarki	w / s8	41.45	14.75	4.22	0.07	8.14	7.89	0.15	6.13	0.68	0.2	0.25
Sarki	w / s10	12.36	4.5	2.02	0.09	17.49	23.38	0.12	1.95	0.2	0.05	0.27
Sarki	w / s12	6.72	2.38	1.35	0.1	19.44	26.64	0.11	0.95	0.11	0.04	0.16
Sarki	w / s15	15.71	4.08	2.11	0.09	16.58	22.53	0.15	1.67	0.28	0.05	0.43
Sarki	w / s18	42.48	14.66	3.5	0.07	7.63	7.43	0.15	6.44	0.73	0.17	0.18
Sarki	w / s21	32.72	14.21	7.99	0.05	6.85	8.48	0.07	5.27	0.67	0.05	0.56
Sarki	w / s28	28.04	12.97	5.60	0.02	4.91	17.73	0.05	3.72	0.97	0.09	0.15
Sarki	w / s31	14.26	5.35	2.55	0.04	11.48	26.43	0.04	2.15	0.34	0.04	0.20
Sehkaniyan	w / s3	23.75	9.98	8.43	0.03	0.84	30.88	0.05	1.92	0.94	0.20	1.31
Sehkaniyan	w / s6	28.14	9.62	4.55	0.03	9.27	16.70	0.04	4.06	0.64	0.04	0.09
Sehkaniyan	w / s21	7.04	3.14	1.27	0.02	5.21	41.51	0.01	0.32	0.22	0.05	0.05
Sargelu	w / s6	1.46	0.42	0.35	<DL	0.24	53.83	0.02	0.10	0.02	0.04	0.29
Sargelu	w / s7	8.87	3.74	2.27	0.04	0.94	45.16	0.04	0.83	0.23	0.23	0.25
Sargelu	w / s8	24.19	10.02	5.22	0.06	0.85	25.77	0.03	1.75	0.68	0.27	1.36
Sargelu	w / s9	13.14	5.78	1.76	0.02	1.58	44.11	0.05	0.94	0.32	0.10	0.33
Sargelu	w / s10	23.71	3.30	2.53	0.01	1.03	34.92	0.06	0.89	0.22	0.21	0.97
Sargelu	w / s11	28.58	2.91	1.80	<DL	0.42	33.22	0.05	0.78	0.20	0.23	2.38
Sargelu	w / s13	24.09	4.35	2.94	<DL	2.07	30.57	0.15	0.99	0.37	0.39	1.28
Naokelekan	w / s1	19.07	4.79	3.42	<DL	4.28	27.58	0.06	1.08	0.41	0.22	2.18
Naokelekan	w / s4	7.56	2.22	1.46	<DL	0.37	45.30	0.07	0.60	0.22	0.13	1.50
Naokelekan	w / s8	17.65	7.53	6.69	<DL	0.59	32.71	0.03	1.52	0.62	0.17	1.32
Barsarin	w / s2	3.69	1.33	0.98	0.03	2.1	48.71	0.01	0.18	0.09	0.02	0.56
Barsarin	w / s5	2.78	0.99	0.53	0.03	0.39	51.82	<DL	0.14	0.06	0.01	0.27
Chia Gara	w / s1	31.80	16.19	8.24	0.01	0.85	16.38	0.10	1.72	1.16	0.35	0.94
Chia Gara	w / s3	1.03	0.62	0.42	<DL	0.37	48.64	0.02	0.04	0.07	0.06	2.71

Chia Gara	w / s4	27.4	13.64	6.06	0.03	0.89	22.69	0.09	1.24	0.85	0.48	2.99
Chia Gara	w / s6	16.63	6.24	3.04	0.02	0.69	37.68	0.04	0.56	0.33	0.14	0.41
Sarki	R / s0	23.54	7.99	2.78	0.04	14	17.8	0.1	3.79	0.38	0.06	0.24
Sarki	R / s2	21.38	7.24	3.16	0.05	14.31	18.6	0.12	3.41	0.33	0.08	0.31
Sarki	R / s5	25.39	8.65	2.96	0.04	13.05	17.15	0.1	4.04	0.41	0.06	0.22
Sarki	R / s8	34.73	12.54	3.95	0.04	10.11	11.79	0.11	5.21	0.55	0.12	0.16
Sarki	R / s10	52.12	19.36	5.52	0.02	4.28	1.14	0.11	8.05	0.84	0.12	0.44
Sarki	R / s11	7.17	2.53	1.79	0.07	19.19	26.06	0.09	1.1	0.11	0.01	0.29
Sarki	R / s13	17.31	5.79	1.85	0.04	16.24	21.26	0.08	2.83	0.25	0.08	0.24
Sarki	R / s15	14.02	4.71	1.92	0.02	12.67	26.66	0.02	2.28	0.33	0.01	0.09
Sarki	R / s17	46.62	16.66	5.1	0.01	4.86	5.49	0.09	8.22	0.61	0.39	0.31
Sarki	R / s20	16	6.01	2.04	0.02	15.98	22.16	0.08	1.98	0.22	0.05	0.08
Sarki	R / s25	41.47	20.42	6.99	0.02	3.91	3.73	0.07	5.69	1.19	0.01	1.62
Sarki	R / s28	34.54	12.4	4.84	0.04	9.14	11.94	0.05	5.08	0.66	0.11	0.36
Sehkaniyan	R / s2	40.8	12.32	4.66	0.04	6.01	12.02	0.1	5.81	0.69	0.06	0.29
Sehkaniyan	R / s4	46.15	16.39	7.31	0.06	3.18	7.5	0.08	6.48	0.91	0.07	0.19
Sehkaniyan	R / s11	52.83	18.95	6.04	0.04	5.17	1.14	0.08	6.59	0.83	0	0.12
Sehkaniyan	R / s13	26.99	9.47	4.18	0.03	13.09	15.34	0.09	3.72	0.46	0.03	0.19
Sehkaniyan	R / s14	52.8	18.44	6.85	0.04	5.13	0.68	0.12	6.88	1.11	0.04	0.24
Sehkaniyan	R / s17	49.27	21.55	4.06	0.02	5.28	1.68	0.17	7.18	1.14	<DL	0.22
Sargelu	R / s10	8.3	4.69	2.93	0.05	14.01	28.88	0.07	0.9	0.22	0.51	0.58
Sargelu	R / s11	10.89	6.41	2.09	0.03	9.99	31.28	0.04	1.1	0.31	0.09	0.77
Sargelu	R / s12	14.97	5.87	2.15	0.02	0.8	38.27	0.04	1.04	0.25	0.17	0.58
Sargelu	R / s13	31.16	1.69	1.02	0.01	1.61	32.63	0.02	0.5	0.11	0.11	0.81
Sargelu	R / s14	32.3	2.1	1.56	0.01	2.68	30.37	0.01	0.56	0.13	0.26	1.85
Naokelekan	R / s1	14.42	1.75	1.06	0.01	0.55	41.81	0.07	0.43	0.13	0.34	0.81
Chia Gara	R / s1	23.14	5.96	2.47	0.01	0.44	35.18	0.04	0.47	0.38	0.04	0.55
Chia Gara	R / s4	7.68	3.5	1.31	0.01	0.4	46.46	0	0.38	0.21	0.08	0.86
Chia Gara	R / s5	12.92	1.96	0.87	0.01	0.34	44.18	0.04	0.26	0.11	0.04	0.97
Chia Gara	R / s6	29.95	13.69	5.52	0.02	0.44	23.2	0.05	0.51	0.83	0.11	0.64

The values for the light rare earth elements (LREE, La, Ce, Pr, Nd, Sm, Eu) and the heavy rare earth elements (HREE, Gd, Tb, Dy, Ho, Er, Tm, Yb and Lu) and the ratio of LREE/HREE are illustrated in Table 2. The LREE/HREE ratios show slight variations between the studied shale samples. The ratio is in general high in lower Jurassic shales (7.6) as compared to middle and upper Jurassic shales (6.1 and 6.0), whereas it increases to 9.3 in the Upper Jurassic to Lower Cretaceous shales of the Chia Gara Formation.

The Eu/Eu* ratios vary between the studied shale samples. The Average Eu/Eu* ratio in the Lower Jurassic shale is 0.91, while it corresponds to 2.25, and 2.14, respectively, in the shales of the Middle Jurassic and the Upper Jurassic to Lower Cretaceous periods.

Table 2. Rare earth and trace elements (ppm) and ratios analysed in the current study

Formation	Section /No.	Ce	Pr	Nd	Sm	Gd	Tb	Dy	Ho	Er	Tm	Yb	Lu	Hf	Zr
Sarki	w / s2	12.3	1.8	6.6	1.4	1.3	0.2	0.9	0.2	0.4	0.1	0.4	0.1	0.4	17.3
Sarki	w / s6	52.7	6.4	22.7	4	3.4	0.5	2.7	0.5	1.3	0.2	1.1	0.2	2.3	86.7
Sarki	w / s8	35.4	4.3	16	2.8	2.7	0.4	2.1	0.4	1.1	0.2	1	0.1	2.5	88.3
Sarki	w / s10	21.5	2.8	10.4	2.2	2.2	0.3	1.7	0.4	0.9	0.1	0.8	0.1	1.3	50.6
Sarki	w / s12	17.5	2.4	9.4	1.8	1.8	0.2	1.4	0.3	0.7	0.1	0.6	0.1	0.4	15.2
Sarki	w / s15	29.4	3.8	14.6	3.3	2.9	0.4	2.4	0.4	1	0.2	1	0.2	1.1	43.2
Sarki	w / s18	56.4	6.4	22.4	4.1	3.1	0.4	2.4	0.5	1.2	0.2	1.1	0.2	2.6	95.7
Sarki	w / s21	14.7	1.9	7.1	1.8	1.8	0.3	1.9	0.4	1.3	0.2	1.3	0.2	3.1	134.2
Sarki	w / s28	29.0	3.2	10	1.6	1.5	0.2	1.8	0.4	1.1	0.2	1.3	0.2	3.0	116.1
Sarki	w / s31	13.2	1.5	5	0.8	0.9	0.1	0.7	0.2	0.4	0.1	0.4	0.1	1.1	37.7
Sehkaniyan	w / s3	53.0	6.2	20.9	3.6	3.3	0.5	2.8	0.5	1.4	0.2	1.4	0.2	2.6	105.5
Sehkaniyan	w / s6	23.4	2.7	9.3	1.7	1.6	0.2	1.9	0.3	0.9	0.2	0.9	0.1	1.4	52.1
Sehkaniyan	w / s21	10.2	1.5	4.9	0.9	0.7	0.1	0.7	0.1	0.4	0.1	0.3	0.1	0.6	20.9
Sargelu	w / s6	2.0	0.6	2.2	0.4	0.6	0.1	0.5	0.1	0.4	0.1	0.3	0.1	0.1	4.8
Sargelu	w / s7	24.7	4.4	15.4	3.1	3.2	0.4	2.8	0.6	1.5	0.2	1.3	0.2	1.0	45.6
Sargelu	w / s8	37.9	4.6	16.6	3.8	3.3	0.5	3.1	0.6	1.5	0.2	1.5	0.2	2.4	84.7
Sargelu	w / s9	15.8	2	7	1.4	1.2	0.1	1.2	0.3	0.7	0.1	0.7	0.1	1.3	47.6
Sargelu	w / s10	12.2	2.2	8.5	1.6	1.9	0.2	1.8	0.4	1.1	0.2	0.9	0.1	0.6	26.4
Sargelu	w / s11	9.4	2.1	8.1	1.4	1.9	0.2	1.6	0.4	1.2	0.1	0.9	0.1	0.5	18.1
Sargelu	w / s13	13.8	3.4	13.1	2.5	3	0.4	2.5	0.6	1.6	0.2	1.3	0.2	0.6	22.8
Naokelekan	w / s1	13.6	3.8	15.1	2.9	3.2	0.5	3.3	0.8	2.2	0.3	1.7	0.3	0.9	32.4
Naokelekan	w / s4	11.3	3.4	12.6	2.2	2.8	0.4	3	0.7	2.1	0.3	1.8	0.3	0.6	22.3
Naokelekan	w / s8	35.8	4.3	16.6	3.5	3.2	0.5	2.9	0.5	1.6	0.2	1.5	0.2	1.9	79.5
Barsarin	w / s2	6.0	0.8	2.5	0.5	0.4	0.1	0.4	0.1	0.2	0.1	0.2	0.1	0.3	11.6
Barsarin	w / s5	4.1	0.5	1.9	0.4	0.3	0.1	0.3	0.1	0.1	0.1	0.2	0.1	0.2	7.2
Chia Gara	w / s1	58.4	6.3	23	4.1	3.3	0.5	3.1	0.6	1.8	0.3	1.7	0.2	3.4	122.8
Chia Gara	w / s3	2.8	0.4	1.1	0.3	0.1	0.1	0.2	0.1	0.1	0.1	0.1	0.1	0.2	8
Chia Gara	w / s4	55.5	6	21.2	4.2	3.1	0.4	3.2	0.6	1.6	0.2	1.6	0.3	3.2	122.1
Chia Gara	w / s6	26.0	3	10.1	2.1	1.6	0.2	1.3	0.3	0.7	0.1	0.6	0.1	1.2	41.9
Sarki	R / s0	31.0	3.6	13.1	2.5	2.1	0.3	2.2	0.4	1.1	0.2	1.1	0.2	2.1	79.5
Sarki	R / s2	23.3	2.8	10.5	2.3	2	0.2	1.6	0.3	0.9	0.1	0.8	0.1	1.7	70.1
Sarki	R / s5	31.8	3.5	13.2	2.6	2.4	0.3	1.9	0.3	1.1	0.2	1	0.1	2.0	76.1

Sarki	R / s8	45.8	5.3	19.3	3.6	3.1	0.4	2.3	0.4	1.1	0.2	1	0.1	2.1	75.3
Sarki	R / s10	23.2	2.8	10.3	1.9	1.8	0.3	1.8	0.4	1.1	0.2	1	0.1	3.9	139.8
Sarki	R / s11	12.8	1.8	6.4	1.2	1.3	0.1	1	0.2	0.5	0.1	0.5	0.1	0.7	28.5
Sarki	R / s13	14.7	1.7	6.6	1.3	1.2	0.2	1.4	0.3	0.8	0.1	0.7	0.1	1.6	61
Sarki	R / s15	25.9	3.4	11.8	2.1	2	0.4	1.9	0.4	1.1	0.2	0.9	0.1	1.6	57.8
Sarki	R / s17	13.8	2.4	10.4	2.3	2.8	0.4	2.6	0.5	1.5	0.2	1.1	0.2	2.6	86.4
Sarki	R / s20	14.1	1.8	5.7	1.4	1.2	0.2	1.3	0.3	0.9	0.2	0.8	0.1	1.5	49.7
Sarki	R / s25	18.5	1.9	5.4	0.8	0.9	0.2	1.4	0.4	1.1	0.2	1.5	0.2	5.1	183.6
Sarki	R / s28	46.8	6.2	21.2	4.2	3.7	0.6	3.6	0.8	2.2	0.3	1.7	0.3	3.3	118.8
Sehkaniyan	R / s2	32.3	3.6	12.4	2.3	2.4	0.4	2.4	0.6	1.7	0.3	1.5	0.2	2.4	90
Sehkaniyan	R / s4	16.1	1.5	4.5	1	1.2	0.2	1.6	0.4	1.5	0.3	1.7	0.3	3.0	104.2
Sehkaniyan	R / s11	7.8	0.8	2.3	0.5	0.4	0.1	0.9	0.2	0.7	0.1	0.8	0.1	2.6	83.5
Sehkaniyan	R / s13	23.7	2.8	9.9	1.9	1.9	0.3	1.8	0.4	1.1	0.2	1.1	0.2	1.6	59.5
Sehkaniyan	R / s14	6.4	0.8	2.8	0.7	0.8	0.2	1.2	0.3	0.9	0.1	1.1	0.2	3.1	109.6
Sehkaniyan	R / s17	13.7	1.7	5.7	1.2	1.7	0.3	2.3	0.6	1.8	0.3	2.1	0.3	5.1	183
Sargelu	R / s10	29.6	4	15.9	2.9	3.6	0.5	2.8	0.6	1.6	0.2	1.2	0.2	1.3	54.7
Sargelu	R / s11	20.7	2.6	8.9	1.7	1.6	0.2	1.5	0.3	1	0.1	0.9	0.1	1.8	59.5
Sargelu	R / s12	20.5	2.8	10.1	2	2.1	0.3	2	0.4	1.2	0.2	1.1	0.2	1.6	66.5
Sargelu	R / s13	6.8	1.5	6.3	1.2	1.4	0.2	1.5	0.3	0.9	0.1	0.7	0.1	0.4	14
Sargelu	R / s14	10.1	1.9	7.4	1.2	1.7	0.2	1.4	0.3	0.9	0.1	0.6	0.1	0.4	16.1
Naokelekan	R / s1	8.1	3.2	12.9	2.3	3.2	0.4	2.8	0.7	2.1	0.3	1.6	0.3	0.4	16.5
Chia Gara	R / s1	31.4	3.9	13.6	3	2.8	0.4	2.3	0.4	1.3	0.2	1.2	0.2	1.6	60.4
Chia Gara	R / s4	12.9	1.5	5.5	1	0.9	0.1	0.8	0.2	0.5	0.1	0.4	0.1	0.7	28.8
Chia Gara	R / s5	12.6	1.5	5.4	1.2	1.3	0.2	1	0.2	0.8	0.1	0.7	0.1	0.5	24.6
Chia Gara	R / s6	66.5	8.1	29.2	5.3	4.7	0.7	3.5	0.7	1.7	0.3	1.5	0.2	2.2	79.1

Table 2. Rare earth and trace elements (ppm) and ratios analysed in the current study, continued.

Formation	Section /No.	La	Eu	Th	U	LREE /HREE	Th/U	La/Th	Eu/Eu*
Sarki	w / s2	5.8	0.2	0.4	1.8	7.8	0.22	14.5	0.81
Sarki	w / s6	27.9	0.8	3.5	1.7	11.6	2.06	8.0	2.95
Sarki	w / s8	16.4	0.5	2.2	2.3	9.4	0.96	7.5	2.09
Sarki	w / s10	11.4	0.4	1.7	2.1	7.5	0.81	6.7	1.74
Sarki	w / s12	9	0.4	0.2	1.4	7.8	0.14	45.0	1.74
Sarki	w / s15	15.6	0.7	3.1	1.9	7.9	1.63	5.0	2.67
Sarki	w / s18	30.9	0.6	4.1	3	13.3	1.37	7.5	1.97
Sarki	w / s21	7.9	0.3	2.7	19	6.0	0.14	2.9	1.30
Sarki	w / s28	19.9	0.3	4.4	20.2	9.5	0.22	4.5	1.22
Sarki	w / s31	7.9	0.2	2.5	12.6	9.9	0.20	3.2	0.98
Sehkaniyan	w / s3	30	0.6	3.3	3.3	11.1	1.00	9.1	2.39

Sehkaniyan	w / s6	13	0.4	3.4	2.1	8.3	1.62	3.8	1.63
Sehkaniyan	w / s21	6.4	0.2	1.6	1.6	9.6	1.00	4.0	0.67
Sargelu	w / s6	4.7	0.1	0.2	11	4.5	0.02	23.5	0.65
Sargelu	w / s7	17.5	0.7	2	7.5	6.5	0.27	8.8	3.13
Sargelu	w / s8	18.3	0.8	5.7	31.4	7.5	0.18	3.2	3.01
Sargelu	w / s9	10.7	0.3	2	5.9	8.4	0.34	5.4	1.12
Sargelu	w / s10	12.8	0.4	1.6	21.1	5.7	0.08	8.0	2.06
Sargelu	w / s11	12.5	0.4	1.3	25	5.3	0.05	9.6	2.36
Sargelu	w / s13	18	0.7	1.8	39.1	5.2	0.05	10.0	3.64
Naokelekan	w / s1	20.6	0.8	2.2	32	4.6	0.07	9.4	3.83
Naokelekan	w / s4	21.7	0.6	1.7	40.7	4.5	0.04	12.8	3.31
Naokelekan	w / s8	17.3	0.8	4.7	28.3	7.4	0.17	3.7	3.17
Barsarin	w / s2	3.6	0.1	0.8	10.3	8.4	0.08	4.5	0.35
Barsarin	w / s5	2.5	0.1	0.4	5.8	7.3	0.07	6.3	0.33
Chia Gara	w / s1	30.3	0.9	9.9	34.9	10.7	0.28	3.1	3.14
Chia Gara	w / s3	1.7	0.1	0.3	5.7	7.1	0.05	5.7	0.14
Chia Gara	w / s4	29.3	0.9	8.5	40.1	10.6	0.21	3.4	2.88
Chia Gara	w / s6	13.4	0.4	3.7	13.1	11.2	0.28	3.6	1.32
Sarki	R / s0	16.5	0.5	2.9	2.2	8.8	1.32	5.7	1.82
Sarki	R / s2	11.7	0.4	3.1	4	8.5	0.78	3.8	1.51
Sarki	R / s5	16.6	0.5	2.8	1.8	9.3	1.56	5.9	2.00
Sarki	R / s8	22.6	0.7	2.9	2.2	11.3	1.32	7.8	2.62
Sarki	R / s10	10.2	0.4	2.9	3.8	7.3	0.76	3.5	1.64
Sarki	R / s11	6.4	0.2	0.2	3.2	7.6	0.06	32.0	0.94
Sarki	R / s13	8.8	0.3	2.2	4.7	6.9	0.47	4.0	1.20
Sarki	R / s15	14.3	0.4	3.7	3	8.3	1.23	3.9	1.65
Sarki	R / s17	9.2	0.5	1.8	19.2	4.1	0.09	5.1	2.64
Sarki	R / s20	9.5	0.3	2.4	8.9	6.5	0.27	4.0	1.12
Sarki	R / s25	10.3	0.2	10	41.8	6.3	0.24	1.0	0.98
Sarki	R / s28	27.7	0.8	4.6	6.1	8.1	0.75	6.0	3.06
Sehkaniyan	R / s2	19.9	0.5	6.2	5.4	7.5	1.15	3.2	2.26
Sehkaniyan	R / s4	11.2	0.2	3.8	6.2	4.8	0.61	2.9	1.04
Sehkaniyan	R / s11	4.9	0.1	4	1.5	5.0	2.67	1.2	0.35
Sehkaniyan	R / s13	13.4	0.3	2.5	4.8	7.4	0.52	5.4	1.30
Sehkaniyan	R / s14	3.2	0.1	2.9	5	2.9	0.58	1.1	0.50
Sehkaniyan	R / s17	9	0.3	15	5.4	3.4	2.78	0.6	1.84
Sargelu	R / s10	17.6	0.7	2.8	14.7	6.6	0.19	6.3	3.77
Sargelu	R / s11	14.2	0.4	3.3	13.9	6.4	0.24	4.3	1.63
Sargelu	R / s12	12.9	0.5	3	23.6	6.5	0.13	4.3	2.28
Sargelu	R / s13	9.2	0.3	0.9	13	4.8	0.07	10.2	1.52
Sargelu	R / s14	11.5	0.3	1.3	22.6	6.1	0.06	8.8	1.84

Naokelekan	R / s1	17.9	0.5	1.2	29.7	3.9	0.04	14.9	3.02
Chia Gara	R / s1	17	0.6	4.7	8.8	7.9	0.53	3.6	2.43
Chia Gara	R / s4	7.5	0.2	2	8.1	9.2	0.25	3.8	0.78
Chia Gara	R / s5	8	0.3	1.4	12.8	6.6	0.11	5.7	1.41
Chia Gara	R / s6	36.6	1	8.9	6.6	11	1.35	4.1	3.85

5. Discussion

In the present study, detailed mineralogical and geochemical analyses were conducted on the Lower Jurassic-Lower Cretaceous shale successions from the Warte and Ranya sections in northeastern Iraq. The results are employed to deduce the source areas and tectonic settings of the examined sediments utilizing both geochemical proxies and mineralogical composition of the studied shale units.

5.1 Proxies for source rock determination

A range of geochemical diagrams which combine various elements and element ratios (e.g., in form of major metal oxides) as well as individual elements (i.e., trace and rare earth elements) have been used to examine provenance in clastic sediments (e.g., Dai et al., 2016; Akkoca et al., 2019; Armstrong-Altrin et al., 2020). Some of these diagrams, e.g., those published by Floyd and Leveridge (1987) and Roser and Korsch (1988), have turned out to be most useful, and are still utilized as discriminant for the provenance signatures of sandstone and shale suites. According to Floyd and Leveridge (1987), the La/Th vs Hf plot can provide valuable information on the composition of the source areas, and provide a useful tool for bulk rock discrimination between different arc compositions and sources. Felsic composition-dominated arcs have low and uniform La/Th ratios (less than 5) and Hf contents of about 3-7 ppm. With the progressive unroofing of the arc and/or an incorporation of sedimentary basement rocks, the Hf content increases via the release of zircon (Floyd and Leveridge, 1987). The La/Th vs Hf plot from the current study (Figure 4) shows that most of the samples from the Sarki, Sehkanyian, Sargelu, Naokelekan, Barsarin and Chia Gara formations, and from both sections, plot in the felsic and intermediate source fields, with plenty of samples being plotted within the field of increasing old sediment components, especially for those from lower Jurassic sediments. Derivation from older rocks has been indicated by using Th/U ratio in the current study. Th/U ratios may be useful in interpreting sedimentary recycling histories and derivation

from older sedimentary rocks (McLennan et al., 1990; Asiedu et al., 2000). The Th/U ratio in most upper crustal rocks is typically about 3.5 to 4.0 (McLennan et al., 1993). An elevation in the Th/U ratio may have happened during sedimentation after oxidation of U to soluble U^{6+} and its loss due to forming other deposits. Thus, Th/U ratios may be useful in interpreting sedimentary recycling histories (McLennan et al., 1990). In sedimentary rocks, Th/U values higher than 4.0 may indicate intense weathering in source areas, or sediment recycling, meaning derivation from older sedimentary rocks (Asiedu et al., 2000). In general, the Th/U ratios in the current study (Table 2) are less than 4.0, with higher values in the Lower Jurassic shale samples.

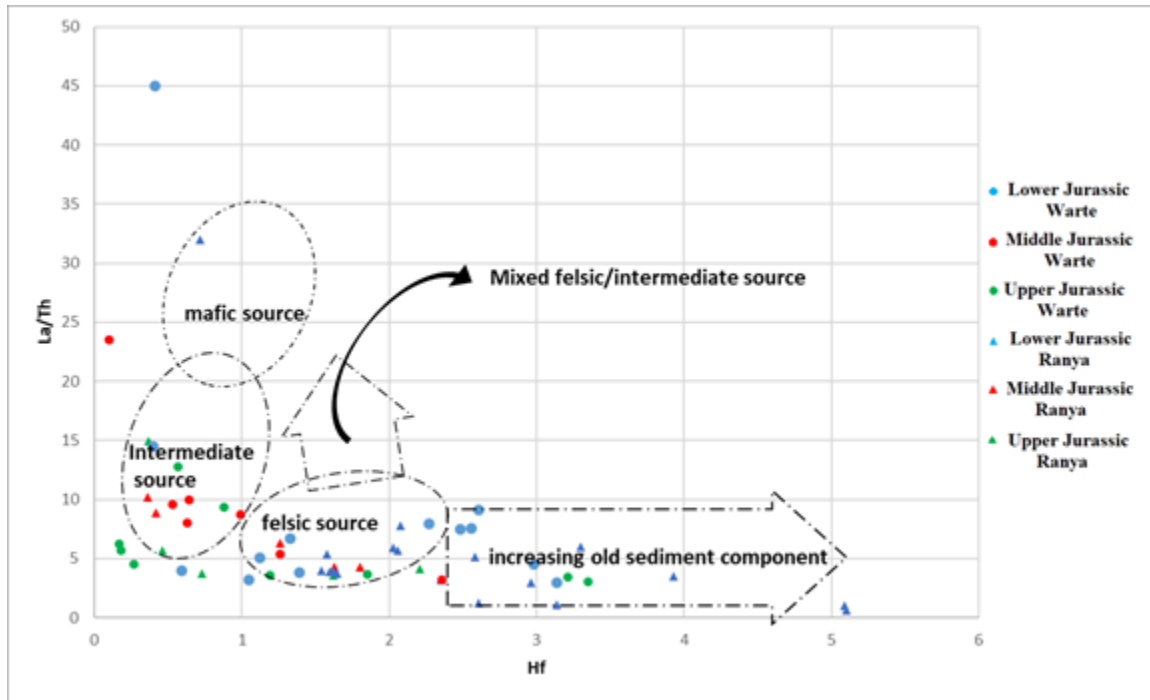


Figure 4. Discriminant Hf versus La/Th diagram for the shales of the Lower Jurassic-Lower Cretaceous formations (assignments according to Floyd and Leveridge, 1987).

In addition, the data obtained from the TiO_2 vs Zr plot (Figure 5) confirms that the shales of both sections (i.e., Warte and Ranya) have been sourced from felsic and intermediate igneous rocks (cf. McLennan et al. 1993).

The $\text{Al}_2\text{O}_3/\text{TiO}_2$ ratio of the Warte and Ranya shales has also been used to assume the structure of the parental materials (Hayashi et al., 1997). The $\text{Al}_2\text{O}_3/\text{TiO}_2$ ratio values for the Warte and Ranya shales range from 12.68 to 28.98 with a mean value of 18.22, thus reflecting intermediate to felsic source rock composition for both studied areas (cf. Fathy et al., 2017). Derivation from felsic and intermediate igneous sources may indicate a significant contribution of detritus from continental settings or rifted continental margins (Vdačný et al., 2013).

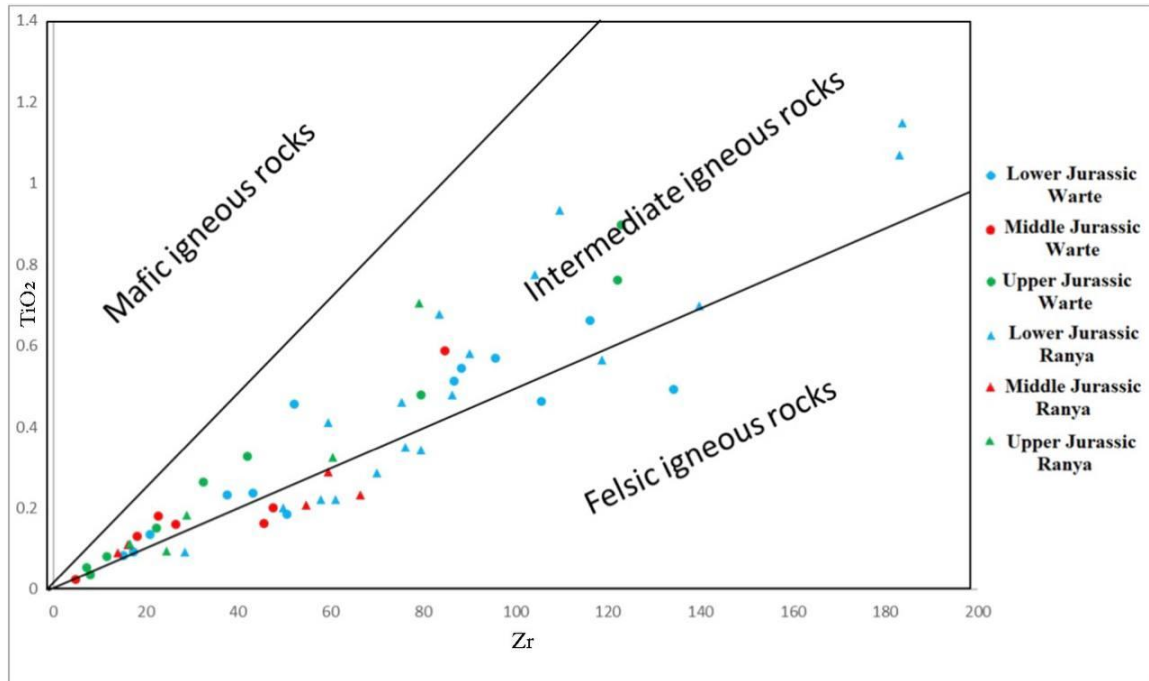


Figure 5. TiO_2 vs Zr diagram of the shales of the Lower Jurassic-Lower Cretaceous formations (McLennan et al., 1993) that discriminates the source rock types.

Based on the type of the igneous rocks using TiO_2 vs Al_2O_3 diagram (Figure 6), the studied samples lie mainly in the granite and basalt (felsic igneous rock) field with very few samples lying in the basalt and granite field.

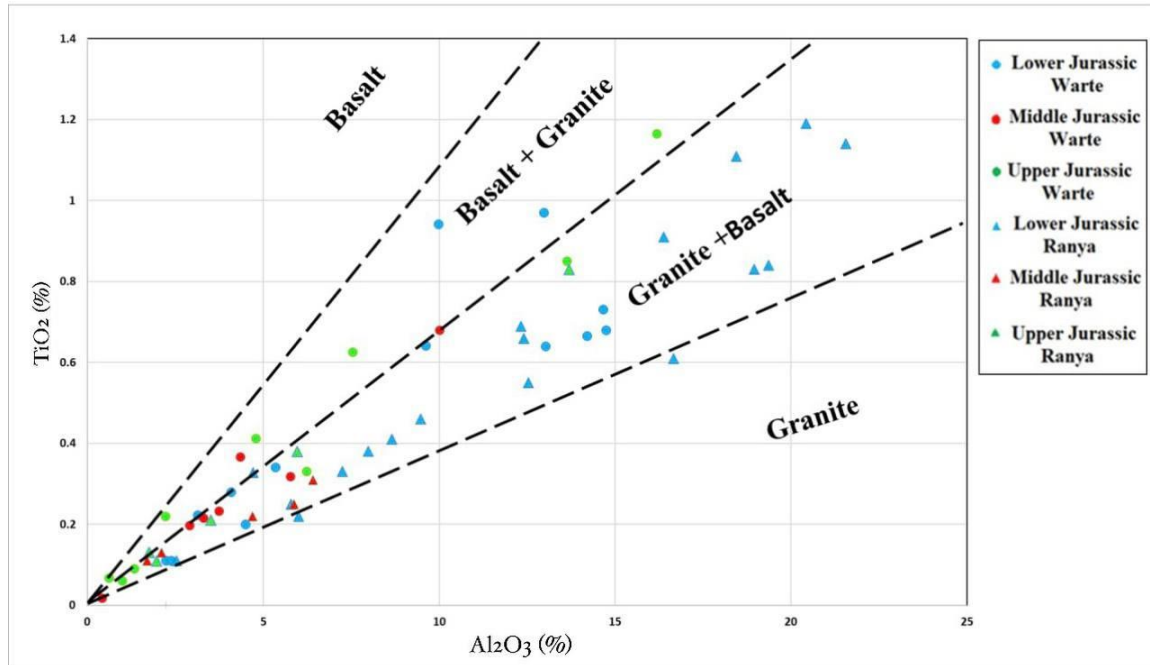


Figure 6. Scatter plot of Al_2O_3 vs TiO_2 , for inferring rock types used in provenance discrimination of the shales from the Lower Jurassic-Lower Cretaceous formations (after Amajor, 1987)

The chondrite-normalized REE patterns for the Lower Jurassic-Lower Cretaceous shales are shown in Figure 7. In general, the REE contents in the shales are lower than in the Post Archean Australian Shale (PAAS) and North American Shale Composite (NASC), (Table 2 and Figure 7). The studied shales are more enriched in Light Rare Earth Elements (LREE, La, Ce, Pr, Nd, Sm and Eu) than Heavy Rare Earth Elements (HREE, Gd, Tb, Dy, Ho, Er, Tm, Yb and Lu) and show almost uniform patterns similar to PAAS and NASC (Figure 7). The Chia Gara shales are more enriched in the LREE and the Naokelekan shales are more enriched in HREE as compared to the other studied shales.

Moreover, the ratios of LREE/HREE have been utilized to infer sources of sedimentary rocks (Taylor and McLennan, 1985). Generally, the felsic rocks contain higher LREE/HREE ratios, whereas the intermediate and mafic rocks contain lower LREE/HREE ratios. In the current study, the ratio of LREE/HREE (average of 7.6) in the shales from the Lower Jurassic Sarki and Sehkanian formations is higher than the average ratio in both Sargelu (Middle Jurassic)

and Naokelekan and Barsarin formations (Upper Jurassic) which have an average of 6.0. This may reflect the higher contribution of felsic than intermediate igneous rocks to the Lower Jurassic sediments.

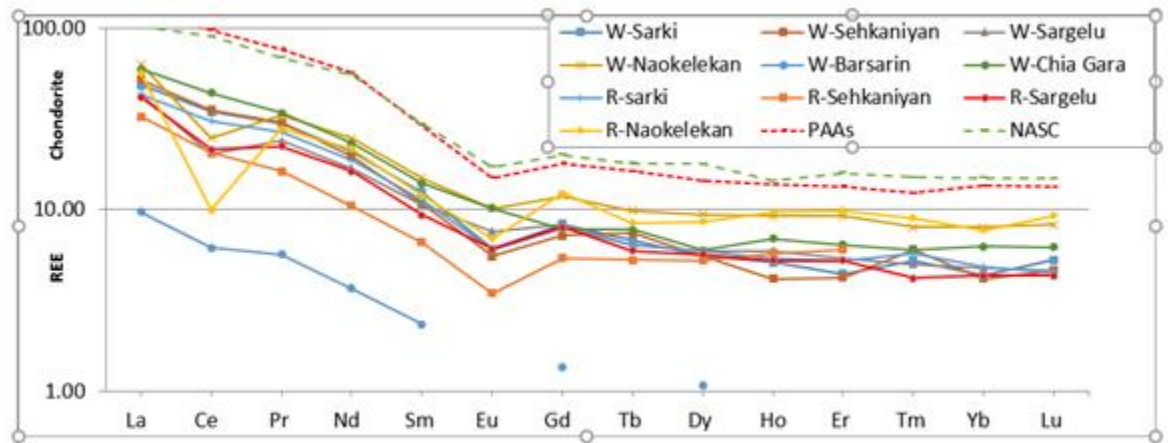


Figure 7. Average chondrite-normalized rare earth element (REE) patterns for the shales from the Lower Jurassic-Lower Cretaceous formations, compared with the PAAS and NASC (Taylor and McLennan, 1985).

Furthermore, the Eu/Eu^* ratio values of the Warte and Ranya shales have been used by many authors to suggest their provenance area (e.g., Tobia et al., 2019; Cai et al., 2022). The Eu/Eu^* ratio of the Warte and Ranya shales shows generally low values (average of 1.89) (Table 2). This would point to their derivation from a provenance dominated by felsic rocks (cf. Tobia et al., 2019; Cai et al., 2022).

The presence of detrital quartz and feldspars in addition to illite and kaolinite clay minerals as revealed by the mineralogical XRD and supported by SEM studies may also suggest the contribution from felsic (acidic) igneous sources. Quartz, feldspar and mica are the common minerals in the felsic rocks, kaolinite is commonly formed under acidic conditions through complex weathering processes or hydrothermal changes in feldspar and other aluminosilicates, while illite is one of the most dominant clay minerals in fine muddy rocks through silicate

weathering (mainly feldspar) during its replacement with other clay minerals due to the dissolution (degradation) of muscovite (Deer et al., 1992).

5.2 Proxies for tectonic setting discrimination

The tectonic setting is largely influenced by sedimentation, diagenesis and composition of sediments (Pettijohn et al., 1972; Bhatia, 1983). The clastic sedimentary rocks from different tectonic settings have a different characteristic of detrital components and chemistry (Dickinson and Suczek, 1979; Dickinson et al., 1983; Bhatia, 1983; Roser and Korsch, 1986; McLennan et al., 1990). Some information on the tectonic setting and the source of sediments can be attained from the elemental composition, including Si, Al, Ti, Fe, Mn, K, Mg, Ca, Na and P, as well as their plot design (Roser and Korsch, 1986; Rollinson, 1993).

Additionally, Verma and Armstrong-Altrin (2013) proposed two discriminant diagrams based on major elements for the tectonic discrimination of siliciclastic sediments, which are successfully used in many studies (e.g., Armstrong-Altrin et al., 2015; Tawfik et al., 2015). According to the differences in SiO₂ values, the diagrams can be divided into a low-silica type (35–63%) and a high-silica type (63–95%). Three different tectonic settings can be classified based on these diagrams including island arc, rift and collisional settings.

In the present study, the SiO₂ contents of the studied shale samples are low being generally below 50% (Table 1). Thus, the shales can be classified as low-silica clastic sediments. The results obtained in this study show that the shale samples from the Warte and Ranya successions are clearly located within the collision and rift tectonic fields (Figure 8).

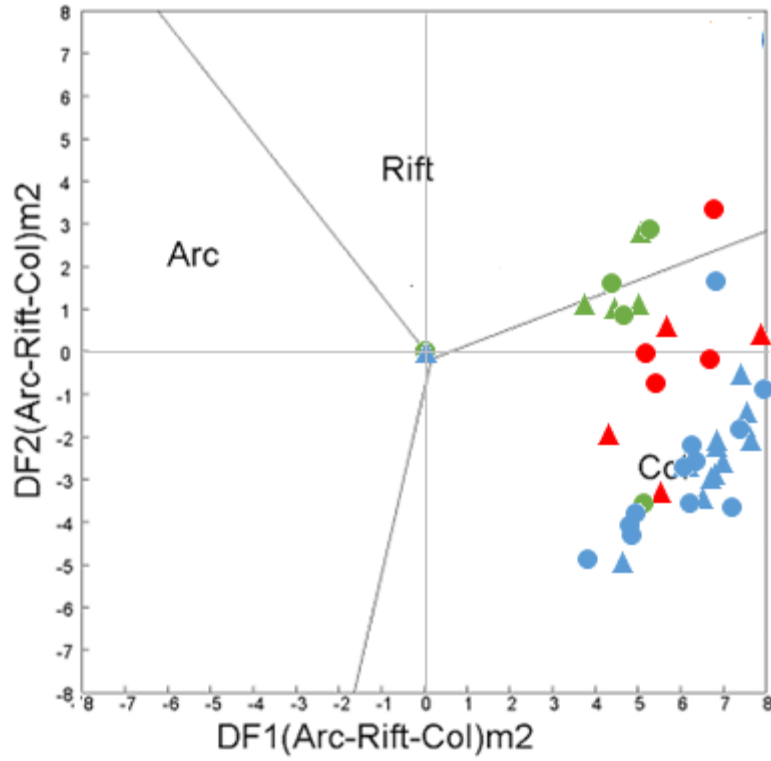


Figure 8. Discriminant function (DF) multidimensional diagram for low-silica clastic sediments (fields after Verma and Armstrong-Altrin, 2013). The subscript m2 in DF1 and DF2 represents the low-silica diagram based on log-ratios of major elements. Discriminant function equations are $DF1(\text{Arc-Rift-Col}) m2 = (0.608 \times \ln (\text{TiO}_2/\text{SiO}_2) \text{ adj}) + (-1.854 \times \ln (\text{Al}_2\text{O}_3/\text{SiO}_2) \text{ adj}) + (0.299 \times \ln (\text{Fe}_2\text{O}_3 \text{ t}/\text{SiO}_2) \text{ adj}) + (-0.550 \times \ln (\text{MnO}/\text{SiO}_2) \text{ adj}) + (0.120 \times \ln (\text{MgO}/\text{SiO}_2) \text{ adj}) + (0.194 \times \ln (\text{CaO}/\text{SiO}_2) \text{ adj}) + (-1.510 \times \ln (\text{Na}_2\text{O} / \text{SiO}_2) \text{ adj}) + (1.941 \times \ln (\text{K}_2\text{O}/\text{SiO}_2) \text{ adj}) + (0.003 \times \ln (\text{P}_2\text{O}_5/\text{SiO}_2) \text{ adj}) - 0.294$. $DF2 (\text{Arc-Rift- Col}) m2 = (-0.554 \times \ln (\text{TiO}_2/\text{SiO}_2) \text{ adj}) + (-0.995 \times \ln (\text{Al}_2\text{O}_3/\text{SiO}_2) \text{ adj}) + (1.765 \times \ln (\text{Fe}_2\text{O}_3\text{t}/\text{SiO}_2) \text{ adj}) + (-1.391 \times \ln (\text{MnO}/\text{SiO}_2) \text{ adj}) + (-1.034 \times \ln (\text{MgO}/\text{SiO}_2) \text{ adj}) + (0.225 \times \ln (\text{CaO}/\text{SiO}_2) \text{ adj}) + (0.713 \times \ln (\text{Na}_2\text{O}/\text{SiO}_2) \text{ adj}) + (0.330 \times \ln (\text{K}_2\text{O}/\text{SiO}_2) \text{ adj}) + (0.637 \times \ln (\text{P}_2\text{O}_5/ \text{SiO}_2) \text{ adj}) - 3.631$.

A further discrimination diagram, which was created by Roser and Korsch (1986), has additionally been used to conclude on the tectonic setting of the shale samples investigated in

this study. The results suggest that the samples were generally derived from the passive margin with a few samples derived from the active continental margin (Figure 9).

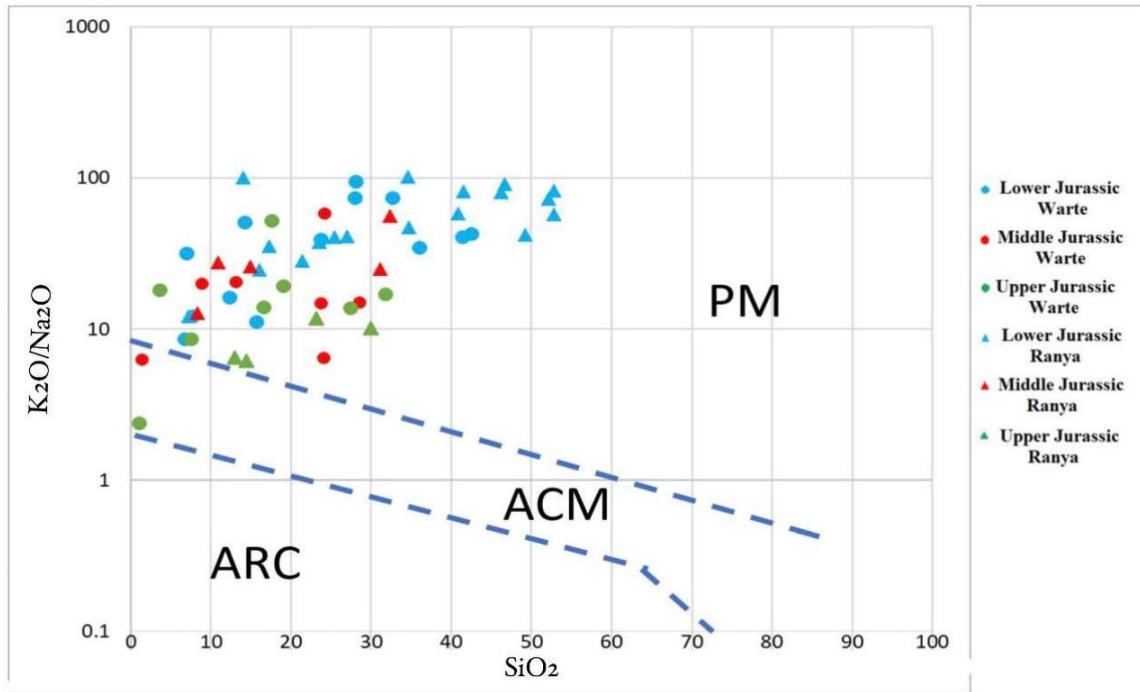


Figure 9. Tectonic discrimination diagram of Roser and Korsch (1986) for the shales from the Lower Jurassic-Lower Cretaceous formations. ARC, oceanic island arc margin, ACM, active continental margin; PM, passive margin.

Additionally, a ternary plot of the trace and rare earth elements (La-Th-Sc), introduced by Bhatia and Crook (1986), has been generated for the shale samples of the Warte and Ranya sections. The results indicate that most of the samples were deposited in a passive margin and continental island arc with some being deposited within the oceanic island arc (Figure 10).

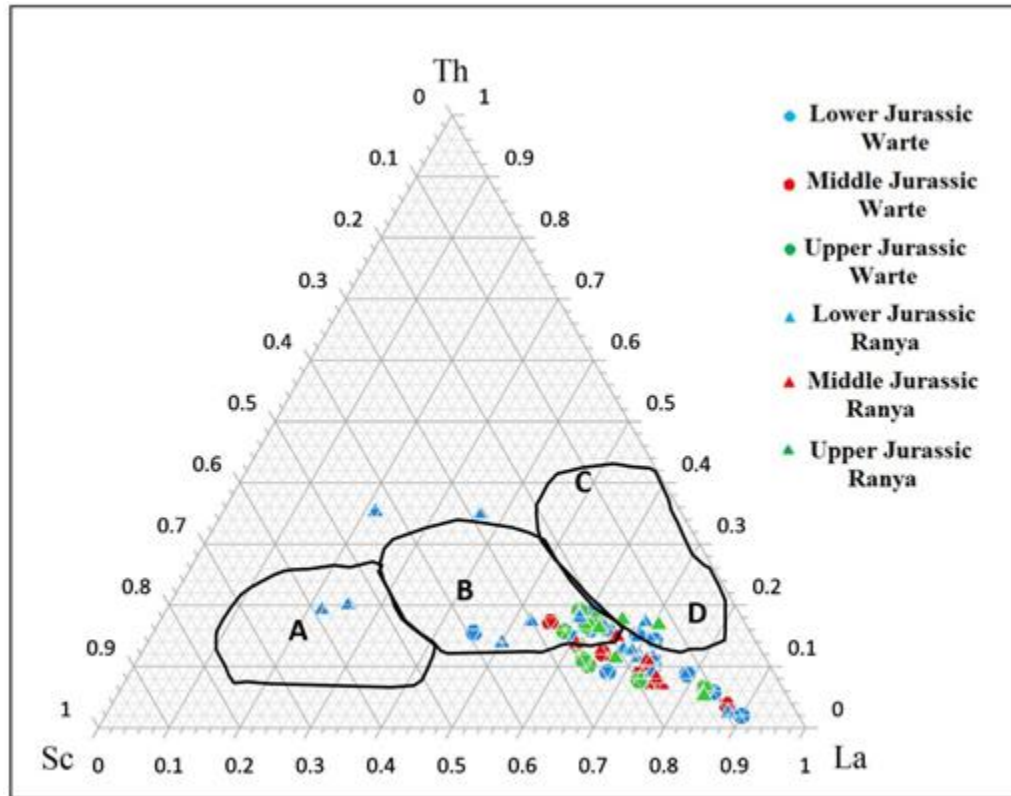


Figure 10. Discrimination diagram of Bhatia and Crook (1986) using Th-Sc-La elements illustrates the tectonic setting fields, **A.** Oceanic Island Arc; **B.** Continental Island Arc; **C.** Passive Margin.

The proposed passive margin, as noted above, being the tectonic province of the Warte and Ranya shale successions, correlates well with the geology of the region of Iraqi Kurdistan, which was exposed to tectonic activity (see also Omar et al., 2020, 2021, 2023). However, the shale samples plotted within the rift field are suggestive of a passive margin. This difference in clastic provenance might be interpreted as being derived from the adjacent Mesopotamian Basin. The Mesopotamian Basin is considered to be a characteristic example for the passive margin setting (Jassim and Goff, 2006).

According to Sharland et al. (2001), the time span from Early Jurassic to Early Cretaceous was, tectonically, critical. During this time the tectonism of the Arabian Plate was converted from

extension because of rifting to compression due to collision and subduction of the Neo-Tethyes oceanic crust beneath the Iranian Plate. This subduction occurred during the Late Jurassic and Early Cretaceous. Accordingly, the formations Sarki, Sehkanyian and Sargelu were deposited in an extension environment, whereas Naokelekan, Barsarin and Chia Gara formations were formed during a compression state. The geochemical and mineralogical analyses showed that all of these formations revealed felsic and intermediate igneous rocks, which indicate quiet passive margin deposits. The dominance of felsic and intermediate origin suggests derivation of the studied shales from a provenance dominated by felsic igneous rocks from the Zagros ophiolites and related igneous rocks in northeastern Iraq (Buday and Jassim, 1987).

Conclusions

The Early Jurassic-Early Cretaceous-age shale successions of northeastern Iraq were deposited in the Warte and Ranya areas within the Zagros Basin.

A combination of extensive mineralogical as well as geochemical analyses of the Early Jurassic-Early Cretaceous shales was undertaken in order to elucidate their provenance history and tectonic setting. The shales of the Early Jurassic-Early Cretaceous-age Warte and Ranya sections are dominated by calcite, dolomite and quartz with traces of feldspar, illite/mica, kaolinite and chlorite. The occurrence of detrital quartz and feldspar with the clay minerals illite and kaolinite indicates their felsic (acidic) igneous origin. The source area, from which these felsic rocks were derived, is suggested to be the Zagros ophiolites and related igneous rocks in northeastern Iraq. The provenance origin of the Early Jurassic-Early Cretaceous-age shale successions has been interpreted as being dominant by felsic and intermediate igneous rocks, whilst a passive margin setting was considered to be the tectonic setting for the Early Jurassic-Early Cretaceous-age shales. This interpretation correlates well with the geological history of the area of northeastern Iraq.

Chapter 7

Chapter 7

Conclusions

This dissertation comprises seven chapters and presents the results of a variety of studies carried out on the Early Jurassic-Early Cretaceous-age formations which crop out in three different areas (Banik, Warte and Ranya) of northern Iraq. The formations include, the Sarki, Sehkanian, Sargelu, Naokelekan, Barsarin and Chia Gara formations. The studies involved the analysis of the sedimentary successions in detail, with the main focus being on the geochemistry and mineralogy of the main lithological components of the studied formations including limestones, dolomitic limestones, dolomites, shales and solid bitumen. The results of these analyses were used as proxies to examine the paleoenvironmental evolution of the region, in particular, the paleoclimate, paleosalinity and paleoredox conditions dominant throughout the period of deposition of the Jurassic successions in northern Iraq.

An initial introductory chapter (Chapter 1) outlines the importance of the studied Jurassic formations and presents the aim of the study. It also describes the general geology of northern Iraq. This is followed by Chapter 2, which examines, in detail, the calcareous nannofossils of the Early Jurassic-Early Cretaceous-age Warte section. Although the preservation of the calcareous nannoplankton is considered to be moderate to poor in the sediments, the recovered nannofossil assemblages were successfully recorded from the Middle Jurassic Sargelu, Upper Jurassic Naokelekan, Barsarin and Chia Gara (Upper Jurassic-Lower Cretaceous) formations, including *Watznaueria barnesiae*, *W. fossacincta*, *W. britannica*, *W. manivitiae* and *Cyclagelosphaera margerelii*, whilst the Lower Jurassic Sarki and Sehkanian formations were found to be barren. A Bajocian-Callovian age was suggested for the Sargelu Formation based on the first occurrence of *C. margerelii*, *W. britannica*, *W. fossacincta*, *W. manivitiae*, *W. barnesiae* and *W. ovata*. The obtained data in Chapter 3 comprise elemental ratios of major and trace elements (Sr, Ca, Al, Sr/Ba, Rb/Sr and Sr/Cu) as well as oxygen isotopic geochemistry of the both Early Jurassic-Early Cretaceous-age Warte and Ranya sections. Analysis of these paleoclimate and paleosalinity proxies, suggested that hot and arid conditions were dominant during the time of deposition of the Early Jurassic-Early Cretaceous-age Warte and Ranya sections. During the Late Jurassic-Early Cretaceous time, the climate changed and

increasing amounts of kaolinite were observed reflecting more humid conditions during this period in northern Iraq.

Petrographic and microfacies analyses of the carbonate units indicated that the Warte and Ranya sections were deposited within tidal flats (supratidal) and in restricted lagoons, as well as in shallow marine and bathyal settings during the Early Jurassic-Early Cretaceous time. Paleoredox proxies (U/Th, V/Cr, Ni/Co, V/Sc and V/(V+Ni)) revealed that conditions during deposition of the Warte and Ranya sediments were likely anoxic with periods of low oxygen. This difference between paleoredox and depositional paleoenvironments is likely related to variations in tectonic settings within the Zagros Basin which extends across the region of northern Iraq, with the formation of semi-enclosed subbasins where water circulation was restricted.

In Chapter 4, the carbonates of the Middle and Upper Jurassic succession of the Banik section from northernmost Iraq were subjected to several analyses including sedimentological, petrographical and microfacies analyses, whilst geochemical analyses were carried out on the shales. The Banik section is dominated by dolomites, limestones, mudstones and rare cherts. Deposition of the Sargelu and Naokelekan formations is interpreted to have occurred in shallow marine and restricted shallow lagoon environments, respectively.

Paleoredox indicators suggested that the sedimentary successions, which are characterized by the deposition of the Middle-Late Jurassic-age Sargelu and Naokelekan formations were accumulated under anoxic conditions. The ongoing tectonic activity might have resulted in the formation of barred subbasins, where the water circulation is topographically restricted. Taken together, the evaporation conditions suggested that permanently anoxic conditions were established within those semi-enclosed subbasins.

In Chapter 5, solid bitumens from the Middle to Upper Jurassic Sargelu and Naokelekan formations in the Banik section from northernmost Iraq were identified and analyzed. Accumulation of solid bitumens in the host shale rocks is interpreted to have occurred as a result of oil migration from other source rocks within the same formations. The results suggest that the source rocks reached a peak for petroleum generation during the Jurassic time. Moreover, due to the ongoing tectonic activity in the region of northernmost Iraq, the occurrence of fractures and faults provided effective pathways for oil migration through the

porous and permeable reservoir rocks (i.e., host shales) in the Banik section. Furthermore, the results from the carbon and oxygen isotopic geochemistry and the paleoredox proxies suggest that the host shales and solid bitumen sources were deposited in a shallow-marine setting and under anoxic conditions.

Chapter 6 combines mineralogical and geochemical analyses of the Early Jurassic-Early Cretaceous-age shale successions in order to elucidate their provenance history and tectonic setting. The occurrence of detrital quartz and feldspar together with the clay minerals illite and kaolinite indicated the influence of felsic (acidic) igneous origins, whilst a passive margin setting was interpreted to be the tectonic setting for the Early Jurassic-Early Cretaceous shales. This interpretation correlates well with the geological history of the area of northern Iraq.

In conclusion, the detailed examination of the paleoenvironmental conditions in the successions of northern Iraq provided a range of novel findings and contributions important for future studies on hydrocarbon explorations of this highly promising Jurassic system. These findings included the elucidation of the paleoclimatic (arid vs humid) conditions and their effect on the internal reservoir architecture of the carbonate rocks. Paleoclimate is an important control on a variety of aspects of carbonate reservoir development, including cyclic variations of the lithological, sedimentological and geochemical properties, and by extension, the depositional patterns (both lateral and vertical) within the sedimentary successions (Ahr, 2008; Samani et al., 2023). In addition, paleoclimate is also an important factor controlling the diagenetic regime of such reservoirs (Worden et al., 2000; Ahr, 2008).

The levels of oxygenation within a depositional setting (i.e., paleoredox) as well as the salinity levels within marine environments (i.e., paleosalinity) are both important controls on the preservation and enrichment of organic material within sedimentary successions (Lu et al., 2013; Sajid et al., 2020). Thus, the quality of source rocks within a hydrocarbon play are also greatly influenced by these two factors (e.g., paleoredox and paleosalinity). Increasing paleosalinity leads to greater reducibility and an increase in the amount of organic matter accumulation (Lu et al., 2013). Lower oxygen conditions (e.g., anoxic/dysoxic) are more favorable for organic matter preservation.

Thus, in summary, the examination of the paleoenvironmental proxies has provided important information with regard to the role that hydrocarbons play in the region of northern Iraq -

elucidating both the depositional settings (i.e., reservoir rocks), as well as the conditions active during deposition (i.e., source rocks). This work represents an important contribution to our knowledge of the geology of northern Iraq, also providing a detailed understanding of the role that hydrocarbons play in the area.

References

- Abdula, R. (2010). Petroleum source rock analysis of the Jurassic Sargelu Formation, northern Iraq. – Master's thesis, Colorado School of Mines: pp. 125. https://www.researchgate.net/publication/280720336_Petroleum_source_rock_analysis_of_the_Jurassic_Sargelu_Formation_northern_Iraq.
- Abdula, R. (2016). Organic geochemical assessment of Jurassic potential source rock from zab-1 well, Iraqi Kurdistan. *Iraqi Bulletin of Geology and Mining*, 12, 53–64.
- Abdula, R. (2017). Source rock assessment of Naokelekan formation in Iraqi Kurdistan. *Journal of Zankoi Sulaimani Part-A-(Pure and Applied Sciences)*, 19, 103–124.
- Abdula, R.A. (2016). Stratigraphy and lithology of Naokelekan Formation in Iraqi Kurdistan Review. *Int. J. Eng. Sci.*, 5, 7–17.
- Abdula, R.A., Balaky, S.M., Nourmohamadi, M.S., Piroui, M. (2015). Microfacies analysis and depositional environment of the Sargelu formation (middle Jurassic) from Kurdistan region, northern Iraq. *Donnish Journal of Geology and Mining Research*, 1, 1–26.
- Abdula, R.A., Kolo, K., Damouliauou, M., Raftopoulou, V., Khanaqa, P., Kalaitzidis, S. (2020). Rock-Eval analysis and organic petrographical characterization of the Upper Jurassic Naokelekan Formation, northern Mesopotamian Basin, Kurdistan Region-Iraq. *BGS* 187–203.
- Afrozi, M., Fralick, P.W., Patry, L., Sans-Jofre, P., Lalonde, S.V. (2021). Carbon and Oxygen Isotope Chemostratigraphy of a Mesoarchean Carbonate Platform (Red Lake, Canada). *Goldschmidt Abstract*. pp. 1.
- Ahlbrandt, T.S., Pollastro, R.M., Klett, T.R., Schenk, C.J., Lindquist, S.J., Fox, J.E. (2000). Region 2 Assessment Summary—Middle East and North Africa. In *USGS World Petroleum Assessment 2000—Description and Results*, Chapter R2: DDS-60, pp. 46.
- Ahr, W.M. (2008). *Geology of carbonate reservoirs: The identification, description, and characterization of hydrocarbon reservoirs in carbonate rocks*, John Wiley & Sons, Inc. Texas, p 277.

- Akkoca, D.B., Eriş, K.K., Çağatay, M.N. and Tekin, DB. (2019). The mineralogical and geochemical composition of Holocene sediments from Lake Hazar, Elazığ, Eastern Turkey: implications for weathering, paleoclimate, redox conditions, provenance, and tectonic setting. *Turkish J. Earth Sci.* 28, 760–785.
- Al-Ahmed, A.A.N. (2006). Organic geochemistry, palynofacies and hydrocarbon potential of Sargelu Formation (Middle Jurassic) northern Iraq. PhD thesis, University of Baghdad.
- Al-Ameri, T.K., Najaf, A.A., Al-Khafaji, A.S., Zumberge, J. & Pitman, J. (2013). Hydrocarbon potential of the Sargelu Formation, North Iraq. – *Arabian Journal of Geosciences*, 7, 987–1000.
- Al-Ameri, T.K., Zumberge, J. (2012). Middle and Upper Jurassic hydrocarbon potential of the Zagross Fold Belt, North Iraq. *Marine and Petroleum Geology*, 36, 13–34.
- Algeo, T.J., Maynard, J.B. (2004). Trace-element behavior and redox facies in core shales of Upper Pennsylvanian Kansas-type cyclothems. *Chem. Geol.* 206, 289–318.
- Al-Juboury, A.I., Hussain, S.H., Al-Lhaebi, S.H. (2021). Geochemistry and mineralogy of the Silurian Akkas Formation, Iraqi western desert: implications for palaeoweathering, provenance and tectonic setting, *Arabian Journal of Geosciences*, 14, 760.
- Al-Juboury, A.I., McCann, T. (2013). Petrological and geochemical interpretation of Triassic-Jurassic boundary sections from north Iraq. *Geological Journal*, 50, 157–172.
- Al-Lhaebi, S.F., Al-Badrani, O.A., Al-Juboury, A.I., Mahanipour, A. (2020). Paleoclimatic insights on the Cenomanian-Turonian Oceanic Anoxic Event (OAE2) from northern Iraq based on calcareous nannofossils and geochemical data. *Iraqi Geol. J.*, 53, 68–86.
- Al-Miamary, F.A., Al-Badrani, O.A., Al-Juboury, A.I. (2020). Calcareous nannofossils and chemostratigraphy of the Early Aptian Oceanic Anoxic Event 1a from northern Iraq. *Bull. Iraq Nat. Hist. Mus.* 16, 363–379.
- Alsharhan, A.S., Nairn, A.E.M. (1997). *Sedimentary Basins and Petroleum Geology of the Middle East*. Elsevier, Amsterdam, pp. 843.

Al-Zubaidi, A.A., Al-Zebari, A.Y. (1998). Prospects for production and marketing of Iraq's heavy oil: Ministry of Oil. State Oil Marketing, Baghdad, Iraq, 221, pp. 10.

Amajor, L.C. (1987). Major and trace elements geochemistry of Albian and Turonian shales from the Southern Benue trough. *Nigeria Jour. African Earth Sci.* 6, 633–641.

Aqrawi, A.A.M. (1998). Paleozoic stratigraphy and petroleum systems of the western and southwestern Deserts of Iraq. *GeoArabia*, 3, 229–247.

Aqrawi, A.A.M., Badics, B. (2015). Geochemical characterisation, volumetric assessment and shale-oil/gas potential of the Middle Jurassic-Lower Cretaceous source rocks of NE Arabian Plate. *GeoArabia* 20, 99–140.

Aqrawi, A.A.M., Horbury, A.D., Goff, J.C., Sadooni, F.N. (2010). *The Petroleum Geology of Iraq*. Scientific Press, pp. 424.

Armstrong-Altrin, J.S., Nagarajan, R., Balaram, V., Natalhy-Pineda, O. (2015). Petrography and geochemistry of sands from the Chachalacas and Veracruz beach areas, western Gulf of Mexico, Mexico: constraints on provenance and tectonic setting. *J. South Am. Earth Sci.* 64, 199–216.

Armstrong-Altrin, J.S., Nagarajan, R., Madhavaraju, J., Rosalez-Hoz, L., Lee, Y.I., Balaram, V., Cruz-Martinez, A., Avila-Ramirez, G. (2013). Geochemistry of the Jurassic and upper Cretaceous shales from the Molango Region, Hidalgo, Eastern Mexico: implications of source-area weathering, provenance, and tectonic setting. *C. R. Geosci.* 345, 185–202.

Armstrong-Altrin, J.S., Ramos-Vázquez, M.A., Hermenegildo-Ruiz, N.Y., Madhavaraju, J. (2021). Microtexture and U–Pb geochronology of detrital zircon grains in the Chachalacas beach, Veracruz State, Gulf of Mexico. *Geological J.* 56, 2418–2438.

Asiedu, D.K., Suzukis, S.I., Nogami, K., Shibata T. (2000). Geochemistry of lower Cretaceous sediments, inner zone of Southwest Japan: constraints on provenance and tectonic environment. *Geochemical J.* 34, 155–173.

Balaky, S.M.H. (2004). *Stratigraphy and Sedimentology of Sargelu Formation (Middle Jurassic) in Selected Sections in Erbil and Duhok Governorates–Iraqi Kurdistan*. MSc thesis, Salahaddin University-Erbil.

- Bartolini, A., Pittet, B., Mattioli, E., Hanziker, J.C. (2003). Shallow-platform paleoenvironmental conditions recorded in deep-shelf sediments: C and O stable isotopes in Upper Jurassic sections of southern Germany (Oxfordian-Kimmeridgian). *Sediment. Geol.* 160, 107–130.
- Bellen, van R.C., Dunnington, H.V., Wetzel, R., Morton, D.M. (1959). *Asie, Fascicule 10a Iraq*; Lexique Stratigraphic International: Paris, France, Volume 3, 333 pp.
- Berberian, M., King, G. (1981). Towards a paleogeography and tectonic evolution of Iran, *Canadian journal of earth sciences.* 18, 210–265.
- Beydoun, Z.R. (1991). Arabian plate hydrocarbon geology and potential. A plate tectonic approach. *American Association of Petroleum Geologists Studies in Geology*, 33, 1–77.
- Beydoun, Z.R., Clarke, M.W.H., Stoneley, R. (1992). Petroleum in the Zagros Basin-a Late Tertiary foreland basin overprinted onto the outer edge of a vast hydrocarbon-rich Paleozoic-Mesozoic passive-margin shelf. In: Mac Queen, R.W., Leckie, D.A. (Eds.), *Foreland Basins and Fold Belts*, vol. 55. AAPG Memoir, Tulsa, OK, USA, pp. 309–339.
- Bhatia, M.R. (1983). Plate tectonics and geochemical composition of sandstones. *J. Geol.* 91, 611–627.
- Bhatia, M.R., Crook, K.A. (1986). Trace element characteristics of gray wackes and tectonic setting discrimination of sedimentary basins. *Contrib Mineralogy Petrology* 92, 181–193.
- Buday, T., Jassim, S.Z. (1987). The Regional Geology of Iraq. Tectonism, magmatism and metamorphism. *Geological Society Iraq*, 2, pp. 275.
- Cai, G., Xu, Y., Zhong, H., Cheng, Y. (2022). Terrigenous and volcanogenic contribution to the deep basin of the South China Sea: Evidence from trace elements and Sr-Nd isotopes. *Marine Geology*, 448, 106811.
- Calvert, S.E., Pedersen, T.F. (1993). Geochemistry of recent oxic and anoxic sediments: implications for the geological record. *Mar. Geol.* 113, 67–88.
- Canet, C., Alfonso, P., Melgarejo, J.C., Belyatsky, B.V. (2004). Geochemical evidences of sedimentary-exhalative origin of the shale-hosted PGEAg-Au-Zn-Cu occurrences of the

Prades Mountains (Catalonia, Spain): trace-element abundances and Sm-Nd isotopes. *J. Geochem. Explor.* 82, 17–33.

Cao, J., Wu, M., Chen, Y., Hu, K., Bian, L.Z., Wang, L.G., Zhang, Y. (2012). Trace and rare earth element geochemistry of Jurassic mudstones in the northern Qaidam Basin, northwest China. *Geochemistry* 72, 245–252.

Chamley, H. (1989). *Clay Sedimentology*. Springer Berlin, Heidelberg, pp. 623.

Condie, C.K., Noll, P.D., Jr., Conway, C.M. (1992). Geochemical and detrital mode evidence for two sources of Early Proterozoic sedimentary rocks from the Tonto Basin Supergroup, central Arizona. *Sedimentary Geology*, 77, 51–76.

Cox, R. Lowe, D.R. (1995). A conceptual review of regional scale controls on the compositions of clastic sediments and the co-evolution of continental blocks and their sedimentary cover. *Journal of Sedimentary Research*, 65, 1–12.

Csató, I., Kiss, K., Szinger, B., Tót, S., Varga, M. (2014). Upper Triassic-Jurassic depositional systems in the Akri-Bijeel exploration block, Iraqi Kurdistan. *Mol Group Scientific Magazine*, 1, 54–72.

Cullers, R.L. (1995). The controls on the major and trace element evolution of shales, siltstones and sandstones of Ordovician to tertiary age in the Wet Mountain region, Colorado, U.S.A. *Chem. Geology* 123, 107–131.

Cullers, R.L. (1995). The controls on the major and trace element evolution of shales, siltstones and sandstones of Ordovician to Tertiary age in the Wet Mountain region. Colorado, USA: *Chem. Geol.* 123, 107–131.

Dai, S., Graham, I.T. and Ward, C.R. (2016). A review of anomalous rare earth elements and yttrium in coal. *Int. J. Coal. Geol.* 159, 82–95.

Daoud, H.S., Karim, K.H. (2010). Types of stromatolites in the Barsarin Formation (late Jurassic), Barzinja area, NE Iraq. *Iraqi Bulletin of Geology and Mining*, 6, 47–57.

Deer, W.A.F., Howie, R.A., Zussman, J. (1992). *An Introduction to the Rock-Forming Minerals*. Longman Scientific & Technical, pp. 696.

- Dickinson, W.R., Beard, L.S., Brakenridge, G.R., Erjavec, J.L., Ferguson, R.C., Inman, K.F., Knepp, R.A., Lindberg, F.A., Ryberg, P.T. (1983). Provenance of North American Phanerozoic sandstones in relation to tectonic setting. *Geological Soc. Am. Bul.* 94, 222–235.
- Dickinson, W.R., Suczek, C.A. (1979). Plate tectonics and sandstone compositions. *Bull. Am. Assoc. Petrol. Geol.* 63, 21–71.
- Dunham, R.L. (1962). Classification of carbonate rocks according to depositional texture. *American Association of Petroleum Geologists Memoir*, 1, 108–121.
- Ekoa Bessa, A.Z., Bela, V.A., Ngueutchoua, G., El Amier, Y.A., Kamani, F.A., Zebaze, L.N., Fotso, C.A., Njong, V.N., Ghomsi, F.E., Valipour, M., Armstrong Altri, J.S. (2022). Characteristics and Source Identification of Environmental Trace Metals in Beach Sediments Along the Littoral Zone of Cameroon. *Earth Systems and Environment*, 6, 175–187.
- El Diasty W.S., El Beialy, S.Y., Peters, K.E., Batten, D.J., Al-Beyati, F.M., Mahdi, A.Q., Hasseb, M.T. (2018). Organic geochemistry of the Middle-Late Jurassic Naokelekan Formation in the Ajil and Balad oil fields, northern Iraq. *J. Pet. Sci. Eng.* 166, 350–362.
- Fadhel, M.S., Al Rahim, A.M. (2019). A new tectonic sedimentary framework of the Jurassic succession in the Merjan oil field, Central Iraq. *Journal of Petroleum Exploration and Production Technology*. 9, 2591–2603.
- Falcon, N. (1974), Southern Iran: Zagros Mountains, Geological Society, London, Special Publications. 4, 199–211.
- Falcon, N., (1969), Problems of the relationship between surface structure and deep displacements illustrated by the zagros range. Geological Society, London, Special Publications. 3, 9–21.
- Fathy, D., Abart, R., Wagreich, M., Gier, S., Ahmed, M.S., Sami, M. (2023). Late Campanian climatic-continental weathering assessment and its influence on source rocks deposition in southern Tethys, Egypt. *Minerals*, 13, 160.
- Fathy, D., Wagreich, M., Zaki, R., Mohamed, R.S.A., Gier, S. (2017). Geochemical fingerprinting of Maastrichtian oil shales from the Central Eastern Desert, Egypt: Implications

for provenance, tectonic setting, and source area weathering. *Geological Journal*, 53, 2597–2612

Fisher, J.K., Price, G.D., Hart, M.B., Leng, M.J. (2005). Stable isotope analysis of the Cenomanian-Turonian (Late Cretaceous) oceanic anoxic event in the Crimea. *Cretac. Res.* 26, 853–863.

Floyd, P.A., Leveridge, B.E. (1987). Tectonic environments of the Devonian Gramscatho basin, south Cornwall: framework mode and geochemical evidence from turbidite sandstones. *Journal of the Geological Society* 144, 531–542.

Floyd, P.A., Winchester, J.A., Park, R.G. (1989). Geochemistry and tectonic setting of Lewisian clastic metasediments from the Early Proterozoic Loch Maree Group of Gairloch, NW Scotland. *Precambrian Res.* 45, 203–214.

Fu, X., Wang, J., Zeng, Y., Tan, F., Feng, X. (2010). REE geochemistry of marine oil shale from the Changshe Mountain area, northern Tibet, China. *Int. J. Coal Geol.* 81, 191–199.

Gao, G., Titi, A., Yang, S., Tang, Y., Kong, Y., He, W. (2017). Geochemistry and depositional environment of fresh lacustrine source rock: a case study from the Triassic Baijiantan Formation shales in Junggar Basin, northwest China. *Org. Geochem.* 113, 75–89.

Hayashi, K.I., Fujisawa, H., Holland, H.D., Ohmoto, H. (1997). Geochemistry of ~1.9 Ga sedimentary rocks from northeastern Labrador, Canada. *Geochimica et Cosmochimica Acta* 61, 4115–4137

Hempton, M.R. (1987). Constraints on Arabian Plate motion and extensional history of the Red Sea. *Tectonics*, 6, 687–705.

Hennhoefer, D., Al Suwaidi, A., Bottini, C., Helja, E., Steuber, T. (2018). The Albian to Turonian carbon isotope record from the Shilaif Basin (United Arab Emirates) and its regional and intercontinental correlation. *Sedimentology* 66, 536–555.

Hill, K.C., Shane, S. (2009). Bayou Bend signs agreements for three highly prospective blocks in Kurdistan. Bayou Bend Petroleum Ltd., <https://shamaranpetroleum.com/news/bayou-bend-signs-agreements-for-three-highly-prosp-122630/>, Accessed November 17, 2023.

- Hussain, S.H., Al-Juboury, A.I., Al-Haj, M.A., Armstrong-Altrin, J.S., Al-Lhaebi, S.F. (2021). Mineralogy and geochemistry of the late triassic baluti formation, northern Iraq. *J. Afr. Earth Sci.* 181, 104243.
- Ismail, S.A., Carr, P.F. (2008). A Brief Review of Ophiolites in Iraq. *Proceedings of the International Symposia on Geoscience Resources and Environments of Asian Terranes*, 4th IGCP 516 and 5th APSEG; Bangkok, Thailand.
- Ivanić, M., Lojen, S., Grozić, D., Jurina, I., Škapin, S., Troskot-Čorbić, T., Mikac, N., Juračić, M., Sondi, I. (2017). Geochemistry of sedimentary organic matter and trace elements in modern lake sediments from transitional karstic land-sea environment of the Neretva River delta (Kuti Lake, Croatia). *Quat. Int.* 494, 286–299.
- Jasim, S.Y. (2013). The potential of hydrocarbons generation in the Chia Gara Formation at Amadia area, north of Iraq. *Arabian Journal of Geosciences*, 6, 3313–3318.
- Jassim, S.Z., Al-Gailani, M. (2006). Hydrocarbons. In: Jassim, S.Z., & Goff, J.C. (eds) *Geology of Iraq*. 1st ed., Brno, Czech Republic, Prague and Moravian Museum, pp. 232–250.
- Jassim, S.Z., Goff, J. (2006). *Geology of Iraq*. Dolin, Prague & Moravian Museum, Brno, pp. 318.
- Jassim, S.Z., Goff, J.C. (2006). *Geology of Iraq*; Dolin. Prague & Moravian Museum, Brno, Czech Republic, pp. 352.
- Jones, B., Manning, D.A.C. (1994). Comparison of geochemical indices used for the interpretation of palaeoredox conditions in ancient mudstones. *Chem. Geol.* 111, 111–129.
- Kimura, H., Watanabe, Y. (2001). Oceanic anoxia at the Precambrian-Cambrian boundary. *Geology*, 29, 995–998.
- Koyi, H., Mansurbeg, H. (2021). The role of multiple weak lithologies in the deformation of cover units in the northwestern segment of the Zagros fold-and thrust belt. *Journal of Petroleum Geology*, 44, 145–166.

- Lalami, H.R.K., Hajjalibeigi, H., Sherkati, S., Adabi, M.H. (2020). Tectonic evolution of the Zagros foreland basin since Early Cretaceous, SW Iran: Regional tectonic implications from subsidence analysis. *Journal of Asian Earth Sciences*, 204, 104550.
- Le Garzica, E., Vergésb, J., Sapinc, F., Saurab, E., Meressec, F., Ringenbach, J.C. (2019). Evolution of the NW Zagros Fold-and-Thrust Belt in Kurdistan Region of Iraq from balanced and restored crustal-scale sections and forward modeling. *Journal of Structural Geology*, 124, 51–69.
- Lee, Y.I. (2009). Geochemistry of shales of the Upper Cretaceous Hayang Group, SE Korea: implications for provenance and source weathering at an active continental margin. *Sedimentary Geology*, 215, 1–12.
- Li, B, Jin, X., Dal Corso, J., Ogg, J.G., Lang, X., Baranyi, V., Preto, N., Franceschi, M., Qiao, P., Shi, Z. (2023). Complex pattern of environmental changes and organic matter preservation in the NE Ordos lacustrine depositional system (China) during the T-OAE (Early Jurassic). *Global and Planetary Change*, 221, 104045.
- Li, X., Wei, Y., Li, Y., Zhang, C. (2016). Carbon isotope records of the early Albian oceanic anoxic event (OAE) 1b from eastern Tethys (southern Tibet, China). *Cretac. Res.* 62, 109–121.
- Liao, W., Wang, Y., Kershaw, S., Weng, Z., Yang, H. (2010). Shallow-marine dysoxia across the Permian–Triassic boundary: Evidence from pyrite framboids in the microbialite in South China. *Sedimentary Geology*, 232, 77–83.
- Liu, L., Shuai Zhang, S., Qinfu Liu, Q., Linsong Liu, L., Deng, Y. (2021). Palaeoclimate, palaeosalinity and redox conditions control palygorskite claystone formation: an example from the Yangtaiwatan Basin, northwest China. *Clay Miner.* 56, 210–221.
- Liu, X., Wen, Z., Wang, Z., Song, C., He, Z. (2018): Structural characteristics and main controlling factors on petroleum accumulation in Zagros Basin, Middle East. *Journal of Natural Gas Geoscience*, 3, 273–281.
- Lu, K., Zuo, Y.H., Bing, M., Cao, H.M., Ding, Y. H. (2013). Paleo-sedimentary environments of the Dongpu depression and their impact on organic matter abundance. *Geol. Exploration*, 49, 0589–0594.

- Madhavaraju, J., Hussain, S.M., Ugeswari, J., Nagarajan, R., Ramasamy, S., Mahalakshmi, S. (2015). Paleo-redox conditions of the albian-danian carbonate rocks of the cauvery basin, south India: implications for chemostratigraphy. In: Ramkumar, M. (Ed.), Chemostratigraphy: Concepts, Techniques and Applications. Elsevier Special Volume, pp. 247–271.
- Madhavaraju, J., Ramírez-Montoya, E., Monreal, R., Gonzalez–Leon, C.M., Pi-Puig, T., Espinoza-Maldonado, I.G., Grijalva–Noriega, F.J. (2016). Paleoclimate, paleoweathering and paleoredox conditions of Lower Cretaceous shales from the Mural Limestone, Tuape section, northern Sonora, Mexico: constraints from clay mineralogy and geochemistry. *Rev. Mex. Ciencias Geol.* 33, 34–48.
- Mahanipour, A., Mutterlose, J., Eftekhari, M. (2019). Calcareous nannofossils of the Barremian-Aptian interval from the southeastern Tethys (Zagros Basin, West Iran) and their paleoceanographic implications: A record of Oceanic Anoxic Event 1a. *Mar. Micropaleontol.* 149, 64–74.
- Mahdi, A.Q., Alshami, A. S., Mohammad, A. H., Al Tarif, A. M. (2021). Geological, mineralogical and geochemical studies of Kolosh Formation, Dokan area, Kurdistan Region, Iraq. *Al-Kitab Journal for Pure Sciences*, 5, 39–49.
- McLennan, S.M., Hemming, S., McDaniel, D.K., Hanson, G.N. (1993). Geochemical approaches to sedimentation, provenance and tectonics. In: Johnsson JM, Basu A (eds) Processes controlling the composition of clastic sediments. Geological Society of America Special, 21–40.
- McLennan, S.M., Taylor, S.R. (1991). Sedimentary rocks and crustal evolution: Tectonic setting and secular trends. *J. Geol.* 99, 1–21.
- McLennan, S.M., Taylor, S.R. and Eriksson, K.A. (1983) Geochemistry of Archean shales from the Pilbara Super group, W. Australia. *Geochim. Cosmochim. Acta*, 47, 1211–1222.
- McLennan, S.M., Taylor, S.R., McCulloch, M.T., Maynard, J.B. (1990). Geochemical and Nd-Sr isotopic composition of deep-sea turbidities: Crustal evolution and plate tectonic associations. *Geochimica et Cosmochimica Acta*, 54, 2015–2050.

- Mehrabi, H., Zamanzadeh, M., Amini, A., Tavokali, V., Sajjadi, F., Mirrabie, S.S., Soltani, B. (2021). Geochemistry and provenance of the lower-middle Pliocene Cheleken formation, Iran. *Acta Geochim.* 40, 787–805.
- Men, X., Mou, Ch, Ge, X. (2022). Changes in palaeoclimate and palaeoenvironment in the upper yangtze area (south China) during the ordovician–silurian transition. *Sci. Rep.* 12, 13186.
- Mohialdeen, I.M.J., Hakimi, M.H., Al-Beyati, F.M. (2013). Geochemical and petrographic characterisation of late jurassic-early cretaceous Chia Gara Formation in northern Iraq: palaeoenvironment and oilgeneration potential. *Mar. Pet. Geol.* 43, 166–177.
- Mondal, M.E.A., Wani, H., Mondal, B. (2012). Geochemical signature of provenance, tectonics and chemical weathering in the Quaternary flood plain sediments of the Hindon River, Gangetic Plain, India. *Tectonophysics*, 566–567, 87–94.
- Moradi, A.V., Sarı, A., Akkaya, P. (2016). Geochemistry of the Miocene oil shale (Hancili Formation) in the Cankırı-Corum Basin, Central Turkey: implications for paleoclimate conditions, source–area weathering, provenance and tectonic setting. *Sedimentary Geol.* 341, 289–303
- Mudoi, N.M., Gogoi, B., Dehingia, P. (2022). Provenance, tectonic setting, paleoweathering and paleoclimatic conditions of early to mid-Eocene sandstones of the Dalbuing Formation, Arunachal Pradesh, NE India: Inferences from petrography and geochemistry, *Physics and Chemistry of the Earth, Parts A/B/C*, 127, 103196.
- Murris, R.J. (1980). Middle East-Stratigraphic evolution and oil habitat. *American Association of Petroleum Geologists Bulletin*, 64, 597–618.
- Mustafa, R.K., Tobia, F.H. (2020). Geochemical application in unraveling paleo-weathering, provenance and environmental setting of the shale from Chia Gara Formation, Kurdistan Region, Iraq. *Iraqi Geological Journal*, 53, 90–116.
- Nesbitt, H.W., Markovics, G., Price, R.C. (1980). Chemical processes affecting alkalis and alkaline earths during continental weathering. *Geochimica et Cosmochimica Acta*, 44, 659–666.

- Nesbitt, H.W., Young, G.M., McLennan, S.M., Keays, R.R. (1996). Effects of chemical weathering and sorting on the petrogenesis of siliciclastic sediment, with implications for provenance studies. *Journal of Geology*, 104, 525–542.
- Numan, N.M.S. (1997). A plate tectonic scenario for the Phanerozoic succession in Iraq. *Journal of the Geological Society of Iraq*, 30, 85–110.
- Numan, N.M.S. (2000). Major cretaceous tectonic events in Iraq. *Rafidain Journal of Science*, 11, 32–54.
- Omar, N., McCann, T., Al- Juboury, A.I., Franz, S.O., Zaroni, G., and Rowe, H., (2023). A comparative study of the mineralogy and geochemistry of Early Jurassic- Early Cretaceous-age formations from NE Iraq: Implications for paleoclimate, paleosalinity and paleoredox conditions. *Marine and Petroleum Geology*, 156, 106430.
- Omar, N., McCann, T., Al-Juboury, A.I. and Suárez-Ruiz, I. (2021). Solid bitumen in shales from the Middle to Upper Jurassic Sargelu and Naokelekan formations of northernmost Iraq: implication for reservoir characterization. *Arabian Journal of Geosciences*, Springer, 14, 755.
- Omar, N., McCann, T., Al-Juboury, A.I., Franz, S.O. (2020). Petrography and geochemistry of the Middle-Upper Jurassic Banik section, northernmost Iraq - implications for paleoredox, evaporitic and diagenetic conditions. *N. Jb. Geol. Paleont. Abh.* 297, 125–152.
- Omar, N., McCann, T., Al-Juboury, A.I., Ustinova, M.A. and Sharezwari, A.O. (2022). Calcareous Nannofossil Biostratigraphy and geochemistry of the Early Jurassic- Early Cretaceous Warte Section, northeastern Iraqi Kurdistan: Implications for paleoclimate conditions. *Geosciences*, 12, 94.
- Pettijohn, F.J., Potter, P.E., Siever, R. (1972). *Sand and sandstones*. Springer, New York, pp. 618.
- Pfiffner, A. (2017). Thick-skinned and thin-skinned tectonics: A global perspective. *Geosciences* 7, 71.
- Pitman, J.K., Steinshouer, D., Lewan, M. (2004). Petroleum generation and migration in the Mesopotamian Basin and Zagros Fold Belt of Iraq: results from a basin-modeling study. *GeoArabia*, 9, 41–72.

- Qin, J., Wang, S., Sanei, H., Jiang, C., Chen, Z., Ren, S., Xu, X., Yang, J., Zhong, N. (2018). Revelation of organic matter sources and sedimentary environment characteristics for shale gas formation by petrographic analysis of middle Jurassic Dameigou formation, northern Qaidam Basin, China. *Int. J. Coal Geol.* 195, 373–385.
- Reolid, M., Emanuela, M., Nieto, L.M., Rodríguez-Tovar, F.J. (2014). The Early Toarcian Oceanic Anoxic Event in the External Subbetic (Southiberian Paleomargin, Westernmost Tethys): Geochemistry, nannofossils and ichnology. *Paleogeogr. Paleoclimatol. Paleoecol.* 411, 79–94.
- Rimmer, S.M. (2004). Geochemical paleoredox indicators in Devonian-Mississippian black shales, central Appalachian Basin. U.S.A.). *Chem. Geol.* 206, 373–391.
- Rollinson, H.R. (1993). *Using Geochemical Data: Evaluation, Presentation, Interpretation.* London, UK: Longman. pp. 384.
- Roser, B.P., Korsch, R.J. (1986). Determination of tectonic setting of sandstone mudstone suites using SiO₂ content and K₂O/Na₂O ratio. *J. Geol.* 94:635–650.
- Roser, B.P., Korsch, R.J. (1988). Provenance signatures of sandstone-mudstone suites determined using discriminant function analysis of major-element data. *Chemical Geology*, 67, 119–139.
- Ruf, M., Link, E., Pross, J., Aigner, T. (2005). Integrated sequence stratigraphy: Facies, stable isotope, and palynofacies analysis in a deeper epicontinental carbonate ramp (Late Jurassic, SW Germany). *Sediment. Geol.* 175, 391–414.
- Ruffell, A.H., McKinley, J.M., Worden, R.H. (2002). Comparison of clay mineral stratigraphy to other proxy palaeoclimate indicators in the Mesozoic of NW Europe. *Philos. Trans. A Math. Phys. Eng. Sci.* 360, 675–693.
- Sadooni, F. (1997). Stratigraphy and petroleum prospects of Upper Jurassic carbonates in Iraq. *Petrol. Geosci.* 3, 233–234.
- Sadooni, F. N. (1995). Petroleum prospects of Upper Triassic carbonates in northern Iraq: *Journal of Petroleum Geology*, 18 (2), 171–190.

- Sajid, Z., Ismail, M.S., Zakariah, M.N.A., Tsegab, H., Vintaned, J.A.G., Hanif, T., Ahmed, N. (2020). Impact of paleosalinity, paleoredox, paleoproductivity/preservation on the organic matter enrichment in Black Shales from Triassic turbidites of Semanggol Basin, Peninsular Malaysia, *Minerals*, 10, 915.
- Salae, A.T.S. (2001). Stratigraphy and sedimentology of the Upper Jurassic succession northeastern Iraq. – Master's thesis, University of Baghdad. pp. 95. (Arabic).
- Samani, Sh., Uromeihy, A., Claes, H., Enayati, A., Mehrgini, B., Pezeshki, M., Mostafavi, I., Swennen, R. (2023). Linking sedimentary properties to mechanical characteristics of carbonate reservoir rock: An example from central Persian Gulf, *Gas Science and Engineering*, 113, 204954
- Sarkarinejad, K., Goftari, F. (2019). Thick-skinned and thin-skinned tectonics of the Zagros orogen, Iran: Constraints from structural, microstructural and kinematics analyses. *Journal of Asian Earth Sciences*, 170, 249–273.
- Sepehr, M., Cosgrove, J.W. (2004). Structural framework of the Zagros Fold–Thrust Belt, Iran, *Marine and Petroleum Geology*, 21, 829–843.
- Severmann, S., Anbar, A.D. (2009). Reconstructing paleoredox conditions through a multitracer approach: the key to the past is the present. *Elements*, 5, 359–364.
- Sharezwari, A.O.H. (2015). Stratigraphy, Microfacies Analysis and Depositional Environment of the Upper Jurassic Naokelekan Formation from Selected Sections in Kurdistan Region, NE Iraq. BSc Thesis, Soran University.
- Sharland, P.R., Archer, R., Casey, D.M., Davies, R.B., Hall, S.H., Heward, A.P., Horbury, A.D., Simmons, M.D. (2001). Arabian plate sequence stratigraphy. *GeoArabia*, Special Publication, 2, pp. 371.
- Simmons, M., Davies, R.B. (2018). Triassic to Middle Jurassic stratigraphy of the Arabian Plate: an introduction. In: Poppelreiter, M.C. (Ed.) *Lower Triassic to Middle Jurassic Sequence of the Arabian Plate*, Chapter 1, EAGE, 9–32.
- Sochava, A.V., Podkovyrov, V.N., Felitsin, S.B. (1994). The Evolution of Terrigenous Rocks in the late Precambrian. *Stratigr. Geol. Correl.* 2, 307–324.

Stampfli, G.M., Borel, G.D. (2002). A plate tectonic model for the Paleozoic and Mesozoic constrained by dynamic plate boundaries and restored synthetic oceanic isochrones. *Earth and Planetary Science Letters*, 196, 17–33.

Talbot, C.J., Alavi, M. (1996). The past of a future syntaxis across the Zagros. In G.I. Alsop, D.J. Blundell and I. Davison (Eds.), *Salt Tectonics*. Geological Society, London, Special Publication, 100, 89–109.

Tawfik, H.A., Ghandour, I.M., Maejima, W., Armstrong-Altrin, J.S., Abdel-Hameed, A.M.T. (2015). Petrography and geochemistry of the siliciclastic Araba Formation (Cambrian), east Sinai, Egypt: implications for provenance, tectonic setting and source weathering. *Geological Magazine*, 154, 1–23.

Taylor, S.R., McLennan, S.H. (1985). The geochemical evolution of the continental crust. *Rev. Geophys.* 33, 241–265.

Tian, L., Tong, J., Algeo, T.J., Song, H., Song, H., Chu, D., Shi, L. and Bottjer, D.J. (2014). Reconstruction of Early Triassic ocean redox conditions based on framboidal pyrite from the Nanpanjiang Basin, South China. *Palaeogeography, Palaeoclimatology, Palaeoecology*, 412, 68–79.

Tobia, F., Mustafa, R. (2022). Geochemical and Clay Mineralogical Characteristics of the Black Shale and Constrains on Diagenesis and Maturation, Chia Gara Formation, Iraqi Kurdistan Region, Iraq. *Iraqi Geological Journal*, 55, 23–37.

Tobia, F.H., Al-Jaleel, H.S., Ahmad, I.N. (2019). Provenance and depositional environment of the Middle-Late Jurassic shales, northern Iraq, *Geosciences Journal*, 23, 747–765.

Tribovillard, N., Algeo, T.W., Lyons, T., Riboulleau, A. (2006). Trace metals as paleoredox and paleoproductivity proxies: an update. *Chem. Geol.* 232, 12–32.

USGS United States Geological Survey World Petroleum Assessment 2000-Description and Results: U.S. Geological Survey Digital Data Series DDS-60, version 1.1, four CD-ROM set.

Vlačný, M., Vozárová, A., Vozár J. (2013). Geochemistry of the Permian sandstones from the Malužiná Formation in the Malé Karpaty Mts (Hronic Unit, Western Carpathians, Slovakia):

implications for source-area weathering, provenance and tectonic setting. *Geologica Carpathica*, 64, 1, 23–38.

Verma, M.K., Ahlbrandt, T.S., Al-Gailani, M. (2004). Petroleum reserves and undiscovered resources in the Total Petroleum Systems of Iraq: Reserve growth and production implications. *GeoArabia*, 9, 51–74.

Verma, S.P., Armstrong-Altrin, J.S. (2013). New multi-dimensional diagrams for tectonic discrimination of siliciclastic sediments and their application to Precambrian basins. *Chem. Geol.* 355, 117–133.

Wang, P., Du, Y., Yu, W., Algeo, T.J., Zhou, Q., Xu, Y., Qi, L., Yuan, L., Pan, W. (2020). The chemical index of alteration (CIA) as a proxy for climate change during glacial-interglacial transitions in Earth history. *Earth Sci. Rev.* 201, 103032.

Wani, H., Mondal, M.E.A. (2011). Evaluation of provenance, tectonic setting, and paleoredox conditions of the Mesoproterozoic–Neoproterozoic basins of the Bastar craton, Central Indian Shield: Using petrography of sandstones and geochemistry of shales *Lithosphere*, 3, 143–154.

Weissert, H., Erba, E. (2004). Volcanism CO₂ and paleoclimate: A late Jurassic—Early Cretaceous carbon and oxygen isotopes record. *J. Geol. Soc. Lond.* 161, 695–702.

Wimbledon, W.A.P., Mohialdeen, I.M.J., Andreini, G., Rehakova, D., Stoykova, K. (2016). The Jurassic/Cretaceous boundary beds in Kurdistan—a preliminary note on wider correlations. *JZS Spec. Issue GeoKurd.* 2, 269–276.

Worden, R.H., Ruffell, A.H. Cornford, C. (2000). Palaeoclimate, sequence stratigraphy and diagenesis. *Journal of Geochemical Exploration*, 69-70, 453–457.

Wronkiewicz, D.J., Condie, K.C. (1987). Geochemistry of Archean shales from the Witwatersrand Supergroup, South Africa: Source-area weathering and provenance. *Geochimica et Cosmochimica Acta.* 51, 2401–2416.

Zainy, M.T., Al-Ansari, N., Bauer, T.E., Ask, M. (2017). The tectonic and structural classifications of the Western part of the Zagros Fold and Thrust Belt, North Iraq, review and discussion. *J. Earth Sci. Geotech. Eng.* 7, 71–89.


Appendices

This section includes the full-length papers, including the supporting information, published during the doctoral studies. The respective introductions to the papers are found in Chapters 2, 3, 4, and 5. In this appendix, the publications are attached in their order of appearance in the dissertation, starting with appendix A “Early Jurassic-Early Cretaceous Calcareous Nannofossil Biostratigraphy and Geochemistry, Northeastern Iraqi Kurdistan: Implications for Paleoclimate and Paleoecological Conditions”, followed by appendix B “A comparative study of the paleoclimate, paleosalinity and paleoredox conditions of Lower Jurassic-Lower Cretaceous sediments in northeastern Iraq”, appendix C “Petrography and geochemistry of the Middle-Upper Jurassic Banik section, northernmost Iraq – Implications for palaeoredox, evaporitic and diagenetic conditions” and appendix D “Solid bitumen in shales from the Middle to Upper Jurassic Sargelu and Naokelekan Formations of northernmost Iraq: implication for reservoir characterization”.

Appendix A

Article

Early Jurassic–Early Cretaceous Calcareous Nannofossil Biostratigraphy and Geochemistry, Northeastern Iraqi Kurdistan: Implications for Paleoclimate and Paleoecological Conditions

Nagham Omar ^{1,*} , Tom McCann ¹, Ali I. Al-Juboury ², Maria A. Ustinova ³ and Arkan O. Sharezwri ⁴

¹ Institut für Geowissenschaften—Geologie, University of Bonn, Nussallee 8, 53115 Bonn, Germany; tmccann@uni-bonn.de

² Geology Department, College of Sciences, University of Mosul, Mosul 41002, Iraq; alialjubory@yahoo.com

³ Geological Institute, Russian Academy of Sciences, 119017 Moscow, Russia; ustinova_masha@mail.ru

⁴ Department of Petroleum Geosciences, Soran University, Soran 44008, Erbil, Kurdistan Region, Iraq; arkan.osman@hotmail.com

* Correspondence: s6naomar@uni-bonn.de; Tel.: +49-228-73-4812; Fax: +49-228-73-9037



Citation: Omar, N.; McCann, T.; Al-Juboury, A.I.; Ustinova, M.A.; Sharezwri, A.O. Early Jurassic–Early Cretaceous Calcareous Nannofossil Biostratigraphy and Geochemistry, Northeastern Iraqi Kurdistan: Implications for Paleoclimate and Paleoecological Conditions.

Geosciences **2022**, *12*, 94. <https://doi.org/10.3390/geosciences12020094>

Academic Editors: Pierre Pellenard, Emanuela Mattioli, Guillaume Dera and Jesus Martinez-Frias

Received: 20 December 2021

Accepted: 13 February 2022

Published: 17 February 2022

Publisher's Note: MDPI stays neutral with regard to jurisdictional claims in published maps and institutional affiliations.



Copyright: © 2022 by the authors. Licensee MDPI, Basel, Switzerland. This article is an open access article distributed under the terms and conditions of the Creative Commons Attribution (CC BY) license (<https://creativecommons.org/licenses/by/4.0/>).

Abstract: Early Jurassic- to Early Cretaceous-age calcareous nannofossils from the Sarki, Sehkanyian, Sargelu, Naokelekan, Barsarin and Chia Gara formations are investigated for the first time from the Warte area, northeastern Iraqi Kurdistan. A range of isotopic and inorganic geochemical analyses are carried out in order to reconstruct the paleoecological and paleoclimatic conditions during which the Sarki, Sehkanyian, Sargelu, Naokelekan, Barsarin and Chia Gara formations were deposited. The age of the Sargelu Formation was determined as Bajocian–Callovian based on the first occurrence of *Cyclagelosphaera margerelii*, *Watznaueria britannica*, *W. fossacincta*, *W. manivittiae*, *Watznaueria barnesiae* and *Watznaueria ovata*. Geochemical proxies (Sr, Ca, Al, Rb/Sr, Sr/Cu and Sr/Ba) for paleoclimate and paleoecological conditions, along with oxygen isotopes ($\delta^{18}\text{O}$) data, suggest that warm and arid climatic conditions were predominant during the Early Jurassic–Early Cretaceous period.

Keywords: calcareous nannofossils; stable isotopes; paleoclimate; paleoecology; Jurassic; Iraq

1. Introduction

Calcareous nannofossils are the most important carbonate-forming organisms since Jurassic times, and their biostratigraphy and carbon-isotope data commonly provide excellent stratigraphic control [1]. In addition, the relationship between calcareous nannofossils and inorganic geochemical data can be used as a tool to interpret paleoenvironmental and paleoclimatic conditions [2–4]. Similarly, the oxygen isotope geochemistry is used as an indicator of the dominant climatic conditions [5–8]. The Jurassic successions in Iraq are of geological and economic importance and, thus, they have been described in numerous academic theses and research papers, the majority of which have focused on the lithology and depositional environments of the successions and their economic significance [9–13]. A few articles on calcareous nannofossils from the Naokelekan and Chia Gara formations in Iraqi Kurdistan have been published [14,15]. However, detailed studies covering the calcareous nannofossil biostratigraphy of all Jurassic-age formations in northeastern Iraqi Kurdistan have not, to date, been attempted.

The current study focuses on calcareous nannofossil biostratigraphy and related isotopic and inorganic geochemistry of the Early Jurassic- to Early Cretaceous-age formations from the Warte section, northeastern Iraqi Kurdistan, including the paleoecology and paleoclimate proxies. This section, i.e., the Warte section, crops up in a region where calcareous nannofossils from the entire Jurassic system were recorded and analyzed for the first time. The location of this section, and its lack of accessibility (partly due to the political situation)

means that this work will remain unique for the foreseeable future. The sedimentary succession from the Warte section comprises interbedded shales and carbonates (dolomites and limestones) and rare chert beds. A total of sixty-five samples were selected, covering the entire Jurassic succession, and including the Sarki, Sehkanyian, Sargelu, Naokelekan, Barsarin and Chia Gara formations. While the presence of a Lower Jurassic–Middle Jurassic boundary and a Middle Jurassic–Upper Jurassic boundary interval was confirmed, the position of these boundaries remains unclear. The aim of the present study, therefore, is to determine the stratigraphic position of the lower and upper boundaries of the Middle Jurassic in the Warte succession from northeastern Iraqi Kurdistan based on the detailed analysis of the calcareous nannofossils. In addition, the study aims to reconstruct the paleoecological and paleoclimatic conditions of the Jurassic–Lower Cretaceous succession of the region by integrating calcareous nannofossil data with geochemical analyses.

2. Geological Setting

The area of study is situated in the Erbil Governorate, within the region of Iraqi Kurdistan, Northern Iraq [13,16]. Northern Iraq lies within the Zagros Basin/Zagros Fold Belt on the northeastern boundary of the Arabian Plate (see Figure 1a for the location and tectonic provinces) [13–18]. The Zagros Basin/Zagros Fold Belt, which covers an area of about $500 \times 103 \text{ km}^2$, has a NW–SE length of c. 2300 km, extending from Turkey to SE Iran, and a NE–SW width of 100–300 km [16]. It formed as a result of the collision between the continental Arabian Plate and the continental segments of the Eurasian margin [19–21]. In Iraq, the Zagros Basin/Zagros Fold Belt contains sedimentary rocks ranging in age from Jurassic to Tertiary, i.e., dominated by a thick Mesozoic succession.

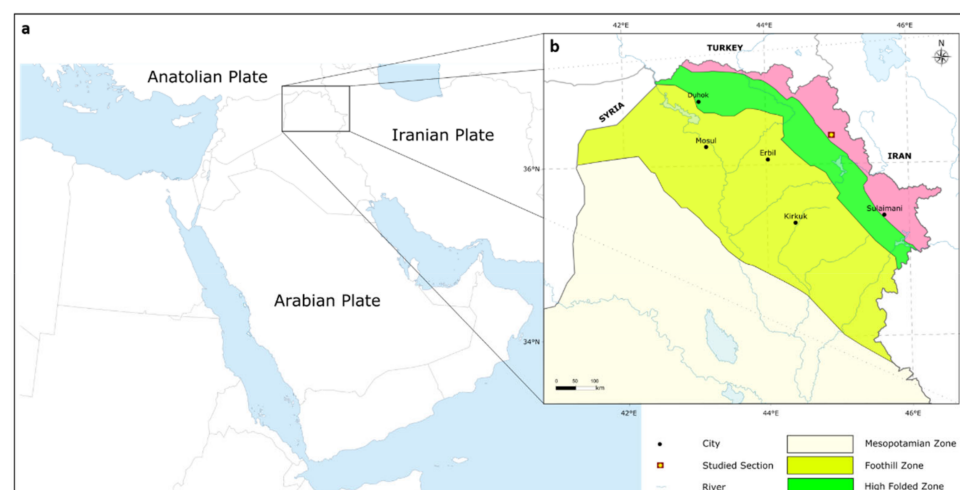


Figure 1. (a) Location of the study area in northeastern Iraqi Kurdistan within the Arabian plate. (b) Geological map of Northern Iraq showing the study area and the structural zones of the Zagros Basin/Zagros Fold Belt.

The present study focusses on the Early to Late Jurassic succession of the Warte area, northeastern Iraqi Kurdistan region. The regional stratigraphy can be subdivided into six formations, namely, the Sarki, Sehkanyian, Sargelu, Naokelekan, Barsarin and Chia Gara formations [22]. The exposed Jurassic formations in Northern Iraq are located as isolated patches within eroded cores and limbs of anticlines in the structural zones of the Zagros Basin/Zagros Fold Belt of Northern Iraq [23]. These structural zones include, from SW to NE, the Low Folded Zone (or Foothills), the High Folded Zone and the Imbricated Zone [24]. The Warte section, which was examined as part of this study, is located within the Imbricated Zone (Figure 1b). The Imbricated Zone of Iraq generally is characterized by marked folding and faulting in the Paleozoic to Cenozoic sedimentary strata [25]. The

impact of tectonic deformation in this zone is clearly visible in the complex fold geometries that are noted [26].

The Early-Jurassic-age Sarki Formation was first described by Dunnington [27] from the Chia Gara Range of N Iraq as a 300 m thick carbonate unit [22,24].

The formation consists of limestones, dolomitic limestones, dolomites and shales. An Early Liassic age has been inferred based on the stratigraphic position of the formation between the underlying Upper Triassic Kurra Chine Formation and the overlying Middle Jurassic Sargelu Formation. The lower and upper contacts of the formation are conformable and gradational. The Sarki Formation was deposited in a restricted lagoonal environment [24].

The Early-Jurassic-age Sehkanian Formation was first described by Wetzel and Morton in 1950 from the Surdash Anticline, NE of Iraq, as a 180 m thick carbonate unit [28]. The formation consists mainly of dolomites and dolomitic limestones. A Liassic age was proposed for the formation based on the faunal content, including bivalve (e.g., *Lithiotis*) and algae (e.g., *Boueina hochstetteri*). The lower and upper contacts of the formation with the Sarki and Sargelu formations are conformable and gradational [22,29]. The formation was deposited in a restricted lagoonal environment [24].

The Middle-Jurassic-age Sargelu Formation was first described by Wetzel from the Surdash Anticline in the High Folded Zone, NE of Iraq [30]. The thickness of the Sargelu Formation in its type section is about 115 m, and consists of bituminous limestones, dolomitic limestones and black shales with streaks of thin black chert. A Bajocian–Bathonian age was suggested for the Sargelu Formation based on the presence of bivalves (e.g., *Bositra buchii*). The lower contact with the Sehkanian Formation in the type area is usually conformable and gradational, and the contact with the overlying Naokelekan Formation is similar. The formation was deposited in a basinal euxinic marine environment [22,24].

The Late-Jurassic-age Naokelekan Formation was first described by Wetzel and Morton from the Balambo-Tanjero Zone near Rowanduz, NE Iraq [28]. The Naokelekan Formation consists of argillaceous bituminous limestones, dolomites, and shales with beds of black shales in its lower part. An Early Callovian–Kimmeridgian age was proposed for the formation based on the recorded fauna, including belemnites, stromatoporoids, foraminifera and algae [31]. The lower and upper contacts of the formation with the Sargelu and Barsarin formations, respectively, appear to be conformable. The formation was deposited in an euxinic environment in a subsiding or starved basin [22,24].

The Late-Jurassic-age Barsarin Formation was first described by Wetzel in 1950 from its type area in the Balambo-Tanjero Zone near Rowanduz, NE Iraq [32]. The Barsarin Formation consists of limestones and dolomitic limestones. A Kimmeridgian–Early Tithonian age was suggested for the formation based on its stratigraphic position below the Late Tithonian Chia Gara Formation and above the Naokelekan Formation. The lower and upper contacts of the formation appear conformable with both the Naokelekan and Chia Gara formations in the type area. The Barsarin Formation was deposited in a lagoonal or evaporitic environment [22,24].

The Late Jurassic–Early Cretaceous-age Chia Gara Formation was first defined by Wetzel in 1950 from the Chia Gara Anticline in the High Folded Zone of Northern Iraq [30]. The Chia Gara Formation consists of thinly bedded limestones and calcareous shales. A Middle Tithonian–Berriasian age was suggested for the formation. The lower contact with the Barsarin Formation is conformable. The contact with the overlying Garagu Formation is gradational and conformable. The Chia Gara Formation was deposited in a mid-deep shelf environment [22,24].

3. Materials and Methods

Sixty-five (65) samples from the Warte section were selected for detailed calcareous nannofossil biostratigraphy, trace element and oxygen stable isotopic geochemistry analyses. The samples cover the entire succession at this location, extending from the Sarki Formation to the Chia Gara Formation (see Figure 2 and Table 1 for sample locations).

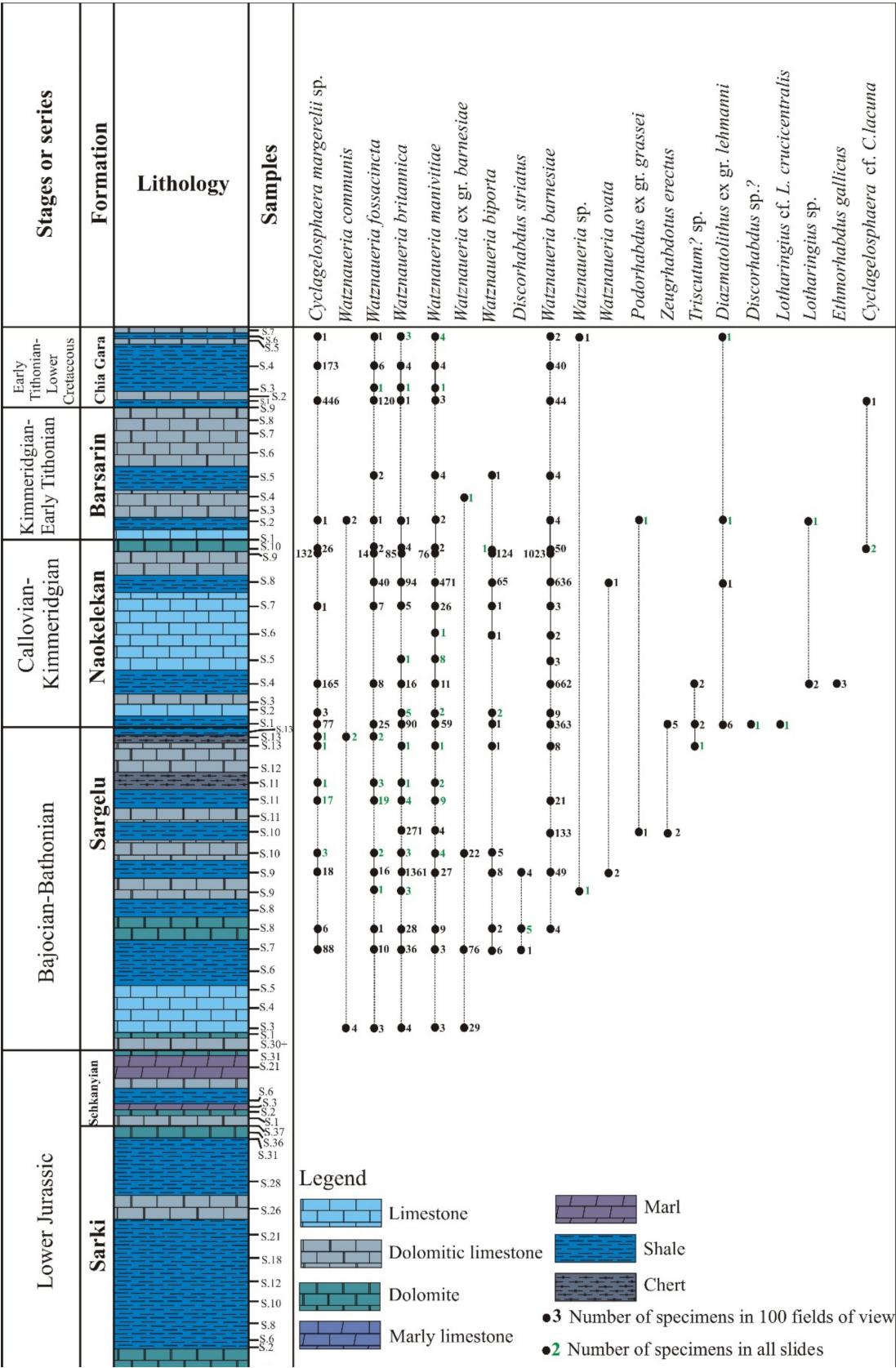


Figure 2. Sample location and distribution of the calcareous nannoplankton of the Warte section.

Table 1. Simplified table showing the precise stratigraphic position of the studied samples from the Sarki, Sehkaniyan, Sargelu, Naokelekan, Barsarin and Chia Gara formations.

Formation	Sample No.	Bed Thickness (m)
Sarki	S 1	0.60
Sarki	S 2	0.20
Sarki	S 6	0.25
Sarki	S 8	0.15
Sarki	S 10	0.25
Sarki	S 12	0.20
Sarki	S 18	0.10
Sarki	S 21	0.30
Sarki	p.c. ¹	30.00
Sarki	S 26	5.00
Sarki	S 28	5.00
Sarki	S 31	7.50
Sarki	S 36	25.00
Sarki	S 37	4.00
Sehkanyian	S 1	0.40
Sehkanyian	S 2	8.00
Sehkanyian	S 3	0.10
Sehkanyian	p.c. ¹	5.00
Sehkanyian	S 6	0.15
Sehkanyian	S 21	0.25
Sehkanyian	S 30	25.00
Sehkanyian	S 31	25.00
Sargelu	S 1	5.00
Sargelu	S 3	4.00
Sargelu	S 4	4.00
Sargelu	S 5	4.00
Sargelu	S 6	0.10
Sargelu	S 7	1.00
Sargelu	S 8	1.50
Sargelu	S 8	1.50
Sargelu	S 9	3.00
Sargelu	S 9	3.00
Sargelu	p.c. ¹	6.00
Sargelu	S 10	3.00
Sargelu	S 10	3.00
Sargelu	S 11	3.00
Sargelu	S 11	3.00
Sargelu	S 11	3.00
Sargelu	S 12	1.00
Sargelu	S 13	2.00
Sargelu	S 13	2.00
Sargelu	S 13	6.00
Naokelekan	S 1	7.00
Naokelekan	S 2	1.00
Naokelekan	S 3	1.80
Naokelekan	S 4	1.80
Naokelekan	S 5	1.80
Naokelekan	S 6	1.80
Naokelekan	S 7	1.80
Naokelekan	S 8	1.50
Naokelekan	S 9	1.50
Naokelekan	S 10	1.00
Barsarin	S 1	6.00
Barsarin	S 2	6.00
Barsarin	S 3	2.00
Barsarin	S 4	3.00

Table 1. *Cont.*

Formation	Sample No.	Bed Thickness (m)
Barsarin	S 5	3.00
Barsarin	S 6	3.00
Barsarin	S 7	5.00
Barsarin	S 8	1.50
Barsarin	S 9	1.50
Chia Gara	S 1	1.43
Chia Gara	S 2	1.43
Chia Gara	S 3	1.43
Chia Gara	S 4	1.43
Chia Gara	S 5	1.43
Chia Gara	S 6	1.43
Chia Gara	S 7	1.43

¹ p.c.: partly covered.

The calcareous nannofossils were investigated using optical methods. Initially, the rock samples were crushed and concentrated using a centrifuge, and smear slides (24 × 24 mm) were prepared using Canada balsam. The slides were then analyzed under the microscope with a 1000× magnification for precise recognition and identification of the nannofossils present. At least 100 fields of view (diameter 0.018 mm) were observed randomly in each slide (in a row-on-row pattern), in order to obtain relative abundances and semi quantitative information about the nannofossil assemblage composition. Species diversity of nannofossils was studied throughout the slide. Additionally, the same samples were analyzed by XRF (X-ray fluorescence) to determine the both the major and trace element compositions. For each sample, 5 g of material was weighed and combined together with 1 g of wax and ground to homogeneity in an agate mortar. This was then pressed into a pellet for 60 s at 20 kbar to prepare for trace element analysis. Measurements were performed in the Institut für Geowissenschaften-Geologie, Bonn University. The isotopic geochemistry analyses for oxygen were conducted at the Ruhr-Universität Bochum, using a mass spectrometer MAT253 (Thermo Fisher Scientific, Bremen, Germany) equipped with a ConFlo IV and a GasBench II (both Thermo Fisher Scientific).

4. Results

4.1. Lithological Analysis

The Warte section, which formed the basis for this study, is located NE Iraq, where, to date, no detailed studies of the entire Jurassic have been attempted. A schematic lithological log was measured illustrating the transition from the Early-Jurassic-age Sarki Formation through to the Late Jurassic–Early Cretaceous-age Chia Gara Formation (see Figure 2). The measured profile is described from base to top, below.

4.1.1. Sarki Formation

The base of the profile referred to the lower part of the Sarki Formation (31.95 m). This generally consists of alternating beds of gray dolomite that are interbedded with dark grey-black shales. Individual dolomite beds range in thickness from c. 0.1 to 3.5 m, whilst the shales range in thickness from c. 0.05 to 0.5 m. Individual dolomite beds are generally medium-to-very-thickly bedded (Figure 3a). Bed boundaries are horizontal and often sharp and are laterally continuous across the outcrop. Internally, some beds show evidence of sedimentary structures, such as lamination, as well as evidence of tectonic deformation in the form of boudinage structures, fractures and joints (Figure 3b). The middle interval (30 m) of the formation is not well exposed and partly covered.



Figure 3. (a) Dolomite beds interbedded with dark grey-black shales in the lower part of the Sarki Formation. (b) Evidence of tectonic deformation in the form of fractures and joints within the Sarki Formation. (c) Veins filled with white calcite within the dolomite beds of the Sarki Formation. (d) Highly fractured dolomite beds of the Sehkaniyan Formation. (e) Quartz geodes within the upper part of the Sehkaniyan Formation. (f) Dolomite beds alternate with limestones and shales in the lower part of the Sargelu Formation. (g) A few ammonites within the Naokelekan Formation. (h) Common stromatolitic structure including stylolite (pressure solution) within the limestone of the contact area between the Naokelekan Formation and the overlying Barsarin Formation. (i) Minor folds in the contact area between the Naokelekan Formation and the overlying Barsarin Formation. (j) Tectonic deformation in the form of box folding within the Barsarin Formation. (k) The contact area between the Barsarin Formation and the overlying Chia Gara Formation. (l) Fissile shales interbedded with dolomitic limestones in the lower part of the Chia Gara Formation. Scales included.

Above the covered interval is the upper part of the formation (119 m), which predominantly comprises dolomites with 9 m of dolomitic limestones and 11 m of shales. Individual dolomite beds, which are grey in color, range from 10 to 50 m in thickness. The dolomites are very thickly bedded; some parts of the beds are cavernous with the presence of veins filled with white calcite (Figure 3c). Bed boundaries are horizontal and often sharp. Internally, some beds show evidence of sedimentary structures, such as hummocky cross stratification, while diagenetic features include liesegang rings and tectonic fractures were also noted. The uppermost bed of the Sarki Formation, i.e., the contact area with the overlying Sehkaniyan Formation, comprises 4 m of marly limestone. It is beige to yellow in color and highly fractured.

4.1.2. Sehkaniyan Formation

The lower part of the Sehkaniyan Formation (12.4 m thick) consists of grey dolomites interbedded with marls and one single dolomitic limestone bed. Individual dolomite beds are highly fractured, laminated and cross laminated, ranging in thickness from c. 0.4 to 7.9 m, whilst the marl is c. 0.1 m thick (Figure 3d). The middle interval (5 m) of the formation is not well exposed and partly covered. The upper part of the formation (455.85 m), overlying the covered interval, comprises dolomites with 0.15 m shale and 0.25 m marl. The dolomites are grey to black in color, very thickly bedded and range from 3.85 to 70 m in thickness. The individual beds are horizontally bedded, with sharp bed boundaries. Deformation, in the form of fracturing and jointing, was noted, with some of the fractures infilled with calcite. Small (2–5 cm) quartz geodes were also noted (Figure 3e).

The uppermost bed of the Sehkanyian Formation (50 m thick) is dolomite, and it marks the gradational contact between the Sehkanyian and Sargelu formations.

4.1.3. Sargelu Formation

The lower part of the formation (33 m thick) comprises thickly bedded, brown-colored dolomites, alternating with medium bedded, black-colored limestones, shales and a 3 m thick dolomitic limestone (Figure 3f). Individual dolomite beds are c. 1 to 5 m in thickness, limestone beds are c. 4 m, whilst the shales are c. 0.1 to 3 m thick. The limestones are organic and bituminous with the presence of calcite veins. The middle interval (6 m) of the formation is not well exposed and partly covered. The upper part of the formation (23 m) consists of dark-brown-to-black dolomitic limestones, alternating with shales and two bands of chert. Individual dolomitic limestone beds are c. 2 to 4 m in thickness, shales are c. 1 to 4 m, whilst the two bands of chert are c. 2 to 3 m thick. Internally, there is no evidence of any sedimentary structures except the dolomitic limestones, which may be laminated. Evidence of deformation, in the form of calcite veins, are present in the dolomitic limestones. The contact with the overlying Naokelekan Formation is gradational.

4.1.4. Naokelekan Formation

The Naokelekan Formation (27 m thick) consists of shales alternating with very thickly bedded limestones and dark-brown-colored dolomitic limestones, while the uppermost bed of the formation is a dark brown dolomite. The shales are c. 2 to 6 m thick; limestone beds are c. 2 to 3 m in thickness with c. 1.5 to 3 m thick dolomitic limestone beds. Both the dolomitic limestones and limestones are organic rich and occasionally mottled. They also contain rare ammonites, preserved as isolated specimens in the middle of the beds (Figure 3g). The dolomitic limestones and limestones include secondary calcite nodules and stylolites, with some beds showing liesegang rings. The sharp contact (6 m thick) between the Naokelekan Formation and the overlying Barsarin Formation is marked by the presence of very thickly bedded, stromatolitic limestones (Figure 3h). The contact area is also marked by the presence of minor folds due to post-depositional deformation in the area (as noted earlier; Figure 3i).

4.1.5. Barsarin Formation

The Barsarin Formation (25 m thick) consists of shales alternating with dark gray dolomitic limestones, and a 6 m thick limestone bed. The shales range in thickness from c. 3 to 6 m, while the dolomitic limestone beds are c. 2 to 5 m thick. Due to tectonic deformation, the studied formation is highly fractured and folded (e.g., box folding; Figure 3j). The contact with the overlying Chia Gara Formation is sharp (Figure 3k).

4.1.6. Chia Gara Formation

The formation (10 m thick) consists of fissile shales interbedded with dolomitic limestones. The studied part of the profile represents the lower part of the Chia Gara Formation which is Late Jurassic–Early Cretaceous in age (Figure 3l).

4.2. Calcareous Nannofossils

Sixty-five samples were collected from the Warte section and investigated using optical microscopy to determine the calcareous nannofossil biostratigraphy. The entire profile was sampled, with sample spacing being closer in the areas coinciding with the formation boundaries (i.e., Sarki/Sehkanyian, Sehkanyian/Sargelu, Sargelu/Naokelekan, Naokelekan/Barsarin, and Barsarin/Chia Gara).

Calcareous nannofossils are not very abundant in the samples, and those that are present tend to be moderately to poorly preserved (Figures 2 and 4). Despite this, calcareous nannofossils were recovered from four of the formations, with the exception of the Sarki and Sehkanyian formations that were barren.

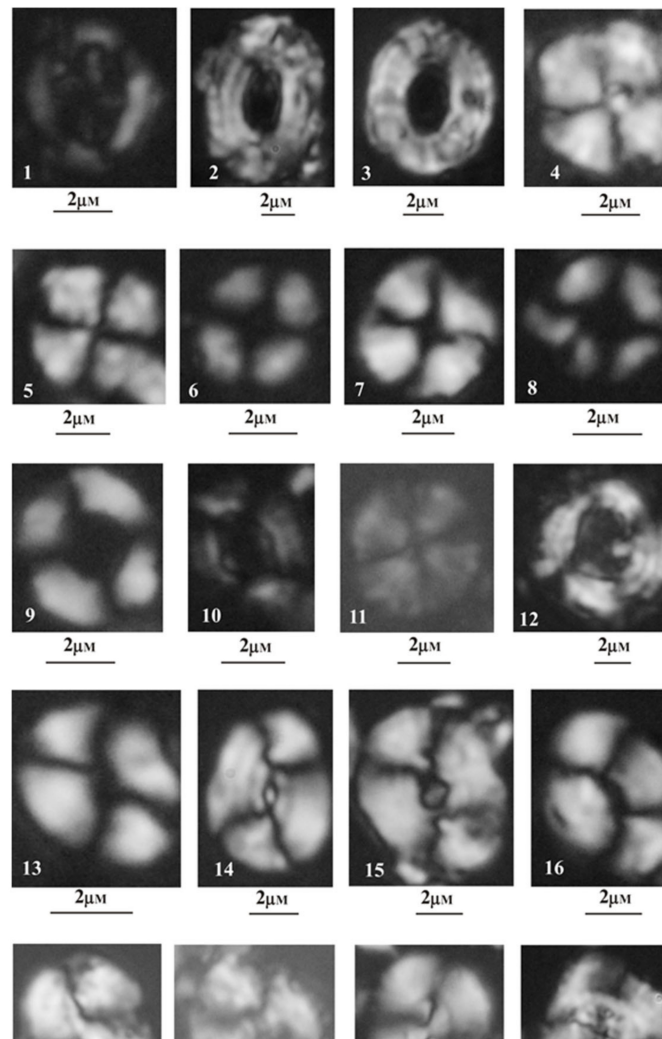


Figure 4. Jurassic species of the Warte section. Abbreviation ‘pol’ denote polarized light. (1) *Lotharingius* ex gr. *crucicentralis* (Medd, 1971), pol. Naokelekan Formation, sample S.1. (2) *Triscutum* sp., pol. Naokelekan Formation, sample S.1. (3) *Triscutum* sp., pol. Naokelekan Formation, sample S.1. (4) *Cyclagelosphaera margerelii* Noël, 1965, pol.; Naokelekan Formation, sample S.1. (5) *Cyclagelosphaera margerelii* Noël, 1965, pol.; Chia Gara Formation, sample S.1. (6) *Cyclagelosphaera* ex gr. *lacuna* Varol and Girgis 1994, pol. Naokelekan Formation, sample S.10. (7) *Cyclagelosphaera* sp., pol. Naokelekan Formation, sample S.1. (8) *Diazomatolithus lehmanii* Noël, 1965, pol. Barsarin Formation, sample S.2. (9) *Diazomatolithus* ex gr. *lehmanii* Noël, 1965, pol. Naokelekan Formation, sample S.8. (10) *Biscutum* sp., pol. Naokelekan Formation, sample S.1. (11) *Discorhabdus striatus* Moshkovitz and Ehrlich, 1976, pol. Sargelu Formation, sample S.9., shale. (12) *Podorhabdus* ex gr. *grassei* Noël, 1965, pol. Barsarin Formation, sample S. 2. (13) *Watznaueria barnesiae* (Black in Black & Barnes, 1959) Perch-Nielsen, 1968, pol. Naokelekan Formation, sample S.1. (14) *Watznaueria Britannica* (Stradner, 1963) Reinhardt, 1964, pol.; Naokelekan Formation, sample S.10. (15) *Watznaueria Britannica* (Stradner, 1963) Reinhardt, 1964, pol.; Naokelekan Formation, sample S.2. (16) *Watznaueria fossacincta* (Black, 1971) Bown in Bown and Cooper, 1989, pol. Naokelekan Formation, sample S.2. (17) *Watznaueria communis* Reinhardt 1964, pol.: Naokelekan Formation, sample S.2. (18) *Watznaueria communis* Reinhardt 1964, pol.: Naokelekan Formation, sample S.2. (19) *Watznaueria biporta* Bukry, 1969, pol.: Naokelekan Formation, sample S.2. (20) *Watznaueria manivitiae* Bukry, 1973, pol. Barsarin Formation, sample S.2.

The nannofossil assemblage identified from the Sargelu, Naokelekan, Barsarin and Chia Gara formations is dominated by the genus *Watznaueria* (Figure 5). Indeed, five species could be recognized, and these varied markedly in terms of their abundance. The percentages of *W. barnesiae* and *W. fossacincta* range from 0.12% to 33% and together they comprise 42% of the entire assemblage. The percentages of *W. britannica* and *W. manivitiae* range from 0.8% up to 67% and 63%, respectively. The percentage of *Cyclagelosphaera magerelii* ranges from 0.1% to 38% of the total assemblage.

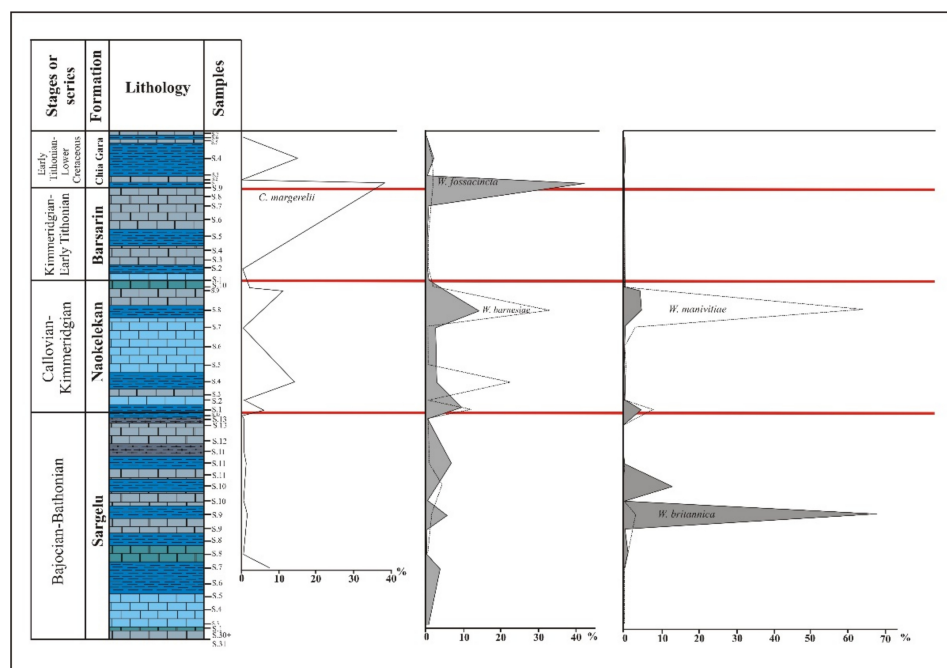


Figure 5. Percentage of the nannofossil *Cyclagelosphaera magerelii* and *Watznaueria* species of the Warte section.

The mudstones and shales of the Sargelu Formation show three distinct abundance peaks for *W. fossacincta* and two peaks for *W. britannica* (Figure 5). Nannofossil assemblage of this formation is most diverse, with biodiversity being significantly reduced in the limestones and dolomitic limestones of the Sargelu, Naokelekan, Barsarin and Chia Gara formations (Figures 2 and 5).

All of the identified species are characterized by very long stratigraphic ranges, extending from the mid-to-late Jurassic (at least). In addition, these species also show a wide geographical distribution. This, together with the lack of precise zonal markers in the Warte profile, makes it difficult to determine the presence or absence of precise nannofossil zones. However, the nannofossils can provide valuable information with regard to ambient oceanic paleotemperatures and the paleoenvironment of the surface waters.

4.3. Geochemistry

Sixty-five samples were collected from the Warte section covering the complete sedimentary succession that is represented by the Sarki, Sehkanyan, Sargelu, Naokelekan, Barsarin and Chia Gara formations. The samples were prepared and analyzed for oxygen stable isotopic geochemistry and trace elements.

4.3.1. Oxygen Isotope Analysis

A total of 65 samples, encompassing all of the formations, were collected for isotopic analysis. At the base of the profile, the Early-Jurassic-age Sarki Formation shows a slightly positive oxygen isotope ($\delta^{18}\text{O}$) value (0.13‰; indeed, this is the only positive value recorded

from the profile), while the values from the rest of the formation vary between -0.65% and -6.99% . The overlying Early-Jurassic-age Sehkanyian Formation values fluctuate between -0.29% and -10.07% , but are all negative. The samples from the Middle-Jurassic-age Sargelu Formation continue this negative trend (ranging from -2.27% to -6.57%). One sample from the latter formation did not provide a good value (Table 2).

Table 2. Oxygen isotope (^{18}O) and carbon isotope (^{13}C) data for the samples from the Sarki, Sehkanyian, Sargelu, Naokelekan, Barsarin and Chia Gara formations.

Formation	Sample No.	$\delta^{18}\text{O}$	$\delta^{13}\text{C}$
Sarki	S1	0.13	-0.76
Sarki	S2	-1.03	-0.52
Sarki	S6	-0.97	-0.80
Sarki	S8	-2.24	-1.23
Sarki	S10	-1.50	-1.43
Sarki	S12	-1.86	-1.08
Sarki	S18	-2.11	-1.49
Sarki	S21	-1.56	-1.95
Sarki	S26	-6.99	-3.47
Sarki	S28	-3.22	0.99
Sarki	S31	-1.70	-3.66
Sarki	S36	-1.28	-3.05
Sarki	S37	-0.65	-2.02
Sehkanyian	S1	-10.07	-3.27
Sehkanyian	S2	-1.23	-5.03
Sehkanyian	S3	-4.48	-5.46
Sehkanyian	S6	-0.29	-0.70
Sehkanyian	S21	-7.29	-7.38
Sehkanyian	S30	-2.67	-0.95
Sehkanyian	S31	-3.34	-0.89
Sargelu	S1	-3.42	-3.02
Sargelu	S3	-4.15	-2.68
Sargelu	S4	-5.06	0.03
Sargelu	S5	-4.25	-0.03
Sargelu	S6	-4.00	-3.30
Sargelu	S7	-4.91	-0.99
Sargelu	S8	-2.27	-1.76
Sargelu	S8	-3.64	-1.21
Sargelu	S9	-2.84	-0.49
Sargelu	S9	-5.28	-2.84
Sargelu	S10	-3.38	-5.82
Sargelu	S10	-4.92	-1.94
Sargelu	S11	-6.57	-3.34
Sargelu	S11	-4.92	-3.34
Sargelu	S11	i.s. ¹	i.s. ¹
Sargelu	S12	-4.21	-4.14
Sargelu	S13	-5.55	-4.00
Sargelu	S13	-3.18	-3.64
Sargelu	S13	-3.70	-4.44
Naokelekan	S1	-2.22	-3.31
Naokelekan	S2	-4.64	-5.81
Naokelekan	S3	-5.03	-5.82
Naokelekan	S4	-4.06	-4.26
Naokelekan	S5	-6.82	-3.73
Naokelekan	S6	-4.26	-3.76
Naokelekan	S7	-3.46	-5.49
Naokelekan	S8	-3.70	-1.61
Naokelekan	S9	-4.25	-4.20
Naokelekan	S10	-0.99	-6.49

Table 2. Cont.

Formation	Sample No.	$\delta^{18}\text{O}$	$\delta^{13}\text{C}$
Barsarin	S1	−3.54	−9.87
Barsarin	S2	−4.01	−9.19
Barsarin	S3	−7.77	−9.97
Barsarin	S4	−4.65	−11.31
Barsarin	S5	−5.24	−9.69
Barsarin	S6	−3.94	−10.40
Barsarin	S7	−4.24	−10.33
Barsarin	S8	−4.25	−10.60
Barsarin	S9	−4.12	−9.49
Chia Gara	S1	−5.70	−4.70
Chia Gara	S2	−5.36	−6.04
Chia Gara	S3	−4.60	−8.21
Chia Gara	S4	−5.39	−4.91
Chia Gara	S5	−3.67	−10.65
Chia Gara	S6	−4.27	−11.18
Chia Gara	S7	−2.13	−9.14

¹ i.s.: insufficient signal.

Moving up profile, the samples from the Late-Jurassic-age Naokelekan and Barsarin formations show consistently negative oxygen isotope ($\delta^{18}\text{O}$) values (range from −0.99‰ to −6.82‰ in the Naokelekan Formation, and from −3.54‰ to −7.77‰ in the Barsarin Formation). The overlying Late Jurassic–Early Cretaceous-age Chia Gara Formation values are also all negative, and fluctuate between −2.13‰ and −5.70‰ (Table 2). However, before starting to study and interpret the oxygen isotope (^{18}O) data, it is necessary to know the extent to which the sediments of the Sarki, Sehkanyian, Sargelu, Naokelekan, Barsarin and Chia Gara formations were influenced by diagenesis. The oxygen isotopes are very sensitive to the diagenetic processes [33] due to the large thermal breakdown of the oxygen isotopes; therefore, the oxygen isotope values were used to indicate ancient water temperatures as they are strongly influenced by water temperature [34,35]. Other authors have suggested that the relationship between the carbon and oxygen isotope values can be used to estimate the influence of diagenesis on the sediments and the extent to which the oxygen isotopes represent the initial imprint of the environment in which these sediments were deposited [33,36,37]. According to these authors, the relationship between the carbon and oxygen isotope values, which is positive and strong, indicates that the oxygen isotopes were strongly influenced by diagenesis as a result of the leakage and transfer of solutions bearing light oxygen and carbon from the diagenetic solutions, such as atmospheric water, whilst weak or negative relationship indicates that the oxygen isotopes were not influenced by diagenesis. Indeed, the relationship established in this study registered weak correlation ($R^2 = 0.0943$) between the carbon and oxygen isotope values. This would indicate, as noted above, that the Sarki, Sehkanyian, Sargelu, Naokelekan, Barsarin and Chia Gara sediments were not or weakly influenced by diagenesis, and thus, the oxygen isotope values represent their initial imprint in the sediments from the Warte section.

4.3.2. Inorganic Geochemistry

Sixty-five samples were collected from the six formations of the Warte section, and then analyzed for their trace elements. Several elemental ratios were calculated and used for paleoclimate and paleoecological interpretations. The latter, including Ca, Al, Rb/Sr, Sr/Cu and Sr/Ba, are considered by many authors to be good paleoclimate proxies [38–41]. Furthermore, the trace element Sr is considered to be a useful salinity indicator [15,42–44].

The Ba values for the samples from the Early-Jurassic-age Sarki Formation fluctuate between 3 and 133 ppm, while the Cu values range from 2.2 to 56.6 ppm. The Sr values vary between 53 and 285 ppm, with the Rb values ranging from 1.0 to 18.4 ppm. The samples from the Sarki Formation also showed variable ranges for Ca (4.4–30.96%) and Al (0.08–5.93%).

The samples from the Early-Jurassic-age Sehkanyian Formation show some fluctuations for Ba (5–108 ppm), with the values for Cu (5.2–17.6 ppm) being lower than those of the Sarki Formation, while the Sr values vary between 62 and 137 ppm, and the Rb values range from 0.9 to 10.7 ppm. The ranges for Ca (8.85–24.46%) and Al (0.15–4.03%) were also variable.

The Ba values for the samples from the Middle-Jurassic-age Sargelu Formation fluctuate between 3 and 586 ppm (values that are considerably higher than the underlying formation). The values for Cu (3.7–87 ppm) are also higher than those measured for the underlying formation, with the Sr values ranging between 46 and 445 ppm being higher than those of the Sehkanyian Formation. The Rb values from the same formation that range from 0.4 to 51.8 ppm, are almost five times higher. The ranges of Ca (1.55–35.11%) and Al (0.03–4.71%) were also measured.

The Late Jurassic-age Naokelekan Formation shows some fluctuations for Ba (18.4–287 ppm), which are considerably lower than those of the underlying formation, while the amounts of Cu (4.51–61.4 ppm), Sr (145–504 ppm) and Rb (0.5–42.5 ppm) were also measured. The samples from the Naokelekan Formation also showed variable ranges for Ca (16.78–34.78%) and Al (0.04–4.18%).

The Ba values for the samples from the Late-Jurassic-age Barsarin Formation fluctuate between 7 and 649 ppm (values that are considerably higher than those of the underlying formation), with the values for Cu (1.2–11.2 ppm) being lower than those of the Naokelekan Formation. In contrast, the highest values for Sr (147.3–1007 ppm) are more than twice those measured for the underlying formation, while the maximum Rb values (0.3–7.2 ppm) are almost five times lower. The amounts of Ca (31.34–38.66%) recorded from the Barsarin Formation are consistently within the 30–40% range. The values for Al (0.04–0.71%), meanwhile, are low.

The samples from the Late Jurassic–Early Cretaceous-age Chia Gara Formation show some fluctuations for Ba (2–112 ppm) (values that are considerably lower than those of the underlying formation), whilst the Cu values (1.1–92.1 ppm) are higher than those of the Barsarin Formation. Sr values from the same formation vary from 274 to 1088 ppm, with the Rb values (1–52.9 ppm) being almost five times higher. The samples from the Chia Gara Formation also showed various ranges for Ca (15.67–36.73%) and Al (0.19–8.12%).

5. Discussion

The Lower Jurassic to Lower Cretaceous of Northern Iraq (Warte area) comprises six lithological units, namely, the Sarki, Sehkanyian, Sargelu, Naokelekan, Barsarin and Chia Gara formations. These formations represent the transition from the Early Jurassic (Sarki Formation) through to the Late Jurassic–Early Cretaceous (Chia Gara Formation). Lithologically, the Warte section succession comprises interbedded carbonates and shales with rare cherts. The carbonates, originally limestones, have since been wholly or partially altered to dolomites, particularly in the Sarki and Sehkanyian formations.

The following discussion investigates a few important points related to the successions, namely, their calcareous nannofossil biostratigraphy, paleoecology and paleoclimate conditions that prevailed during the Early Jurassic–Early Cretaceous of Northern Iraq.

5.1. Calcareous Nannofossil Biostratigraphy

As mentioned above, calcareous nannofossils are moderately to poorly preserved throughout the investigated interval, and thus, the precise determination of the ages of the various formation boundaries was not possible. This was due to the absence of specific age markers, for example, *Cyclagelosphaera weidmanni* Reale and Monechi. This species, absent from the studied section, is a marker species of the Middle Jurassic–Upper Jurassic boundary as it only common in the Callovian of the Tethys Realm [45]. Moreover, *Nannoconus steinmannii* subsp. *minor* Deres and Achéritéguy, which was also not found in the studied section, is the marker species for the Jurassic–Cretaceous boundary. Indeed, the species is considered to be the characteristic species of the Lower Cretaceous of the Tethys Realm [46,47].

Despite the lack of specific age markers noted above, some markers were recovered. For example, in the upper part of the Sargelu Formation, *Cyclagelosphaera margerelii*, *Watznaueria britannica*, *W. fossacincta* and *W. manivittiae* were all recorded for the first time. These species are indicative of the Bajocian Stage [45]. Furthermore, *Watznaueria barnesiae* indicative of the Bathonian Stage was also recovered [48,49]. In addition, the first occurrence of *Watznaueria ovata* is indicative of the Callovian Stage [48,50,51]. Thus, the age range for the Sargelu Formation is clearly Bajocian–Callovian.

5.2. Paleoclimate Proxies

As noted above, a range of geochemical proxies were measured from the various formations from NE Iraq in order to provide information about the paleoclimate at the time of deposition. The proxies used include Ca, Al, Sr/Ba, Rb/Sr and Sr/Cu (Table 3 and Figure 6) [38–40].

Table 3. Trace (in ppm) element concentrations, including geochemical proxies for paleoclimate conditions, Ca, Al, Sr/Ba, Rb/Sr and Sr/Cu, for the samples from the Sarki, Sehkanyian, Sargelu, Naokelekan, Barsarin and Chia Gara formations.

Formation	Sample No.	Ba (ppm)	Cu (ppm)	Sr (ppm)	Rb (ppm)	Ca (%)	Al (%)	Sr/Cu	Sr/Ba	Rb/Sr
Sarki	S1	4	4.3	87	6.8	17.74	0.36	20.23	21.75	0.08
Sarki	S2	7	6.2	77	10.2	17.01	0.94	12.42	11	0.13
Sarki	S6	103	18.8	102	10.1	6.21	4.83	5.43	0.99	0.09
Sarki	S8	122	24	96	18.4	4.91	5.27	4.00	0.79	0.19
Sarki	S10	30	9.4	105	9.3	14.35	1.49	11.17	3.50	0.09
Sarki	S12	8	3.2	113	11.3	17.06	0.95	35.31	14.13	0.1
Sarki	S18	133	22.4	100	13.3	4.4	5.93	4.46	0.75	0.13
Sarki	S21	102	49.8	53	11.6	4.32	5.77	1.06	0.52	0.22
Sarki	S26	6.0	5.19	203.1	1.0	30.96	0.08	39.13	33.85	0.005
Sarki	S28	88	17.2	116	8.9	10.51	4.64	6.74	1.32	0.08
Sarki	S31	115	56.6	285	12.8	15.32	2.02	5.04	2.48	0.04
Sarki	S36	3	2.2	79	2.5	21.26	0.21	35.91	26.33	0.03
Sarki	S37	24.9	12.28	61.1	3.3	14.49	0.22	4.98	2.45	0.05
Sehkanyian	S1	23	5.2	111	7.7	24.32	0.66	21.35	4.83	0.07
Sehkanyian	S2	7.2	4.93	108.3	0.9	17.69	0.25	21.97	15.04	0.008
Sehkanyian	S3	108	7.5	62	6.2	8.85	4.03	8.27	0.57	0.1
Sehkanyian	S6	74	13.2	82	9.1	8.87	3.35	6.21	1.11	0.11
Sehkanyian	S21	31	10.2	92	10.7	24.46	1.52	9.02	2.97	0.12
Sehkanyian	S30	6.2	14.92	101.5	2.0	17.60	0.15	6.80	16.37	0.02
Sehkanyian	S31	5	17.6	137	4.1	21.18	0.54	7.78	27.40	0.03
Sargelu	S1	3	18	112	1.7	21.86	0.29	6.22	37.33	0.02
Sargelu	S3	67	8.7	416	1.3	35.11	0.22	47.82	6.21	0.003
Sargelu	S4	5.0	10.39	164.4	0.9	31.57	0.11	15.82	32.88	0.005
Sargelu	S5	9	9.4	223	2.5	33.75	0.47	23.72	24.78	0.01
Sargelu	S6	65	10	367	2.9	31.19	0.23	36.70	5.65	0.008
Sargelu	S7	44	77.8	260	20.6	27.77	1.94	3.34	5.91	0.08
Sargelu	S8	23	50.7	194	8.9	22.17	1.38	3.83	8.43	0.05
Sargelu	S8	159	63.5	302	51.8	16.63	4.71	4.76	1.90	0.17
Sargelu	S9	24	27.4	286	9.5	30.35	1.44	10.44	11.92	0.03
Sargelu	S9	46	59.7	194	21.5	25.38	2.69	3.25	4.22	0.11
Sargelu	S10	586	5.8	317	5.2	32.97	0.55	54.66	0.54	0.02
Sargelu	S10	68	87	330	18.6	21.34	1.68	3.79	4.85	0.06
Sargelu	S11	7	14.3	46	8.7	1.55	0.15	3.22	6.57	0.19
Sargelu	S11	12	16	86	2	3.92	0.2	5.38	7.17	0.02
Sargelu	S11	38	54.6	445	16.5	19.66	1.37	8.15	11.71	0.04
Sargelu	S12	8	3.7	242	1.1	33.91	0.11	65.41	30.25	0.005
Sargelu	S13	139	41.5	293	21.1	18.79	1.68	7.06	2.11	0.07
Sargelu	S13	41.1	16.06	73.1	0.4	4.40	0.03	4.55	1.78	0.005
Sargelu	S13	77.5	14.34	256.9	1.6	21.23	0.12	17.91	3.31	0.006
Naokelekan	S1	140	56.5	251	30.7	16.78	2.2	4.44	1.79	0.12
Naokelekan	S2	89	16.1	399	5.9	34.05	0.42	24.78	4.48	0.01
Naokelekan	S3	23	7.2	145	2.7	34.78	0.22	20.14	6.30	0.02
Naokelekan	S4	124	44.3	504	18.1	27.75	1.29	11.38	4.06	0.04

Table 3. Cont.

Formation	Sample No.	Ba (ppm)	Cu (ppm)	Sr (ppm)	Rb (ppm)	Ca (%)	Al (%)	Sr/Cu	Sr/Ba	Rb/Sr
Naokelekan	S5	128.2	6.52	265.6	0.5	33.98	0.04	40.74	2.07	0.002
Naokelekan	S6	57	8.8	416	2.4	34.5	0.19	47.27	7.30	0.006
Naokelekan	S7	18.4	4.51	174.4	0.5	32.80	0.07	38.67	9.48	0.003
Naokelekan	S8	268	61.4	333	42.5	19.51	4.18	5.42	1.24	0.13
Naokelekan	S9	96.6	40.01	317.2	4.4	24.82	0.51	7.93	3.28	0.01
Naokelekan	S10	287	11.7	372	14.1	25.13	1.28	31.79	1.30	0.04
Barsarin	S1	649	1.2	446	1.1	38.07	0.16	371.67	0.69	0.002
Barsarin	S2	22	9.6	364	7.2	33.39	0.71	37.92	16.55	0.02
Barsarin	S3	27	5.5	1007	4.3	38.57	0.51	183.09	37.30	0.004
Barsarin	S4	4.2	4.23	241.4	0.5	33.16	0.05	57.07	57.48	0.002
Barsarin	S5	19	5.6	377	5.1	31.34	0.59	67.32	19.84	0.01
Barsarin	S6	7	4.2	269	2.5	38.66	0.46	64.05	38.43	0.009
Barsarin	S7	3.3	4.07	163.3	0.4	33.91	0.04	40.12	49.48	0.002
Barsarin	S8	4.0	3.02	147.3	0.3	33.50	0.04	48.77	36.83	0.002
Barsarin	S9	12	11.2	391	4.4	36.91	0.63	34.91	32.58	0.01
Chia Gara	S1	102	75.9	764	52.9	10.04	8.12	10.07	7.49	0.07
Chia Gara	S2	27	21.9	761	11.6	35.78	1.77	34.75	28.19	0.02
Chia Gara	S3	10	7.2	314	1.4	33.22	0.28	43.61	31.40	0.004
Chia Gara	S4	112	92.1	1088	51.7	15.67	6.79	11.81	9.71	0.05
Chia Gara	S5	25	7.8	274	5.5	36.73	0.94	35.13	10.96	0.02
Chia Gara	S6	54	58.3	549	22	25.61	3.39	9.42	10.17	0.04
Chia Gara	S7	2	1.1	321	1	30.06	0.19	291.82	160.50	0.003

The inverse relationship between the Ca and Al contents has been used by a range of authors as a proxy for both salinity and/or aridity [15,41]. In general, the values measured from the various formations show an overall increase in Ca content (e.g., 15.32, 25.13, 38.66), moving up through the stratigraphy (i.e., from the basal Sarki Formation through to the Chia Gara Formation at the top) with a corresponding decrease in Al content (e.g., 2.02, 1.28, 0.46) (see Table 3). The increase in Ca and the corresponding decrease in Al would suggest that deposition occurred under arid conditions [17,41]. Interestingly, a recent study on the petrography and geochemistry of the Middle–Upper Jurassic Banik section from northernmost Iraq (a region that is located close to the northwestern boundary of the Warte section) suggested that the deposition of the Middle–Upper Jurassic formations occurred under arid conditions [17]. This conclusion was based on the results obtained from selected geochemical proxies for evaporitic conditions, including the inverse relationship between the Ca and Al contents.

The high Sr/Ba ratio values were also interpreted in terms of salinity and/or aridity [40]. According to Wang et al. (2017), high Sr/Ba ratio values can indicate high salinity and/or arid climates, whilst low Sr/Ba ratio values suggest low salinity and/or humid climates. Relatively high values of Sr/Ba ratio are recorded within the samples in this study (e.g., 5.65, 38.43, 160.50) (see Table 3), which may indicate an arid climate and high salinity conditions during the time of their deposition.

A number of authors, including Yandoka et al. and Song et al., have suggested that the Sr/Cu ratio can be used as an indicator of paleoclimate conditions [52,53]. According to these authors, the ratio values of Sr/Cu, which ranges from 1.3–5, indicate a warm humid climate, whilst values of >5 indicate a hot and arid climate. High Sr/Cu values (i.e., >5) were observed from the samples of the Sarki, Sehkanyian, Sargelu, Naokelekan, Barsarin and Chia Gara formations (see Table 3). Thus, the climate was most probably hot and arid. These results agree with the results obtained from the Sr/Ba ratio (see above).

The inverse relationship between the Sr/Cu ratio and the Rb/Sr ratio values are also used as paleoclimatic indications [38,39]. Within the samples of the Sarki, Sehkanyian, Sargelu, Naokelekan, Barsarin and Chia Gara formations, the Sr/Cu ratio values increase (e.g., 20.23, 67.32, 183.09) with a consistent decrease in the Rb/Sr ratio values (e.g., 0.34, 0.08, 0.02) (see Table 3). The inverse relationship between the two ratios (i.e., Sr/Cu and Rb/Sr) would suggest that the depositional area underwent a warm climate during the deposition of the Sarki, Sehkanyian, Sargelu, Naokelekan, Barsarin and Chia Gara formations [38,39]. Similarly, Al-Lhaebi et al. examined the Cenomanian–Turonian boundary of the Gulneri

Formation in the Azmir, Dokan and Degala sections in Northern Iraq using some selected geochemical data, including Rb/Sr, Sr/Cu and Sr/Ba ratios, and suggested that warm and arid conditions were predominant in the Cenomanian–Turonian transition [3]. Another study used Rb/Sr, Sr/Cu and Sr/Ba ratios as paleoclimate and paleosalinity indicators in their mineralogical and geochemical study of the Late Triassic Baluti Formation in the Baluti (formerly Zewa) village in northern Iraq [54]. They also suggested that the climate during the time of deposition of the Baluti sediments was hot and arid to semi-arid.

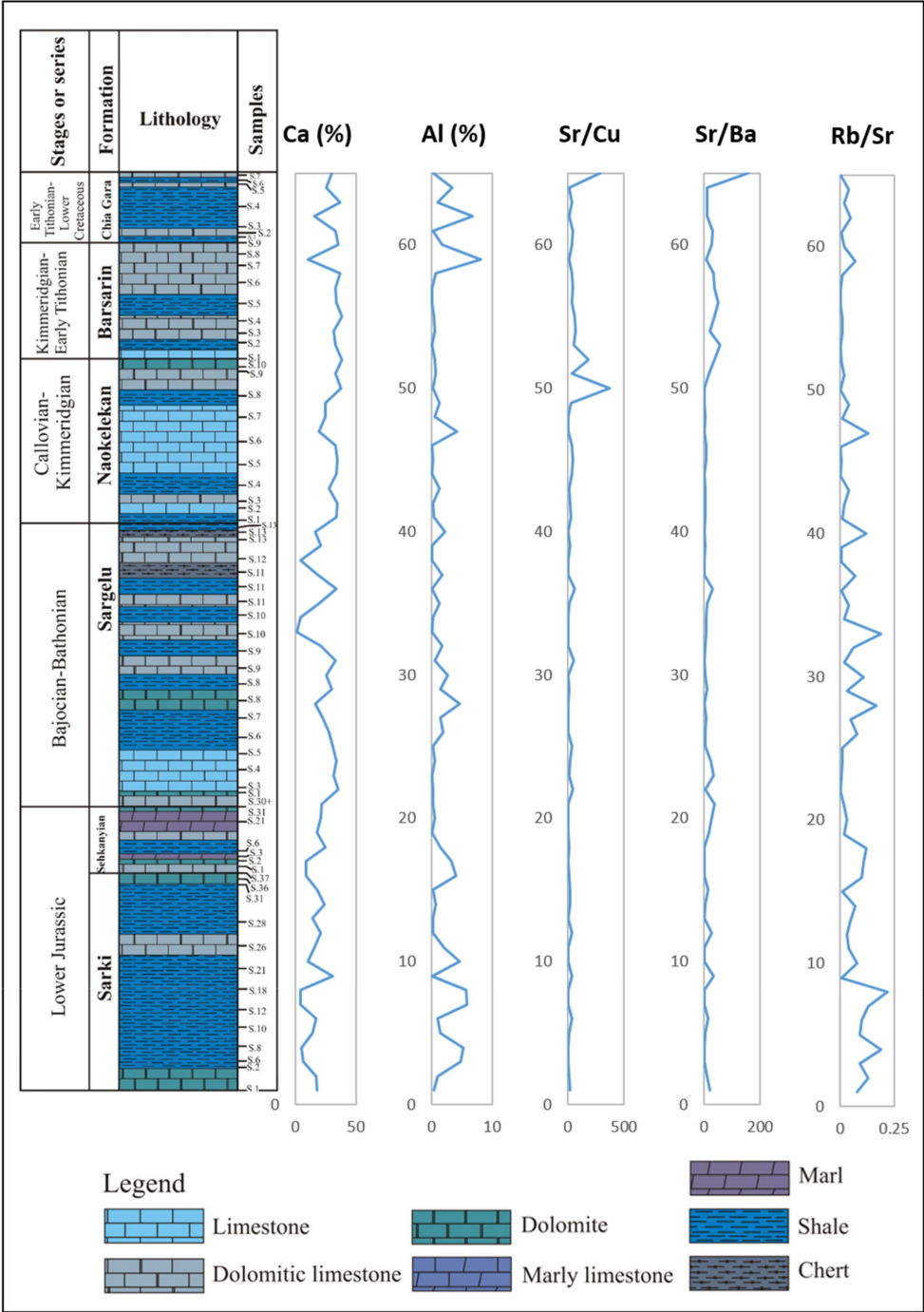


Figure 6. Chart showing geochemical proxies for paleoclimate conditions along the measured log of the Warte section, northeastern Iraqi Kurdistan.

In summary, the analysis of the various elemental ratios used in this study would suggest that the climate at the time of deposition was one that was warm and arid. Furthermore, these conditions prevailed throughout much of the Jurassic and extended into the Early Cretaceous. The aridity of the Jurassic correlates well with the dominance of warming that characterized the Jurassic period globally [55,56]. In addition, the deposition of the upper part of the Early-Cretaceous-age Qamchuqa Formation in northeastern Iraq coincided with increased temperatures and salinities in the region, related to restriction of circulation [57].

5.3. Paleoecological Proxies

Calcareous nannofossils and geochemical analyses were used to reconstruct the paleoecological conditions of the depositional area of the Sarki, Sehkanyian, Sargelu, Naokelekan, Barsarin and Chia Gara formations, including examination of water temperatures and salinities.

According to Svobodová and Košťák [58], calcareous nannofossils can provide important information about the paleoecological conditions of the depositional settings, in terms of water temperature and salinity [59–62]. The calcareous nannofossil *Watznaueria manivitiae* is considered by a variety of authors to be indicative of warm waters [63,64], and thus, the increase in the number of *Watznaueria manivitiae* (see above) may indicate episodes of water warming.

In addition to geochemical proxies, oxygen isotope analysis was also used. Oxygen isotopes have been used by a variety of authors to indicate ancient water temperatures [5–7]. In general, negative values are considered to be indicative of warm waters [5–7], while positive values are indicative of cool waters. As noted above, the values from the various formations of NE Iraq are all negative, with one exception. The lowermost sample from the Sarki Formation is slightly positive (Table 2 and Figure 7). This persistence of negative oxygen isotope values from the Early Jurassic–Early Cretaceous-age formations of NE Iraq in this study resembles the results obtained for the same stratigraphic interval in the Duhok Governorate of NW Iraq. There, the results were interpreted as being indicative of warm waters during the period [65].

As noted above, calcareous nannofossils can also provide important information regarding ancient water salinities. According to Tremolada et al. and Abdula, the presence of the nannofossil *Cyclagelosphaera margerelii* is considered to be indicative of high salinities [14,66]. In four of the formations from NE Iraq (i.e., Sargelu, Naokelekan, Barsarin and Chia Gara), up to 38% of the recovered nannofossil species were *Cyclagelosphaera margerelii*, which is suggestive of high salinities at that time.

Values of the trace element Sr have been used by a number of authors as a proxy for salinity and/or evaporation conditions [17,42–44]. According to these authors, increased Sr values are considered to be indicative of high salinity and/or evaporation conditions within the depositional setting. High Sr values were noted from the samples of the Sarki, Sehkanyian, Sargelu, Naokelekan, Barsarin and Chia Gara formations of NE Iraq (e.g., 82, 223, 504) (see Table 3 and Figure 7), which would suggest that both salinities and evaporation rates within the depositional area were high. Omar et al. has also suggested that salinity conditions and rates of evaporation (controlled by arid climate) were high within the depositional area of the Middle–Late Jurassic-age Sargelu and Naokelekan formations in northernmost Iraq [17]. This suggestion was based on the observed high Sr values within the samples of these Middle–Upper Jurassic formations.

In conclusion, these paleoecological findings correspond strongly with those from the paleoclimate proxies as detailed above; therefore, this study suggests that the deposition of the Sarki, Sehkanyian, Sargelu, Naokelekan, Barsarin and Chia Gara formations of NE Iraq occurred under arid conditions, with elevated salinities and high evaporation rates. These environmentally stressful conditions may also explain the poor preservation of the calcareous nannoplankton specimens throughout the entire investigated interval.



Calcareous nannofossils from the Lower Jurassic to Lower Cretaceous succession of the Warte section from northeastern Iraqi Kurdistan region were investigated for the first time. The calcareous nannoplankton are moderately to poorly preserved in the Warte sediments. The recovered nannofossil assemblages were recorded from the Middle Jurassic–Early Cretaceous-age Sargelu, Naokelekan, Barsarin and Chia Gara formations, including *W. barnesiae*, *W. fossacincta*, *W. britannica*, *W. manivitiae* and *C. margerelii*, whilst the Early-Jurassic-age Sarki and Sehkanyian formations were barren.

102

More detailed geochemical analyses, including oxygen isotopes and paleoclimate and paleoecological proxies, indicated warm and arid conditions prevailing during the Early Jurassic–Early Cretaceous transition.

Author Contributions: Conceptualization, N.O., T.M. and A.I.A.-J.; methodology, N.O., T.M. and A.I.A.-J.; validation, N.O., T.M., A.I.A.-J. and M.A.U.; formal analysis, N.O., T.M. and M.A.U.; investigation, N.O., A.I.A.-J. and A.O.S.; resources, N.O., A.I.A.-J. and A.O.S.; writing—original draft preparation, N.O.; writing—review and editing, N.O., T.M., A.I.A.-J. and M.A.U.; supervision, T.M. and A.I.A.-J.; funding acquisition, N.O. All authors have read and agreed to the published version of the manuscript.

Funding: This work was supported by the Arab-German Young Academy of Sciences and Humanities (AGYA) that is funded under the German Ministry of Education and Research (BMBF) grant 01DL20003.

Data Availability Statement: Not applicable.

Conflicts of Interest: The authors declare no conflict of interest.

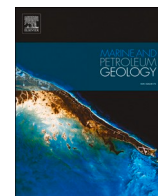
References

1. Mutterlose, J.; Bottini, C. Early Cretaceous chalks from the North Sea giving evidence for global change. *Nat. Commun.* **2013**, *4*, 1686. [\[CrossRef\]](#)
2. Reolid, M.; Emanuela, M.; Nieto, L.M.; Rodríguez-Tovar, F.J. The Early Toarcian Oceanic Anoxic Event in the External Subbetic (Southiberian Paleomargin, Westernmost Tethys): Geochemistry, nannofossils and ichnology. *Paleogeogr. Paleoclimatol. Paleoecol.* **2014**, *411*, 79–94. [\[CrossRef\]](#)
3. Al-Lhaebi, S.F.; Al-Badrani, O.A.; Al-Juboury, A.I.; Mahanipour, A. Paleoclimatic insights on the Cenomanian-Turonian Oceanic Anoxic Event (OAE2) from Northern Iraq based on calcareous nannofossils and geochemical data. *Iraqi Geol. J.* **2020**, *53*, 68–86. [\[CrossRef\]](#)
4. Al-Miarny, F.A.; Al-Badrani, O.A.; Al-Juboury, A.I. Calcareous nannofossils and chemostratigraphy of the Early Aptian Oceanic Anoxic Event 1a from Northern Iraq. *Bull. Iraq Nat. Hist. Mus.* **2020**, *16*, 363–379. [\[CrossRef\]](#)
5. Bartolini, A.; Pittet, B.; Mattioli, E.; Hanziker, J.C. Shallow-platform paleoenvironmental conditions recorded in deep-shelf sediments: C and O stable isotopes in Upper Jurassic sections of southern Germany (Oxfordian–Kimmeridgian). *Sediment. Geol.* **2003**, *160*, 107–130. [\[CrossRef\]](#)
6. Weissert, H.; Erba, E. Volcanism CO₂ and paleoclimate: A late Jurassic—Early Cretaceous carbon and oxygen isotopes record. *J. Geol. Soc. Lond.* **2004**, *161*, 695–702. [\[CrossRef\]](#)
7. Ruf, M.; Link, E.; Pross, J.; Aigner, T. Integrated sequence stratigraphy: Facies, stable isotope, and palynofacies analysis in a deeper epicontinental carbonate ramp (Late Jurassic, SW Germany). *Sediment. Geol.* **2005**, *175*, 391–414. [\[CrossRef\]](#)
8. Mahanipour, A.; Mutterlose, J.; Eftekhari, M. Calcareous nannofossils of the Barremian—Aptian interval from the southeastern Tethys (Zagros Basin, West Iran) and their paleoceanographic implications: A record of Oceanic Anoxic Event 1a. *Mar. Micropaleontol.* **2019**, *149*, 64–74. [\[CrossRef\]](#)
9. Daoud, H.S.; Karim, K.H. Types of stromatolites in the Barsarin Formation (late Jurassic), Barzinja area, NE Iraq. *Iraqi Bull. Geol. Min.* **2006**, *6*, 47–57.
10. Al-Ameri, T.K.; Zumberge, J. Middle and Upper Jurassic hydrocarbon potential of the Zagross Fold Belt, North Iraq. *Mar. Pet. Geol.* **2012**, *36*, 13–34. [\[CrossRef\]](#)
11. Al-Juboury, A.I.; McCann, T. Petrological and geochemical interpretation of Triassic-Jurassic boundary sections from North Iraq. *Geol. J.* **2013**, *50*, 157–172. [\[CrossRef\]](#)
12. Jasim, S.Y. The potential of hydrocarbons generation in the Chia Gara Formation at Amadia area, north of Iraq. *Arab. J. Geosci.* **2013**, *6*, 3313–3318. [\[CrossRef\]](#)
13. Abdula, R. Source rock assessment of Naokelekan formation in Iraqi Kurdistan. *JZS Part A* **2017**, *19*, 103–124. [\[CrossRef\]](#)
14. Abdula, R.A. Stratigraphy and lithology of Naokelekan Formation in Iraqi Kurdistan Review. *Int. J. Eng. Sci.* **2016**, *5*, 7–17.
15. Wimbledon, W.A.P.; Mohialdeen, I.M.J.; Andreini, G.; Rehakova, D.; Stoykova, K. The Jurassic /Cretaceous boundary beds in Kurdistan—a preliminary note on wider correlations. *JZS Spec. Issue GeoKurd.* **2016**, *2*, 269–276. [\[CrossRef\]](#)
16. Liu, X.; Wen, Z.; Wang, Z.; Song, C.; He, Z. Structural characteristics and main controlling factors on petroleum accumulation in Zagros Basin, Middle East. *J. Nat. Gas. Geosci.* **2018**, *5*, 273–281. [\[CrossRef\]](#)
17. Omar, N.; McCann, T.; Al-Juboury, A.I.; Franz, S.O. Petrography and geochemistry of the Middle-Upper Jurassic Banik section, northernmost Iraq—implications for paleoredox, evaporitic and diagenetic conditions. *N. Jb. Geol. Paleont. Abh.* **2020**, *297*, 125–152. [\[CrossRef\]](#)
18. Omar, N.; McCann, T.; Al-Juboury, A.I.; Suárez-Ruiz, I. Solid bitumen in shales from the Middle to Upper Jurassic Sargelu and Naokelekan Formations of northernmost Iraq: Implication for reservoir characterization. *Arab. J. Geos.* **2021**, *14*, 755. [\[CrossRef\]](#)

19. Beydoun, Z.R.; Clarke, M.W.H.; Stoneley, R. Petroleum in the Zagros Basin a Late Tertiary foreland basin overprinted onto the outer edge of a vast hydrocarbon-rich Paleozoic Mesozoic passive margin shelf. In *Foreland Basins and Fold Belts*; MacQueen, R.W., Leckie, D.A., Eds.; AAPG Memoir: Tulsa, OK, USA, 1992; Volume 55, pp. 309–339. [\[CrossRef\]](#)
20. Talbot, C.J.; Alavi, M. The past of a future syntax is across the Zagros. In *Salt Tectonics*; Alsop, G.I., Blundell, D.J., Davison, I., Eds.; Special Publication; Geological Society: London, UK, 1996; Volume 100, pp. 89–109. [\[CrossRef\]](#)
21. Stampfli, G.M.; Borel, G.D. A plate tectonic model for the Paleozoic and Mesozoic constrained by dynamic plate boundaries and restored synthetic oceanic isochrons. *Earth Planet. Sci. Lett.* **2002**, *196*, 17–33. [\[CrossRef\]](#)
22. Bellen, R.C.V.; Dunnington, H.V.; Wetzel, R.; Morton, D.M. *Asie, Fascicule 10a Iraq*; Lexique Stratigraphic International: Paris, France, 1959; Volume 3, p. 333.
23. Numan, N.M.S. Major cretaceous tectonic events in Iraq. *Raf. J. Sci.* **2000**, *11*, 32–52.
24. Jassim, S.Z.; Goff, J.C. *Geology of Iraq*; Dolin, Prague & Moravian Museum: Brno, Czech Republic, 2006; p. 352.
25. Fouad, S.F.A. *Tectonic Map of Iraq, Scale 1: 1000,000*, 3rd ed.; Iraqi Bulletin of Geology and Mining: Baghdad, Iraq, 2015; Volume 11, pp. 1–7.
26. Balaky, S.M.; Asaad, I.S.; Al-Juboury, A.I. Facies analysis and sequence stratigraphy of Kometan Formation (Upper Cretaceous) in the imbricated zone, northeastern Iraq. *Arab. J. Geosci.* **2016**, *9*, 747. [\[CrossRef\]](#)
27. Dunnington, H.V. Generation, migration, accumulation and dissipation of oil in Northern Iraq. In *Habitat of Oil, a Symposium; Weeks*; American Association of Petroleum Geologists: Tulsa, OK, USA, 1958; pp. 1194–1251.
28. Wetzel, R.; Morton, D.M.; Formation, S.; Van Bellen, R.C.; Dunnington, H.V.; Wetzel, R.; Morton, D.M. (Eds.) *Paris, III, Asie, Fascicule 10a Iraq*; Lexique Stratigraphic International: Paris, France, 1950; pp. 211–215.
29. Sissakian, V.K. Geological Maps in the Kurdistan Region. *UKH J. Sci. Eng.* **2018**, *2*, 39–42. [\[CrossRef\]](#)
30. Al-Omari, F.S.; Sadiq, A. *Geology of Northern Iraq: Mosul, Iraq*; Mosul University Press: Mosul, Iraq, 1977; p. 198.
31. Jassim, S.Z.; Buday, T. Late Toarcian-Early Tithonian (Mid-Late Jurassic) Megasequence AP7. In *Geology of Iraq*; Jassim, S.Z., Goff, J.C., Eds.; Moravian Museum: Brno, Prague, 2006; pp. 117–123.
32. Buday, T. *The Regional Geology of Iraq. Stratigraphy and Palaeogeography*; Publication of GEOSURV: Baghdad, Iraq, 1980; Volume 1, p. 445.
33. Fisher, J.K.; Price, G.D.; Hart, M.B.; Leng, M.J. Stable isotope analysis of the Cenomanian-Turonian (Late Cretaceous) oceanic anoxic event in the Crimea. *Cretac. Res.* **2005**, *26*, 853–863. [\[CrossRef\]](#)
34. Allan, J.R.; Matthews, R.K. Isotope signatures associated with early meteoric diagenesis. *Sedimentology* **1982**, *29*, 797–817. [\[CrossRef\]](#)
35. Azmy, K.; Poty, E.; Brand, U. High-resolution isotope stratigraphy of the Devonian–Carboniferous boundary in the Namur–Dinant Basin, Belgium. *Sediment. Geol.* **2009**, *216*, 117–124. [\[CrossRef\]](#)
36. Li, X.; Wei, Y.; Li, Y.; Zhang, C. Carbon isotope records of the early Albian oceanic anoxic event (OAE) 1b from eastern Tethys (southern Tibet, China). *Cretac. Res.* **2016**, *62*, 109–121. [\[CrossRef\]](#)
37. Hennhofer, D.; Al Suwaidi, A.; Bottini, C.; Helja, E.; Steuber, T. The Albian to Turonian carbon isotope record from the Shilaif Basin (United Arab Emirates) and its regional and intercontinental correlation. *Sedimentology* **2018**, *66*, 536–555. [\[CrossRef\]](#)
38. Sinha, R.; Smykatz-Kloss, W.; Stüben, D.; Harrison, S.P.; Berner, Z.; Kramar, U. Late Quaternary paleoclimatic reconstruction from the lacustrine sediments of the Sambhar playa core, Thar Desert margin, India. *Paleogeogr. Paleoclimatol. Paleocol.* **2006**, *233*, 252–270. [\[CrossRef\]](#)
39. Xu, H.; Liu, B.; Wu, F. Spatial and temporal variations of Rb/Sr ratios of the bulk surface sediments in Lake Qinghai. *Geochem. Trans.* **2010**, *11*, 1–8. [\[CrossRef\]](#)
40. Wang, Z.; Fu, X.; Feng, X.; Song, C.; Wang, D.; Chen, W.; Zeng, S. Geochemical features of the black shales from the Wuyu Basin, southern Tibet: Implications for paleoenvironment and paleoclimate. *Geol. J.* **2017**, *52*, 282297. [\[CrossRef\]](#)
41. Orhan, H.; Delikan, A.; Demir, A.; Kapan, S.; Olgun, K.; Özmen, A.; Sayin, Ü.; Ekici, G.; Aydin, H.; Nazik, A. Geochemical evidences of paleoenvironmental changes in Late Quaternary lacustrine sediments of the Konya Closed Basin (Konya, Turkey). In *Patterns and Mechanisms of Climate, Paleoclimate and Paleoenvironmental Changes from Low Latitude Regions*; Zhang, Z., Khelifi, N., Mezghani, A., Heggy, E., Eds.; Springer: Berlin, Germany, 2019; pp. 73–76. [\[CrossRef\]](#)
42. Read, J.F.; Kerans, C.; Weber, L.J.; Sarg, H.F.; Wright, F.M. Milankovitch sea level changes, cycles and reservoirs on carbonate platforms in greenhouse and ice-house worlds. *SEPM Soc. Sediment. Geol.* **1995**, *35*, 1–81. [\[CrossRef\]](#)
43. Price, G.D. The evidence and implications of polar ice during the Mesozoic. *Earth Sci. Rev.* **1999**, *48*, 183–210. [\[CrossRef\]](#)
44. Vincent, B.; Rambeau, C.; Emmanuel, L.; Loreaue, J.P. Sedimentology and trace element geochemistry of shallow-marine carbonates: An approach to paleoenvironmental analysis along the Pagny-sur-Meuse Section (Upper Jurassic, France). *Facies* **2006**, *52*, 69–84. [\[CrossRef\]](#)
45. Gradstein, F.M.; Ogg, J.G.; Schmitz, M.; Ogg, G. *Geologic Time Scale 2020*, 1st ed.; Elsevier: Amsterdam, The Netherlands, 2020; p. 1357. [\[CrossRef\]](#)
46. Bralower, T.J.; Monechi, S.; Thierstein, H.R. Calcareous nannofossil zonation of the Jurassic-Cretaceous boundary interval and correlation with the geomagnetic polarity timescale. *Mar. Micropaleontol.* **1989**, *14*, 153–235. [\[CrossRef\]](#)
47. Bown, P.R.; Cooper, M.K.E. Jurassic. In *Calcareous Nannofossil Biostratigraphy*; British Micropaleontological Society Publication Series; Springer: Berlin, Germany, 1998; pp. 34–85.

48. Grün, W.; Zweili, F. Das kalkige Nannoplankton der Dogger-Malm-Grenze im Berner Jura bei Liesberg (Schweiz). *Jb. Geol. B-A* **1980**, *123*, 231–341.
49. Gollain, G.; Mattioli, E.; Kenjo, S.; Bartolini, A.; Reboulet, S. Size patterns of the coccolith *Watznaueria barnesia* in the lower Cretaceous: Biotic versus abiotic forcing. *Mar. Micropaleontol.* **2019**, *152*, 101740. [[CrossRef](#)]
50. Rai, J.; Garg, R. Early Callovian nannofossils from the Kuldhar section, Jaisalmer, Rajasthan. *Curr. Sci.* **2007**, *92*, 816–820.
51. Jain, S.; Singh, A. First calcareous nannofossil record from the Jurassic strata exposed in the Blue Nile Basin (Ethiopia). *J. Afr. Earth Sci.* **2019**, *158*, 103553. [[CrossRef](#)]
52. Yandoka, B.M.S.; Abdullah, W.H.; Abubakar, M.B.; Hakimi, M.H.; Adegoke, A.K. Geochemical characterization of early Cretaceous lacustrine sediments of Bima Formation, Yola Sub-basin, northern Benue trough, NE Nigeria: Organic matter input, preservation, paleoenvironment and paleoclimatic conditions. *Mar. Petrol. Geol.* **2015**, *61*, 82–94. [[CrossRef](#)]
53. Song, Y.; Liu, Z.; Meng, Q.; Xu, J.; Sun, P.; Cheng, L.; Zheng, G. Multiple controlling factors of the enrichment of organic matter in the upper cretaceous oil shale sequences of the Songliao basin, NE China: Implications from geochemical analyses. *Oil Shale* **2016**, *33*, 142–166. [[CrossRef](#)]
54. Hussain, S.H.; Al-Juboury, A.I.; Al-Haj, M.A.; Armstrong-Altrin, J.S.; Al-Lhaebi, S.F. Mineralogy and geochemistry of the Late Triassic Baluti Formation, Northern Iraq. *J. Afr. Earth Sci.* **2021**, *181*, 104243. [[CrossRef](#)]
55. Hallam, A. The Jurassic climate. In *Climate in Earth History: Studies in Geophysics*; The National Academies Press: Washington, DC, USA, 1982; pp. 159–163. [[CrossRef](#)]
56. Chao, H.; Hou, M.; Jiang, W.; Cao, H.; Chang, X.; Luo, W.; Ogg, J.G. Paleoclimatic and Redox Condition Changes during Early-Middle Jurassic in the Yili Basin, Northwest China. *Minerals* **2021**, *11*, 675. [[CrossRef](#)]
57. Ameen, B.M.; Karim, K.H. Depositional Environment of Early Cretaceous Arabian Platform: An example from Kurdistan Region, NE-Iraq. In Proceedings of the 3rd Scientific Conference of the College of Science, University of Baghdad, Baghdad, Iraq, 24–26 March 2009; pp. 1949–1961.
58. Svobodová, A.; Košťák, M. Calcareous nannofossils of the Jurassic/Cretaceous boundary strata in the Puerto Escaño section (southern Spain)—Biostratigraphy and paleoecology. *Geol. Carpath.* **2016**, *67*, 223–238. [[CrossRef](#)]
59. Erba, E. Middle Cretaceous calcareous nannofossils from the western Pacific (Leg 129): Evidence for paleoequatorial crossings. In *Proceedings of the Ocean Drilling Program, Scientific Results*; Texas A&M University: College Station, TX, USA, 1992; Volume 129, pp. 189–201. [[CrossRef](#)]
60. Tremolada, F.; Erba, E.; Bralower, T.J. Late Barremian to early Aptian calcareous nannofossils paleoceanography and paleoecology from the Ocean Drilling Program Hole 641C (Calicia Margin). *Cretac. Res.* **2006**, *27*, 887–897. [[CrossRef](#)]
61. Aguado, R.; O'Dogherty, L.; Sandoval, J. Fertility changes in surface waters during the Aalenian (mid-Jurassic) of the Western Tethys as revealed by calcareous nannofossils and carbon-cycle perturbations. *Mar. Micropaleontol.* **2008**, *68*, 268–285. [[CrossRef](#)]
62. Mattioli, E.; Pittet, B.; Suan, G.; Mailliot, S. Calcareous nannoplankton changes across the early Toarcian oceanic anoxic event in the western Tethys. *Paleoceanography* **2008**, *23*, PA3208. [[CrossRef](#)]
63. Tremolada, F.; Erba, E.; van de Schootbrugge, B.; Mattioli, E. Calcareous nannofossil changes during the late Callovian–early Oxfordian cooling phase. *Mar. Micropaleontol.* **2006**, *59*, 197–209. [[CrossRef](#)]
64. Giraud, F. Calcareous nannofossil productivity and carbonate production across the Middle-Late Jurassic transition in the French Subalpine Basin. *Geobios* **2009**, *42*, 699–714. [[CrossRef](#)]
65. AL-Badry, A.M.S. Stratigraphy and Geochemistry of Jurassic Formations in Selected Sections—North Iraq. Ph.D. Thesis, College of Science, University of Baghdad, Baghdad, Iraq, 2012; p. 162.
66. Tremolada, F.; Bornemann, A.; Bralower, T.J.; Koeberl, C.; van de Schootbrugge, B. Paleooceanographic changes across the Jurassic/Cretaceous boundary—The calcareous phytoplankton response. *Earth Planet. Sci. Lett.* **2006**, *241*, 361–371. [[CrossRef](#)]

Appendix B



A comparative study of the paleoclimate, paleosalinity and paleoredox conditions of Lower Jurassic-Lower Cretaceous sediments in northeastern Iraq

Nagham Omar^{a,*}, Tom McCann^a, Ali I. Al-Juboury^b, Sven Oliver Franz^a, Giovanni Zanoni^c, Harry Rowe^c

^a Institut für Geowissenschaften, Geologie, University of Bonn, Nussallee 8, 53115, Bonn, Germany

^b Petroleum Engineering Department, College of Engineering, Al-Kitab University, Kirkuk, Iraq

^c Premier Corex Laboratories, Houston, TX, 77041, USA

ARTICLE INFO

Keywords:

Geochemistry

Anoxia

Depositional conditions

Paleoclimate

Jurassic

NE Iraq

ABSTRACT

The findings of this study are considered to be of great importance given their singularity in northeastern (NE) Iraq, as the first broader study that discusses various paleoenvironmental proxies (i.e., paleoclimate, paleosalinity and paleoredox proxies) which were predominant during the Early Jurassic-Early Cretaceous period of NE Iraq. To this end, a comparative study of the mineralogical and geochemical features of the Sarki, Sehkanyan, Sargelu, Naokelekan, Barsarin and Chia Gara formations from the Early Jurassic-Early Cretaceous-age Ranya section, was carried out together with a study of the same formations from the Warte section (both sections are located in NE Iraq). Petrographic and microfacies analyses show that all six formations in both sections were deposited in tidal flat (supratidal), restricted lagoons and shallow marine to bathyal depositional environments. The paleoclimate proxies (Ca, Al, Sr/Ba, Rb/Sr and Sr/Cu) and paleosalinity proxies (Sr, Ca, Al and Sr/Ba) together with oxygen isotopes, suggest that the climate was predominantly hot and arid during the period of deposition, contrasting with periods of warm and humid climates during the deposition of the Late Jurassic-Early Cretaceous-age Chia Gara Formation. This climatic change was revealed by a shift in clay mineralogy, from a dominance of illite to increasing amounts (and even dominance) of kaolinite marking the change to more humid conditions within the Late Jurassic-Early Cretaceous period. Geochemical proxies for redox conditions (U/Th, V/Cr, Ni/Co, V/Sc and V/(V+Ni)) indicate that deposition of the sediments in the examined areas occurred under anoxic (or reduced oxygen) conditions. This difference in paleoclimate, paleosalinity and paleoredox conditions is likely to be controlled by tectonic activity in the region of northern Iraq, with the development of small silled sub-basins within the broader Zagros Basin/Zagros Fold Belt.

1. Introduction

The Jurassic-Lower Cretaceous successions of Iraq are considered to be of great importance (e.g., Daoud and Karim, 2006; Al-Ameri and Zumberge, 2012; Al-Juboury and McCann, 2013; Jasim, 2013; Abdula, 2017) given the fact that most of the petroleum, which was discovered in Iraq, has been sourced from the Jurassic-age rocks and trapped in the Cretaceous- and Tertiary-age reservoirs of the Mesopotamian Basin and the Zagros Basin/Zagros Fold Belt (Pitman et al., 2004). The studied Early Jurassic-Early Cretaceous-age Warte and Ranya sections are located within the Zagros Basin/Zagros Fold Belt, NE Iraq. According to

Sadooni (1997), Al-Ameri and Zumberge (2012), Mohialdeen et al. (2013), Hakimi et al. (2018), and Tobia et al. (2019), most of the discovered oil in northern Iraq was sourced from the Middle Jurassic-age Sargelu Formation, Late Jurassic-age Naokelekan Formation, and Late Jurassic-Early Cretaceous-age Chia Gara Formation. Thus, understanding the paleoenvironmental conditions, in which the Jurassic-Lower Cretaceous successions are found, would provide important information for future hydrocarbon exploration studies since the Jurassic system in Iraq is highly promising harboring great potential in this respect.

Reconstructing paleoclimates, paleosalinities and paleoredox conditions is a major aim of paleoenvironmental reconstructions (Jones and

* Corresponding author.

E-mail address: s6naomar@uni-bonn.de (N. Omar).

<https://doi.org/10.1016/j.marpetgeo.2023.106430>

Received 23 January 2023; Received in revised form 23 July 2023; Accepted 26 July 2023

Available online 30 July 2023

0264-8172/© 2023 Elsevier Ltd. All rights reserved.

Manning, 1994; Tribouvillard et al., 2006; Wang et al., 2020; Men et al., 2022; Li et al., 2023). Knowledge about paleoenvironmental conditions is essential for reconstructing how the oxygenation, climatic changes and paleosalinity of the Earth's surface environment have changed through time (Severmann and Anbar, 2009).

The geochemical features of specific major and trace elements and/or some of their elemental ratios have been utilized by many authors (e.g., Cullers, 1995; Canet et al., 2004; Gao et al., 2017; Ivanić et al., 2017; Qin et al., 2018; Hussain et al., 2021; Fathy et al., 2023) to provide important information about the paleoenvironmental conditions during deposition. In addition, some ratios of rare earth and trace elements have also been used to understand the variations in paleoredox conditions in both modern marine sediments and ancient rocks (Calvert and Pedersen, 1993; Kimura and Watanabe, 2001; Algeo and Maynard, 2004; Rimmer, 2004; Fu et al., 2010; Madhavaraju et al., 2015). Other authors have used mineralogical studies (XRD, SEM and EDX analyses) of clay minerals as evidence to trace climatic conditions due to the effects of weather conditions and the paleoclimate on these minerals in the source area (e.g., Chamley, 1989; Ruffell et al., 2002; Cao et al., 2012; Madhavaraju et al., 2016; Liu et al., 2021; Hussain et al., 2021).

Certain isotopes (e.g., carbon and oxygen isotopes) can be used to provide insights into paleoenvironmental conditions (e.g., Bartolini et al., 2003; Weissert and Erba, 2004; Ruf et al., 2005; Fisher et al., 2005; Li et al., 2016; Hennhoefer et al., 2018; Afrozi et al., 2021). More recently, we examined the calcareous nannofossil biostratigraphy and related this to the isotopic and inorganic geochemistry of the Warte section in NE Iraq (Omar et al., 2022). Although such studies are relatively common, there is, however, to date, a lack of broader comparative geochemical studies of the Jurassic-Cretaceous successions of Iraq.

The studied sections are located at the towns of Warte and Ranya, NE Iraq. Both the Warte and Ranya sections comprise six formations. The lowermost formations (Sarki, Sehkanyian) represent the Early Jurassic, the Middle Jurassic Formation (Sargelu), the Upper Jurassic formations (Naokelekan, Barsarin) with the uppermost Formation (Chia Gara) being Late Jurassic-Early Cretaceous in age. A total of one hundred and forty-one carbonate and shale samples were collected, covering the entire Jurassic-Lower Cretaceous Warte and Ranya successions in NE Iraq.

The aim of this work is to reconstruct the paleoclimate, paleosalinity and paleoredox conditions during the deposition of the Early Jurassic-Early Cretaceous-age formations in both sections, in order to evaluate the variations and/or similarities in the depositional conditions that prevailed during the Early Jurassic-Early Cretaceous time of the region of NE Iraq. Thus, this pioneering multi-proxies paleoenvironmental study presents a comparative mineralogical and geochemical characterization of major, trace and rare earth elements, as well as carbon and oxygen isotopes, from two Early Jurassic-Early Cretaceous-age sections (Warte and Ranya sections) in NE Iraq.

2. Geological setting

The studied sections are located in the Kurdistan region, northern Iraq and within the Zagros Basin/Zagros Fold Belt. This latter region lies within the NE boundary of the Arabian Plate, covering an area of about $500 \times 103 \text{ km}^2$, and marking the collision between the continental Arabian Plate and the continental segments of the Eurasian margin (Beydoun et al., 1992; Talbot and Alavi, 1996; Stampfli and Borel, 2002; Abdula, 2017; Liu et al., 2018). The Zagros Basin/Zagros Fold Belt extends in a NW-SE direction, over a distance of ca. 2300 km and with a width of 100–300 km, from Turkey to SE Iran (Abdula, 2017; Liu et al., 2018). According to Jassim and Goff (2006), the Zagros Basin/Zagros Fold Belt can be subdivided into three structural zones, including, from SW to NE, the Low Folded Zone (or Foothills), the High Folded Zone, and the Imbricated Zone. It is within this latter zone that the Early Jurassic-Early Cretaceous-age succession in the area of the town of Warte is exposed, whilst the area of the Ranya town is located within the

High Folded Zone (Fig. 1).

The Jurassic-Early Cretaceous stratigraphical succession of NE Iraq comprises six formations, namely, the Sarki, Sehkanyian, Sargelu, Naokelekan, Barsarin and Chia Gara formations. The lowermost Sarki Formation is composed of dolomites, dolomitic limestones, limestones and shales (Jassim and Goff, 2006). The formation was first described by Dunnington (1958) in Bellen et al. (1959) from the Chia Gara Range (N Iraq) as a 300 m-thick carbonate unit. The formation is Hettangian-Sinemurian in age (Bellen et al., 1959; Jassim and Buday, 2006). The lower and upper contacts of the Sarki Formation are conformable and gradational. Sediment deposition most probably occurred within a restricted lagoonal environment (Jassim and Goff, 2006).

The overlying Sehkanyian Formation comprises mainly dolomites and dolomitic limestones (Bellen et al., 1959). The formation was first described by Wetzel and Morton (1950) in Bellen et al. (1959) from the Surdash Anticline (NE Iraq), as a 180 m-thick carbonate unit. Based on its stratigraphic position and due to the lack of index fossils as a result of extensive dolomitization, the age of the Sehkanyian Formation is believed to be Pliensbachian to Toarcian (Bellen et al., 1959). The lower and upper contacts of the Sehkanyian Formation are conformable and gradational (Bellen et al., 1959). Jassim and Goff (2006) have also suggested that deposition occurred within a restricted lagoonal environment.

The overlying Sargelu Formation comprises bituminous limestones, dolomitic limestones, black shales and bands of thin black chert (Bellen et al., 1959; Jassim and Goff, 2006). The formation was first described by Wetzel and Morton (1950) in Bellen et al. (1959) from the Surdash Anticline in the High Folded Zone, NE Iraq. The thickness of the formation is about 115 m in the type section (Bellen et al., 1959; Jassim and Goff, 2006). It has been suggested (Al-Dujaily, 1994; Omar et al., 2022) that the age of the Sargelu Formation is Aalenian-Callovian. The lower contact of the Sargelu Formation with the Sehkanyian Formation in the type area is conformable and gradational. Similarly, the upper contact of the Sargelu Formation with the Naokelekan Formation is conformable and gradational. Deposition occurred within a basinal euxinic marine environment (Bellen et al., 1959; Jassim and Goff, 2006).

The overlying Naokelekan Formation contains argillaceous bituminous limestones, dolomites and beds of black shales in the lower part (Jassim and Buday, 2006). The formation was first described, from the Balambo-Tanjero Zone near Rowanduz (NE Iraq), by Wetzel and Morton (1950) in Bellen et al. (1959). The age of the Naokelekan Formation has been suggested as Early Tithonian (Kharajany and Mohialdeen, 2018). The lower contact of the Naokelekan Formation with the Sargelu Formation is conformable, and the upper contact with the Barsarin Formation appears to be similar. The depositional setting of the Naokelekan Formation was suggested as an euxinic environment in a subsiding or starved basin (Bellen et al., 1959; Jassim and Goff, 2006).

The overlying Barsarin Formation comprises limestones and dolomitic limestones (Bellen et al., 1959; Jassim and Goff, 2006). The formation was first described, in the type area, by Wetzel and Morton (1950) in Bellen et al. (1959) from the Balambo-Tanjero Zone near Rowanduz, NE Iraq (Buday, 1980). The age of the formation has been suggested as late Early-Middle Tithonian based on its stratigraphic position below the Chia Gara Formation and above the Naokelekan Formation (Kharajany and Mohialdeen, 2018). The lower and upper contacts with these two formations in the type area are both conformable. Sedimentation occurred within a lagoonal or evaporitic environment (Bellen et al., 1959; Jassim and Goff, 2006).

The overlying Chia Gara Formation is composed of thinly bedded limestones and calcareous shales (Bellen et al., 1959; Jassim and Goff, 2006). The Chia Gara Formation was first defined by Wetzel and Morton (1950) in Bellen et al. (1959) from the Chia Gara Anticline in the High Folded Zone, northern Iraq (Al-Ameri and Zumberge, 2012). The age of the Chia Gara Formation has been determined as Late Tithonian (Al-Abbasi et al., 2018). The lower contact of the Chia Gara Formation

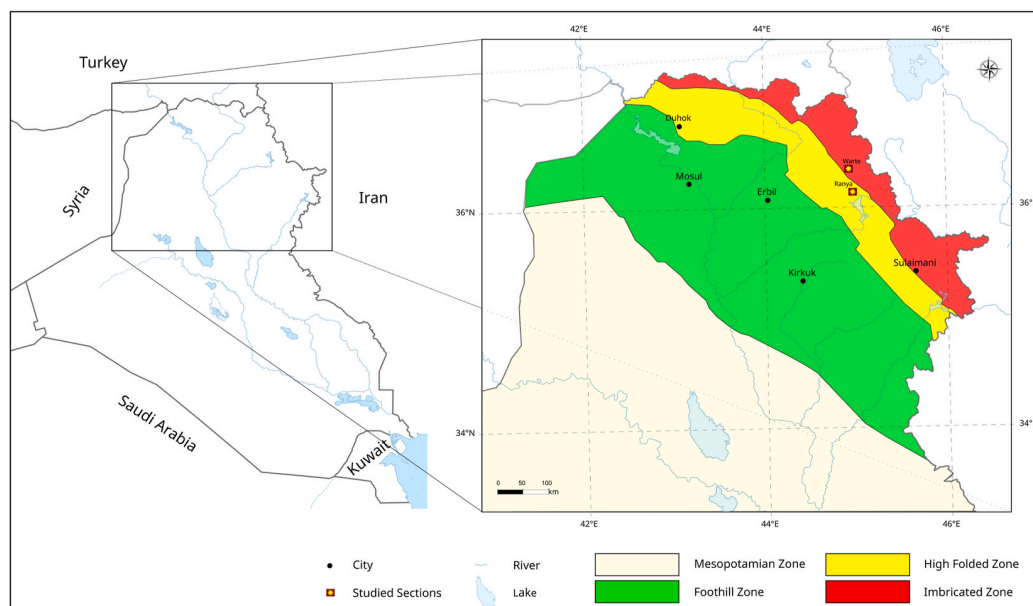


Fig. 1. Geological map of Iraqi Kurdistan showing the location of the studied sections and the structural zones of the Zagros Basin/Zagros Fold Belt (after Awdal et al., 2016).

with the Barsarin Formation is conformable. The upper contact with the Garagu Formation is both gradational and conformable. The sediments of the Chia Gara Formation were deposited in a mid-deep shelf setting (Bellen et al., 1959; Jassim and Goff, 2006).

3. Materials and methods

3.1. Petrography

Petrographic determination for the main components and diagenetic processes of the Lower Jurassic-Lower Cretaceous carbonate rocks of the Warte and Ranya sections (both sections in NE Iraq) has been conducted at the Institute for Geosciences-Geology of Bonn University, Germany. Microfacies analysis is carried out based on carbonate classification model of Dunham (1962), whereas standard depositional environment models and distribution of facies were based primarily on Wilson (1975) and Flügel (2010).

3.2. X-ray diffraction

Seventy-one samples from the Sarki, Sehkaniyan, Sargelu, Naokelkan, Barsarin and Chia Gara formations from the Warte section, and seventy samples from the same formations from the Ranya section were collected for detailed mineralogical and geochemical analyses. The selected samples were examined mineralogically, as powder preparation for bulk sediment using X-ray diffraction (XRD, using a D8 Advance from the company Bruker AXS GmbH) at the Institute for Geosciences-Geology of Bonn University, Germany. The data obtained from X-ray diffraction analysis was then analyzed and quantitatively evaluated using the software MacDiff 4.2.6 (Petschick, 2002) and the Rietveld method (Döbelin and Kleeberg, 2015).

3.3. Scanning electron microscopy (SEM)

This technique with energy-dispersive X-ray microanalysis (EDX) was conducted at the Premier Corex Group, Houston, USA, using an FEI Quanta FEG 650 F E-SEM instrument equipped with two Bruker EDS XFlash 5030 energy dispersive X-ray spectroscopy (EDS) detectors, and an FEI R580 Everhart-Thornley (ETD) electron detector. Freshly broken

surfaces were prepared by breaking rock segments perpendicular to the bedding. All samples were mounted on aluminum stubs using a conductive high viscosity glue. They were then sputter-coated with 10 nm of iridium using a Leica EM ACE600 sputter coater prior to being placed in the SEM. The measurements were performed at high vacuum, with an accelerating voltage of 10 kV. Each sample was imaged in secondary electron and backscattered electron mode, at seven different horizontal field widths (HFWs) – 5 µm, 10 µm, 25 µm, 50 µm, 100 µm, 200 µm, 500 µm, 1000 µm.

3.4. X-ray fluorescence

Geochemical analyses of the same samples were analyzed using X-ray fluorescence (XRF analysis for major, trace and rare earth elements) at the Bureau Veritas Laboratory, Canada. The prepared sample is digested to complete dryness with an acid solution of (2:2:1:1) of H₂O–HF–HClO₄–HNO₃. Aqueous HCl solution (50%) is added to the residue and heated using a mixing hot block. After cooling, the solutions are transferred to test tubes and brought to a defined volume using dilute aqueous HCl solution (2-N). Samples of 0.25 g are analyzed. The accuracy and analytical precision were determined using analyses of reference material (STD OREAS45E_IG and STD SO-18), and duplicate samples were measured in each analytical set. Duplicate measurements were conducted for 10% of the analyzed samples (precision 2–3%).

3.5. Stable isotopic C and O analysis

Stable carbon and oxygen isotopes were analyzed using a mass spectrometer MAT253 (Thermo Fisher Scientific, Bremen, Germany) equipped with a ConFlo IV and a GasBench II (both Thermo Fisher Scientific) at the Ruhr University Bochum, Germany.

Carbonate samples ({0.17}0.02 g) were reacted for 90 min at 90 °C in 100% phosphoric acid to produce CO₂. The acid fractionation factor for calcite was used to calculate the isotope composition. The measured isotope ratios were calibrated to those measured for the international calcite standards NBS18 ($\delta^{13}\text{C} = -5.00$, $\delta^{18}\text{O} = -22.96\text{‰}$, relative to VPDB) and NBS19 ($\delta^{13}\text{C} = 1.95$, $\delta^{18}\text{O} = -2.20\text{‰}$, relative to VPDB). The external precision is 0.1‰ for both $\delta^{13}\text{C}$ and $\delta^{18}\text{O}$ values.

4. Results

4.1. Studied sections

The studied sections represent the Lower Jurassic-Lower Cretaceous Warte and Ranya successions that are located in NE Iraq. The Sarki, Sehkanian, Sargelu, Naokelekan, Barsarin and Chia Gara formations can be recognized in both sections. These latter six formations will be described from base to top, below.

The Early Jurassic-age Sarki Formation from the Ranya section contains shales, dolomitic limestones, limestones and dolomites. The dolomitic limestone and limestone beds are fractured, with the veins infilled by calcite. Load structures were noted within the dolomitic limestone beds with some parts of the beds also being cavernous (i.e., vugs) (Fig. 2A). A range of deformational features were noted, including stylolites within individual beds as well as joints and thrust faults. In comparison, the Sarki Formation from the Warte section comprises dolomites, dolomitic limestones and shales. Internally, some beds show evidence of sedimentary structures, such as lamination, hummocky cross stratification as well as evidence of tectonic deformation in the form of boudinage structures (Fig. 2B), fractures and joints, while diagenetic features including liesegang rings were also noted.

The Early Jurassic-age Sehkanian Formation from the Ranya section consists of shales, dolomitic limestones and limestones with two

nodular and lenticular chert bands. Internally, some beds show evidence of sedimentary structures, such as lamination. The dolomitic limestone and limestone beds are fractured with the presence of calcite veins and nodules, some parts of the dolomitic limestone beds are cavernous. Small calcite and quartz geodes were also observed (Fig. 2C). In comparison, the Sehkanian Formation from the Warte section contains dolomites, marls and shales with one single dolomitic limestone bed. Internally, some beds may show evidence of deformation, in the form of fracturing and jointing (Fig. 2D), or the presence of fractures filled with calcite. Small quartz geodes were also noted.

The Middle Jurassic-age Sargelu Formation from the Ranya section comprises dolomitic limestones, limestones and shales with a few bands of chert (Fig. 2E). The dolomitic limestone and limestone beds are marked by the presence of calcite veins. Rare bivalves, preserved as isolated specimens, were recorded within the limestone beds. In contrast, the Sargelu Formation from the Warte section consists of dolomites, dolomitic limestones, limestones and shales with two bands of chert (Fig. 2F). Internally, there is no evidence of any sedimentary structures. However, the dolomitic limestones might be laminated. Deformation, in the form of calcite veins, was noticed within the dolomitic limestones.

The Late Jurassic-age Naokelekan Formation from the Ranya section comprises mainly shales and limestones. The limestone beds contain stylolites (Fig. 3A) and calcite veins with one single bed being rich in

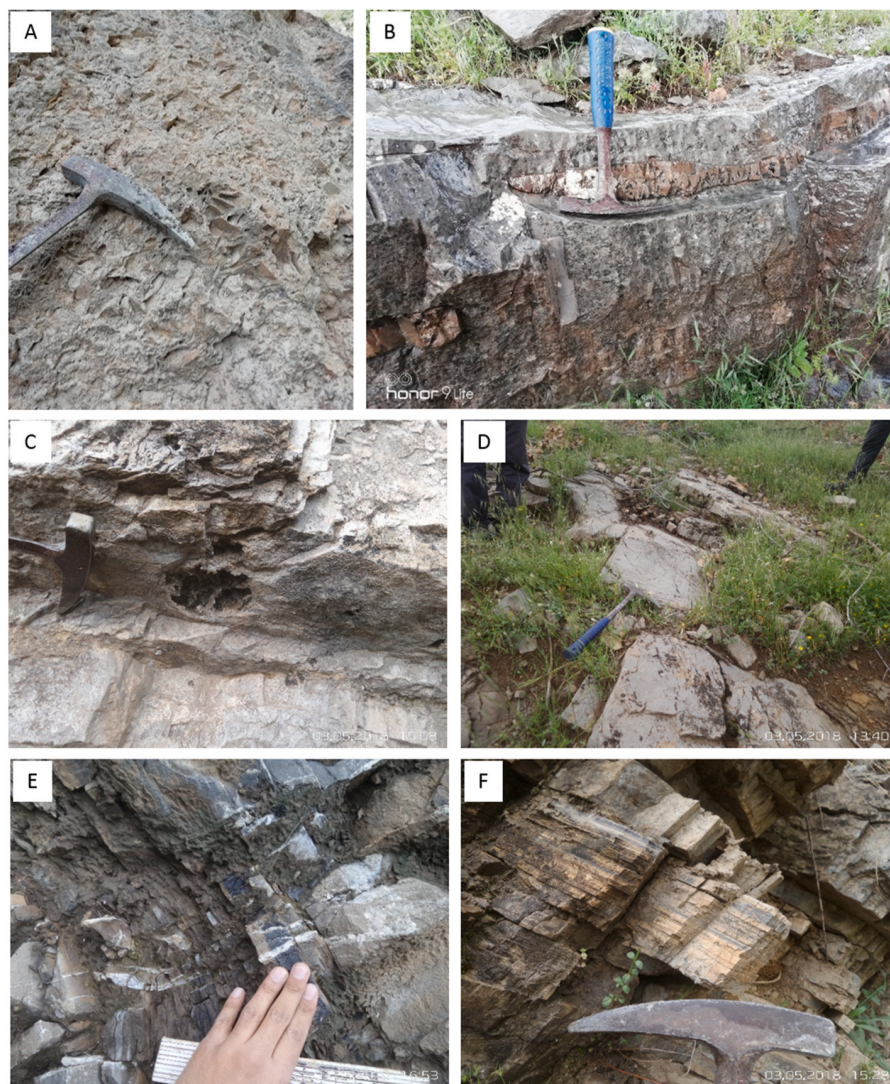


Fig. 2. Field photos. A. Cavernous features with box-work (melikaria) structures in the gray shale, blocky marl and dolomitic limestone in the Lower Jurassic Sarki Formation at the Ranya section. B. Boudinage structure of a dolomite within the dolomitic limestone of the Lower Jurassic Sarki Formation at the Warte section. C. Calcite and quartz geodes in the dolomitic limestone of the Lower Jurassic Sehkanian Formation at the Ranya section. D. Fracturing and jointing in the dolomite, Lower Jurassic Sehkanian Formation at the Warte section. E. A band of chert (black band) within the Middle Jurassic Sargelu Formation at the Ranya section. F. Two bands of chert (black bands) within the Middle Jurassic Sargelu Formation at the Warte section. Scales included.

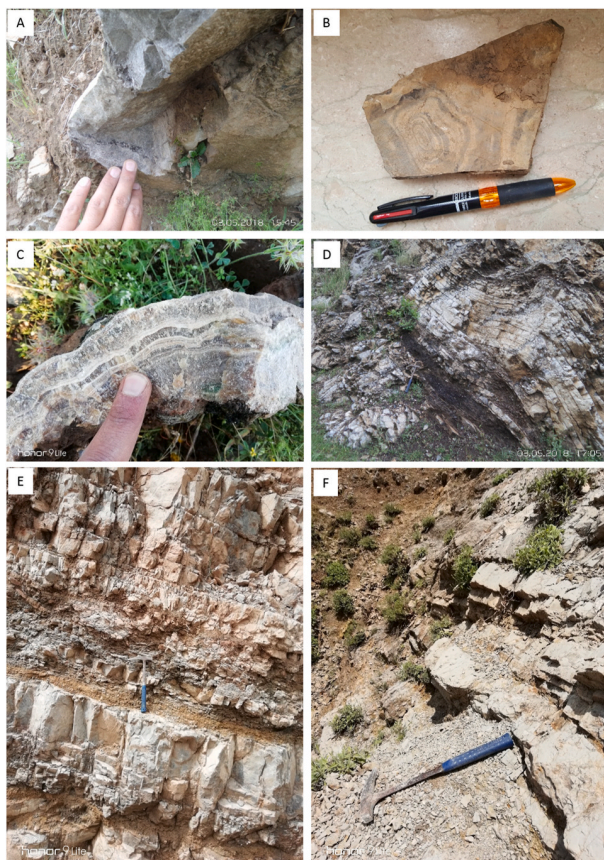


Fig. 3. Field photos. A. Stylolite in the dolomitic limestone, the Upper Jurassic Naokelekan Formation at the Ranya section. B. Liesegang rings in the limestone, the Upper Jurassic Naokelekan Formation at the Warte section. C. Wavy stromatolite in the Upper Jurassic limestone in the Barsarin Formation at the Ranya section. D. Folded beds within the Upper Jurassic Barsarin Formation at the Warte section. E. The shale and limestone beds in the lower part of the Upper Jurassic-Lower Cretaceous Chia Gara Formation at the Ranya section. F. Fissile shales interbedded with dolomitic limestone beds in the lower part of the Upper Jurassic-Lower Cretaceous Chia Gara Formation at the Warte section. Scales included.

ammonites. In comparison, the Naokelekan Formation from the Warte section comprises shales, limestones, and dolomitic limestones, with one single dolomite bed. Rare ammonites, preserved as isolated specimens, were recorded within the dolomitic limestone and limestone beds. The latter beds also contain secondary calcite nodules and stylolites, with some beds showing liesegang rings (Fig. 3B). Post-depositional deformation in the form of minor folds was also observed in the contact area (Omar et al., 2022).

The Late Jurassic-age Barsarin Formation from the Ranya section consists of limestones and shales with chert nodules. The limestone beds contain planar and wavy stromatolites (Fig. 3C) as well as calcite veins. In comparison, the Barsarin Formation from the Warte section contains shales and dolomitic limestones, with only one single limestone bed. It is also highly fractured and folded (Fig. 3D) due to tectonic deformation (e.g., box folding).

The Late Jurassic–Early Cretaceous-age Chia Gara Formation from the Ranya section contains mainly shales and limestones (Fig. 3E). Internally, there is no evidence of any sedimentary structures. In contrast, the Chia Gara Formation from the Warte section comprises mainly fissile shales and dolomitic limestones (Fig. 3F). Internally, there is no evidence of any sedimentary structures (Omar et al., 2022). It should be noted that the studied part of the Chia Gara Formation from both sections (i.e., Warte and Ranya sections) represents the lower part

of the Chia Gara Formation which is Late Jurassic–Early Cretaceous in age.

4.2. Petrography

Petrographic investigation of the carbonate units of the Lower Jurassic Sarki and Sehkaniyan formations from both the Warte and Ranya sections revealed that the main components are dominated by skeletal constituents (e.g., bivalves, ostracods, gastropods and echinoderms) and non-skeletal fragments (e.g., peloids, intraclasts and aggregated grains). These components are embedded in a micritic matrix. Subsequent post-depositional and diagenetic changes included compaction as well as severe dolomitization, cementation, and micritization.

In the Middle Jurassic Sargelu Formation, the main components of the carbonate rocks show a variety of open-marine faunas, including radiolaria, posidonia (thin-shell pelecypods), planktonic foraminifera, calcispheres and ostracods. These skeletal components are also embedded in micritic matrix, they suffered from various post-depositional and diagenetic processes including compaction, dolomitization (as well as dedolomitization), silicification, cementation, and recrystallization.

In the Upper Jurassic Naokelekan and Barsarin formations, stromatolitic structures, in the form of stratified and domal stromatolites, are predominant. The main skeletal components are represented by foraminifera, calcispheres, ostracods and bioclastic fragments, in addition to non-skeletal peloids. Various post-depositional and diagenetic processes affected these rocks including severe dolomitization (especially in the Barsarin Formation), cementation, recrystallization and chemical compaction (stylolite formation).

The petrographic components of the Upper Jurassic to Lower Cretaceous Chia Gara Formation include radiolaria, sponge spicules, calcispheres and ostracods.

4.3. Microfacies and depositional environments

A brief description of the main microfacies and their related Standard Microfacies (SMF; Flügel, 2010) is presented below, together with the suggested environments of deposition (Figs. 4 and 5).

4.3.1. Lower Jurassic Sarki and Sehkaniyan formations

4.3.1.1. Mudstone microfacies. This microfacies is commonly dolomitized with an aphanotopic texture of dolomite embedded in micritic groundmass and common veins filled by sparry calcite (Fig. 4A), it dominates in the lowermost part of the Lower Jurassic Sarki Formation, which corresponds to SMF 23 of Flügel (2010) which represents a supratidal environment of deposition.

4.3.1.2. Bioclastic wackstone microfacies. Bioclasts form more than 10% of the components of this microfacies which is mostly dolomitized. This microfacies exists in the Lower Jurassic Sarki and Sehkaniyan formations in both the Warte and Ranya sections (Fig. 4B–D) that corresponds to SMF 9 of Flügel (2010) and is considered to be indicative of supratidal and occasional shallow-marine lagoonal environments.

4.3.1.3. Peloidal packstones microfacies. Peloids dominate this microfacies in the lower part of the Sarki Formation at the Ranya section (Fig. 4E) and in the Sehkaniyan Formation in both the Warte and Ranya sections (Fig. 4F) which corresponds to SMF 16 of Flügel (2010) and represents subtidal to shallow restricted lagoonal depositional environments.

4.3.1.4. Dolostone microfacies. This is the common microfacies in the carbonate succession of the Lower Jurassic Sehkaniyan Formation

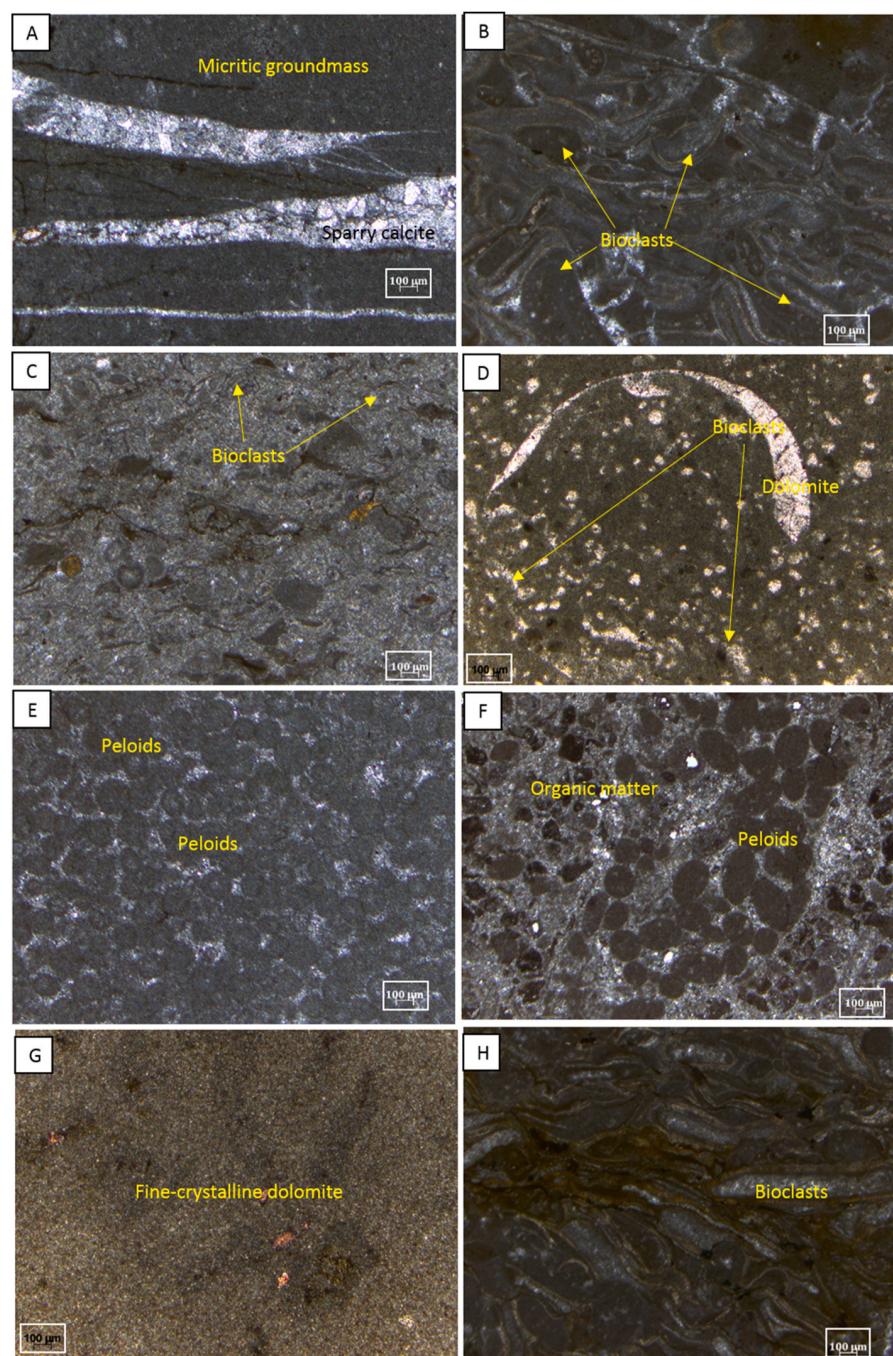


Fig. 4. Main microfacies of the Warte and Ranya sections. A. Mudstone microfacies with an aphanitic texture of dolomite and fractures filled by sparry calcite (sample 1 from the Sarki Formation at the Warte section). B. Bioclastic wackstone microfacies, dolomitized (sample 16 from the Sarki Formation at the Warte section). C. Bioclastic wackstone microfacies (sample 33 from the Sarki Formation at the Ranya section). D. Bioclastic wackstone microfacies with common dolomite (sample 12 from the Sehkanian Formation at the Ranya section). E. Peloidal packstone microfacies (sample 4 from the Sarki Formation at the Ranya section). F. Peloidal packstone microfacies, dolomitized with organic matter (sample 10 from the Sehkanian Formation at the Warte section). G. Dolostone microfacies (sample 1 from the Sehkanian Formation at the Ranya section). H. Bioclastic wackstone microfacies, crenulated bioclasts due to compaction (sample 13 from the Sargelu Formation at the Ranya section). See Figs. 10 and 11 for sample locations.

constituting fine-crystalline dolomite (Fig. 4G) and corresponding to SMF 23, representing deposition in supratidal settings.

In general, the microfacies, as mentioned above, suggest that the Lower Jurassic formations (i.e., the Sarki and Sehkanian formations) were deposited in tidal flats (supratidal) and restricted lagoons.

4.3.2. Middle Jurassic Sargelu Formation

In the Middle Jurassic Sargelu Formation, several microfacies were identified in both sections (i.e., the Warte and Ranya sections) as detailed below.

4.3.2.1. Bioclastic wackstone microfacies. In this microfacies, bioclastic material forms more than 10% of the total components (Fig. 4H), some

of which are dissolved and then filled by sparry calcite cement.

4.3.2.2. Planktonic foraminifera-Bositra wackstone microfacies. Planktonic foraminifera and Bositra (formerly known as Posidonia) or thin shelly pelagic pelecypod are common forming more than 10% of the total components (Fig. 5A). This microfacies correlates with SMF 10 (Flügel, 2010) and represents deposition in an outer shelf environment.

4.3.2.3. Radiolarian wackstone and Bositra-Radiolarian packstone microfacies. Radiolarian wackstone microfacies (Fig. 5B) and Bositra-Radiolarian packstone microfacies (Fig. 5C) both correspond to SMF 3 and represent deposition in middle to lower bathyal settings.

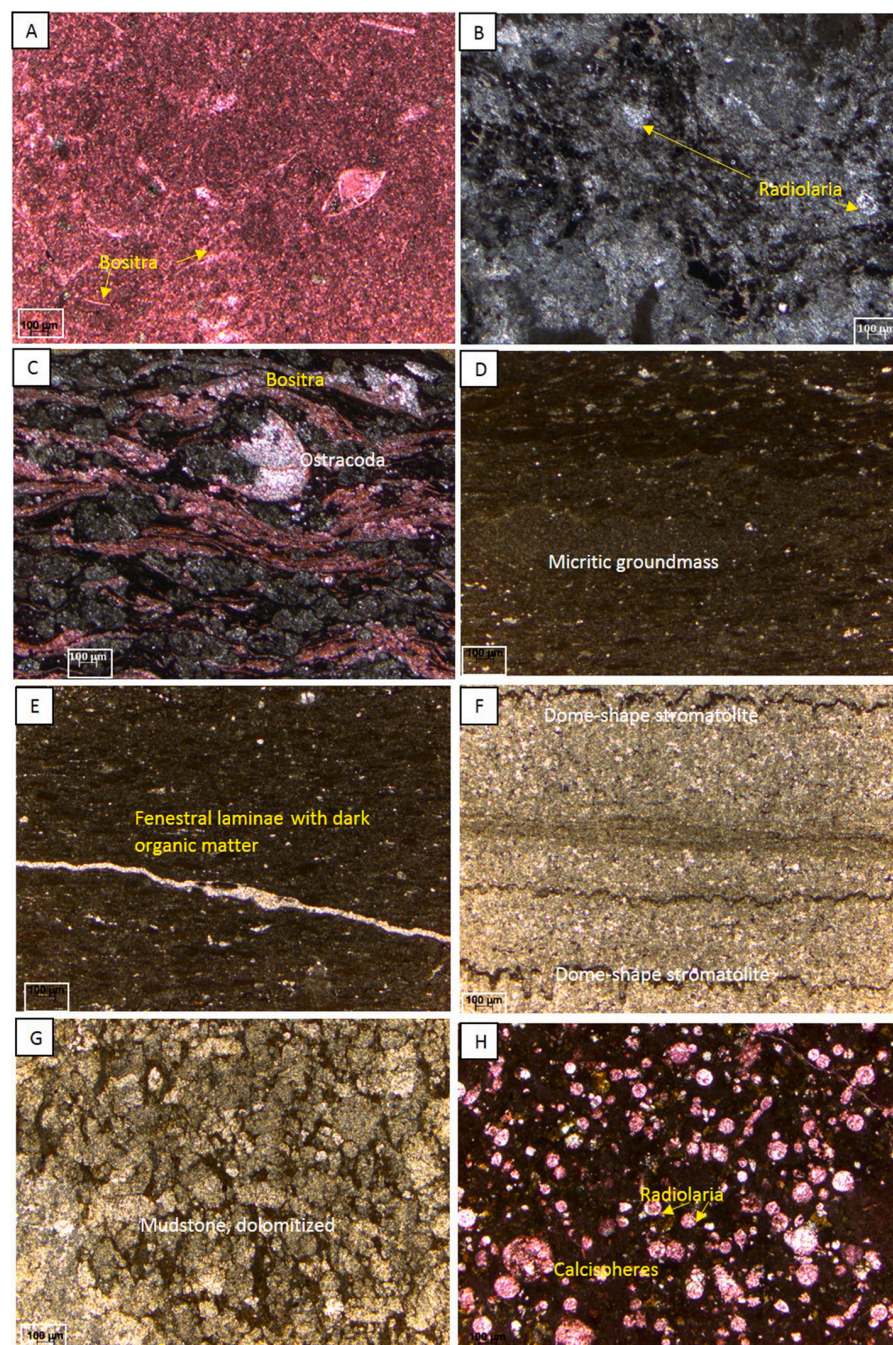


Fig. 5. Main microfacies of the Warte and Ranya sections. A. Planktonic foraminifera-Bositra wackestone microfacies (sample 7 from the Sargelu Formation at the Ranya section). B. Radiolarian wackestone microfacies (sample 3 from the Sargelu Formation at the Warte section). C. Bositra-radiolarian packstone microfacies (sample 13 from the Sargelu Formation at the Warte section). D. Laminated mudstone microfacies, stratified stromatolite (sample 3 from the Naokelekan Formation at the Ranya section). E. Foraminiferal-calcisphere wackestone microfacies (sample 2 from the Naokelekan Formation at the Ranya section). F. Dome-shaped stromatolitic microfacies (sample 2 from the Barsarin Formation at the Ranya section). G. Mudstone microfacies, severely dolomitized (sample 2 from the Chia Gara Formation at the Ranya section). H. Radiolarian calcisphere wackestone to packstone microfacies (sample 7 from the Chia Gara Formation at the Ranya section). See Figs. 10 and 11 for sample locations.

4.3.3. Upper Jurassic Naokelekan and Barsarin formations

In the Upper Jurassic Naokelekan Formation, a number of different microfacies were identified as described below.

4.3.3.1. Laminated mudstone microfacies. This microfacies includes dark organic matter filling fenestral laminae (Fig. 5D) indicating supratidal (pond brackish water) deposition.

4.3.3.2. Stratified stromatolite microfacies. Stromatolites dominate this microfacies (Fig. 5D) that represents deposition in an intertidal to subtidal depositional environments (Logan et al., 1964).

4.3.3.3. Foraminiferal-calcisphere wackestone microfacies. Foraminifera and calcispheres form together more than 10% of the total components

of the facies (Fig. 5E). They correlate with SMF 3 representing deposition in an open marine shelf setting.

4.3.3.4. Dome-shaped stromatolitic microfacies. This microfacies is the dominant one in the Barsarin Formation (Fig. 5F) and corresponds to SMF 20 representing deposition in an intertidal to subtidal setting.

4.3.4. Upper Jurassic-Lower Cretaceous Chia Gara Formation

The recorded microfacies in the Upper Jurassic to Lower Cretaceous Chia Gara Formation are described below.

4.3.4.1. Mudstone microfacies. This microfacies is composed dominantly of mudstone which is severely dolomitized (Fig. 5G) representing an intertidal to subtidal setting.

4.3.4.2. *Radiolarian-calcisphere wackstone to packstone microfacies.* Radiolaria and calcispheres form more than 10% of the total component of this facies (Fig. 5H) and may represent deposition in bathyal settings.

4.4. Mineralogy

X-ray diffraction analysis indicates that calcite and quartz are the dominant constituents present within the samples. Dolomite has also been noted, as well as traces of feldspar and some clay minerals. These latter minerals include illite and kaolinite (Figs. 6 and 7). Detailed examination of fifteen shale samples using SEM confirms the presence of these various clays, providing evidence for the presence of illite and kaolinite (Figs. 8 and 9).

Illite is commonly found in the form of fibers and laths or as platelets (Figs. 8A, E and 9A, C, F). Kaolinite occurs in hexagonal or booklet-like grains, some of which are degraded (Fig. 8C and D).

Various polymorphs of calcite have been identified. These include, euhedral (hexagonal) crystals, star-shaped calcite microcrystals and clusters of hexagonal and columnar calcite crystals (Fig. 8). These crystals occur individually, or as infill of chambers in coccoliths (Fig. 9E and F). Pyrite is found as framboidal clusters (Fig. 9B) and within sedimentary pore spaces. Pores have also been noted (Figs. 8C and 9D). Dolomites are present in euhedral shapes (Fig. 8B), while quartz is commonly found in euhedral quartz crystals with overgrowth (Fig. 8A).

4.5. Geochemistry

XRF analysis of the major, trace and rare earth elements of the six formations from the Warte and Ranya sections, NE Iraq, was carried out. A variety of elemental ratios, including Sr/Ba (0.5–160.5 Warte section; 0.2–185 Ranya section), Rb/Sr (0–0.22 Warte section; 0–4.08 Ranya section), Sr/Cu (1.1–371.7 Warte section; 0.4–126 Ranya section), U/Th (0.5–55 Warte section; 0.4–54 Ranya section), V/Cr (1–27 Warte section; 1–15 Ranya section), Ni/Co (0.5–199 Warte section; 0.3–211.1 Ranya section), V/Sc (9–927.5 Warte section; 5.5–385.5 Ranya section) and V/(V+Ni) (0.3–1 Warte section; 0.33–1 Ranya section) were calculated (see Tables 1–4). These data were used to interpret the paleoclimate, paleosalinity and paleoredox conditions prevailing during the deposition of the studied formations (Figs. 10 and 11).

4.6. Carbon and oxygen isotope analysis

The relationship between the ratios of carbon ($\delta^{13}\text{C}$) and oxygen ($\delta^{18}\text{O}$) isotopes has been utilized by many authors (Fisher et al., 2005; Li et al., 2016; Hennhoefter et al., 2018) to evaluate the impact of diagenesis, and the extent to which the oxygen isotopes represent the initial imprint of the depositional environment. Fisher et al. (2005), Li et al. (2016), and Hennhoefter et al. (2018) suggested that a positive relationship between the carbon and oxygen isotope values would indicate a strong influence of diagenesis on the oxygen isotopes, while a weak or negative relationship between the carbon and oxygen isotope values would indicate that the oxygen isotopes were not influenced by diagenesis.

The carbon and oxygen isotope values, which were calculated as part of this study, displayed a weak correlation for both the Warte ($R^2 = -0.07$) and Ranya ($R^2 = -0.021$) sections. This weak relationship between the carbon and oxygen isotope values would suggest that the oxygen isotopes reflect their initial imprint in these sediments. Thus, the oxygen isotope data provided can be used to evaluate the paleoclimate conditions present during the deposition of the Early Jurassic–Early Cretaceous-age Warte and Ranya sediments (Tables 5 and 6), (Figs. 10 and 11).

5. Discussion

Comparative mineralogical and geochemical analyses were carried

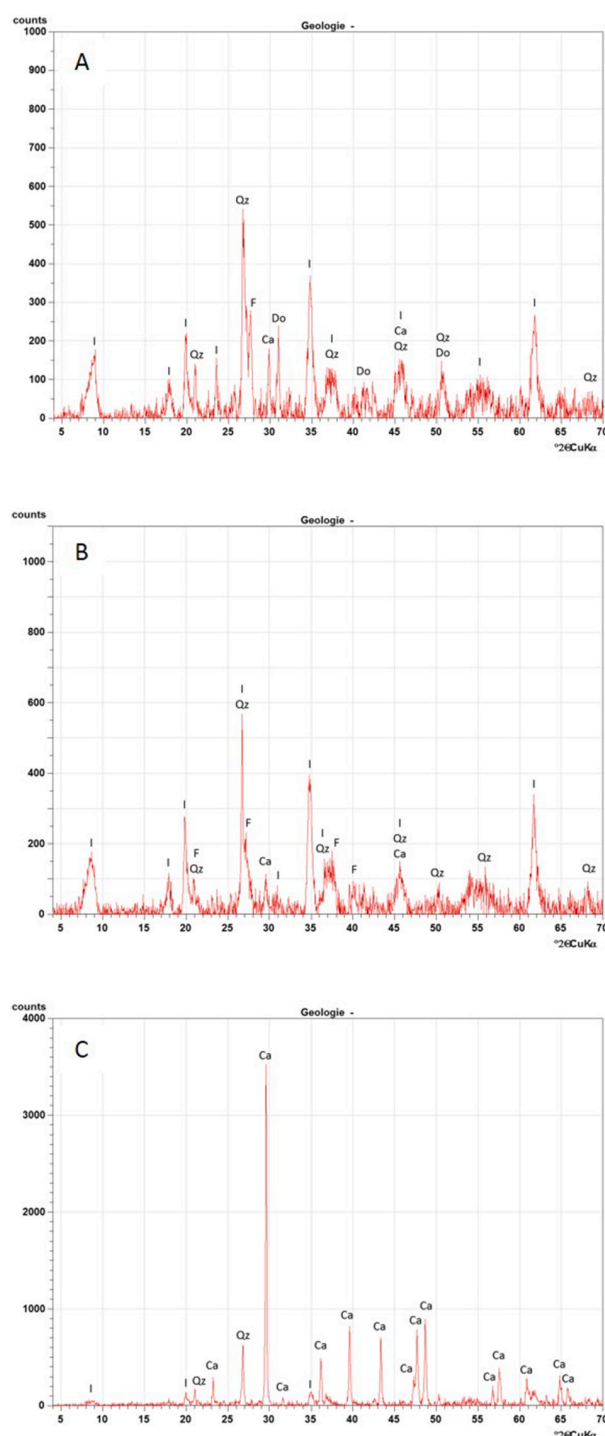


Fig. 6. X-ray diffractograms showing the clay and non-clay minerals in selected samples from the Lower and Middle Jurassic succession in the Warte and Ranya sections. A. Sample 10 from the Sarki Formation at the Ranya section. B. Sample 11 from the Sehkanian Formation at the Ranya section. C. Sample 8 from the Sargelu Formation at the Warte section. I = illite; Qz= quartz; F= feldspar; Ca= calcite; Do= dolomite.

out on the Early Jurassic–Early Cretaceous-age Warte and Ranya sections from NE Iraq. The six formations representing these periods are the Lower Jurassic formations (Sarki, Sehkanian) through the Middle Jurassic Formation (Sargelu) and the Upper Jurassic formations (Naokalekan, Barsarin) to the Upper Jurassic–Lower Cretaceous Formation (Chia Gara).

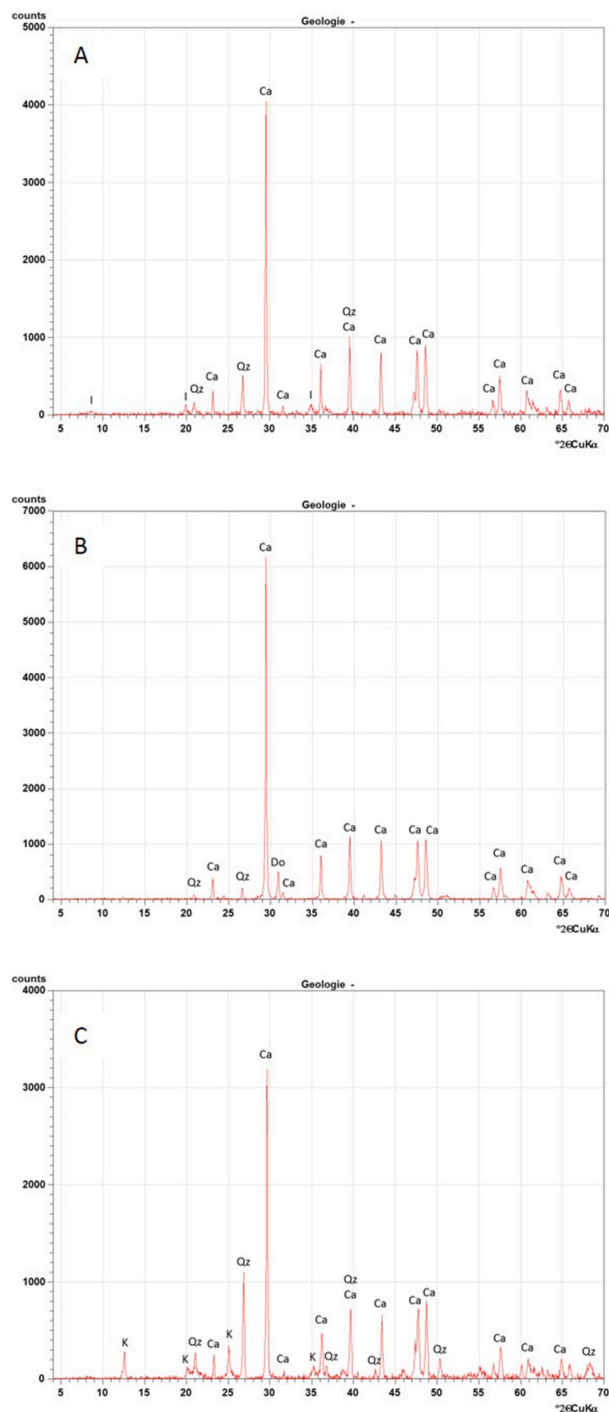


Fig. 7. X-ray diffractograms showing the clay and non-clay minerals in selected samples from the Upper Jurassic and Upper Jurassic-Lower Cretaceous succession in the Warte and Ranya sections. A. Sample 8 from the Naokelekan Formation at the Warte section. B. Sample 2 from the Barsarin Formation at the Warte section. C. Sample 6 from the Chia Gara Formation at the Ranya section. I = illite; Qz = quartz; Ca = calcite; Do = dolomite; K = kaolinite.

The following discussion will consider a number of important proxies (i.e., paleoclimate proxies, paleosalinity proxies and paleoredox proxies) associated with the depositional conditions during which the Lower Jurassic-Lower Cretaceous successions of NE Iraq were deposited.

5.1. Paleoclimate proxies

As noted above, a variety of paleoclimate proxies were measured from the six formations of the Ranya and Warte sections. Geochemical proxies used include Ca, Al, Sr/Ba, Rb/Sr and Sr/Cu data (Xu et al., 2010; Song et al., 2016; Wang et al., 2017; Omar et al., 2020). Additionally, oxygen isotope values (Bartolini et al., 2003; Weissert and Erba, 2004; Ruf et al., 2005), and some indicative clay and non-clay minerals including illite, kaolinite, calcite and quartz (Singer, 1984; Chamley, 1989; Liu et al., 2020) were considered.

Despite the predominance of strontium in carbonate rocks, and the impact of depositional/diagenetic conditions on redistribution of Sr and Ca, this element is commonly used as paleoclimate and paleosalinity proxy along with other trace elements such as Ba, Cu, Rb and Ga (Marshall and Fairbridge, 1999). Sr is more soluble in aqueous solution than other elements, and the solubility product of strontium sulfate (SrSO_4) is larger than, for example, that of BaSO_4 . Therefore, with increasing salinity in a waterbody, the initial precipitation of BaSO_4 results in higher Sr than Ba concentration. This is one of the properties that led to an increase in the ratios of both elements from fresh to marine sediments, and it can be affected by dry and humid paleoclimatic conditions (Zuo et al., 2020). Additionally, some redox-sensitive elements such as (Cu, Ni, Zn) tend to be more soluble under oxidizing conditions and less soluble under reducing conditions, and they are delivered to the sediment mainly in association with organic matter, whilst other paleoproductivity proxies such as Ba are solubilized under reducing conditions and may be lost from oxygen-deprived sediments (Tribouillard et al., 2006).

The Sr/Cu ratio has been used by many authors as an indicator of paleoclimate conditions. Yandoka et al. (2015) and Song et al. (2016) suggested that Sr/Cu ratio values of more than 5 denote a hot and arid climate, while those between 1.3 and 5 indicate a warm, humid climate. Generally, the Sr/Cu ratio values observed in the samples of all six of the formations from the Ranya section, NE Iraq, are higher than 5 (see Table 2), indicating hot and arid climate conditions during deposition. This conclusion is also supported by the low Rb/Sr ratio values of the same samples from the Ranya section, where a continuous decrease in the Rb/Sr ratio values was observed, with a concurrent increase in the Sr/Cu ratio values (see Table 2), (Fig. 11). It has been suggested (Sinha et al., 2006; Xu et al., 2010) that an inverse relationship between the Sr/Cu ratio values and the Rb/Sr ratio values indicates a warm climate during deposition. The present results are consistent with the results obtained from the samples of the same studied formations from the Warte section, which also showed an inverse relationship between the Sr/Cu ratio values and the Rb/Sr ratio values (see Table 1), (Fig. 10) (Omar et al., 2022).

The Sr/Ba ratio can be considered as an indicator of salinity and/or aridity (Wang et al., 2017). High values of the Sr/Ba ratio suggest high salinity and/or arid climates, while low values would suggest low salinity and/or humid climates (Wang et al., 2017). Relatively high Sr/Ba ratio values were recorded from the samples of all six formations from the Ranya section (Table 2), (Fig. 11). This result suggests that the climate was characterized by arid conditions, and that salinity values were high during the deposition of the Jurassic-Lower Cretaceous sediments in the Ranya area. Additionally, the Sr/Ba ratio values attained from the samples of the same six formations from the Warte section, display a similar trend (see Table 1 and Fig. 10) which is also indicative of high salinity and an arid climate (Omar et al., 2022).

The inverse relationship between the Ca and Al values was also interpreted in terms of salinity and/or aridity (Orhan et al., 2019; Omar et al., 2020). According to the literature (Orhan et al., 2019; Omar et al., 2020), a decrease in Al and a corresponding increase in Ca content suggests that sedimentation occurred during arid conditions. Generally, the recorded results from the samples of the six formations from the Ranya section show an inverse relationship between the Ca values and the Al values (see Table 2, Fig. 11). Therefore, these elemental variations

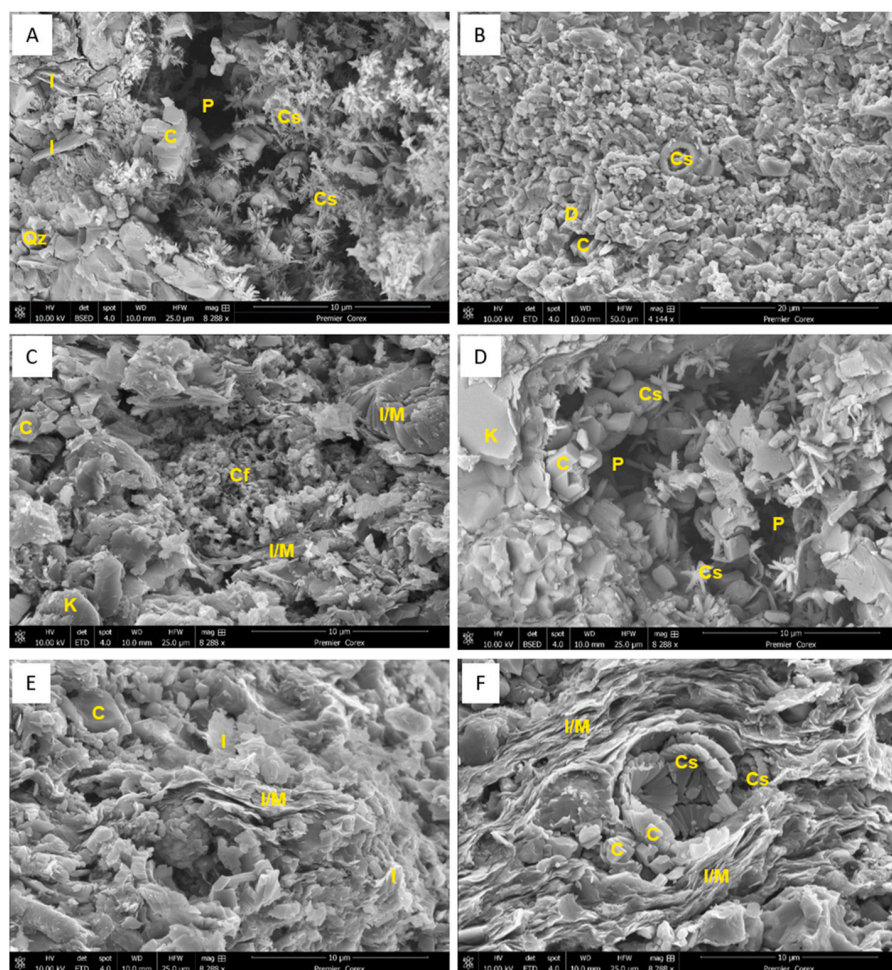


Fig. 8. Scanning electron microscopic (SEM) images showing: A. Illite platelets (I), calcite in the form of columnar (hexagonal) (C) and star-shaped forms (Cs), quartz (Qz) and pores (P), (sample 1 from the Naokelekan Formation at the Ranya section). B. Common presence of calcite as hexagonal, columnar (C) and filling fossil (cocolith) chambers (Cs) and dolomite rhombs (D), (sample 1 from the Naokelekan Formation at the Ranya section). C. Finely crystalline calcite grains in the middle part of the photo (Cf), degraded kaolinite (K) and columnar calcite (C), (sample 8 from the Naokelekan Formation at the Warte section). D. Star-shaped calcite (Cs), columnar and hexagonal calcite (C), in addition to hexagonal kaolinite plate (K) with common pores (P), (sample 2 from the Barsarin Formation at the Warte section). E. Illite plates and laths (I), calcite grains (C), (sample 6 from the Chia Gara Formation at the Ranya section). F. Common calcite in hexagonal and columnar forms (C) and infills of cocolith chambers (Cs), illite plates (I), (sample 1 from the Chia Gara Formation at the Warte section).

would indicate high salinities with arid conditions being predominant during sedimentation. Similarly, the recorded results from the six formations of the Warte section, also revealed an inverse relationship between the Ca and the Al contents (see Table 1, Fig. 10) indicating similar conditions (Omar et al., 2022).

Oxygen isotope values have been used by a number of authors to provide some indications regarding ancient water temperatures (Bartolini et al., 2003; Weissert and Erba, 2004; Ruf et al., 2005). According to these authors, negative values of the oxygen isotopes are suggestive of warm waters, while positive values are suggestive of cool waters. The samples measured from the six formations of the Ranya section, show overall negative values for the oxygen isotopes (see Table 6, Fig. 11). Analysis of the oxygen isotopes from the samples of the same six formations from the Warte section also shows broadly negative values (see Table 5), (Fig. 10) (Omar et al., 2022). These results might thus be interpreted as being indicative of warm waters (Bartolini et al., 2003; Weissert and Erba, 2004; Ruf et al., 2005; Omar et al., 2022) during the deposition of the Early Jurassic-Early Cretaceous-age sediments in the Warte and Ranya areas.

Clay minerals can be useful indicators of paleoclimatic conditions, particularly in sediments that were deposited in marine environments (Singer, 1984; Chamley, 1989; Li et al., 2016). The clay mineral assemblage of the studied samples of the six formations from both the Warte and Ranya sections, as revealed by XRD and SEM studies, is dominated by illite and kaolinite (especially within a few samples of the Chia Gara Formation), whilst non-clay minerals are mainly represented by calcite and quartz. Arid, dry climatic conditions deduced from elemental geochemical proxies are also suggested by the presence of

common illite in the studied rocks (Chamley, 1989). Sediments rich in illite, chlorite and quartz are interpreted as corresponding to relatively dry periods (Singer, 1984). Additionally, kaolinite is a good indicator of humid climates (Chamley, 1989).

The presence of illite in the studied samples from both sections reflects the dominance of hot and dry, arid conditions during deposition. This is also suggested by the common presence of calcite and quartz which may suggest saline conditions in addition to hot climates (Singer, 1984; Liu et al., 2020).

As noted above, kaolinite is the dominant clay mineral in some Chia Gara Formation samples (3 samples from the Warte section and the uppermost sample from the Ranya section). Its presence is suggestive of periods of warm and humid climatic conditions during the deposition of this formation (Late Jurassic to Early Cretaceous in age). This climatic change from hot and arid to warm and humid conditions of the Chia Gara Formation was similar, in some ways, to the Jurassic-Cretaceous transition of the Fårarp-1 core (southern Sweden), where the climatic conditions in the area shifted from more seasonally dry to more humid over the Tithonian-lowermost Berriasian interval (Lindström and Erlström, 2011).

5.2. Paleosalinity proxies

As outlined above, some geochemical proxies including Ca, Al and Sr/Ba can be used as proxies for both salinity and/or aridity (Wang et al., 2017; Orhan et al., 2019; Remírez and Algeo, 2020; Omar et al., 2020; Sun et al., 2022) and the values are indicative of a strong relationship between climates and salinity.

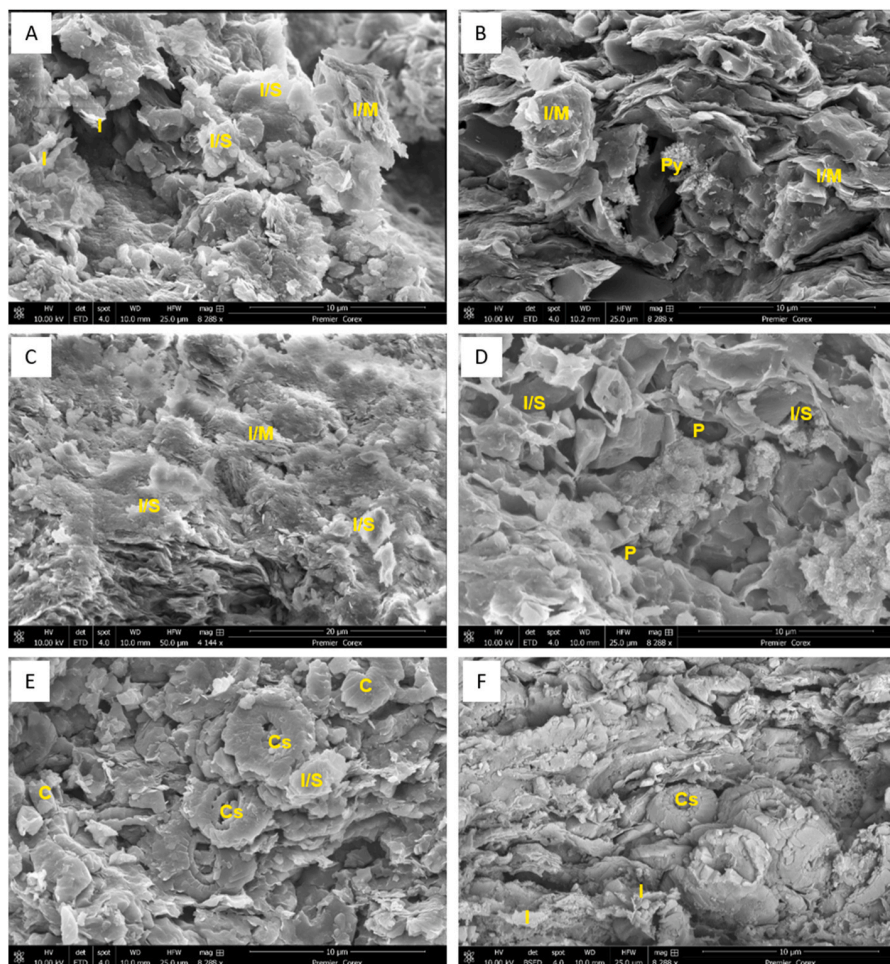


Fig. 9. Scanning electron microscopic (SEM) images showing: A. Illite laths and fibers (I), (sample 10 from the Sarki Formation at the Ranya section). B. Framboidal pyrite (Py) and platy illite (I), (sample 8 from the Sarki Formation at the Warte section). C. Illite, platy and fibrous (I), (sample 11 from the Sehkanian Formation at the Ranya section). D. Illite (platy, I), and pores (P), (sample 6 from the Sehkanian Formation at the Warte section). E. Calcite either in the form of disseminated grains (C) or infills of cocoliths (Cs), (sample 12 from the Sargelu Formation at the Ranya section). F. Illite flakes (I) and common calcite in hexagonal and columnar forms (C), mostly filling fossil (cocolith) chamber (Cs), (sample 8 from the Sargelu Formation at the Warte section).

In addition, the trace element Sr has been used by a variety of authors as a proxy for salinity and/or evaporation conditions (Read et al., 1995; Price, 1999; Vincent et al., 2006; Omar et al., 2020; Dashtgard et al., 2022). It has been suggested that high values of the trace element Sr can indicate high salinity and/or evaporation conditions within the depositional area. Indeed, the samples of the six formations from the Ranya section registered high Sr values (see Table 2, Fig. 11) which support the suggestion of high salinities and evaporation rates (as a result of the arid climates) during deposition of the sediments. Similarly, high Sr values (see Table 1, Fig. 10) were measured in the samples of the same six formations from the Warte section, which support the idea of high salinities and evaporation rates within the depositional setting of the Warte section (Omar et al., 2022).

Omar et al. (2020) used a variety of geochemical proxies (i.e., Sr, Ca and Al) to indicate evaporitic conditions in their study on the petrography and geochemistry of the Middle-Upper Jurassic Banik section from northernmost Iraq. The results obtained from the latter geochemical proxies indicated high salinities and high rates of evaporation (controlled by aridity) within the depositional environments of the Middle-Late Jurassic-age Sargelu and Naokelekan formations from the Banik section in northernmost Iraq.

In summary, the findings from the paleosalinity and paleoclimate proxies suggest that the depositional areas of the Sarki, Sehkanian, Sargelu, Naokelekan and Barsarin formations from both the Warte and Ranya sections of NE Iraq underwent hot and arid climates with a shift to warm and humid conditions encompassing the Upper Jurassic to the Lower Cretaceous strata (Chia Gara Formation).

In addition, deposition of the Middle-Late Jurassic-age successions

from the Banik section in northernmost Iraq was also interpreted to have occurred under warm and arid conditions (Omar et al., 2020, 2021). This interpretation was based on the geochemical proxies used for evaporitic conditions, as noted above, in addition to the observed negative oxygen isotope values within the samples of the Middle-Upper Jurassic formations of northernmost Iraq. Furthermore, dominance of warming and aridity during the Jurassic, across the region of northern Iraq, coincided with a global warming that governed the Jurassic period (Hallam, 1982; Chao et al., 2021).

5.3. Paleoredox proxies

As noted earlier, a selection of paleoredox proxies were measured from the studied formations of the Warte and Ranya sections. The measured proxies, including U/Th, V/Cr, Ni/Co, V/Sc and V/(V+Ni) ratios (e.g., Hatch and Leventhal, 1992; Jones and Manning, 1994; Kimura and Watanabe, 2001; Deepul et al., 2012; Armstrong-Altrin et al., 2019; Bennett and Canfield, 2020) can provide important information about the redox conditions, however, factors other than redox can also impact the ratios, such as organic matter and enrichment in some trace elements (S and Fe), (Algeo and Liu, 2020).

Some trace elements such as V, Mo, U and Ni are insoluble in reducing environments, and they are suggested by many authors (e.g., Algeo and Maynard, 2004; Tribouillard et al., 2006) to be sensitive to redox environments and to allow differentiation of anoxic conditions, due to their enrichment under these oxic conditions resulting in their deficiency.

The U/Th ratio has been used by Jones and Manning (1994) as a

Table 1

Selected major and trace element compositions, including paleoclimate and paleosalinity proxies of the samples from the Sarki, Sehkanian, Sargelu, Naokelekan, Barsarin and Chia Gara formations from the Warte section.

Formation	Lithology	Cu (ppm)	Sr (ppm)	Ca (%)	Ba (ppm)	Al (%)	Rb (ppm)	Sr/Ba	Rb/Sr	Sr/Cu
Sa 1	dolomite	4.3	87	17.74	4	0.36	6.8	21.8	0.08	20.2
Sa 2	shale	6.2	77	17.01	7	0.94	10.2	11	0.13	12.4
Sa 4	dolomite	1.7	84	19.59	2	0.07	1.9	42	0.02	49.4
Sa 6	shale	18.8	102	6.21	103	4.83	10.1	1	0.1	5.4
Sa 7	dolomite	4.3	136	19.14	4	0.21	5.2	34	0.04	31.6
Sa 8	shale	24	96	4.91	122	5.27	18.4	0.8	0.19	4
Sa 9	dolomite	4	94	19.05	6	0.29	7	15.7	0.07	23.5
Sa 10	shale	9.4	105	14.35	30	1.49	9.3	3.5	0.09	11.2
Sa 11	dolomite	2	126	18.49	100	0.28	7.2	1.3	0.06	63
Sa 12	shale	3.2	113	17.06	8	0.95	11.3	14.1	0.1	35.3
Sa 14	dolomite	1.6	84	17.67	3	0.31	6.9	28	0.08	52.5
Sa 15	shale	15.4	103	14.82	48	1.7	11.7	2.1	0.11	6.7
Sa 17	dolomite	4.6	100	18.44	70	0.67	13.8	1.4	0.14	21.7
Sa 18	shale	22.4	100	4.4	133	5.93	13.3	0.8	0.13	4.5
Sa 20	dolomite	3.7	120	19.18	8	0.24	6.6	15	0.06	32.4
Sa 21	shale	49.8	53	4.32	102	5.77	11.6	0.5	0.22	1.1
Sa 24	dolomite	3	89	19.72	4	0.3	4.7	22.3	0.05	29.7
Sa 28	shale	17.2	116	10.51	88	4.64	8.9	1.3	0.08	6.7
Sa 30	dolomite	2.3	100	20.12	9	0.01	0.6	11.1	0.01	43.5
Sa 31	shale	56.6	285	15.32	115	2.02	12.8	2.5	0.05	5
Sa 34	dolomite	4.9	101	18.53	4	0.52	11.1	25.3	0.11	20.6
Sa 36	dolomite	2.2	79	21.26	3	0.21	2	26.3	0.03	35.9
Se 1	d.m.	5.2	111	24.32	23	0.66	7.7	4.8	0.07	21.3
Se 3	shale	7.5	62	8.85	108	4.03	6.2	0.6	0.1	8.3
Se 4	dolomite	6.4	205	19.83	97	0.28	6.4	2.1	0.03	32
Se 6	shale	13.2	82	8.87	74	3.35	9.1	1.1	0.11	6.2
Se 10	dolomite	1.7	106	19.67	2	0.02	0.8	53	0.01	62.4
Se 13	dolomite	1	47	18.01	2	0.01	0.2	23.5	0.00	47
Se 16	dolomite	0.9	81	20.14	1	0.01	0.4	81	0.00	90
Se 19	dolomite	1.1	36	19.38	1	0.01	0.1	36	0.00	32.7
Se 21	shale	10.2	92	24.46	31	1.52	10.7	3	0.12	9
Se 24	dolomite	1.2	57	19.71	1	0.01	0.4	57	0.01	47.5
Se 27	dolomite	1.9	106	21.11	1	0.09	1.8	106	0.02	55.8
Se 31	shale	17.6	137	21.18	5	0.54	7.7	27.4	0.06	7.8
Sg 1	dolomite	18	112	21.86	3	0.29	4.6	37.3	0.04	6.2
Sg 3	limestone	8.7	416	35.11	67	0.22	3.1	6.2	0.01	47.8
Sg 5	limestone	9.4	223	33.75	9	0.47	4.8	24.8	0.02	23.7
Sg 6	shale	10	367	31.19	65	0.23	2.9	5.6	0.01	36.7
Sg 7	limestone	5.8	232	33.12	24	0.36	4.1	9.7	0.02	40
Sg 7	shale	77.8	260	27.77	44	1.94	20.6	5.9	0.08	3.3
Sg 8	d.m.	50.7	194	22.17	23	1.38	15.7	8.4	0.08	3.8
Sg 8	shale	63.5	302	16.63	159	4.71	51.8	1.9	0.17	4.8
Sg 9	d.m.	27.4	286	30.35	24	1.44	14	11.9	0.05	10.4
Sg 9	shale	59.7	194	25.38	46	2.69	21.5	4.2	0.11	3.2
Sg 10	d.m.	5.8	317	32.97	586	0.55	6	0.5	0.02	54.7
Sg 10	shale	87	330	21.34	68	1.68	18.6	4.9	0.06	3.8
Sg 11	limestone	14.3	46	1.55	7	0.15	1.5	6.6	0.03	3.2
Sg 11	chert	16	86	3.92	12	0.2	2	7.2	0.02	5.4
Sg 11	shale	54.6	445	19.66	38	1.37	16.5	11.7	0.04	8.2
Sg 12	d.m.	3.7	242	33.91	8	0.11	1.1	30.3	0.00	65.4
Sg 13	shale	41.5	293	18.79	139	1.68	21.1	2.1	0.07	7.1
Na 1	shale	56.5	251	16.78	140	2.2	30.7	1.8	0.12	4.4
Na 2	limestone	16.1	399	34.05	89	0.42	5.9	4.5	0.01	24.8
Na 3	d.m.	7.2	145	34.78	23	0.22	2.7	6.3	0.02	20.1
Na 4	shale	44.3	504	27.75	124	1.29	18.1	4.1	0.04	11.4
Na 6	limestone	8.8	416	34.5	57	0.19	2.4	7.3	0.01	47.3
Na 8	shale	61.4	333	19.51	268	4.18	42.5	1.2	0.13	5.4
Na 10	dolomite	11.7	372	25.13	287	1.28	14.1	1.3	0.04	31.8
Ba 1	limestone	1.2	446	38.07	649	0.16	1.1	0.7	0.00	371.7
Ba 2	shale	9.6	364	33.39	22	0.71	7.2	16.5	0.020	37.9
Ba 3	d.m.	5.5	1007	38.57	27	0.51	4.3	37.3	0.00	183.1
Ba 5	shale	5.6	377	31.34	19	0.59	5.1	19.8	0.014	67.3
Ba 6	limestone	4.2	269	38.66	7	0.46	2.5	38.4	0.01	64.0
Ba 9	d.m.	11.2	391	36.91	12	0.63	4.4	32.6	0.01	34.9
Ch 1	shale	75.9	764	10.04	102	8.12	52.9	7.5	0.069	10.1
Ch 2	d.m.	21.9	761	35.78	27	1.77	11.6	28.2	0.02	34.7
Ch 3	shale	7.2	314	33.22	10	0.28	1.4	31.4	0.004	43.6
Ch 4	shale	92.1	1088	15.67	112	6.79	51.7	9.7	0.048	11.8
Ch 5	d.m.	7.8	274	36.73	25	0.94	5.5	11	0.02	35.1
Ch 6	shale	58.3	549	25.61	54	3.39	22	10.2	0.040	9.4
Ch 7	d.m.	1.1	321	30.06	2	0.19	1	160.5	0.00	291.8
Average		19.6	242	22.10	66	1.43	10.4	18.1	0.055	36.7

Formation: Sa= Sarki, Se= Sehkanian, Sg= Sargelu, Na= Naokelekan, Ba= Barsarin, Ch= Chia Gara.

Lithology: d.m.= dolomitic limestone.

Table 2

Selected major and trace element compositions, including paleoclimate and paleosalinity proxies of the samples from the Sarki, Sehkaniyan, Sargelu, Naokelekan, Barsarin and Chia Gara formations from the Ranya section.

Formation	Lithology	Cu (ppm)	Sr (ppm)	Ca (%)	Ba (ppm)	Al (%)	Rb (ppm)	Sr/Ba	Rb/Sr	Sr/Cu
Sa 0	shale	16.9	82	10.79	68	2.86	11.2	1.2	0.14	4.9
Sa 1	dolomite	4.6	88	19.82	22	0.64	9.8	4	0.11	19.1
Sa 2	shale	22.4	77	11.28	66	2.63	12.9	1.2	0.17	3.4
Sa 4	dolomite	2.7	74	21.37	3	0.19	2.9	24.7	0.04	27.4
Sa 5	shale	16.3	75	10.03	66	2.91	10.2	1.1	0.14	4.6
Sa 7	dolomite	1.9	84	20.96	15	0.16	2.2	5.6	0.03	44.2
Sa 8	shale	19	82	6.42	121	4.19	8.1	0.7	0.1	4.3
Sa 9	dolomite	2.3	77	20.89	8	0.3	3.4	9.6	0.04	33.5
Sa 10	shale	33.8	59	0.69	159	7.43	36.1	0.4	0.61	1.7
Sa 11	dolomite	8.6	123	19.65	87	1.08	18.9	1.4	0.15	14.3
Sa 11	shale	6.4	106	16.68	98	0.81	11.9	1.1	0.11	16.6
Sa 12	dolomite	2.7	74	20.23	23	0.2	2.6	3.2	0.04	27.4
Sa 13	shale	21.1	66	13.19	66	1.84	8.4	1	0.13	3.1
Sa 14	limestone	1.4	78	33.61	4	0.06	0.7	19.5	0.01	55.7
Sa 15	shale	2.4	70	14.24	18	2.06	22.4	3.9	0.32	29.2
Sa 16	dolomite	1.5	59	20.99	1	0.28	3.3	59	0.06	39.3
Sa 17	shale	28.2	49	3.6	80	5.86	14.1	0.6	0.29	1.7
Sa 19	d.m.	1.3	72	20.99	1	0.03	0.4	72	0.01	55.4
Sa 20	shale	15	90	13.3	52	3.07	37.8	1.7	0.42	6.0
Sa 22	d.m.	1.6	101	22.44	2	0.05	0.9	50.5	0.01	63.1
Sa 24	dolomite	1.5	80	22.85	1	0.07	0.6	80	0.01	53.3
Sa 25	shale	112.3	49	2.58	134	11.88	46.7	0.4	0.95	0.4
Sa 27	dolomite	1.7	72	21.39	1	0.31	3.3	72	0.05	42.4
Sa 28	shale	23.2	57	7.1	93	5.05	23.2	0.6	0.41	2.5
Sa 30	dolomite	1.7	82	21.88	1	0.08	1.4	82	0.02	48.2
Se 1	dolomite	4.3	94	19.06	15	1.23	17	6.3	0.18	21.9
Se 2	shale	28.9	57	7.95	92	5.51	29.6	0.6	0.52	2
Se 3	dolomite	3.5	83	20.83	2	0.16	2.4	41.5	0.03	23.7
Se 4	shale	37.1	42	4.93	177	7.14	19	0.2	0.45	1.1
Se 7	dolomite	1	126	21.99	3	0.1	1.5	42	0.01	126
Se 10	dolomite	1.5	76	20.87	2	0.72	1.6	38	0.02	50.7
Se 11	shale	19.1	18	0.66	88	6.33	73.5	0.2	4.08	0.9
Se 12	dolomite	1.5	84	19.4	2	0.07	1.3	42	0.02	56
Se 13	shale	22.6	54	8.54	83	3	18.2	0.7	0.34	2.4
Se 14	shale	64.5	24	0.38	69	6.27	53.4	0.3	2.23	0.4
Se 15	dolomite	1.1	90	20.38	1	0.16	3.7	90	0.04	81.8
Se 17	shale	19.4	50	1.14	161	10.89	190.6	0.3	3.81	2.6
Se 18	dolomite	0.8	87	20.4	1	0.1	1	87	0.01	108.8
Se 19	limestone	3.1	295	31.16	10	0.23	1.8	29.5	0.01	95.2
Se 21	dolomite	0.9	81	21.99	1	0.08	0.6	81	0.01	90
Se 24	dolomite	0.9	35	20.02	1	0.01	0.2	35	0.01	38.9
Se 27	dolomite	1.4	79	24.1	1	0.07	0.6	79	0.01	56.4
Se 31	dolomite	1.9	60	21.57	1	0.07	1	60	0.02	31.6
Sg 1	dolomite	2.9	60	21.85	1	0.2	3	60	0.05	20.7
Sg 4	dolomite	2.6	103	22.79	1	0.23	3.7	103	0.04	39.6
Sg 7	limestone	3.3	188	36.12	9	0.55	5.5	20.9	0.03	57
Sg 9	dolomite	15.9	111	19.72	3	0.36	5	37	0.05	7
Sg 10	shale	151.9	155	17.61	42	2.4	22.2	3.7	0.14	1
Sg 11	dolomite	46.3	191	18.19	30	1.5	5.6	6.4	0.03	4.1
Sg 11	shale	89.6	181	18.76	52	3.4	30.6	3.5	0.17	2
Sg 12	dolomite	7.4	164	22.18	2	0.1	1.7	82	0.01	22.2
Sg 12	shale	179.3	258	23.15	59	3.22	32.6	4.4	0.13	1.4
Sg 13	chert	14.4	89	4.69	93	0.24	2.3	1	0.03	6.2
Sg 13	limestone	36.5	448	28.41	38	0.93	13.9	11.8	0.03	12.3
Sg 13	shale	31.7	260	20.25	43	0.89	11.3	6	0.04	8.2
Sg 14	chert	11.5	126	6.1	22	0.22	1.8	5.7	0.01	11
Sg 14	limestone	6	352	33.97	12	0.11	1.2	29.3	0.00	58.7
Sg 14	shale	50.9	265	17.58	52	1.1	14.2	5.1	0.05	5.2
Na 1	limestone	29.2	380	33.29	91	0.67	13.3	4.2	0.04	13
Na 1	shale	37.3	384	24.47	139	0.88	13.6	2.8	0.04	10.3
Na 3	limestone	2	203	35.16	22	0.16	1.3	9.2	0.01	101.5
Ba 1	limestone	2.3	222	35.49	31	0.17	1.9	7.2	0.01	96.5
Ba 4	dolomite	4.1	370	21.46	2	0.28	2.7	185	0.01	90.2
Ba 6	d.m.	5.4	358	35.91	9	0.32	2.7	39.8	0.01	66.3
Ch 1	shale	15.8	1089	18.89	36	3.03	13	30.3	0.01	68.9
Ch 2	d.m.	7.5	607	32.37	20	1.5	8.2	30.4	0.01	80.9
Ch 4	shale	12.7	488	27.2	26	1.76	11.2	18.8	0.02	38.4
Ch 5	shale	18.5	1644	27.12	30	1.04	5.8	54.8	0.01	88.9
Ch 6	shale	28	603	14.11	73	6.2	16.1	8.3	0.03	21.5
Ch 7	limestone	11.4	842	27.1	33	2.81	10.2	25.5	0.01	73.9
Average		19.8	193	18.95	41	1.86	13.8	27.5	0.25	34.3

Formation: Sa= Sarki, Se= Sehkaniyan, Sg= Sargelu, Na= Naokelekan, Ba= Barsarin, Ch= Chia Gara.

Lithology: d.m.= dolomitic limestone.

Table 3

Selected trace and rare earth element compositions, including paleoredox proxies of the samples from the Sarki, Sehkaniyan, Sargelu, Naokelekan, Barsarin and Chia Gara formations from the Warte section.

Formation	Lithology	Ni	Co	U	Th	V	Cr	Sc	U/Th	V/Cr	Ni/Co	V/Sc	V/(V + Ni)
Sa 1	dolomite	2.8	2.2	0.9	0.5	9	4	0.3	1.8	2.3	1.3	30	0.8
Sa 2	shale	8.6	3.8	1.8	0.4	16	7	0.7	4.5	2	2.3	23	0.65
Sa 4	dolomite	1.2	0.5	1.2	0.3	6	2	0.1	4	3	2.4	60	0.8
Sa 6	shale	30.5	15.1	1.7	3.5	80	35	6.4	0.5	2	2	13	0.72
Sa 7	dolomite	3.7	1.2	0.9	0.3	8	3	0.1	3	2.7	3.1	80	0.7
Sa 8	shale	28.7	14.2	2.3	2.2	96	45	5.7	1	2	2	17	0.77
Sa 9	dolomite	4.5	3.2	2.2	0.2	8	3	0.2	11	2.7	1.4	40	0.6
Sa 10	shale	10.7	5.1	2.1	1.7	31	13	2.5	1.2	2	2.1	12	0.74
Sa 11	dolomite	2.4	1.2	1.1	0.2	8	3	0.2	5.5	2.7	2	40	0.8
Sa 12	shale	3	1.9	1.4	0.2	14	6	0.8	7	2	1.6	18	0.82
Sa 14	dolomite	1.2	1.1	1	0.2	10	4	0.2	5	2.5	1.1	50	0.9
Sa 15	shale	11.4	7	1.9	3.1	27	13	3.1	0.6	2	1.6	9	0.70
Sa 17	dolomite	7.3	3.1	2.2	0.3	14	6	0.5	7.3	2.3	2.4	28	0.7
Sa 18	shale	27.7	12.1	3	4.1	92	47	7.2	0.7	2	2.3	13	0.77
Sa 20	dolomite	3.2	2.6	3.1	0.1	16	3	0.2	31	5.3	1.2	80	0.8
Sa 21	shale	84	39.6	19	2.7	181	68	6.8	7	3	2.1	27	0.68
Sa 24	dolomite	1	0.9	1.1	0.1	7	3	0.1	11	2.3	1.1	70	0.9
Sa 28	shale	46.9	13	20.2	4.4	132	54	4.7	4.6	2	3.6	28	0.74
Sa 30	dolomite	0.1	0.2	1.4	0.1	7	2	0.1	14	3.5	0.5	70	1.0
Sa 31	shale	19.7	7.4	12.6	2.5	139	22	2.6	5	6	2.7	53	0.88
Sa 34	dolomite	9	2.1	5.2	0.1	57	5	0.2	52	11.4	4.3	285	0.9
Sa 36	dolomite	1.5	0.7	1.6	0.2	6	2	0.1	8	3	2.1	60	0.8
Se 1	d.m.	3.1	0.9	2.4	1	20	5	1	2.4	4	3.4	20	0.9
Se 3	shale	20.2	7.1	3.3	3.3	101	32	4.7	1	3	2.8	21	0.83
Se 4	dolomite	3	1.3	1.6	0.1	14	4	0.2	16	3.5	2.3	70	0.8
Se 6	shale	28.9	13.8	2.1	3.4	60	33	4.7	0.6	2	2.1	13	0.68
Se 10	dolomite	1.3	0.2	1.1	0.1	4	1	0.1	11	4	6.5	40	0.8
Se 13	dolomite	3.3	0.2	1.1	0.1	9	2	0.1	11	4.5	16.5	90	0.7
Se 16	dolomite	0.3	0.2	0.8	0.1	3	1	0.1	8	3	1.5	30	0.9
Se 19	dolomite	0.5	0.2	0.4	0.1	1	1	0.1	4	1	2.5	10	0.7
Se 21	shale	56.3	4.8	1.6	1.6	45	28	2	1	2	11.7	23	0.44
Se 24	dolomite	1.3	0.2	0.9	0.1	2	1	0.1	9	2	6.5	20	0.6
Se 27	dolomite	2.7	0.4	0.9	0.1	5	2	0.2	9	2.5	6.8	25	0.6
Se 31	shale	13.6	1.4	6.7	0.3	24	6	0.6	22.3	4	9.7	40	0.6
Sg 1	dolomite	9.5	1.4	3.8	0.1	28	4	0.3	38	7	6.8	93.3	0.7
Sg 3	limestone	25.5	0.2	8.4	0.3	371	31	0.4	28	12	127.5	927.5	0.9
Sg 5	limestone	8.7	0.9	2	0.5	14	7	1.5	4	2	9.7	9.3	0.6
Sg 6	shale	41	0.9	11	0.2	311	33	0.5	55	9	45.6	622	0.88
Sg 7	limestone	18.6	0.3	4.2	0.5	59	19	0.9	8.4	3.1	62	65.6	0.8
Sg 7	shale	91.6	10.3	7.5	2	65	29	4.2	3.8	2	8.9	15	0.42
Sg 8	d.m.	29.6	4	4.4	1.6	40	14	3.1	2.8	2.9	7.4	12.9	0.6
Sg 8	shale	340.3	30.9	31.4	5.7	650	66	9.1	5.5	10	11	71	0.66
Sg 9	d.m.	37.1	7.5	4.9	1.6	54	16	2.5	3.1	3.4	4.9	21.6	0.6
Sg 9	shale	78.2	10.7	5.9	2	101	36	3.7	3	3	7.3	27	0.56
Sg 10	d.m.	22.2	2	4.4	0.7	109	11	1.5	6.3	9.9	11.1	72.7	0.8
Sg 10	shale	324.8	9.1	21.1	1.6	484	65	3.3	13.2	7	35.7	147	0.6
Sg 11	limestone	117.4	1.5	1.7	0.1	43	9	0.1	17	4.8	78.3	430	0.3
Sg 11	chert	37.8	1.6	2.2	0.2	64	10	0.4	11	6.4	23.6	160	0.6
Sg 11	shale	369.3	6.1	25	1.3	367	49	3.2	19.2	7	60.5	115	0.5
Sg 12	d.m.	19.5	0.5	3.5	0.2	28	5	0.4	17.5	5.6	39	70	0.6
Sg 13	shale	270	5.7	39.1	1.8	293	50	4.2	21.7	6	47.4	70	0.52
Na 1	shale	387.8	11.5	32	2.2	323	46	5.6	14.5	7	33.7	58	0.45
Na 2	limestone	69.2	1.6	18.4	0.6	185	24	1.4	30.7	7.7	43.3	132.1	0.7
Na 3	d.m.	39.8	0.2	6.5	0.3	101	10	0.7	21.7	10.1	199	144.3	0.7
Na 4	shale	397.4	3	40.7	1.7	1124	121	2.9	23.9	9	132.5	388	0.74
Na 6	limestone	38.3	0.5	9.2	0.3	293	27	0.5	30.7	10.9	76.6	586	0.9
Na 8	shale	369.4	32.6	28.3	4.7	603	64	7.8	6	9	11.3	77	0.62
Na 10	dolomite	39.1	6.3	6.2	1.7	194	25	2.7	3.6	7.8	6.2	71.9	0.8
Ba 1	limestone	4.3	0.6	1.1	0.2	19	4	0.3	5.5	4.8	7.2	63.3	0.8
Ba 2	shale	39.9	2.6	10.3	0.8	63	14	1.5	12.9	5	15.3	42	0.61
Ba 3	d.m.	40.2	2.4	24.3	0.6	60	7	1	40.5	8.6	16.8	60	0.6
Ba 5	shale	24.9	1.7	5.8	0.4	46	11	1	14.5	4	14.6	46	0.65
Ba 6	limestone	15.9	1	4.8	0.6	40	7	0.8	8	5.7	15.9	50	0.7
Ba 9	d.m.	17.8	7.5	13.3	0.7	175	10	1.5	19	17.5	2.4	116.7	0.9
Ch 1	shale	228.3	36.6	34.9	9.9	640	76	11.6	3.5	8	6.2	55	0.74
Ch 2	d.m.	59.4	13.6	6.6	2.2	238	28	3	3	8.5	4.4	79.3	0.8
Ch 3	shale	37.6	5.1	5.7	0.3	188	7	0.7	19	27	7.4	269	0.83
Ch 4	shale	295.7	59.4	40.1	8.5	929	76	9.6	4.7	12	5	97	0.76
Ch 5	d.m.	13.5	3.8	4.2	0.7	74	10	1.2	6	7.4	3.6	61.7	0.8
Ch 6	shale	107.6	21.6	13.1	3.7	210	46	5	3.5	5	5	42	0.66
Ch 7	d.m.	1.8	0.9	2.7	0.1	25	3	0.2	27	8.3	2	125	0.9
Average		63.6	6.7	8.4	1.4	139	22	2.2	11.8	5.5	18.5	98.6	0.7

Formation: Sa= Sarki, Se= Sehkanyian, Sg= Sargelu, Na= Naokelekan, Ba= Barsarin, Ch= Chia Gara.

Lithology: d.m.= dolomitic limestone.

Table 4

Selected trace and rare earth element compositions, including paleoredox proxies of the samples from the Sarki, Sehkaniyan, Sargelu, Naokelekan, Barsarin and Chia Gara formations from the Ranya section.

Formation	Lithology	Ni	Co	U	Th	V	Cr	Sc	U/Th	V/Cr	Ni/Co	V/Sc	V/(V + Ni)
Sa 0	shale	20.2	10.3	2.2	2.9	49	24	4.1	0.8	2	2	12	0.71
Sa 1	dolomite	4.4	2.4	1.7	0.3	12	5	0.5	5.7	2.4	1.8	24	0.7
Sa 2	shale	27.6	11.8	4	3.1	54	23	3.7	1.3	2	2.3	15	0.66
Sa 4	dolomite	2.2	0.7	0.7	0.1	8	2	0.1	7	4	3.1	80	0.8
Sa 5	shale	21.1	13.1	1.8	2.8	51	25	4.2	0.6	2	1.6	12	0.71
Sa 7	dolomite	1.4	0.6	1.6	0.1	9	2	0.1	16	4.5	2.3	90	0.9
Sa 8	shale	30.7	15.9	2.2	2.9	86	36	5.2	0.8	2	1.9	17	0.74
Sa 9	dolomite	3.7	1.5	0.7	0.1	9	3	0.1	7	3	2.5	90	0.7
Sa 10	shale	47.3	21	3.8	2.9	126	79	7.3	1.3	2	2.3	17	0.73
Sa 11	dolomite	11.7	6.3	3.5	0.8	19	8	1.4	4.4	2.4	1.9	13.6	0.6
Sa 11	shale	8	2.6	3.2	0.2	21	8	0.7	16	3	3.1	30	0.72
Sa 12	dolomite	2.1	0.7	1.2	0.1	12	2	0.1	12	6	3	120	0.9
Sa 13	shale	12.4	5.4	4.7	2.2	38	27	2.7	2.1	1	2.3	14	0.75
Sa 14	limestone	0.6	0.2	1.7	0.1	7	2	0.1	17	3.5	3	70	0.9
Sa 15	shale	8.8	3.6	3	3.7	35	14	2.9	0.8	3	2.4	12	0.80
Sa 16	dolomite	1.7	0.4	1.5	0.1	7	4	0.1	15	1.8	4.3	70	0.8
Sa 17	shale	42	7.4	19.2	1.8	130	63	2.6	10.7	2	5.7	50	0.76
Sa 19	d.m.	0.1	0.3	4.8	0.1	8	1	0.1	48	8	0.3	80	1.0
Sa 20	shale	21.3	7.4	8.9	2.4	61	24	4	3.7	3	2.9	15	0.74
Sa 22	d.m.	0.9	0.5	3	0.1	14	2	0.1	30	7	1.8	140	0.9
Sa 24	dolomite	2	0.4	3.1	0.1	11	1	0.1	31	11	5	110	0.8
Sa 25	shale	143.4	13.9	41.8	10	724	138	8	4.2	5	10.3	91	0.84
Sa 27	dolomite	1.8	0.7	2	0.1	9	2	0.1	20	4.5	2.6	90	0.8
Sa 28	shale	44.4	12.9	6.1	4.6	98	40	6	1.3	2	3.4	16	0.69
Sa 30	dolomite	1.7	0.3	5.4	0.1	14	2	0.1	54	7	5.7	140	0.9
Se 1	dolomite	13	3.6	1.4	0.9	25	6	1.7	1.6	4.2	3.6	14.7	0.7
Se 2	shale	44.2	15.7	5.4	6.2	98	39	7.7	0.9	3	2.8	13	0.69
Se 3	dolomite	1.7	0.4	1.3	0.1	7	1	0.1	13	7	4.3	70	0.8
Se 4	shale	59.4	24.5	6.2	3.8	159	75	6.4	1.6	2	2.4	25	0.73
Se 7	dolomite	1.9	0.5	2.8	0.1	10	2	0.1	28	5	3.8	100	0.8
Se 10	dolomite	3.5	0.9	1.1	0.1	7	3	0.1	11	2.3	3.9	70	0.7
Se 11	shale	30	12.2	1.5	4	133	77	10.6	0.4	2	2.5	13	0.82
Se 12	dolomite	2.7	0.6	0.7	0.1	3	1	0.1	7	3	4.5	30	0.5
Se 13	shale	31	12.1	4.8	2.5	68	28	3.5	1.9	2	2.6	19	0.69
Se 14	shale	52.8	24.4	5	2.9	145	79	8.6	1.7	2	2.2	17	0.73
Se 15	dolomite	1.3	0.6	0.9	0.1	5	3	0.1	9	1.7	2.2	50	0.8
Se 17	shale	47.6	12.1	5.4	15	138	86	18.1	0.4	2	3.9	8	0.74
Se 18	dolomite	0.8	0.2	1.2	0.1	4	1	0.1	12	4	4	40	0.8
Se 19	limestone	4.8	1	1.8	0.3	12	3	0.4	6	4	4.8	30	0.7
Se 21	dolomite	2.8	0.4	1	0.1	4	1	0.1	10	4	7	40	0.6
Se 24	dolomite	0.1	0.3	0.2	0.1	1	1	0.1	2	1	0.3	10	0.9
Se 27	dolomite	1.2	0.3	0.9	0.1	3	1	0.1	9	3	4	30	0.7
Se 31	dolomite	2.3	0.3	2	0.1	5	2	0.1	20	2.5	7.7	50	0.7
Sg 1	dolomite	3.4	0.6	1.7	0.1	8	4	0.1	17	2	5.7	80	0.7
Sg 4	dolomite	2.3	1	1.7	0.1	10	4	0.1	17	2.5	2.3	100	0.8
Sg 7	limestone	1.6	0.8	0.6	0.6	6	6	1.1	1	1	2	5.5	0.8
Sg 9	dolomite	33.7	1.5	3.6	2	29	6	0.6	1.8	4.8	22.5	48.3	0.5
Sg 10	shale	199.9	19.3	14.7	2.8	139	37	4.1	5.3	4	10.4	34	0.41
Sg 11	dolomite	76.4	7.2	6.5	2.1	84	31	2.9	3.1	2.7	10.6	29	0.5
Sg 11	shale	167.3	13.3	13.9	3.3	121	36	4.1	4.2	3	12.6	30	0.42
Sg 12	dolomite	8.8	1.6	3.7	0.1	28	3	0.1	37	9.3	5.5	280	0.8
Sg 12	shale	324.8	32.1	23.6	3	163	64	5.4	7.9	3	10.1	30	0.33
Sg 13	chert	58.1	2.2	2	0.2	74	15	0.3	10	4.9	26.4	246.7	0.6
Sg 13	limestone	295.2	3	14.7	1.2	358	43	2.8	12.3	8.3	98.4	127.9	0.5
Sg 13	shale	232	4.7	13	0.9	320	29	2	14.4	11	49.4	160	0.58
Sg 14	chert	53.9	3.3	3.6	0.2	41	13	0.5	18	3.2	16.3	82	0.4
Sg 14	limestone	23.4	1.1	4.7	0.1	60	7	0.4	47	8.6	21.3	150	0.7
Sg 14	shale	268.3	8.7	22.6	1.3	179	31	2.6	17.4	6	30.8	69	0.4
Na 1	limestone	156.7	0.9	24.1	1.2	424	54	1.1	20.1	7.9	174.1	385.5	0.7
Na 1	shale	295.6	1.4	29.7	1.2	578	56	2.5	24.8	10	211.1	231	0.66
Na 3	limestone	3.3	0.2	3	0.2	16	6	0.4	15	2.7	16.5	40	0.8
Ba 1	limestone	6.8	0.2	6.3	0.3	22	4	0.2	21	5.5	34	110	0.8
Ba 4	dolomite	9.4	3.5	2	0.1	26	3	0.1	20	8.7	2.7	260	0.7
Ba 6	d.m.	10	2.2	4.4	0.5	71	6	0.8	8.8	11.8	4.5	88.8	0.9
Ch 1	shale	59.7	4.4	8.8	4.7	277	32	4.4	1.9	9	13.6	63	0.82
Ch 2	d.m.	26.7	2.8	2.4	2.8	100	21	2.2	0.9	4.8	9.5	45.5	0.8
Ch 4	shale	37.8	5	8.1	2	143	23	2.5	4.1	6	7.6	57	0.79
Ch 5	shale	49.9	2.4	12.8	1.4	307	21	2.5	9.1	15	20.8	123	0.86
Ch 6	shale	98.4	10.3	6.6	8.9	291	53	6.3	0.7	5	9.6	46	0.75
Ch 7	limestone	34.6	4.3	3.1	3.9	108	45	4.4	0.8	2.4	8	24.5	0.8
Average		47.2	5.5	6.0	1.8	92	23	2.4	11.2	4.5	14.0	71.4	0.7

Formation: Sa= Sarki, Se= Sehkaniyan, Sg= Sargelu, Na= Naokelekan, Ba= Barsarin, Ch= Chia Gara.

Lithology: d.m.= dolomitic limestone.

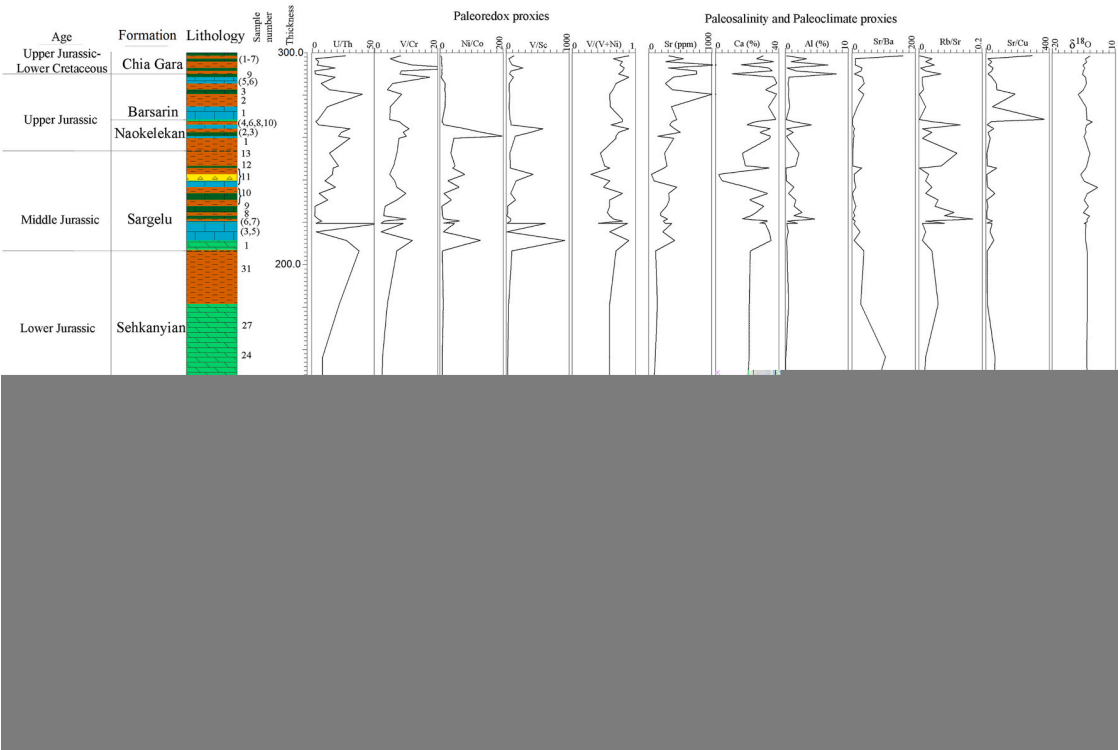


Fig. 10. Distribution of the values of paleoclimate, paleosalinity and paleoredox proxies along the sedimentary log of the Warte section, NE Iraq (see also sample locations).

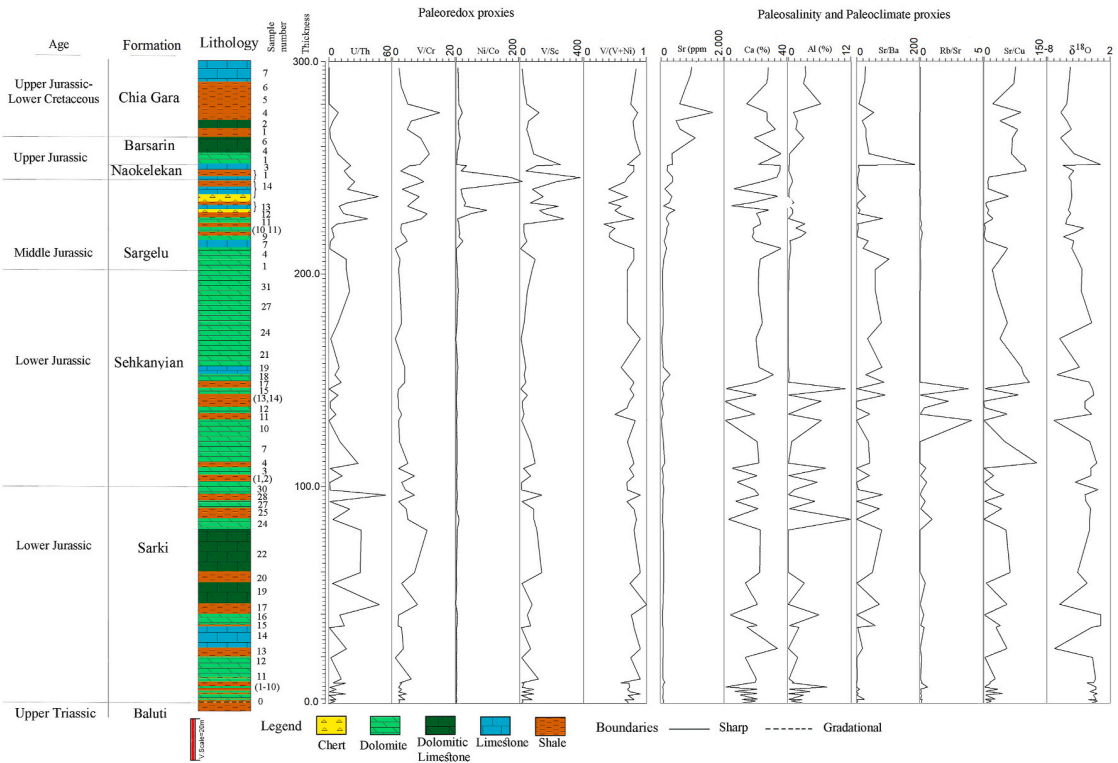


Fig. 11. Distribution of the values of paleoclimate, paleosalinity and paleoredox proxies along the sedimentary log of the Ranya section, NE Iraq (see also sample locations).

Table 5

Carbon isotope (^{13}C) and oxygen isotope (^{18}O) records of the samples from the Sarki, Sehkanyian, Sargelu, Naokelekan, Barsarin and Chia Gara formations from the Warte section.

Formation	lithology	^{13}C [‰]	^{18}O [‰]
Sa 1	dolomite	-0.76	0.13
Sa 2	shale	-0.52	-1.03
Sa 4	dolomite	0.82	0.71
Sa 6	shale	-0.80	-0.97
Sa 7	dolomite	-0.90	-0.29
Sa 8	shale	-1.23	-2.24
Sa 9	dolomite	-1.33	-0.32
Sa 10	shale	-1.43	-1.50
Sa 11	dolomite	2.45	-1.11
Sa 12	shale	-1.08	-1.86
Sa 14	dolomite	0.13	0.37
Sa 15	shale	-0.69	-0.79
Sa 17	dolomite	-1.24	-0.30
Sa 18	shale	-1.49	-2.11
Sa 20	dolomite	-1.40	-0.44
Sa 21	shale	-1.95	-1.56
Sa 24	dolomite	-1.21	-0.10
Sa 28	shale	0.99	-3.22
Sa 30	dolomite	1.30	-0.94
Sa 31	shale	-3.66	-1.70
Sa 34	dolomite	-0.87	-0.07
Sa 36	dolomite	-3.05	-1.28
Se 1	d.m.	-3.27	-10.07
Se 3	shale	-5.46	-4.48
Se 4	dolomite	-4.44	-0.97
Se 6	shale	-0.70	-0.29
Se 10	dolomite	-1.48	-0.04
Se 13	dolomite	0.53	-1.18
Se 16	dolomite	-2.10	-5.00
Se 19	dolomite	1.47	-6.58
Se 21	shale	-7.38	-7.29
Se 24	dolomite	0.14	-3.09
Se 27	dolomite	-1.79	-3.79
Se 31	shale	-0.89	-3.34
Sg 1	dolomite	-3.02	-3.42
Sg 3	limestone	-2.68	-4.15
Sg 5	limestone	-0.03	-4.25
Sg 6	shale	-3.30	-4.00
Sg 7	limestone	-5.21	-3.30
Sg 7	shale	-0.99	-4.91
Sg 8	d.m.	-1.76	-2.27
Sg 8	shale	-1.21	-3.64
Sg 9	d.m.	-0.49	-2.84
Sg 9	shale	-2.84	-5.28
Sg 10	d.m.	-5.82	-3.38
Sg 10	shale	-1.94	-4.92
Sg 11	limestone	-3.34	-6.57
Sg 11	chert	-3.34	-4.92
Sg 11	shale	i.s.	i.s.
Sg 12	d.m.	-4.14	-4.21
Sg 13	shale	-4.44	-3.70
Na 1	shale	-3.31	-2.22
Na 2	limestone	-5.81	-4.64
Na 3	d.m.	-5.82	-5.03
Na 4	shale	-4.26	-4.06
Na 6	limestone	-3.76	-4.26
Na 8	shale	-1.61	-3.70
Na 10	dolomite	-6.49	-0.99
Ba 1	limestone	-9.91	-3.57
Ba 2	shale	-9.19	-4.01
Ba 3	d.m.	-9.97	-7.77
Ba 5	shale	-9.69	-5.24
Ba 6	limestone	-10.40	-3.94
Ba 9	d.m.	-9.49	-4.12
Ch 1	shale	-4.70	-5.70
Ch 2	d.m.	-6.04	-5.36
Ch 3	shale	-8.21	-4.60
Ch 4	shale	-4.91	-5.39
Ch 5	d.m.	-10.65	-3.67
Ch 6	shale	-11.18	-4.27
Ch 7	d.m.	-9.14	-2.13

Formation: Sa= Sarki, Se= Sehkanyian, Sg= Sargelu, Na= Naokelekan, Ba= Barsarin.

Ch= Chia Gara. Lithology: d.m.= dolomitic limestone. i.s.= insufficient signal.

proxy for paleoredox conditions. According to these authors, U/Th ratio values of greater than 1.25 are considered to be indicative of deposition under anoxic conditions. Generally, the values recorded from the samples of the six formations from the Ranya and Warte sections are higher than 1.25 (Tables 3 and 4, Figs. 10 and 11) suggesting that the sediments were deposited under anoxic conditions.

Krejci-Graf (1966), Ernst (1970), Dill (1986), Jones and Manning (1994), and Deepulal et al. (2012) suggested that the ratio of Ni/Co could be used to provide information with regard to the paleoredox conditions. According to Krejci-Graf (1966) and Ernst (1970), values of less than 1 for the Ni/Co ratio may indicate deposition under oxic conditions, while values more than 1 would indicate anoxic conditions. Indeed, the values obtained from all six formations are higher than 1 (see Tables 3 and 4, Figs. 10 and 11) strongly suggesting that deposition occurred under anoxic conditions.

The V/Cr ratio has been considered by Jones and Manning (1994) to provide some indication to oxygenation conditions in the environment of deposition. They suggested that in case of ratios of greater than 4.5, anoxic conditions were predominant, while values of less than 2 suggest that oxic conditions prevailed (Jones and Manning, 1994). The V/Cr ratio values of the samples from the Sarki and Sehkanyian formations from the Warte section, are less than 4.5 (see Table 3, Fig. 10) suggesting that anoxia was less prevalent within the period during which they were deposited. Upon moving up one section, the V/Cr ratio values of the samples from the Sargelu, Naokelekan, Barsarin and Chia Gara formations are moderately increased to above 4.5. This would suggest, as noted before, that anoxic conditions became dominant during the time of their deposition.

In comparison, the samples of the Sarki, Sehkanyian and Sargelu formations from the Ranya section of NE Iraq, show values of less than 4.5 for the V/Cr ratio (see Table 4, Fig. 11). This would suggest that sediments of the Sarki, Sehkanyian and Sargelu formations of the Ranya section were deposited within a time during which anoxia was less prevalent, except for the uppermost sediments from the Sargelu Formation which have high V/Cr values (see Table 4, Fig. 11). This increase might support the suggestion of a marked increase in anoxia at this time.

The overlying Naokelekan, Barsarin and Chia Gara formations from the same section (i.e., Ranya) also have V/Cr values of greater than 4.5 (see Table 4, Fig. 11). Again, this would indicate that anoxic conditions were common during the period of their deposition.

According to Kimura and Watanabe (2001), the V/Sc ratio is indicative of oxygenation conditions. Ratio values of less than 9 suggest oxidizing conditions, while values greater than 9 suggest that conditions were suboxic (Kimura and Watanabe, 2001). The V/Sc ratio values of the samples from the six formations from both sections (i.e., the Warte and Ranya sections) are all greater than 9, which would suggest deposition within a zone of suboxic conditions (see Tables 3 and 4, Figs. 10 and 11).

Hatch and Leventhal (1992) have suggested that values for the V/(V + Ni) ratio that are between 0.54 and 0.84 would suggest anoxic conditions, whilst values greater than 0.84 would indicate euxinic conditions. Commonly, values of the V/(V + Ni) ratio from the samples of the six formations from both sections range from 0.54 to 0.84 (see Tables 3 and 4, Figs. 10 and 11) again suggesting that anoxic conditions were predominant during the time of deposition of the sediments of the Warte and Ranya sections.

In summary, the results obtained from the paleoredox proxies, as detailed above, indicate that the deposition of the Early Jurassic-Early Cretaceous-age sediments of NE Iraq probably occurred under anoxic conditions, with interspersed (and shorter) periods of reduced oxygen levels. According to Haq (2018), sedimentation through the Hettangian and Early Sinemurian coincided with low sea-levels, whilst the Late

Table 6

Carbon isotope (^{13}C) and oxygen isotope (^{18}O) records of the samples from the Sarki, Sehkanyian, Sargelu, Naokelekan, Barsarin and Chia Gara formations from the Ranya section.

Formation	Lithology	^{13}C [‰]	^{18}O [‰]
Sa 0	shale	-1.01	-0.97
Sa 1	dolomite	-0.92	-0.10
Sa 2	shale	-0.73	-1.46
Sa 4	dolomite	-0.30	-0.28
Sa 5	shale	-1.25	-0.71
Sa 7	dolomite	0.27	-0.13
Sa 8	shale	-0.53	-1.21
Sa 9	dolomite	-0.13	-0.26
Sa 10	shale	i.s.	i.s.
Sa 11	dolomite	-1.41	-0.65
Sa 11	shale	-1.43	-1.69
Sa 12	dolomite	-0.97	-0.38
Sa 13	shale	-0.71	-0.83
Sa 14	limestone	-2.82	-6.86
Sa 15	shale	0.79	-0.98
Sa 16	dolomite	1.43	0.49
Sa 17	shale	i.s.	i.s.
Sa 19	d.m.	-3.30	-6.02
Sa 20	shale	1.13	-1.70
Sa 22	d.m.	-0.91	-3.19
Sa 24	dolomite	-0.88	-1.31
Sa 25	shale	i.s.	i.s.
Sa 27	dolomite	-2.96	-1.10
Sa 28	shale	-3.71	-1.90
Sa 30	dolomite	-1.25	-2.02
Se 1	dolomite	-0.76	0.02
Se 2	shale	-1.07	-3.57
Se 3	dolomite	-0.50	-1.08
Se 4	shale	-1.47	-1.14
Se 7	dolomite	-0.89	-0.19
Se 10	dolomite	-1.55	-1.28
Se 11	shale	-11.06	-6.93
Se 12	dolomite	-0.47	-0.99
Se 13	shale	-0.39	-2.07
Se 14	shale	i.s.	i.s.
Se 15	dolomite	-1.78	-0.63
Se 17	shale	i.s.	i.s.
Se 18	dolomite	-2.47	-1.36
Se 19	limestone	-3.93	-6.45
Se 21	dolomite	-2.69	-2.90
Se 24	dolomite	1.40	-6.04
Se 27	dolomite	1.13	-0.98
Se 31	dolomite	-0.75	-2.64
Sg 1	dolomite	-0.64	-2.51
Sg 4	dolomite	-0.92	-3.26
Sg 7	limestone	0.55	-4.10
Sg 9	dolomite	-2.49	-3.84
Sg 10	shale	-4.17	-5.43
Sg 11	dolomite	-1.76	-2.26
Sg 11	shale	-1.47	-3.63
Sg 12	dolomite	-2.99	-4.85
Sg 12	shale	-2.51	-5.08
Sg 13	chert	-3.31	-4.43
Sg 13	limestone	-3.48	-4.67
Sg 13	shale	-3.69	-4.30
Sg 14	chert	-4.25	-4.21
Sg 14	limestone	i.s.	i.s.
Sg 14	shale	-3.74	-4.33
Na 1	limestone	-8.97	-4.18
Na 1	shale	-4.39	-4.63
Na 3	limestone	-5.70	-3.82
Ba 1	limestone	-8.45	-5.53
Ba 4	dolomite	-10.07	0.39
Ba 6	d.m.	-11.15	-3.77
Ch 1	shale	-3.22	-5.90
Ch 2	d.m.	-2.13	-4.18
Ch 4	shale	-4.86	-4.89
Ch 5	shale	-3.16	-5.83
Ch 6	shale	-0.75	-4.93
Ch 7	limestone	-0.52	-4.56

Formation: Sa= Sarki, Se= Sehkanyian, Sg= Sargelu, Na= Naokelekan, Ba= Barsarin.

Ch= Chia Gara. Lithology: d.m.= dolomitic limestone. i.s.= insufficient signal.

Sinemurian-Pliensbachian (i.e., the boundary between the Sarki and Sehkanyian formations) coincided with an eustatic rise. In the Toarcian (i.e., late Sehkanyian Formation times), there was another eustatic rise (Haq, 2018). As noted above, the depositional history of both formations is one which is predominantly supratidal (according to the carbonate microfacies), with little variation, apart from a deepening to a coast-adjacent lagoonal setting in the middle of the Sehkanyian Formation. However, the sea-level at this time would have been lower than at both the beginning and end of the depositional period, which does not quite equate with a deepening. A possible explanation would be that the water level recorded by the two sections is one which reflects the local conditions (i.e., relative sea-level) where tectonics also played a major role (e.g., Murris, 1980; Sharland et al., 2001). As noted by Tavani et al. (2018), the tectonic architecture of the Zagros region is strongly controlled by both sedimentary and structural inheritance (e.g., Hessami et al., 2001; Alavi, 2004; Mouthereau et al., 2012; Tavakoli-Shirazi et al., 2013). The Mesozoic succession suggests that there was a major Early Jurassic-age phase of extension with a coeval change from shallow-to deep-marine environments (Tavani et al., 2018). Clearly, the pattern observed in Iraq does not correlate suggesting a disconnect between the two areas. The Sarki and Sehkanyian formations record mainly a coastal environment with short periods of deepening (but only to coast-adjacent lagoons). This would suggest that the major phase of Early Jurassic extension in the Zagros Belt did not extend to N Iraq. Instead, it would appear that the tectonic evolution of the N Iraq region was, to a degree, independent - certainly based on the stability of the observed sediment microfacies. One important aspect, however, which must be discussed is the possibility that the dolomitization which is predominant in both the Sarki and Sehkanyian formations has obscured, or even destroyed, any primary evidence of the original depositional setting (here, presuming that the setting was one that was different from the one which is reconstructed on the basis of the existing record) (e.g., Purser et al., 1994a, b; Al-Langawi, 2006). The dolomites of the region at this time mostly show an equiplanar texture which is planar (idiotopic) (Csató et al., 2014; Delizy and Shingaly, 2022).

An eustatic fall of sea-level occurred in the Early Aalenian, with a subsequent rise from the Late Aalenian onwards (Haq, 2018). There were two short falls in sea-level in the Bajocian and the latest Callovian (Haq, 2018). The depositional record of the Sargelu Formation covers the period from the Aalenian through to the Callovian, and could be expected to reflect the sea-level rise, which is the case, to an extent. The environment of deposition is interpreted as being supratidal/subtidal for much of the formation, with shelf or even bathyal settings recorded from the uppermost parts of the formation. Such settings would agree broadly with the eustatic record (cf. Haq, 2018) of a gradual deepening of the basin. As with the underlying formations, however, the supratidal/subtidal signal may be one that is secondary, given the degree of dolomitization which the rocks underwent (cf. Zenger, 1972; Al-Juboury and Durovic, 1996; Sena et al., 2014; Al-Haj et al., 2019). The lack of fabrics within the dolomites (i.e., possibly fabric destructive rather than fabric retentive) would suggest that the degree of diagenesis was significant. The dolomitization most probably occurred as a result of seaward hydrodynamic reflux of Mg-enriched brines, with the continental supratidal sabkhas providing ideal conditions for brine evolution.

The Oxfordian and Kimmeridgian are absent from the succession, with the disconformable Naokelekan Formation representing the Early Tithonian, whilst the conformable overlying Barsarin Formation represents late Early Tithonian to Middle Tithonian. As noted by Haq (2018), there was a sea-level rise at the Kimmeridgian-Tithonian boundary. Deposition within the Naokelekan Formation has been interpreted as being bathyal in the Ranya section, but supratidal in the Warte area. These two sections (i.e., Warte and Ranya sections) are ca. 70 km apart but located in different structural zones of the Zagros Belt, namely, the High Folded Zone, and the Imbricated Zone. These two zones are separated from one another by folding and faulting (Murris, 1980; Sharland et al., 2001; Abdunaby, 2019). This distance, as well as the

fact that the sections are located in different tectonic units, may explain the observed differences in terms of depositional setting.

In contrast, the overlying Barsarin Formation in both the Warte and Ranya sections has been interpreted as having been deposited in an intertidal to subtidal setting, and this despite the different tectonic zones (see above). As noted above, the Naokelekan Formation sedimentation in the Ranya section, which has been suggested to have occurred in deep waters, contrasts with the depositional case of the Naokelekan Formation elsewhere in NE Iraq (i.e., the Warte section) which has been interpreted as having occurred in shallower waters. This disparity in terms of sea-level rising versus the suggested shallower depositional environments (i.e., intertidal to subtidal) in the area of the Warte and Ranya sections, has also been observed in the Barsarin Formation. A reasonable interpretation is that ongoing tectonic activity related to the period of Cimmerian uplift (Buday, 1980) resulted in the formation of small silled sub-basins (see also Omar et al., 2020, 2021) within the broader Zagros Basin/Zagros Fold Belt and the depositional settings of the Upper Jurassic (Naokelekan and Barsarin) formations. This tectonic fragmentation within the marine depositional settings (i.e., areas of higher and lower relief) can also be observed in the lowermost part of the Chia Gara Formation in the Ranya section, which has been interpreted as having been deposited in an intertidal to subtidal setting. On the other hand, sedimentation of the overlying parts of the Chia Gara Formation in the same section and in the Warte section, was interpreted to have occurred within bathyal settings. This latter interpretation correlates well with the sea-level signal through the Late Tithonian, which remained high (Haq, 2018).

The observed differences in depositional settings within the stratigraphic units may also explain the differences in oxygen levels measured, where anoxic facies were predominant within the sub-basins active in the region.

6. Conclusions

Various elemental ratios of major and trace elements (Sr, Ca, Al, Sr/Ba, Rb/Sr and Sr/Cu) integrated with oxygen isotopic geochemistry of the Early Jurassic-Early Cretaceous-age Warte and Ranya sections, were utilized to reconstruct the climate conditions prevailing during the Early Jurassic-Early Cretaceous period of NE Iraq. The obtained results suggest that a hot and arid climate dominated most of the Jurassic time.

During the deposition of the Late Jurassic-Early Cretaceous-age Chia Gara Formation in both the Warte and Ranya sections, the climate changed from predominantly arid to more humid conditions. A change in clay mineralogy was observed, from the dominance of illite to increasing amounts of kaolinite within the Chia Gara Formation, where the presence of the latter mineral clearly reflects more humid conditions during this period (Late Jurassic-Early Cretaceous) in NE Iraq.

Petrographic and microfacies analyses of the carbonate units of Early Jurassic-Early Cretaceous-age Warte and Ranya sections in NE Iraq indicated that the Warte and Ranya sediments had mainly formed within tidal flats (supratidal) and in restricted lagoons, as well as in shallow marine and bathyal settings during the Early Jurassic-Early Cretaceous period.

Geochemical proxies for the redox state (U/Th, V/Cr, Ni/Co, V/Sc and V/(V+Ni)) revealed that conditions during deposition of the Warte and Ranya sediments were likely anoxic with periods of low oxygen. This difference between paleoredox and depositional conditions is likely related to variations in tectonic settings within the Zagros Belt, which extends across the region of northern Iraq.

Declaration of competing interest

The authors declare that they have no known competing financial interests or personal relationships that could have appeared to influence the work reported in this paper.

Data availability

No data was used for the research described in the article.

Acknowledgements

This work was supported by the Arab-German Young Academy of Sciences and Humanities (AGYA) that is funded under the German Federal Ministry of Education and Research (BMBF) grant 01DL20003.

References

- Abdula, R., 2017. Source rock assessment of Naokelekan formation in Iraqi Kurdistan. *JZS-A* 19, 103–124. <https://doi.org/10.17656/jzs.10589>.
- Abdulnaby, W., 2019. Structural geology and neotectonics of Iraq, northwest Zagros (chapter 4). In: *Developments in Structural Geology and Tectonics*, vol. 3. Elsevier, pp. 53–73. <https://doi.org/10.1016/B978-0-12-815048-1.00004-4>.
- Afrozi, M., Fralick, P.W., Patry, L., Sans-Jofre, P., Lalonde, S.V., 2021. Carbon and Oxygen Isotope Chemostratigraphy of a Mesoproterozoic Carbonate Platform (Red Lake, Canada). *Goldschmidt*. <https://doi.org/10.7185/gold2021.7598>, 2021 Abstract.
- Al-Abbasi, M.W., Al-Mutwali, M.M., Al-Banna, N.Y., 2018. Late tithonian ammonites from Chia Gara Formation at maten anticline, northern Iraq. *Iraqi National J. Earth Sci.* 18, 41–54. https://earth.mosuljournals.com/article_159271_57e9f9ca850b864727cec6a273cd86a7.pdf.
- Al-Ameri, T.K., Zumberge, J., 2012. Middle and upper jurassic hydrocarbon potential of the Zagros Fold Belt, north Iraq. *Mar. Pet. Geol.* 36, 13–34. <https://doi.org/10.1016/j.marpetgeo.2012.04.004>.
- Alavi, M., 2004. Regional stratigraphy of the Zagros fold-thrust belt of Iran and its proforeland evolution. *Am. J. Sci.* 304, 1–20. <https://doi.org/10.2475/ajs.304.1.1>.
- Al-Dujaili, L.S., 1994. Stratigraphy Section of Middle-Upper Jurassic System and Lower Cretaceous, Northern Iraq: Master's Thesis (Unpublished). Science College, University of Baghdad, Baghdad, Iraq, p. 98 (in Arabic).
- Algeo, T.J., Maynard, J.B., 2004. Trace-element behavior and redox facies in core shales of Upper Pennsylvanian Kansas-type cyclothems. *Chem. Geol.* 206, 289–318. <https://doi.org/10.1016/j.chemgeo.2003.12.009>.
- Algeo, T.J., Liu, J.S., 2020. A re-assessment of elemental proxies for paleoredox analysis. *Chem. Geol.* 540, 119549.
- Al-Haj, M.A., Al-Juboury, A.I., Al-Hadidy, A.H., Hassan, D.K., 2019. Cenomanian-early Campanian carbonate reservoir rocks of northwestern Iraq: diagenesis and porosity development. *Al-Kitab Journal for Pure Science* 2 (2), 1–19.
- Al-Juboury, A.I., McCann, T., 2013. Petrological and geochemical interpretation of Triassic-Jurassic boundary sections from North Iraq. *Geol. J.* 50, 157–172. <https://doi.org/10.1002/gj.2537>.
- Al-Juboury, A.I., Durovic, V., 1996. Supratidal origin of carpathian keuper dolostones. *Miner. Slovaca* 28, 12–20.
- Al-Langawi, A.J., 2006. Fabric preserving and fabric destroying dolomitization: a case of seawater dolomitization. *SQU J. Sci.* 11, 39. <https://doi.org/10.24200/squjs.voll1iss0pp39-67>.
- Armstrong-Altrin, J.S., Botello, A.V., Villanueva, S.F., Soto, L.A., 2019. Geochemistry of surface sediments from the northwestern Gulf of Mexico: implications for provenance and heavy metal contamination. *Geol. Q.* 63, 522–538. <https://doi.org/10.7306/gq.1484>.
- Awad, A., Healy, D., Alsop, G.I., 2016. Fracture patterns and petrophysical properties of carbonates undergoing regional folding: a case study from Kurdistan, N Iraq. *Mar. Pet. Geol.* 71, 149–167. <https://doi.org/10.1016/j.marpetgeo.2015.12.017>.
- Bartolini, A., Pittet, B., Mattioli, E., Hanziker, J.C., 2003. Shallow-platform paleoenvironmental conditions recorded in deep-shelf sediments: C and O stable isotopes in Upper Jurassic sections of southern Germany (Oxfordian-Kimmeridgian). *Sediment. Geol.* 160, 107–130. [https://doi.org/10.1016/S0037-0738\(02\)00369-X](https://doi.org/10.1016/S0037-0738(02)00369-X).
- Bellen, R.C.V., Dunnington, H.V., Wetzel, R., Morton, D.M., 1959. *Asie, fascicule 10a Iraq. Lexique Stratigraphic International: Paris, France* 3, 333.
- Bennett, W.W., Canfield, D.E., 2020. Redox-sensitive trace metals as paleoredox proxies: a review and analysis of data from modern sediments. *Earth Sci. Rev.* 204, 103175. <https://doi.org/10.1016/j.earscirev.2020.103175>.
- Beydoun, Z.R., Clarke, M.W.H., Stoneley, R., 1992. Petroleum in the Zagros Basin—a Late Tertiary foreland basin overprinted onto the outer edge of a vast hydrocarbon-rich Paleozoic-Mesozoic passive-margin shelf. In: MacQueen, R.W., Leckie, D.A. (Eds.), *Foreland Basins and Fold Belts*, vol. 55. AAPG Memoir, Tulsa, OK, USA, pp. 309–339.
- Buday, T., 1980. The Regional Geology of Iraq. Stratigraphy and Palaeogeography, vol. 1. Publication of GEOSURV: Baghdad, Iraq, p. 445.
- Calvert, S.E., Pedersen, T.F., 1993. Geochemistry of recent oxic and anoxic sediments: implications for the geological record. *Mar. Geol.* 113, 67–88. [https://doi.org/10.1016/0025-3227\(93\)90150-T](https://doi.org/10.1016/0025-3227(93)90150-T).
- Canet, C., Alfonso, P., Melgarejo, J.C., Belyatsky, B.V., 2004. Geochemical evidences of sedimentary-exhalative origin of the shale-hosted PGE-Ag-Au-Zn-Cu occurrences of the Prades Mountains (Catalonia, Spain): trace-element abundances and Sm-Nd isotopes. *J. Geochem. Explor.* 82, 17–33. <https://doi.org/10.1016/j.gexplo.2004.01.002>.
- Cao, J., Wu, M., Chen, Y., Hu, K., Bian, L.Z., Wang, L.G., Zhang, Y., 2012. Trace and rare earth element geochemistry of Jurassic mudstones in the northern Qaidam Basin, northwest China. *Geochemistry* 72, 245–252. <https://doi.org/10.1016/j.chemer.2011.12.002>.

- Chamley, H., 1989. *Clay Sedimentology*. Springer Berlin, Heidelberg, p. 623.
- Chao, H., Hou, M., Jiang, W., Cao, H., Chang, X., Luo, W., Ogg, J.G., 2021. Paleoclimatic and redox condition changes during early-middle jurassic in the yili basin, northwest China. *Minerals* 11, 675. <https://doi.org/10.3390/min11070675>.
- Csató, I., Kiss, K., Balázs, S., Tóth, S., Varga, M., 2014. Upper Triassic-Jurassic depositional systems in the Akri-Bijel exploration block, Iraqi Kurdistan. *MOL Group Scientific Magazine* 54–71.
- Cullers, R.L., 1995. The controls on the major and trace element evolution of shales, siltstones and sandstones of Ordovician to Tertiary age in the Wet Mountain region. Colorado, USA: *Chem. Geol.* 123, 107–131. [https://doi.org/10.1016/0009-2541\(95\)00050-V](https://doi.org/10.1016/0009-2541(95)00050-V).
- Daoud, H.S., Karim, K.H., 2006. Types of stromatolites in the Barsarin Formation (late jurassic), barzinja area, NE Iraq. *Iraqi Bull. Geol. Min.* 6, 47–57. <https://www.iasj.net/iasj/download/8fe0c8cef9e56ebc>.
- Dashtgard, Sh.E., Wang, A., Pospelova, V., Wang, P.-L., La Croix, A., Ayranci, K., 2022. Salinity indicators in sediment through the fluvial-to-marine transition (Fraser River, Canada). *Sci. Rep.* 12, 14303 <https://doi.org/10.1038/s41598-022-18466-4>.
- Deepulal, P.M., Gireesh Kumar, T.R., Sujatha, C.H., George, R., 2012. Chemometric study on the trace metal accumulation in the sediments of the Cochin Estuary-Southwest coast of India. *Environ. Monit. Assess.* 184, 6261–6279. <https://doi.org/10.1007/s10661-011-2418-7>.
- Delizy, B.A., Shingaly, W.S., 2022. Microfacies analysis and depositional environment of Sarki Formation (early jurassic), rawanduz area, kurdistan region, northern Iraq. *Tikrit J. Pure Sci.* 27, 24–35. <https://doi.org/10.25130/tjps.v27i1.79>.
- Dill, H., 1986. Metallogenesis of early paleozoic graptolite shales from the grafenthal horst (northern bavaria, Federal Republic of Germany). *Econ. Geol.* 81, 889–903. <https://doi.org/10.2113/gsecongeo.81.4.889>.
- Döbelin, N., Kleeberg, R., 2015. Preface: a graphical user interface for the Rietveld refinement program BGMN. *J. Appl. Crystallogr.* 48, 1573–1580. <https://doi.org/10.1107/S1600576715014685>.
- Dunham, R.J., 1962. Classification of carbonate rocks according to depositional textures. In: Ham, William, E. (Eds.), *Classification of Carbonate Rocks — A Symposium*. AAPG Memoir AAPG (American Association of Petroleum Geologists), Tulsa, Oklahoma, pp. 108–121.
- Ernst, W., 1970. *Geochemical Facies Analysis. Methods in Geochemistry and Geophysics*, vol. 11. Elsevier, Amsterdam, p. 151.
- Fathy, D., Abart, R., Wagreich, M., Gier, S., Ahmed, M.S., Sami, M., 2023. Late campanian climatic-continental weathering assessment and its influence on source rocks deposition in southern Tethys, Egypt. *Minerals* 13, 160. <https://doi.org/10.3390/min13020160>.
- Fisher, J.K., Price, G.D., Hart, M.B., Leng, M.J., 2005. Stable isotope analysis of the Cenomanian-Turonian (Late Cretaceous) oceanic anoxic event in the Crimea. *Cretac. Res.* 26, 853–863. <https://doi.org/10.1016/j.cretres.2005.05.010>.
- Flügel, E., 2010. *Microfacies of Carbonate Rocks, Analysis, Interpretation and Application*, second ed. Springer Verlag, Berlin, Heidelberg, p. 984.
- Fu, X., Wang, J., Zeng, Y., Tan, F., Feng, X., 2010. REE geochemistry of marine oil shale from the Changshe Mountain area, northern Tibet, China. *Int. J. Coal Geol.* 81, 191–199. <https://doi.org/10.1016/j.coal.2009.12.006>.
- Gao, G., Titi, A., Yang, S., Tang, Y., Kong, Y., He, W., 2017. Geochemistry and depositional environment of fresh lacustrine source rock: a case study from the Triassic Bajiantan Formation shales in Junggar Basin, northwest China, Org. Geochem. (Tokyo. 1967) 113, 75–89. <https://doi.org/10.1016/j.orggeochem.2017.08.002>.
- Hakimi, M.H., Najaf, A.A., Abdula, R.A., Mohialdeen, I.M.J., 2018. Generation and expulsion history of oil-source rock (Middle Jurassic Sargelu Formation) in the Kurdistan of north Iraq, Zagros folded belt: implications from 1D basin modeling study. *J. Petrol. Sci. Eng.* 162, 852–872. <https://doi.org/10.1016/j.petrol.2017.11.0013>.
- Hallam, A., 1982. The Jurassic climate. In: *Climate in Earth History: Studies in Geophysics*. The National Academies Press, Washington, DC, USA, pp. 159–163.
- Haq, B.U., 2018. Jurassic sea-level variations: a reappraisal. *GSA Today (Geol. Soc. Am.)* 28, 4–10. <https://doi.org/10.1130/GSATG359A.1>.
- Hatch, J.R., Leventhal, J.S., 1992. Relationship between inferred redox potential of the depositional environment and geochemistry of the upper pennsylvanian (missourian) Stark shale member of the dennis limestone, wabaunsee county, Kansas, USA. *Chem. Geol.* 99, 65–82. [https://doi.org/10.1016/0009-2541\(92\)90031-Y](https://doi.org/10.1016/0009-2541(92)90031-Y).
- Hennhofer, D., Al Suwaidi, A., Bottini, C., Helja, E., Steuber, T., 2018. The Albian to Turonian carbon isotope record from the Shilaif Basin (United Arab Emirates) and its regional and intercontinental correlation. *Sedimentology* 66, 536–555. <https://doi.org/10.1111/sed.12493>.
- Hessami, K., Koyi, H.A., Talbot, C.J., 2001. The significance of strike-slip faulting in the basement of the Zagros fold and thrust belt. *J. Petrol. Geol.* 241, 5–28. <https://doi.org/10.1111/j.1747-5457.2001.tb00659.x>.
- Hussain, S.H., Al-Juboury, A.I., Al-Haj, M.A., Armstrong-Altrin, J.S., Al-Lhaebi, S.F., 2021. Mineralogy and geochemistry of the late triassic baluti formation, northern Iraq. *J. Afr. Earth Sci.* 181, 104243 <https://doi.org/10.1016/j.jafrearsci.2021.104243>.
- Ivančić, M., Lojen, S., Grozić, D., Jurina, I., Škapin, S., Troskot-Čorbić, T., Mikac, N., Jurčić, M., Sondi, I., 2017. Geochemistry of sedimentary organic matter and trace elements in modern lake sediments from transitional karstic land-sea environment of the Neretva River delta (Kuti Lake, Croatia). *Quat. Int.* 494, 286–299. <https://doi.org/10.1016/j.quaint.2017.03.050>.
- Jasim, S.Y., 2013. The potential of hydrocarbons generation in the Chia Gara Formation at Amadia area, north of Iraq. *Arabian J. Geosci.* 6, 3313–3318. <https://doi.org/10.1007/s12517-012-0619-1>.
- Jassim, S.Z., Buday, T., 2006. Late toarcian-early titonian (Mid-Late jurassic) megasequence AP7. In: Jassim, S.Z., Goff, J.C. (Eds.), *Geology of Iraq*. Moravian Museum, Brno, Prague, pp. 117–123.
- Jassim, S.Z., Goff, J.C., 2006. *Geology of Iraq: Dolin. Prague & Moravian Museum, Brno, Czech Republic*, p. 352.
- Jones, B., Manning, D.A.C., 1994. Comparison of geochemical indices used for the interpretation of palaeoredox conditions in ancient mudstones. *Chem. Geol.* 111, 111–129. [https://doi.org/10.1016/0009-2541\(94\)90085-X](https://doi.org/10.1016/0009-2541(94)90085-X).
- Kharajany, S.O.A., Mohialdeen, I.M.J., 2018. Nanofossil distribution in the late jurassic naokalekan and Barsarin formations, miran oil field, well-2-, kurdistan, northeastern Iraq. *J. Zankoy Sulaimani - Part A - Pure Appl. Sci.* 20, 53–66. <https://doi.org/10.17656/jzs.10724>.
- Kimura, H., Watanabe, Y., 2001. Oceanic anoxia at the Precambrian-Cambrian boundary. *Geology* 29, 995–998. [https://doi.org/10.1130/0091-7613\(2001\)029<0995:OATPC>2.0.CO;2](https://doi.org/10.1130/0091-7613(2001)029<0995:OATPC>2.0.CO;2).
- Krejci-Graf, K., 1966. *Geochemische faziesdiagnostik. Freiburger Forschungshefte - A C* 224, 80.
- Li, X., Wei, Y., Li, Y., Zhang, C., 2016. Carbon isotope records of the early Albian oceanic anoxic event (OAE) 1b from eastern Tethys (southern Tibet, China). *Cretac. Res.* 62, 109–121. <https://doi.org/10.1016/j.cretres.2015.08.015>.
- Li, B.B., Jin, X., Dal Corso, J., et al., 2023. Complex pattern of environmental changes and organic matter preservation in the NE Ordos lacustrine depositional system (China) during the T-OAE (Early Jurassic). *Global Planet. Change* 221, 104045.
- Lindström, S., Erlström, M., 2011. The Jurassic-Cretaceous transition of the Fårarp-1 core, southern Sweden: sedimentological and phytochemical indications of climate change. *Paleogeogr. Paleoclimatol. Paleoecon.* 308, 445–475. <https://doi.org/10.1016/j.palaeo.2011.05.052>.
- Liu, L., Shuai Zhang, S., Qinfu Liu, Q., Linsong Liu, L., Deng, Y., 2021. Palaeoclimate, palaeosalinity and redox conditions control palysorskite claystone formation: an example from the Yangtaiwan Basin, northwest China. *Clay Miner.* 56, 210–221.
- Liu, X., Wen, Z., Wang, Z., Song, C., He, Z., 2018. Structural characteristics and main controlling factors on petroleum accumulation in Zagros Basin, Middle East. *J. Nat. Gas. Geosci.* 5, 273–281. <https://doi.org/10.1016/j.jnggs.2018.11.004>.
- Liu, Y., Song, Ch, Meng, Q., He, P., Yang, R., Huang, R., Chen, S., Wang, D., Xing, Z., 2020. Palaeoclimate change since the Miocene inferred from clay-mineral records of the Jiuquan Basin, NW China. *Paleogeogr. Paleoclimatol. Paleoecon.* 550, 109730 <https://doi.org/10.1016/j.palaeo.2020.109730>.
- Logan, B.W., Rezak, R., Ginsburg, R.N., 1964. Classification and environmental significance of algal stromatolites. *J. Geol.* 72, 68–83. <https://www.jstor.org/stable/30071097>.
- Madhavaraju, J., Hussain, S.M., Ugeswari, J., Nagarajan, R., Ramasamy, S., Mahalakshmi, S., 2015. Paleo-redox conditions of the albian-danian carbonate rocks of the cauvery basin, south India: implications for chemostratigraphy. In: Ramkumar, M. (Ed.), *Chemostratigraphy: Concepts, Techniques and Applications*. Elsevier Special Volume, pp. 247–271.
- Madhavaraju, J., Ramírez-Montoya, E., Monreal, R., González-León, C.M., Pi-Puig, T., Espinoza-Maldonado, I.G., Grijalva-Noriega, F.J., 2016. Paleoclimate, paleoweathering and paleoredox conditions of Lower Cretaceous shales from the Mural Limestone, Tuape section, northern Sonora, Mexico: constraints from clay mineralogy and geochemistry. *Rev. Mex. Ciencias Geol.* 33, 34–48. <https://www.scielo.org.mx/pdf/rmcg/v33n1/2007-2902-rmcg-33-01-00034>.
- Marshall, C.P., Fairbridge, R.W., 1999. *Encyclopedia of Geochemistry*. Springer, p. 644.
- Men, X., Mou, Ch, Ge, X., 2022. Changes in palaeoclimate and palaeoenvironment in the upper yangtze area (south China) during the ordovician-silurian transition. *Sci. Rep.* 12, 13186 <https://doi.org/10.1038/s41598-022-17105-2>.
- Mohialdeen, I.M.J., Hakimi, M.H., Al-Beyati, F.M., 2013. Geochemical and petrographic characterisation of late jurassic-early cretaceous Chia Gara Formation in northern Iraq: palaeoenvironment and oilgeneration potential. *Mar. Pet. Geol.* 43, 166–177. <https://doi.org/10.1016/j.marpetgeo.2013.02.010>.
- Mouthereau, F., Lacombe, O., Vergès, J., 2012. Building the Zagros collisional orogen: timing, strain distribution and the dynamics of Arabia/Eurasia plate convergence. *Tectonophysics* 532, 27–60. <https://doi.org/10.1016/j.tecto.2012.01.022>.
- Murris, R.J., 1980. Middle East: stratigraphic evolution and oil habitat. *AAPG Bull.* 64, 597–618. <https://doi.org/10.1306/M35439C20>.
- Omar, N., McCann, T., Al-Juboury, A.I., Franz, S.O., 2020. Petrography and geochemistry of the Middle-Upper Jurassic Banik section, northernmost Iraq - implications for paleoredox, evaporitic and diagenetic conditions. *N. Jb. Geol. Paleont. Abh.* 297, 125–152. <https://doi.org/10.1127/njgpa/2020/0916>.
- Omar, N., McCann, T., Al-Juboury, A.I., Suárez-Ruiz, I., 2021. Solid bitumen in shales from the middle to upper jurassic Sargelu and naokalekan formations of northernmost Iraq: implication for reservoir characterization. *Arabian J. Geosci.* 14, 755. <https://doi.org/10.1007/s12517-021-07048-9>.
- Omar, N., McCann, T., Al-Juboury, A.I., Ustinova, M.A., Sharezwri, A.O., 2022. Early jurassic-early cretaceous calcareous nanofossil biostratigraphy and geochemistry, northeastern Iraqi kurdistan: implications for paleoclimate and paleoecological conditions. *Geosciences* 12, 94. <https://doi.org/10.3390/geosciences12020094>.
- Orhan, H., Delikan, A., Demir, A., Kapan, S., Olgun, K., Özmen, A., Sayin, Ü., Ekici, G., Aydin, H., Nazik, A., 2019. Geochemical evidences of paleoenvironmental changes in late quaternary lacustrine sediments of the konya closed basin (konya, Turkey). In: Zhang, Z., Khelifi, N., Mezghani, A., Heggy, E. (Eds.), *Patterns and Mechanisms of Climate, Palaeoclimate and Palaeoenvironmental Changes from Low Latitude Regions*. Springer Berlin, Germany, pp. 73–76.
- Petschick, R., 2002. Röntgendiffraktometrie in der Sedimentologie (K5). *Z. Dtsch. Geol. Ges.* 18, 99–118.

- Pitman, J.K., Steinshouer, D., Lewan, M.D., 2004. Petroleum generation and migration in the Mesopotamian Basin and Zagros Fold Belt of Iraq: results from a basin-modeling study. *GeoArabia* 9, 41–72. <https://doi.org/10.2113/geoarabia090441>.
- Price, G.D., 1999. The evidence and implications of polar-ice during the Mesozoic. *Earth Sci. Rev.* 48, 183–210. [https://doi.org/10.1016/S00128252\(99\)000483](https://doi.org/10.1016/S00128252(99)000483).
- Purser, B.H., Brown, A., Assouli, D.M., 1994b. Nature, origin and evolution of porosity in dolomites. In: Purser, B.H., Tucker, M.E., Zenger, D.H. (Eds.), *Dolomites: A Volume in Honour of Dolomieu*, vol. 21. International Association of Sedimentologists, Special Publication, pp. 283–308.
- Purser, B.H., Tucker, M.E., Zenger, D.H., 1994a. Problems, progress and future research concerning dolomites and dolomitization. In: Purser, B.H., Tucker, M.E., Zenger, D. H. (Eds.), *Dolomites: A Volume in Honour of Dolomieu*, vol. 21. International Association of Sedimentologists, Special Publication, pp. 3–20.
- Qin, J., Wang, S., Sanei, H., Jiang, C., Chen, Z., Ren, S., Xu, X., Yang, J., Zhong, N., 2018. Revelation of organic matter sources and sedimentary environment characteristics for shale gas formation by petrographic analysis of middle Jurassic Dameigou formation, northern Qaidam Basin, China. *Int. J. Coal Geol.* 195, 373–385. <https://doi.org/10.1016/j.coal.2018.06.015>.
- Remírez, M.N., Algeo, T.J., 2020. Paleosalinity determination in ancient epicontinental seas: a case study of the T-OAE in the Cleveland Basin (UK). *Earth Sci. Rev.* 201, 103072.
- Read, J.F., Kerans, C., Weber, L.J., Sarg, H.F., Wright, F.M., 1995. Milankovitch sea-level changes, cycles and reservoirs on carbonate platforms in green-house and ice-house worlds. *SEPM Short. Course* 35, 1–81. <https://doi.org/10.2110/scn.95.35>.
- Rimmer, S.M., 2004. Geochemical paleoredox indicators in Devonian-Mississippian black shales, central Appalachian Basin, U.S.A.). *Chem. Geol.* 206, 373–391. <https://doi.org/10.1016/j.chemgeo.2003.12.029>.
- Ruf, M., Link, E., Pross, J., Aigner, T., 2005. Integrated sequence stratigraphy: facies, stable isotope, and palynofacies analysis in a deeper epicontinental carbonate ramp (Late Jurassic, SW Germany). *Sediment. Geol.* 175, 391–414. <https://doi.org/10.1016/j.sedgeo.2004.12.023>.
- Ruffell, A.H., McKinley, J.M., Worden, R.H., 2002. Comparison of clay mineral stratigraphy to other proxy palaeoclimate indicators in the Mesozoic of NW Europe. *Philos. Trans. A Math. Phys. Eng. Sci.* 360, 675–693. <https://doi.org/10.1098/rsta.2001.0961>.
- Sadooni, F., 1997. Stratigraphy and petroleum prospects of Upper Jurassic carbonates in Iraq. *Petrol. Geosci.* 3, 233–234. <https://doi.org/10.1144/petgeo.3.3.233>.
- Sena, C.M., John, C.M., Jourdan, A., Vandeginste, V., Manning, C., 2014. Dolomitization of Lower Cretaceous peritidal carbonates by modified seawater: constraints from clumped isotopic paleothermometry, elemental chemistry and strontium isotopes. *J. Sediment. Res.* 84, 552–566. <https://doi.org/10.2110/jsr.2014.45>.
- Severmann, S., Anbar, A.D., 2009. Reconstructing paleoredox conditions through a multitracer approach: the key to the past is the present. *Elements* 5, 359–364. <https://doi.org/10.2113/gselements.5.6.359>.
- Sharland, P.R., Archer, R., Casey, D.M., Hall, S.H., Heward, A.P., Horbury, A.D., Simmons, M.D., 2001. *Arabian Plate Sequence Stratigraphy*, *GeoArabia, Special Publication 2*. Gulf Petrolink, Bahrain, p. 371.
- Singer, A., 1984. The paleoclimatic interpretation of clay minerals in sediments — a review. *Earth Sci. Rev.* 21, 251–293. [https://doi.org/10.1016/0012-8252\(84\)90055-2](https://doi.org/10.1016/0012-8252(84)90055-2).
- Sinha, R., Smykatz-Kloss, W., Stüben, D., Harrison, S.P., Berner, Z., Kramar, U., 2006. Late Quaternary paleoclimatic reconstruction from the lacustrine sediments of the Sambhar playa core, Thar Desert margin, India. *Paleogeogr. Paleoclimatol. Paleocool.* 233, 252–270. <https://doi.org/10.1016/j.palaeo.2005.09.012>.
- Song, Y., Liu, Z., Meng, Q., Xu, J., Sun, P., Cheng, L., Zheng, G., 2016. Multiple controlling factors of the enrichment of organic matter in the upper cretaceous oil shale sequences of the Songliao basin, NE China: implications from geochemical analyses. *Oil Shale* 33, 142–166. <https://doi.org/10.3176/oil.2016.2.04>.
- Stampfli, G.M., Borel, G.D., 2002. A plate tectonic model for the Paleozoic and Mesozoic constrained by dynamic plate boundaries and restored synthetic oceanic isochrons. *Earth Planet Sci. Lett.* 196, 17–33. [https://doi.org/10.1016/S0012-821X\(01\)00588-X](https://doi.org/10.1016/S0012-821X(01)00588-X).
- Talbot, C.J., Alavi, M., 1996. The past of a future syntaxis across the Zagros. In: Alsop, G. I., Blundell, D.J., Davison, I. (Eds.), *Salt Tectonics*, vol. 100. Special Publication of Geological Society, London, pp. 89–109. <https://doi.org/10.1144/gsl.sp.1996.100.01.08>.
- Tavakoli-Shirazi, S., Frizon de Lamotte, F., Wrobel-Daveau, J.C., Ringenbach, J.C., 2013. Pre-Permian uplift and diffuse extensional deformation in the High Zagros Belt (Iran): integration in the geodynamic evolution of the Arabian plate. *Arabian J. Geosci.* 6, 2329–2342. <https://doi.org/10.1007/s12517-012-0542-5>.
- Tavani, S., Parente, M., Vitale, S., Iannace, A., Corradetti, A., Bottini, C., Morsalnejad, D., Mazzoli, S., 2018. Early Jurassic rifting of the Arabian passive continental margin of the Neo-Tethys. Field evidence from the Lurestan region of the Zagros fold-and-thrust belt, Iran. *Tectonics* 37, 2586–2607. <https://doi.org/10.1029/2018TC005192>.
- Tobia, F.H., Al-Jaleel, H.S., Ahmad, I.N., 2019. Provenance and depositional environment of the Middle-Late Jurassic shales, northern Iraq. *Geosci. J.* 23, 747–765. <https://doi.org/10.1007/s12303-018-0072-6>.
- Tribouillard, N., Algeo, T.W., Lyons, T., Riboulleau, A., 2006. Trace metals as paleoredox and paleoproductivity proxies: an update. *Chem. Geol.* 232, 12–32. <https://doi.org/10.1016/j.chemgeo.2006.02.012>.
- Vincent, B., Rambeau, C., Emmanuel, L., Loreau, J.P., 2006. Sedimentology and trace element geochemistry of shallow-marine carbonates: an approach to paleoenvironmental analysis along the Pagny-sur-Meuse section (Upper Jurassic, France). *Facies* 52, 69–84. <https://doi.org/10.1007/s1034700500260>.
- Wang, P., Du, Y., Yu, W., Algeo, T.J., Zhou, Q., Xu, Y., Qi, L., Yuan, L., Pan, W., 2020. The chemical index of alteration (CIA) as a proxy for climate change during glacial-interglacial transitions in Earth history. *Earth Sci. Rev.* 201, 103032. <https://doi.org/10.1016/j.earscirev.2019.103032>.
- Wang, Z., Fu, X., Feng, X., Song, C., Wang, D., Chen, W., Zeng, S., 2017. Geochemical features of the black shales from the Wuyu Basin, southern Tibet: implications for paleoenvironment and paleoclimate. *Geol. J.* 52, 282297. <https://doi.org/10.1002/gj.2756>.
- Weissert, H., Erba, E., 2004. Volcanism CO₂ and paleoclimate: a late Jurassic-Early Cretaceous carbon and oxygen isotopes record. *J. Geol. Soc. Lond.* 161, 695–702. <https://doi.org/10.1144/0016-764903-087>.
- Wilson, J.L., 1975. *Carbonate Facies in Geological History*. Springer-Verlag New York, Heidelberg Berlin, p. 471.
- Xu, H., Liu, B., Wu, F., 2010. Spatial and temporal variations of Rb/Sr ratios of the bulk surface sediments in Lake Qinghai. *Geochem. Trans.* 11, 1–8. <https://doi.org/10.1186/1467-4866-11-3>.
- Yandoka, B.M.S., Abdullah, W.H., Abubakar, M.B., Hakimi, M.H., Adegoko, A.K., 2015. Geochemical characterization of early Cretaceous lacustrine sediments of Bima Formation, Yola Sub-basin, northern Benue trough, NE Nigeria: organic matter input, preservation, paleoenvironment and paleoclimatic conditions. *Mar. Petrol. Geol.* 61, 82–94. <https://doi.org/10.1016/j.marpetgeo.2014.12.010>.
- Zenger, D.H., 1972. Significance of supratidal dolomitization in the geologic record. *GSA Bull.* 83, 1–12. <https://doi.org/10.1130/0016-7606>.
- Zuo, X., Li, C., Zhang, J., Ma, G., Chen, P., 2020. Geochemical characteristics and depositional environment of the shahejie Formation in the binnan oilfield, China. *J. Geophys. Eng.* 17, 539–551. <https://doi.org/10.1093/jge/gxaa013>.

Appendix C

Petrography and geochemistry of the Middle–Upper Jurassic Banik section, northernmost Iraq – Implications for palaeoredox, evaporitic and diagenetic conditions

Nagham Omar, Tom McCann, Ali I. Al-Juboury, and Sven Oliver Franz

With 11 figures and 4 tables

Abstract: Lithological, petrographic, and geochemical analysis of the Middle to Upper Jurassic succession (i.e. Sargelu and Naokelekan formations) from northernmost Iraq were undertaken with the aim of providing an updated discussion for their sedimentary and diagenetic histories, as well as examining the evaporation proxies and palaeoredox conditions under which these two formations were deposited. Lithologically, the Sargelu Formation comprises massive dolomites, interbedded with shales, rare cherts and one single limestone bed, whilst the Naokelekan Formation consists of shales overlain by limestones and one single dolomite bed. Petrographic analysis of both formations revealed the presence of rare ostracods, bioclastic fragments as well as calcispheres. Five main microfacies were recognized, including bioclastic wackestone, mudstone, dolorudite, dolarenite and dolomicrite microfacies. The shales comprise clay minerals assemblages (illite/muscovite and kaolinite) with some quartz, alkali feldspar and rare pyrite. The Sargelu Formation was probably deposited in a shallow-marine environment. In contrast, the Naokelekan Formation is hypothesized to be deposited in a restricted shallow-lagoon environment. Palaeoredox indicators suggest that both formations were accumulated under anoxic conditions, most probably in silled basins where water circulation was restricted. Tectonic activity thus resulted in basin compartmentalization across the region, which also explains the marked differences which are often observed.

Key words: Palaeoenvironment, geochemistry, deposition, carbonate.

1. Introduction

Northern Iraq is situated within the Zagros Basin/Zagros Fold Belt, an area which is rich in hydrocarbons, and which forms part of the broader, oil-rich Arabian Plate (Fig. 1) (JASSIM & GOFF 2006; ABDULA 2010; SORKHABI 2010; LE GARZIC *et al.* 2019). Estimates of the oil reserves suggest that the area contains approx. 45 billion barrels of Iraq's total of 115 billion barrels of oil reserves (AL-ZUBAIDI & AL-ZEBARI 1998; JASSIM & AL-GAILANI 2006; HILL & SHANE 2009; AL-AMERI & ZUMBERGE 2012; MOHIALDEEN *et al.* 2013; AL-AMERI *et al.* 2013). The Middle and Upper Jurassic sedimentary successions of Northern Iraq contain very significant carbonate source units interbedded with

highly porous and permeable siliciclastic reservoir units (OMAR *et al.* in preparation). That these carbonate units are excellent source rocks is due to the high total organic carbon (TOC) contents in the Sargelu and Naokelekan formations (OMAR *et al.* in preparation).

The present study focuses on the Middle to Upper Jurassic succession of the Banik section from northernmost Iraq. The two formations representing these periods are the Sargelu and Naokelekan formations, respectively. Although much work has been carried out on these formations, particularly on the petrology and organic geochemistry (e.g., AL-AHMED 2006; ABDULA 2010; AL-AMERI & ZUMBERGE 2012; AL-AMERI *et al.* 2013; ABDULA 2017), the sedimentology (e.g., SALAE 2001; SHAREZWRI 2015; ABDULA *et al.* 2015)



Fig. 1. Location of the study area in northernmost Iraq within the Arabian Plate.

and the shale geochemistry (e.g., [TOBIA et al. 2019](#)), to date, there has not been a comprehensive examination of the petrography and microfacies of the carbonates integrated with the geochemistry of the clastic rocks.

This study initially describes the lithological, petrographic and microfacies of the carbonates of both Jurassic formations from the Banik area, in order to provide an updated interpretation for their depositional environment. Subsequent geochemical analysis of the intercalated shales will provide additional information on palaeoredox, evaporitic and diagenetic conditions, which can be integrated into a new depositional environment for the region.

2. Geological setting

The study area, situated within the Kurdistan region of Iraq, forms part of the northeastern margin of the Arabian Plate ([ABDULA 2017](#); [KONERT et al. 2001](#)), which can be subdivided into three broad geological areas:

the Arabian Shield to the west, the Arabian Platform in the centre and the Arabian Gulf in the east (Fig. 2) ([JAJU et al. 2016](#)). Located at the junction of the Arabian Plate (i.e. Arabian Platform area) and the Eurasian Plate, the region of northernmost Iraqi Kurdistan, is situated within the Zagros Basin/Zagros Fold Belt on the northeastern boundary of the Arabian Plate ([ABDULA 2017](#); [LIU et al. 2018](#)). This foreland basin, covering an area of about $500 \times 103 \text{ km}^2$ has a NW–SE length of c. 2300 km, extending from Turkey to SE Iran, and a NE–SW width of 100–300 km ([LIU et al. 2018](#)). It formed as a result of the collision between the continental Arabian Plate and the continental segments of the Eurasian margin ([BEYDOUN et al. 1992](#); [TALBOT & ALAVI 1996](#); [STAMPFLI & BOREL 2002](#)). In Iraq, the foreland basin is bounded by the Khleisia Uplift (a Mesozoic-age stable shelf region) to the west, and by the Mesopotamian Basin to the south (see Fig. 3). As noted above, the Zagros Basin/Zagros Fold Belt contains sedimentary rocks ranging in age from Jurassic to Tertiary, i.e. dominated by a thick Mesozoic succession.

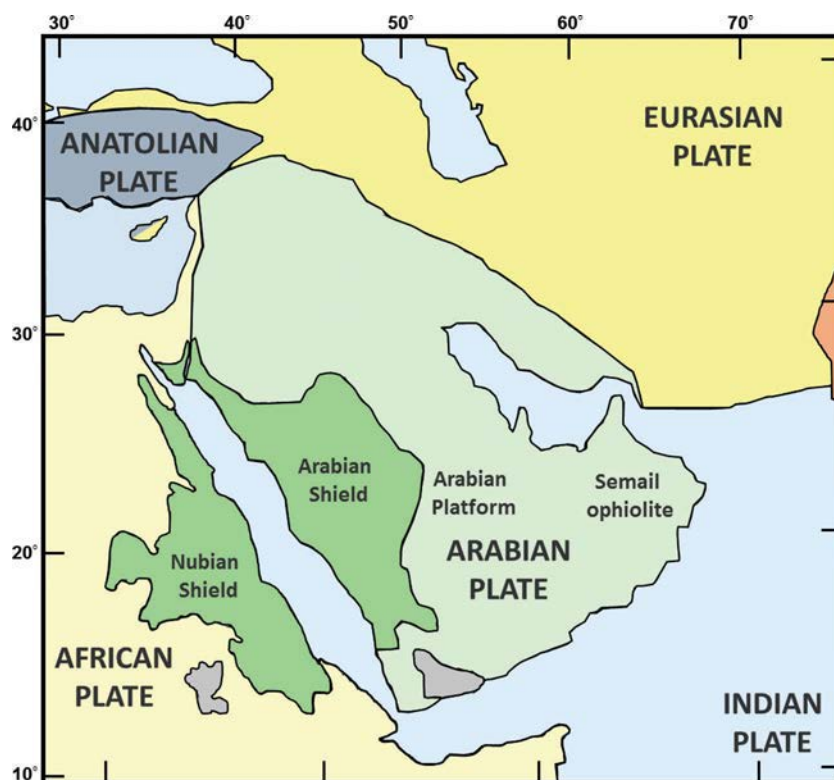


Fig. 2. The main geological subdivisions of the Arabian Plate (after KONERT *et al.* 2001).

The exposed Jurassic formations in the Kurdistan region of Iraq crop out as isolated patches within the eroded cores and limbs of anticlines in the structural zones of the broader Zagros Basin (NUMAN 2000). These structural zones include, from SW to NE, the Low Folded Zone (or Foothills), the High Folded Zone and the Thrust Zone (JASSIM & GOFF 2006). In a recent review, ZAINY *et al.* (2017) noted that the Thrust Zone could be considered to be a subzone (i.e. the Northern (Ora) Thrust Subzone) within the Imbricated zone, with this latter zone being subdivided into two sub-zones, namely, the Balambo-Tanjero Subzone and the Northern (Ora) Thrust Subzone. The Banik section, which was examined as part of this study, is located near the boundary between the High Folded Zone and the Thrust Zone (Fig. 3).

The Sargelu Formation was first recognized and described by WETZEL (1948) and subsequently correlated with successions in Iran (JAMES & WYND 1965), Turkey and Syria (ALTINLI 1966; DUBERTRET 1966). AL-OMARI & SADIQ (1977) suggested that the Sargelu Formation was Middle Jurassic in age, and an Aalenian–Bajocian age was later confirmed by

AL-DUJAILY (1994). However, more recently a palynomorph study by AL-AMERI *et al.* (2012) suggested a Bajocian–Bathonian, and possibly Early Callovian age. Thus, while a Middle Jurassic age was confirmed, there are still problems in terms of the stratigraphic precision. Further age analysis of the formation would be useful. The lower contact in the type area, as well as to the N and NE, is usually gradational and conformable. In the subsurface, the boundary is defined by the last occurrence of anhydrite (JASSIM & BUDAY 2006b). SALAE (2001) described the upper contact of the Sargelu Formation with the overlying Naokelekan Formation, noting that it is concordant. Recognition of the upper contact in northernmost Iraq, however, is difficult but it is generally assumed to be gradational (BUDAY 1980). The lack of chert and abundant *Bositra* bivalves and ammonites distinguish the Sargelu Formation from the overlying Naokelekan Formation (WETZEL 1948; SALAE 2001; BALAKY 2004). In addition, the Naokelekan Formation contains bitumen (WETZEL 1948), although bitumen was also noted within the underlying Sargelu Formation (OMAR *et al.* in preparation).

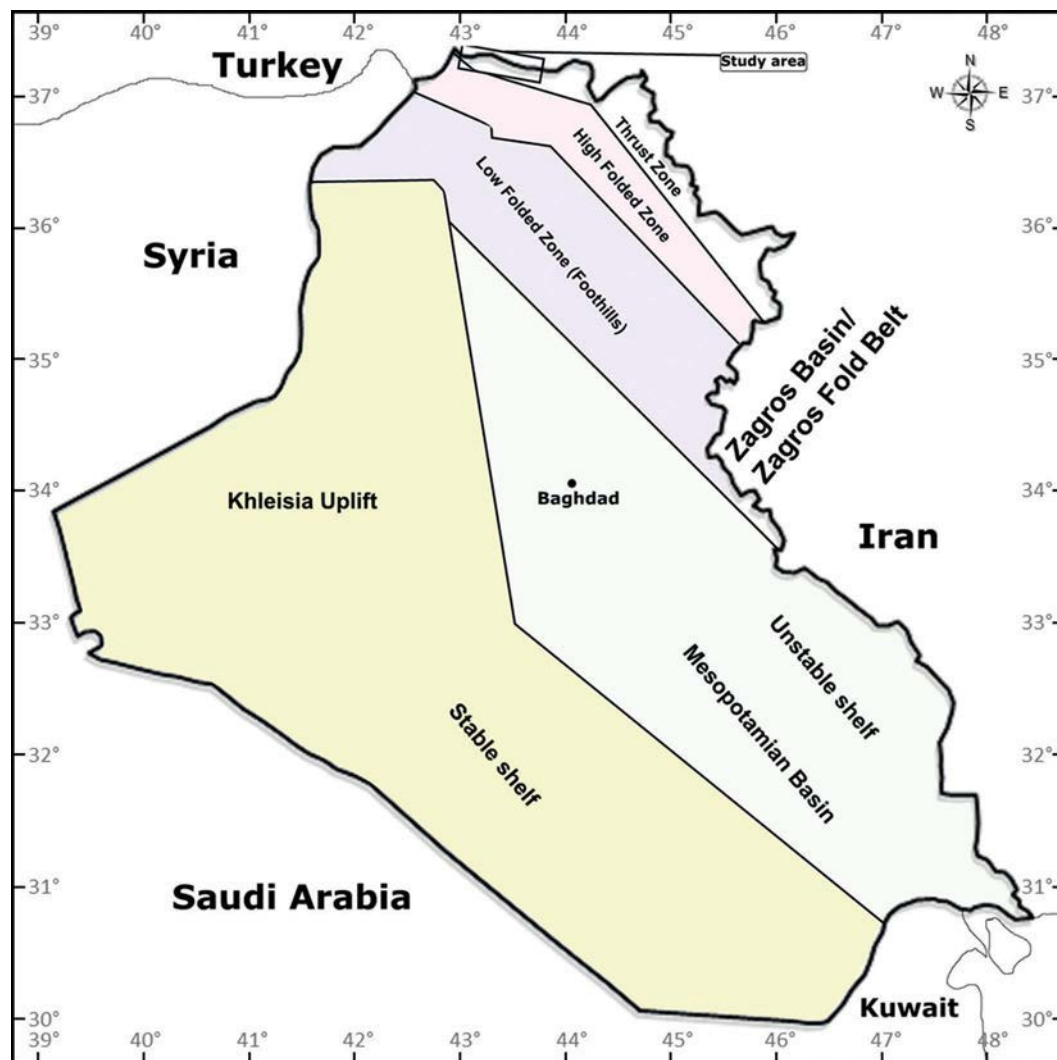


Fig. 3. Geological map of Iraq showing the study area and the structural zones of the Zagros Basin/Zagros Fold Belt (after AL-AMERI et al. 2012).

Lithologically, the Sargelu Formation, in its type section, comprises 115m of thinly-bedded, bituminous limestones, dolomitic limestones and black shales. Towards the top of the formation, thin chert beds occur (WETZEL 1948; JASSIM & BUDAY 2006b). In the subsurface, higher proportions of shale as well as rare fine-grained sandstones have also been noted (JASSIM & BUDAY 2006b). In addition, formation thicknesses in Iraq can vary from 74–447 m (JASSIM & BUDAY 2006b). Fossils are abundant and typically pelagic, including pelecypods, gastropods, echinoderms (including sponge spicules), radiolarians, algae (*Globochaeta*), calcispheres, ostracods, and foraminifera (van BELLEN et al. 1959; JASSIM & BUDAY 2006b).

In addition, the upper part of the Sargelu Formation comprises a microfacies with thin-shelled pelecypods as well as ammonites (JASSIM & BUDAY 2006b).

The type section of the overlying Naokelekan Formation comprises 20m of sediment. It can be subdivided into three units (WETZEL & MORTON 1950) although the original order of the succession was subsequently altered by newer work from AL-SAYYAB et al. (1982) and JASSIM & BUDAY (2006b). In addition, a better-exposed supplementary type section was described by van BELLEN et al. (1959). From base to top, the three units include, a) thinly-bedded, bituminous limestones with intercalated bituminous black shales and limestones, b) thinly-bedded, fossiliferous dolo-

mitic limestones, and, c) thinly-bedded, highly bituminous dolomites and limestones interbedded with black shales in the lower part (this upper unit is mostly obscured in the type section). The age of the Naokelekan Formation has been determined on the basis of fossil content, including belemnites, stromatoporoids, foraminifera and algae, and is considered to be Early Callovian–Kimmeridgian (JASSIM & BUDAY 2006b).

3. Palaeogeography

During the Late Mesozoic and Early Cenozoic, sedimentation in the Zagros Basin/Zagros Fold Belt was controlled by local tectonics, eustatic sea-level changes, and climate variations (EDILBI & SHERWANI 2019) and was intimately associated with the evolution of the Neo-Tethys Ocean (e.g., KORDI 2019). The opening of this ocean took place in two stages, the initial stage (Permian through to the Middle Triassic) coincided with rifting along the Zagros Suture and the separation of the Iranian Plate, which moved from the Arabian Plate towards the Eurasian Plate (BEYDOUN 1991; SADOONI & ALSHARHAN 2004; MUTTONI *et al.* 2009; LIU *et al.* 2018). The second stage occurred in Late Triassic–Middle Jurassic times, the period during which Neo-Tethys attained its maximum width (4000 km) (SADOONI & ALSHARHAN 2004). From Jurassic through to Late Cretaceous times, sea-level fluctuations, in conjunction with slow subsidence, led to the development of large, but shallow, intrashelf basins on the passive margins of the Neo-Tethys Ocean and the Arabian Plate (MURRIS 1980).

The Phanerozoic history of the region can be subdivided, on the basis of tectonic and geological analysis, into five evolutionary phases, which can be further subdivided into 11 tectonostratigraphic megasequences (SHARLAND *et al.* 2001). These are termed AP1–AP11 (SHARLAND *et al.* 2001). Of particular interest to this study is AP7 (Mid-Late Jurassic Megasequence) which was deposited during a period of isolation of the Mesopotamian Basin from the Neo-Tethys Ocean, probably as a result of renewed rifting along the NE margin of the Arabian Plate (JASSIM & BUDAY 2006b). The base of the AP7 megasequence coincides with the deposition of the deeper-water argillaceous-calcareous Sargelu Formation (corresponding to the shallow-water, sandy-calcareous Muhaiwir Formation on the shelf) in Iraq (AL-SAYYAB *et al.* 1982; JASSIM & BUDAY 2006a).

The Late Jurassic formations of the AP7 megasequence include the Naokelekan Formation which represents a period of extremely low productivity, probably due to basin restriction (SHARLAND *et al.* 2001). This corresponds to shallow-water shelf environments located along the western basin margin (clastic-carbonate: Najmah and Saggara formations, and carbonate-evaporite: Najmah and Gotnia formations) (JASSIM & BUDAY 2006b). These differences are also reflected in the recorded sediment thicknesses, for example, the Najmah-29 well on the western basin margin (Najmah Formation) contains almost 700 m of carbonates, whereas the sediments in the basin centre (Iraqi Zagros Basin/Zagros Fold belt) are only 130 m thick (van BELLEN *et al.* 1959).

In general, the AP7 sediments can be characterized as organic rich (i.e. hydrocarbon source units). These units were intercalated with highly porous and permeable shallow-marine carbonates and siliciclastic sediments (i.e. reservoir units) and subsequently overlain by evaporites or non-permeable sediments (i.e. seal units). The Jurassic- and overlying Cretaceous-age sedimentary succession of Northern Iraq thus forms a closed petroleum system (i.e. petroleum play) (MURRIS 1980; BEYDOUN 1991; SHARLAND *et al.* 2001).

4. Materials and methods

A total of 34 carbonate and shale samples from the Sargelu and Naokelekan formations in northernmost Iraq were collected for detailed analysis (i.e. mineralogy, geochemistry, microfacies). The samples were collected along a 32 m thick profile – the Banik section. This lithological profile comprises the Middle to Upper Jurassic succession (i.e. Sargelu and Naokelekan formations; see Fig. 4 for a detailed sedimentary log).

Twenty-two carbonate samples (dolomites, limestones) were examined petrographically. Thin sections were prepared in the Institut für Geowissenschaften-Geologie, Bonn University and were stained with Alizarin Red solution (ARS) following the procedure of FRIEDMAN (1959). Microfacies analysis, based on the DUNHAM (1962) classification, was used to interpret the depositional environment. The major and trace elements of 12 shale samples were analysed (XRF) while mineralogical constituents were determined using the XRD in order to provide additional information concerning the depositional environments. Eight carbonate and shale samples from both the Sargelu and Naokelekan formations were examined using scanning electron microscopy (SEM) with energy-dispersive X-ray microanalysis (EDX). These latter were measured at the Nees Institute laboratory, Bonn University.

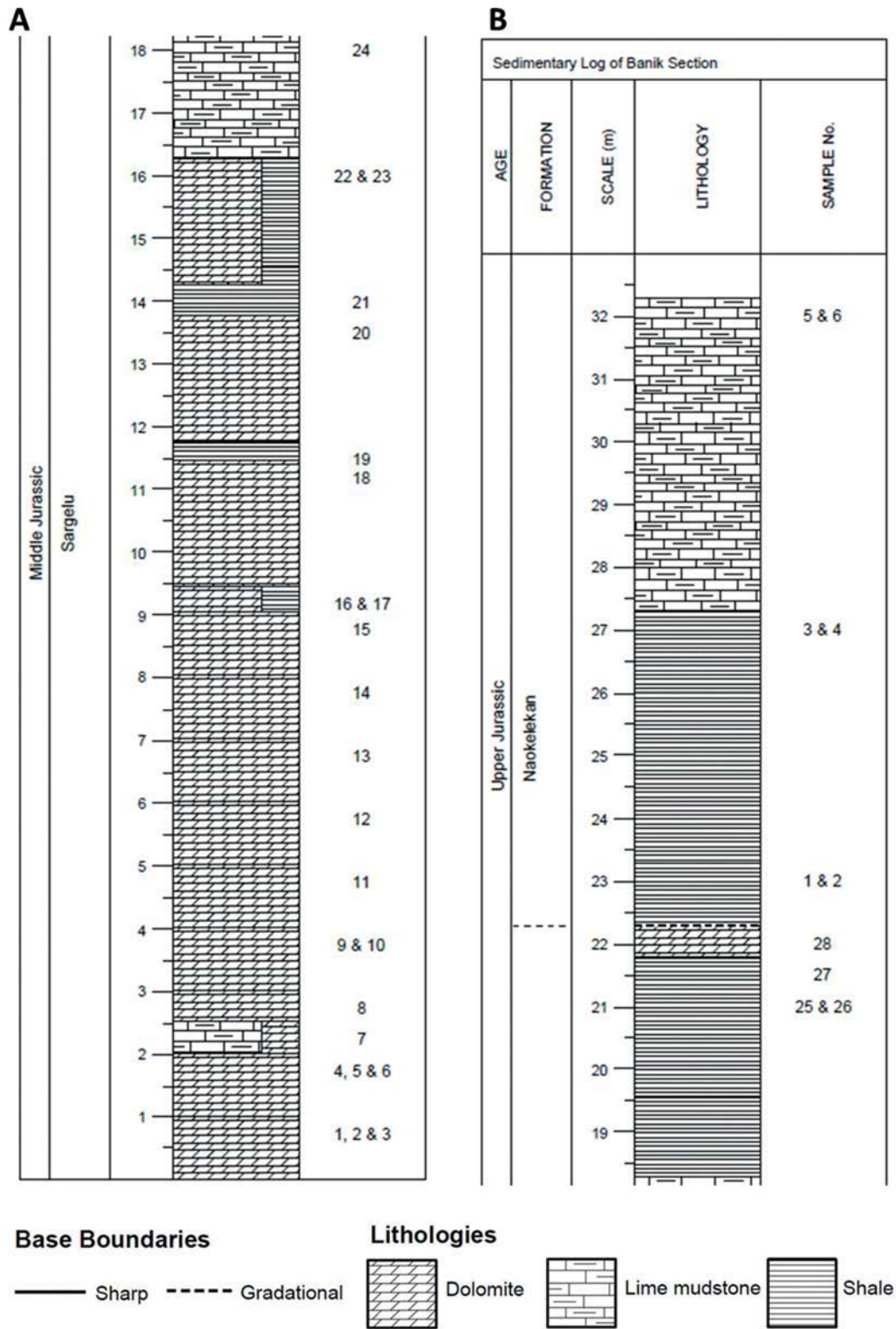


Fig. 4. Lithological section of the studied formations at Banik area of northernmost Iraq with sample locations.

5. Lithological analysis

The present study was carried out at one important outcrop (Banik section) where a high-resolution lithological profile was measured illustrating the transition from the Middle Jurassic-age Sargelu Formation through to the Late Jurassic-age Naokelekan Formation (Fig. 4). This profile was measured in a region where, due to recent political upheavals, access is now forbidden. Thus, this work – presenting as it does a length of nearly 32 m – will remain unique for the foreseeable future. The profile will be described from base to top, below.

5.1. Sargelu Formation

The base of the profile commences with the lower part of the Sargelu Formation (8 m). This generally consists of grey dolomites, with individual beds ranging in thickness from c. 1.0 to 4.0 m. Individual dolomite beds are generally massive, although some may show evidence of vuggy porosity, or the presence of veins filled with white calcite (Fig. 5A). Bed boundaries are horizontal and often sharp, and are laterally continuous across the outcrop (up to 21 m). Internally, there is no evidence of any sedimentary structures.

Moving up section, the dolomites pass into alternating beds of dolomite which are interbedded with grey-dark grey, friable bituminous shales as well as rare cherts and one single limestone bed (Fig. 5B). This interval is 13 m thick. Dolomite beds range in thickness from 0.3 to 2.0 m, while the shales range from 0.1 to 1.5 m (Fig. 5C).

The single limestone bed, which is 2.0 m thick, can be classified petrographically as a bioclastic wackestone (cf. DUNHAM 1962). This microfacies comprises a wackestone (i.e. 40% grains in a micritic matrix) where the individual grains consist of some bioclasts and rare ostracods (*Loricoecia loricata*) (Fig. 6A). These latter skeletal grains range in size from 300–500 µm, while the individual clasts are fine grained (i.e. 100 to 250 µm in size), and moderately sorted. The surrounding matrix is, as noted above, micritic with rare, patchily distributed, organic matter. SEM and EDX analysis revealed that the grains are mainly CaCO₃ (main elements: Ca, C, O) (Figs. 7A and 8A area 2), while the organic matter comprises mainly C and S (Figs. 7A and 8A area 1).

Several chert beds occurring near the top of the Sargelu Formation range in thickness from 0.2–0.5 m. The cherts are grey to black in colour, with calcite veins present (Fig. 5D). The chert beds are parallel to bedding with sharp upper and lower contacts. The uppermost part of the Sargelu Formation, i.e. the transition to the Naokelekan Formation, is marked by a final bed of dolomite, which represents the boundary between the Middle and Upper Jurassic.

5.2. Naokelekan Formation

The lower part of the Naokelekan Formation (5 m thick) consists of grey-black, friable shales. Bed thickness ranges from 0.5 to 2.0 m (Fig. 5E). The shales are bituminous and appear to be rich in organic material. Above this shale-rich interval is the upper part of the formation (5 m) which comprises limestones. Individual limestone beds, which are grey to yellow in colour, range from 0.5 to 3 m in thickness (Fig. 5F). The beds of limestones are horizontally bedded, with sharp beds boundaries. Internally there is no evidence of any sedimentary structures, with the beds being essentially massive. Petrographic analysis has revealed that the limestones are mainly mudstones (cf. DUNHAM 1962), with rare floating skeletal grains such as calcispheres (less than 10% of the facies composition). Fe-oxides were also noted, as well as rare, patchily-distributed organic matter (Fig. 6B). SEM and EDX analysis revealed the presence of Fe and O in the oxides (Figs. 7B and 8B area 2), with C and S being noted from the organic material (Figs. 7B and 8B area 3). The uppermost bed of the Naokelekan Formation, i.e. the contact area with the overlying Barsarin Formation, is 1.0 m of dolomite. It is grey to yellow in color, horizontally bedded, and with sharp upper and lower boundaries.

5.3. Dolomite in the Sargelu and Naokelekan formations

As noted above, dolomite is a common mineral within the two formations of the Banik section. Three types of dolomite have been noted and are described below. Medium-crystalline dolomites (dolorudites): Comprising a variety of grains in a micritic matrix (20%), this microfacies is widespread throughout the upper part of the Sargelu Formation, with a particular concentra-



Fig. 5. (A) Massive dolomites of the lower part of the Sargelu Formation. (B) The upper part of the Sargelu Formation. (C) Thin shale beds alternates with dolomites (black arrows) in the upper part of the Sargelu Formation. (D) Chert beds (black arrows) within the upper part of the Sargelu Formation. (E) Shales of the lower part of the Naokelekan Formation. (F) The limestones of the upper part of the Naokelekan Formation. Scales included.

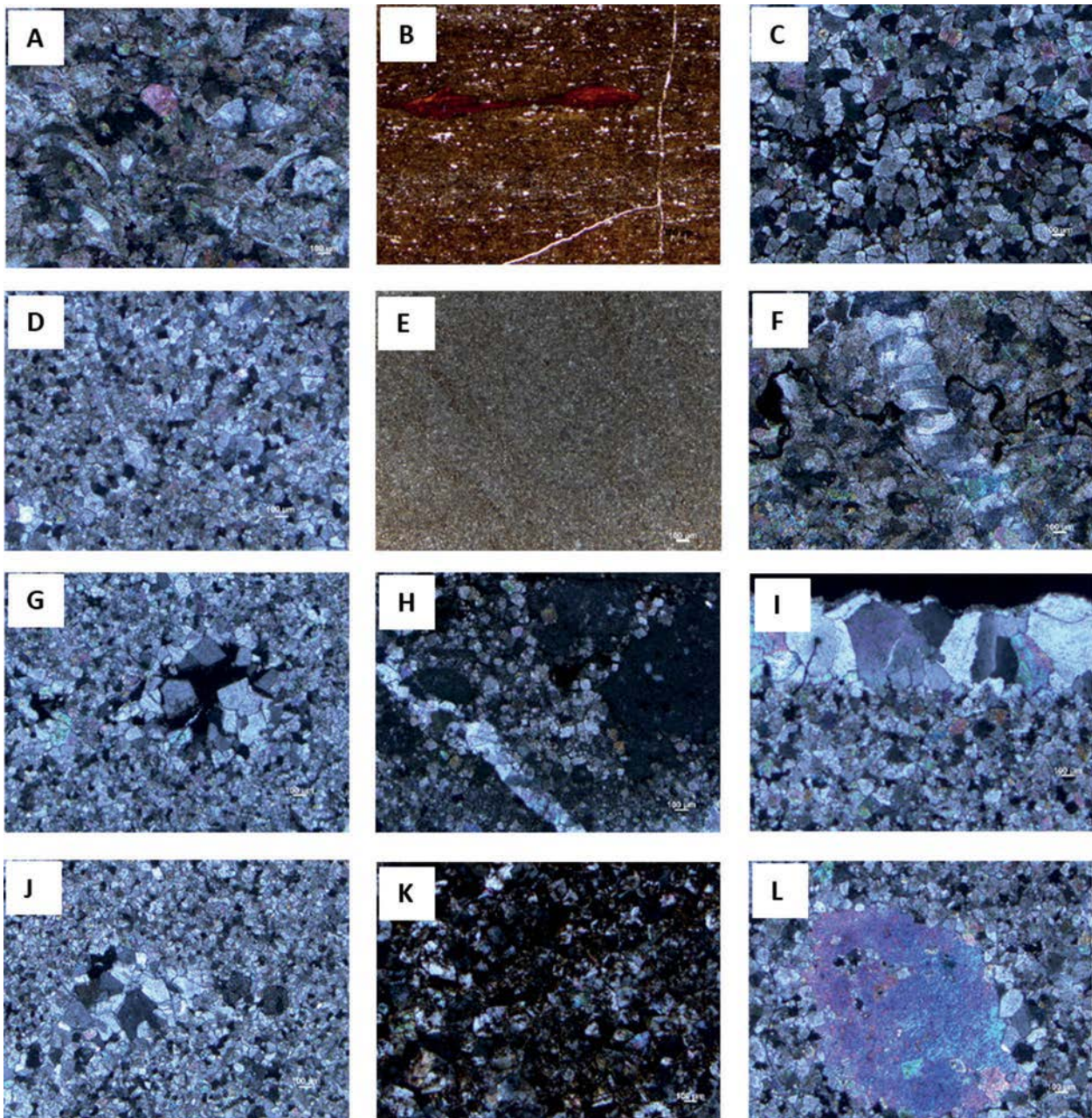
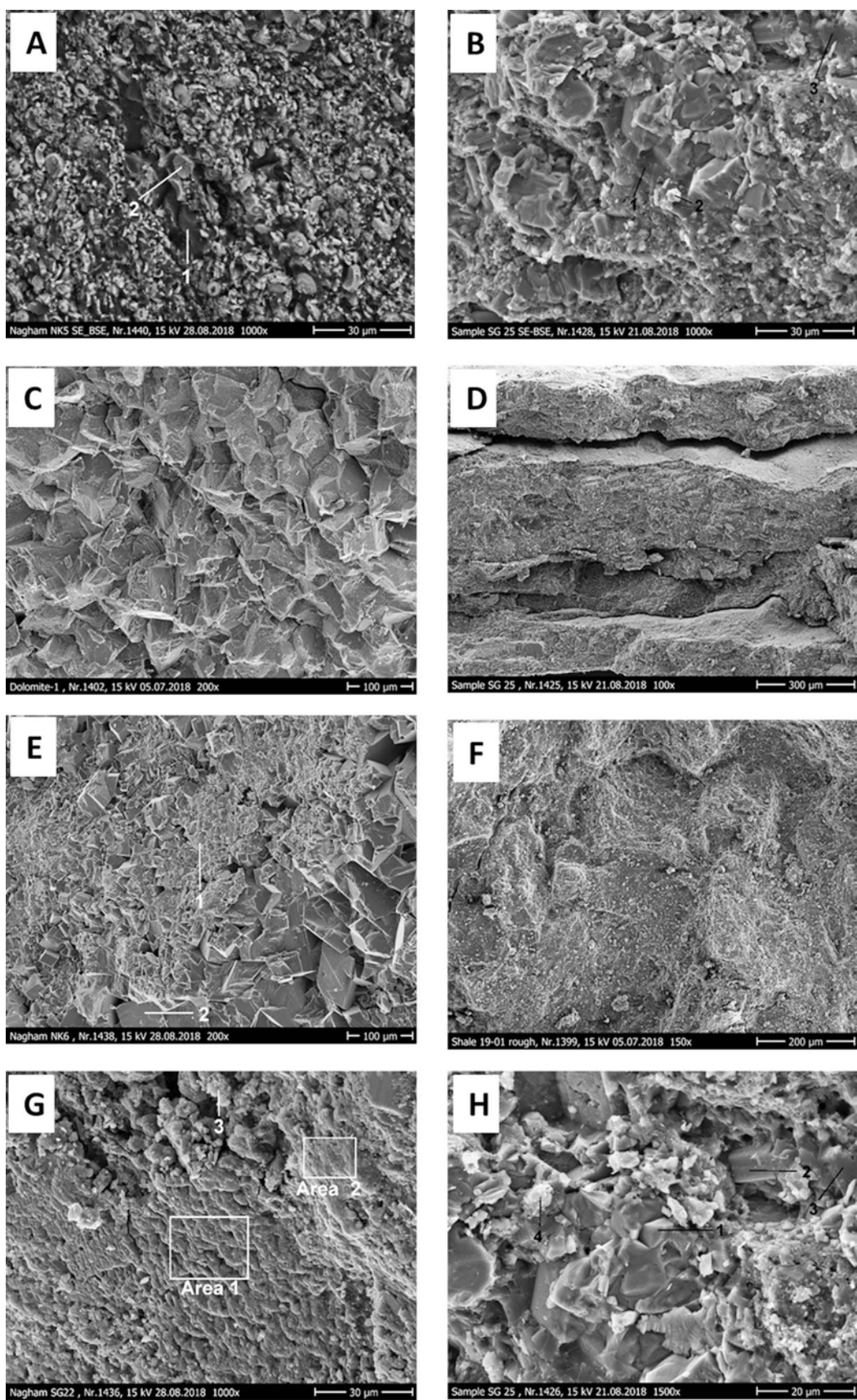


Fig. 6. Microfacies and diagenetic features of the Sargelu and Naokelekan formations. (A) An ostracod shell with some bioclasts within the bioclastic wackestone microfacies. (B) Iron oxides, fracture porosity, and rare floating skeletal grains within the mudstone microfacies. (C) Peaked low amplitude stylolites within the dolorudite microfacies. (D) Scattered crystals of pyrite within the dolarenite microfacies. (E) Dolomicrite microfacies. (F) Peaked high amplitude stylolites and channel porosity filled with bladed calcite cement. (G) Vuggy porosity. (H) Drusy calcite cement. (I) Saddle dolomite cement. (J) Aggrading neomorphism. (K) Micrite envelopes coating some of the carbonate grains. (L) Anhydrite cement. Scales included.

tion in the contact area with the overlying Naokelekan Formation. The dolomite crystals are mainly medium sized (c. 100–250 µm) and the microfacies also includes rare limestone lithoclasts (c. 400–600 µm). The

dolomites are characterized as planar e and s (euhe-
dral to subhedral) crystals in a hypidiotopic mosaic
(cf. [SIBLEY & GREGG 1987](#)). Patchily-distributed and
rare organic matter was also noted (Fig. 6C).



Fine-crystalline dolomites (dolarenites): This microfacies is restricted in terms of its occurrence to the lower part of the Sargelu Formation. The microfacies is dominated by fine dolomite crystals (30 to 60 μm in size), with the micritic matrix comprising <10% of the rock. These dolomites are composed of planar e and s (euhedral to subhedral) crystals in a hypidiotopic mosaic (cf. SIBLEY & GREGG 1987). Rare limestone lithoclasts (c. 350–500 μm) and pyrite crystals (c. 30–50 μm) were also noted (Fig. 6D).

Very Fine-crystalline dolomites (dolomicrites): This microfacies is found in only one bed, in the uppermost part of the Naokelekan Formation, i.e. the contact area with the overlying Barsarin Formation. The microfacies consists of mostly, very-fine dolomite crystals (4 to 14 μm in size) with <7% micritic matrix. The dolomite crystals are densely packed and can be characterized as non-planar a crystals (anhedral) in a xenotopic mosaic (Fig. 6E) (cf. SIBLEY & GREGG 1987).

6. Diagenetic features of the Sargelu and Naokelekan formations

As noted above, the lithologies within the Sargelu and Naokelekan formations comprise mainly limestones and dolomites. Evidence of diagenesis is present within both formations, but is particularly common within the Sargelu Formation. Estimated porosity is >10% for this formation, and <4% for the overlying Naokelekan Formation.

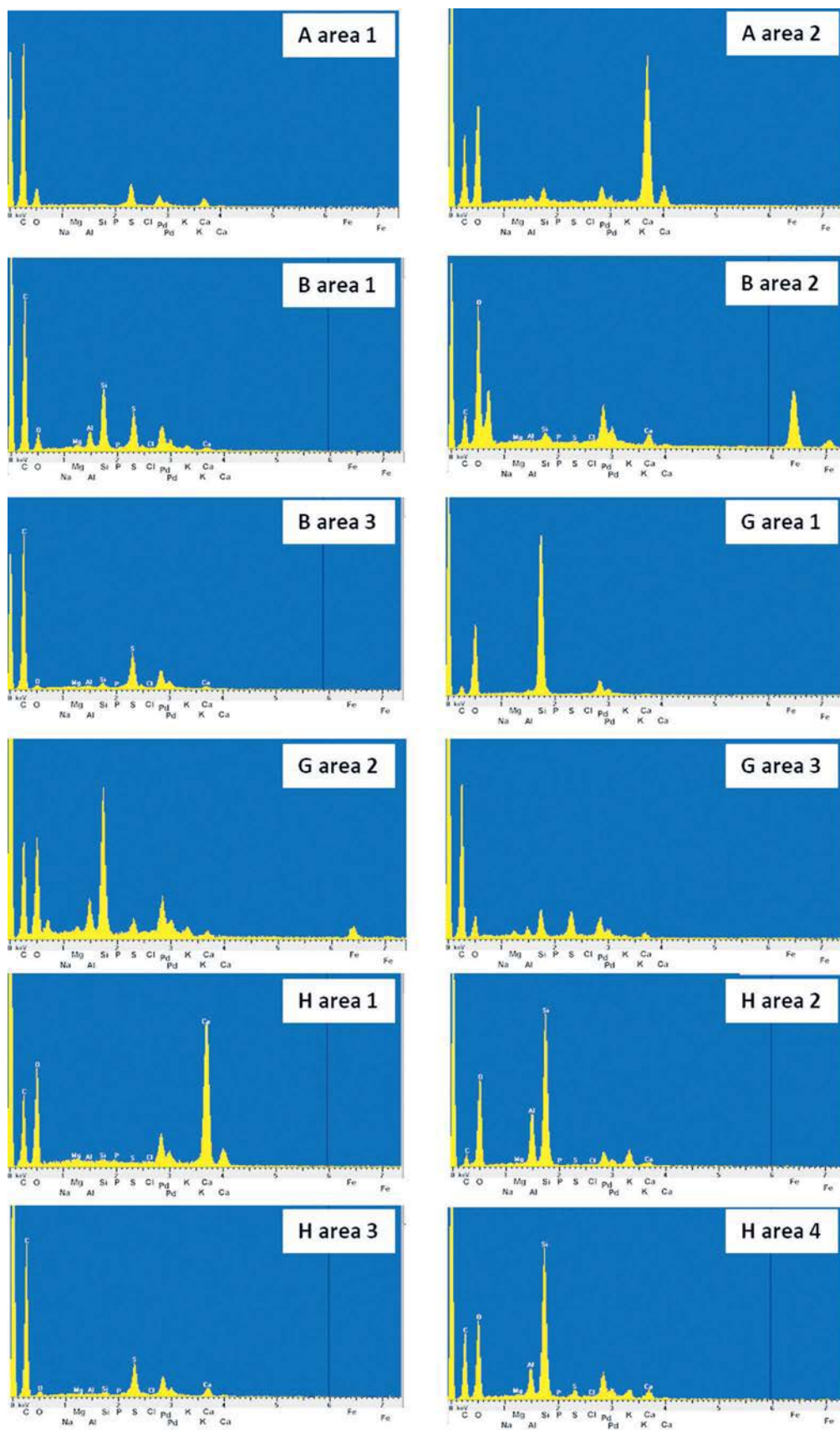
Both primary and secondary porosity were recorded in the carbonates of the Banik section. The primary porosity comprises only interparticle porosity, which was reduced as a result of subsequent mechanical compaction and cementation (Fig. 7C). Secondary porosity was generated by dissolution which resulted in the formation of molds, vugs, channels and fractures (cf. FLÜGEL 2004). The molds are generally formed as a result of the dissolution of fossils. Both fractures (up to 25 μm wide, noted in both formations) (Figs. 6B, 7D) and channels (up to 1.5 mm wide, only present with-

in the Sargelu Formation) porosities (Fig. 6F) were also generated. Vugs of various sizes (0.5–1.5 mm) were noted (Fig. 6G), although these were restricted to the Sargelu Formation. Organic matter often filled the molds as well as the channels and fractures of the Sargelu Formation, while in the Naokelekan Formation they tended to be empty.

The oldest evidence of diagenesis noted within the profile is the physical compactional features within the Sargelu Formation. These are mainly grain-grain point, long and concave-convex contacts (Fig. 6C; FLÜGEL 2004). Stylolites were noted only from the Sargelu Formation (FLÜGEL 2004). They are often found in the lower and upper parts of the formation, except in the contact area with the overlying Naokelekan Formation. Peaked low amplitude stylolites were more common in the lower part of the Sargelu Formation (Fig. 6C), whilst peaked high amplitude stylolites were restricted to the upper part of the formation (Fig. 6F). The various stylolites could be easily recognized due to the presence of insoluble organic matter (stylocumulate).

Cementation was an important process in the carbonates of the two formations. Three types of cements were recognized including, drusy calcite cement, bladed calcite cement, and dolomite cement. Drusy cement occurs in the form of anhedral to subhedral non-ferroan calcite crystals and forms in near-surface meteoric, as well as burial, environments (FLÜGEL 2004). In this study, drusy cement was found in the lower part of the Sargelu Formation, filling the veins and interparticle pores. The crystal size is usually 60–100 μm , increasing towards the center of the void (Fig. 6H). In contrast, bladed calcite cement was present only in the single limestone bed from the upper part of the Sargelu Formation (Fig. 6F), and was characterized by non-equidimensional and non-fibrous crystals. These latter are elongate crystals somewhat wider than fibrous crystals (cf. FLÜGEL 2004). Crystal sizes of up to 10 μm in width and lengths ranged from <20 to >100 μm . This particular cement type is typically marine-phreatic (and abundant in shallow-marine settings) and marine-vadose. It is usually a High-Mg calcite or may also be aragonite (cf. FLÜGEL 2004).

Fig. 7. SEM microimages of the Sargelu and Naokelekan formations. (A) Organic matter with some calcareous bioclasts. (B) Iron oxides with rare organic matter. (C) Tightly locked crystals of dolomite, indicative of physical compaction. (D) Fracture porosity. (E) Recrystallization of dolomite from fine crystals (area 1) to coarse crystals (area 2). (F) Broad view of a shale sample showing the convergent nature of the clay minerals. (G) Selected areas within a shale with quartz, montmorillonite and kaolinite. (H) Calcite and illite with an anhydrite cement. Scales included.



Dolomite cement, as noted above, was observed in both formations (i.e. Sargelu and Naokelekan), although the volume of cement is small when compared to the total volume of dolomite present (Fig. 6I). The dolomite cement present is a saddle dolomite (=baroque dolomite) (cf. MEHMOOD *et al.* 2018). Saddle dolomite is irregular, both in terms of its shape and size, where the individual crystals are coarse, generally a millimeter or larger and commonly found within fractures and pores. This would suggest that these crystals have a late origin (cf. RAHIMI *et al.* 2016). Saddle dolomites are also indicative of high-temperature conditions (i.e. 60–1500 °C) (SPÖTL & PITMAN 1998; MERINO *et al.* 2006; RAMEIL 2008) and are generally derived from high-salinity brines (MERINO *et al.* 2006; RAMEIL 2008).

Dolomitization has resulted in the precursor limestones of the Sargelu Formation being wholly or partly converted to dolomite rock. In the present study, dolomitization is mainly pervasive. Pervasive dolomite is represented by the presence of extensive and pervasive dolomite with a range of different crystal sizes (e.g., 30–250 µm) being present.

Neomorphism was also noted within the dolomites of the Sargelu Formation, and was confined to the growth of dolomite crystals (i.e. aggrading neomorphism) (Figs. 6J, 7E). Evidence of neomorphism includes the presence of irregular patches of recrystallized dolomite crystals. Individual recrystallized dolomite crystals range in size from fine to medium (c. 50–200 µm) or medium to coarse (c. 200–400 µm) (cf. BATHURST 1975).

Micritization of dolomite has also been noted in the upper part of the Sargelu Formation, while rare calcite crystals have been micritized in the upper part of the Naokelekan Formation. The micritization is recognised by the presence of micrite envelopes. In this study, the darker golden brown color of the micrite envelopes is considered to be a characteristic feature coating some of the carbonate grains (Fig. 6K). Micritization is a primary process which occurs in marine diagenesis at the sediment–water interface (SAMANKASSOU *et al.* 2005) and under low-energy conditions (FLÜGEL 2004).

7. Mineralogy

X-ray diffraction of twelve shale samples from the Sargelu and Naokelekan formations was carried out in order to investigate their mineralogical content. The predominant clay and non-clay minerals in the analysed shale samples are listed in Table 1. Illite (14.96–64.77%), and kaolinite (12.61%), constitute the only clay minerals present within the shales of the Middle to Late Jurassic-age succession of the Banik profile. The common, non-clay minerals include quartz (2.15–57.10%), dolomite/ankerite (0.70–90.60%), calcite (1.31–87.94%), alkali feldspar (2.60–51.30%), gypsum (0.78–1.31%), goethite (2.21–4.14%), and pyrite (1.16%).

In the shales of the Sargelu Formation, illite is the predominant clay mineral, followed by kaolinite – although they are only dominant in one sample (S16), whilst illite is the sole constituent clay mineral in the shales of the Naokelekan Formation (N4; see Table 1 & Fig. 9). Additional electron scanning microscopy (SEM) and EDX analysis confirmed the XRD analysis (Fig. 7F) (Figs. 7B area 1; 7G area 3; 7H area 2 and 4) (Figs. 8B area 1; 8G area 3; 8H area 2 and 4), as well as the presence of rare montmorillonite in the Sargelu Formation (Fig. 7G area 2) (Fig. 8G area 2).

In addition to the shale samples, a single sample from a chert bed within the upper part of the Sargelu Formation was also analysed using XRD. As expected, high values of SiO₂ were noted, as well as evidence of dolomite and calcite. Chert formation could possibly be related to silicification, post-dating the dolomitization.

8. Geochemistry

Twelve shale samples (8 Sargelu Formation, 4 Naokelekan Formation) were analysed using XRF in order to investigate their major and trace element compositions. The Sargelu Formation samples have moderately varied major element contents, including, SiO₂ (c. 9–30%), CaO (c. 5–20%), Al₂O₃ (c. 2–15%), Fe₂O₃ (c. 2–8%), MgO (c. 1.5–8%), SO₃ (c. 1–6%)

Fig. 8. EDX spectral analyses of selected areas of the Sargelu and Naokelekan formations. A area 1. organic matter. A area 2. calcium carbonate. B area 1. illite. B area 2. iron oxides. B area 3. organic matter. G area 1. quartz. G area 2. montmorillonite. G area 3. kaolinite. H area 1. calcite. H areas 2 & 4. illite. H area 3. anhydrite cement. Corresponding data is included in all analyses.

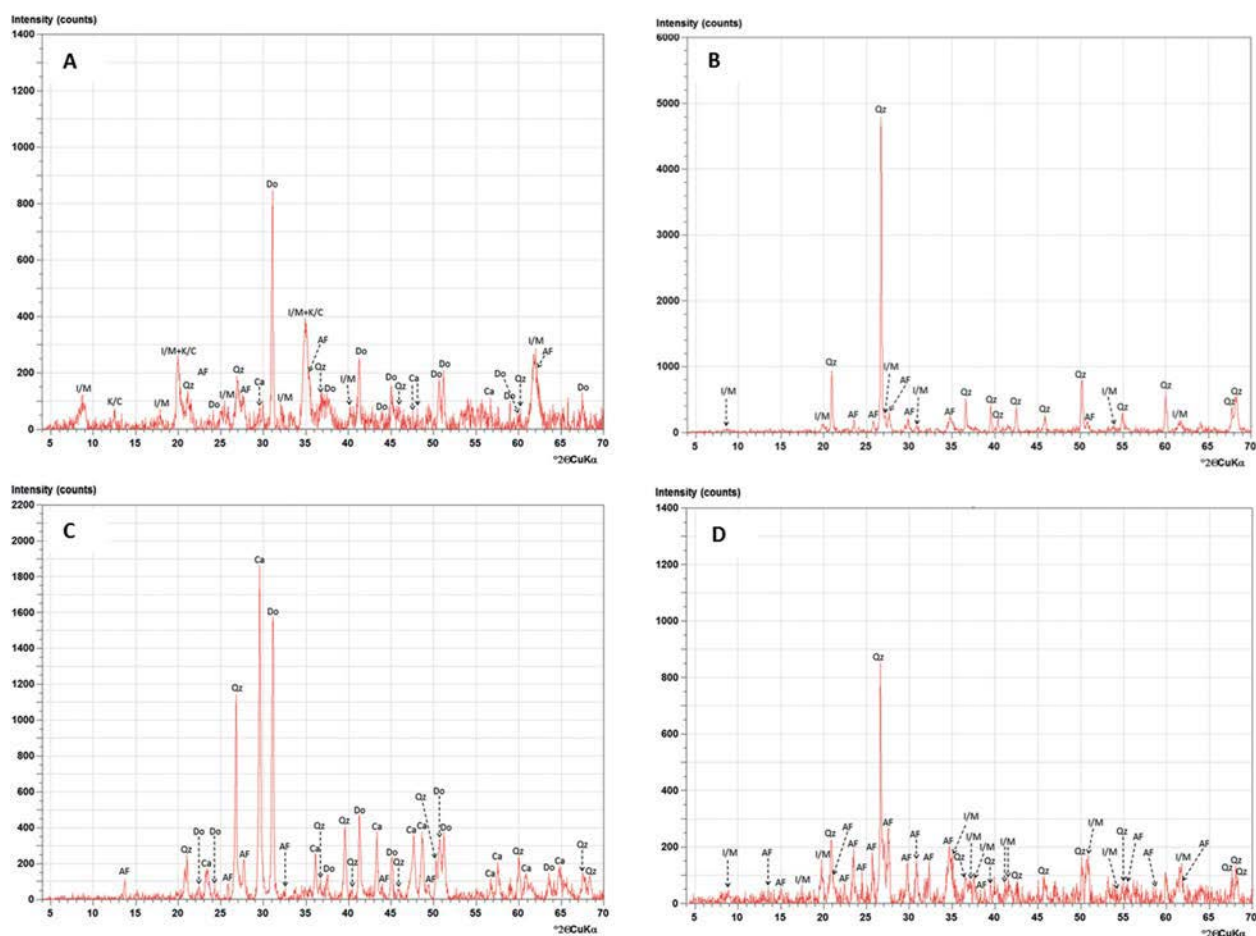


Fig. 9. X-ray diffractograms of selected samples from the Sargelu and Naokelekan formations illustrating the clay and non-clay minerals in the studied rocks. (A) Sample 16 Sargelu Fm. (B) Sample 22 Sargelu Fm. (C) Sample 27 Sargelu Fm. (D) sample 4 Naokelekan Fm, see Figure 4 for sample location.

and K_2O (c. 1–5 %). Two shale samples from the upper part of the Sargelu Formation have unusually high values of CaO (i.e. 42.26, 44.75 %). The shales show low values of TiO_2 (c. 0.10–1 %), P_2O_5 (c. 0.10–0.80 %), Na_2O (c. 0.04–0.09 %) and MnO (c. <0.02 %) (see Table 2).

Trace element distributions from the Sargelu Formation showed that the samples have high amounts of Ba, V, Mo, Cu, Zr, W, Pb, La, Ce, Zn, Sr, Cr and Rb. Some of the observed values differed markedly from the general values within the formation. For example, the Ba value from the lowest sampled shale in the formation is 1000 ppm, which is higher than the general range of values (c. 22–141 ppm). Higher values were also observed in V (a single shale sample from the middle part of the formation is 827 ppm vs general values

of c. 200–450 ppm), Mo (two shale samples from the middle part of the formation with values of 662 ppm and 526 ppm vs general values of c. 100–300 ppm), Cu (two shale samples from the lower part of the formation are 287 ppm and 217 ppm vs general values of c. 20–120 ppm), Zr (two shale samples from the lower part of the formation with values of 277 ppm and 144 ppm vs general values of c. 10–60 ppm), W (a single shale sample from the upper part of the formation is 144 ppm vs general values of c. 20–40 ppm), Pb (a single shale sample at the lowest part of the formation is 119 ppm vs general values of c. 15–24 ppm), La (a single shale sample at the lowest part of the formation is 91 ppm, vs general values of c. 10–30 ppm), Ce (a single shale sample at the lowest part of the formation is 84 ppm vs general values of c. 15–24 ppm).

Lower values were also observed, for example, in Zn (a single shale sample from the uppermost part of the formation is 74 ppm vs general range of values of c. 200–500 ppm), Sr (a single shale sample from the middle part in the formation is 52 ppm vs the general range of c. 80–150 ppm). Similar observations were made from two shale samples from the upper part of the formation in Cr (28 ppm and 18 ppm vs general values of c. 60–180 ppm) and a single sample from the upper part of the formation in Rb (6 ppm vs general values of c. 20–80 ppm).

The shales from the Sargelu Formation also showed varied ranges for Ni (c. 200–500 ppm), Mn (c. 30–85 ppm), As (c. 20–65 ppm), U (c. 20–50 ppm), Y (c. 15–40 ppm), Nd (c. 10–35 ppm) and Co (c. 10–30 ppm). The Th, Hf, Sm, Cs, Nb, Sc, and Ga from the same shale samples have considerably lower ranges of (c. 1–9 ppm), except for the Ga value from a single shale sample from the lowest part of the formation, which has a value of c. 43 ppm (see Table 3).

In contrast, the samples from the Naokelekan Formation have major element contents which are considerably lower than those recorded from the underlying Sargelu Formation. SiO₂ values (c. 3–8%) are c. 22% lower, CaO values (c. 3–30%) are c. 10% lower, Al₂O₃ values (c. 0.90–2.50%) are c. 13% lower, Fe₂O₃ values (c. 1–4%) are c. 4% lower, MgO values (c. 0.10–2%) are c. 6% lower, and K₂O values (c. 0.50–1.80%) are c. 3% lower. In contrast, the SO₃ values (c. 4–10%) are c. 6% higher than those recorded from the Sargelu Formation. The shales show low values of TiO₂ (c. 0.14–0.36%), P₂O₅ (c. 0.14–0.41%), Na₂O (c. 0.04–0.09%) and MnO (c. <0.01%), which are very similar to those recorded from the underlying Sargelu Formation (see Table 2).

Trace element distributions from the Naokelekan Formation show values of Ba (c. 150–300 ppm), V (c. 800–2000 ppm), Zn (c. 200–1000 ppm), Cr (c. 70–300 ppm), As (c. 25–77 ppm), U (c. 33–68 ppm) and Y (c. 26–85 ppm), which are higher than those from the underlying Sargelu Formation, whilst Mn (c. 20–58 ppm), Nd (c. 10–27 ppm) and Co (c. 3–11 ppm) values are slightly lower than those recorded from the underlying Sargelu Formation.

The general range of the trace element distributions in the two formations (i.e. Sargelu and Naokelekan) is similar for Mo (c. 100–300 ppm), Cu (c. 20–87 ppm), Zr (c. 10–55 ppm), W (c. 10–29 ppm), Pb (c. 14–22 ppm), La (c. 10–35 ppm), Ce (c. 5–20 ppm), Sr (c. 94–200 ppm), Rb (c. 15–37 ppm), and, Ni (c. 200–500 ppm). The range of values for Th, Hf, Sm,

Cs, Nb, Sc, and Ga from the same shale samples are low (i.e. <1–9 ppm), and thus very similar to those from the underlying Sargelu Formation (see Table 3).

9. Discussion

Carbonates interbedded with shales and rare cherts occurs within the Middle to Upper Jurassic Sargelu and Naokelekan formations from the Banik section, northernmost Iraq. These two formations have been described according to a number of different criteria mainly based on their lithological, petrographical and geochemical compositions. Determining the precise conditions present within the depositional environment and, in particular, the importance of evaporitic processes, can be difficult (e.g., MOORE *et al.* 1992). However, a multidisciplinary approach can provide more information. The following discussion will investigate a number of important points related to the two formations, namely, their depositional settings, diagenetic histories, evaporation proxies and palaeo-redox conditions.

9.1. Depositional setting

Limestones can be deposited in a variety of settings, ranging from terrestrial (e.g., BUCHHEIM *et al.* 2000) through to deep marine (e.g., ZADEH *et al.* 2019). Based on the lithological and microfacies descriptions of the limestones of the Sargelu and Naokelekan formations, it can be concluded that they were deposited in a marine setting. This can be confirmed by the presence of fossils (including microfossils) in both formations. The Sargelu Formation, comprising carbonates, shales and rare cherts, includes evidence of bioclastic fragments (ghost features) – and these fragments would appear to be pelecypods, although because of subsequent diagenesis it is not possible to identify them more accurately. In addition, the ostracod *Loricoecia loricata* is also present. This species is commonly found in shallow to intermediate depths (ANTEZANA *et al.* 1997). In other areas of Northern Iraq, a range of fossils have also been noted from the Sargelu Formation, including pelecypods (e.g., *Bositra*), gastropods, radiolaria, ostracods, calcispheres and algal filaments (e.g., ABDULA *et al.* 2015). *Bositra* is a marine benthic bivalve (e.g., JACH 2007), sometimes associated with

oxygen-depleted settings (CASWELL & COE 2013; ETTER 1996). Gastropods are pervasive in intertidal and shallow-marine settings (MCQUAID 1996). Radiolaria are useful indicators of open-ocean conditions, but may also be associated with coastal and brackish estuarine palaeoenvironments (BOLTOVSKOY et al. 2003). Ostracods are common lacustrine calcitic microfossils (McCORMACK et al. 2019). Calcspheres and filaments have been recorded in mid and outer ramp settings (REHMAN et al. 2016). In summary, these fossils are generally typical of marine environments, at depths ranging from shallow to deeper areas.

The amount of fossils present in the Sargelu Formation of northernmost Iraq is relatively low, and their condition is generally poor. Both of these aspects are most probably related to the degree of diagenesis (see below) which has been noted in the Sargelu Formation. However, our results would support the suggestion of JASSIM & BUDAY (2006b) that the Sargelu Formation was deposited across a range of marine environments (shallow to deep).

As noted above, the interbedded limestones are bioclastic wackestones. Such wackestones are comparable to the standard microfacies types of FLÜGEL (2004), particularly SMF-8 (wackestones and floatstones with whole fossils and well-preserved infauna and epifauna) and SMF-9 (strongly burrowed bioclastic wackestone). Both of these wackestones were deposited in low-energy environments below fair-weather wave base (cf. FLÜGEL 2004). They are found in environments ranging from shelf lagoons, outer- and mid-ramp settings as well as deeper shelf areas (FLÜGEL 2004). Based on the detailed study of the microfacies, their classification and the fossil content in the area of deposition, and related/adjacent areas, we would suggest that the Sargelu Formation of northernmost Iraq was deposited in a shallow-marine setting.

The Naokelekan Formation, comprising carbonates and shales, includes evidence of rare floating calcspheres. In other areas of Northern Iraq fossils have been noted from the Naokelekan Formation. The fossil suite includes planktonic foraminifers (*Globigerina*), small planktonic gastropods and pelagic ostracods, with ammonites and pelecypods (e.g., SHAREZWRI 2015). The planktonic foraminifers (*Globigerina*) are typical of nutrient-rich surface marine areas (KEMLE-VON MÜCKE & OBERHÄNSLI 1999), while also extending to the subsurface (REBOTIM et al. 2017). Small planktonic gastropod faunas are found in areas of oxygen depletion (MAPES & NUETZEL 2009). Pelagic ostracods are predominant in shelf topographic lows to

marginal/off-shelf environments (PERRIER et al. 2008). Ammonites have a transitional range from 20–550 m at submarine depth along continental shelf and slope environments (JIARUN & XIAOQIAO 1996). Unfortunately, there is no published information on the precise ammonite species present within the formation.

The limestones of the Naokelekan Formation are mainly mudstones (cf. FLÜGEL 2004), and were interpreted to be deposited in a low-energy setting water based on the absence skeletal material. Much of the lime mud was derived from the abrasion and micritization of the skeletal particles present, particularly in areas which were restricted (i.e. cut off from open ocean current activity). Mudstone microfacies are comparable to the microfacies type SMF-23 of FLÜGEL (2004), which consists of non-laminated homogeneous micrite and microsparite without fossils. These mudstones were deposited in saline or evaporitic environments, e.g. in tidal ponds (FLÜGEL 2004).

As noted above, and based on the fossil content in the area of deposition and related/adjacent areas, it would appear that the Naokelekan Formation of northernmost Iraq was deposited in a restricted shallow lagoon environment.

9.2. Diagenetic history

As noted above, parts of the carbonate succession have been altered to dolomite. The alteration of limestone to dolomite can be explained by a number of models including the evaporite brine-residue model, the groundwater mixing model, evaporation pumping model and the formation water model (e.g., WARREN 2000; MEHMOOD et al. 2018). Determining the appropriate model for a region, however, is not always easy. MEHMOOD et al. (2018) noted that the formation of dolomite within a carbonate succession results in the formation of a number of fabric-damaging to fabric-retaining features, and the development of new fabrics (selective to persistent). They also noted that the important factors to be observed include grain mineralogy, crystal extent, the timing of the dolomitization and the nature of the dolomitizing fluids (MEHMOOD et al. 2018). As noted earlier, the lower part of the Sargelu Formation comprises massive dolomites, while the upper part comprises dolomites interbedded with shales and rare cherts (with the exception of one limestone). In contrast, the Naokelekan Formation comprises shales in the lower part overlain by limestones (one bed is dolomite). Thus, a model to explain the dolo-

mitization would have to explain these differences between the two formations.

SIBLEY & GREGG (1987) noted the range of crystal boundary shapes in dolomites. Based on crystal size and crystal geometry two textural types of dolomite were distinguished within the Sargelu Formation. These are: fine crystalline planar e (=euhedral) and planar s (=subhedral) dolomite, medium crystalline planar e and planar s dolomite, whilst one common dolomite texture is present within the Naokelekan Formation represented by very fine crystalline non-planar a (=anhedral) dolomite (SIBLEY & GREGG 1987). The planar textures, which characterize the replacement dolomite in the Sargelu Formation, are consistent with an early diagenetic origin (cf. GREGG & SIBLEY 1984; SIBLEY & GREGG 1987). Fine-crystalline dolomites, comprising the lower part of the Sargelu Formation, are more commonly found in proximal shelf areas although they also occur closer to shore (NAGY *et al.* 2004). These dolomites are represented by extensive and pervasive dolomites comprising fine individual dolomite crystals (30 to 60 µm in size) and planar (euhedral to subhedral) morphologies. This type of dolomite is equivalent to the hypidiotopic mosaic texture of SIBLEY & GREGG (1987). Fine-crystalline dolomites have been described from peritidal sequences in the coastal sabkhas of Abu Dhabi (PATTERSON & KINSMAN 1982) and in hypersaline environments from Bonaire in the Netherlands Antilles (DEFFEYES *et al.* 1965). MCKENZIE *et al.* (1980) have suggested that fine-crystalline dolomites occur in areas where capillary evaporation and evaporative pumping were prevalent. Thus, it is possible that the evaporation pumping model would explain the presence of these dolomites in the Sargelu Formation. The presence of anhydrite (Fig. 6L) (Figs. 7H and 8H area 3), often in the form of a cement, within the lower part of the formation also supports the idea of evaporation being a defining process within the diagenetic environment.

Medium-crystalline dolomites, comprising a significant proportion of the upper part of the Sargelu Formation, are both extensive and pervasive. The individual dolomite crystals are medium sized (100 to 250 µm) and show planar (euhedral to subhedral) morphologies. This type of dolomite is also equivalent to the hypidiotopic mosaic texture of SIBLEY & GREGG (1987). Medium-crystalline dolomites are believed to be developed after considerable burial, and involve the replacement of subtidal to supratidal mudstones by wackestones (AMTHOR & FRIEDMAN 1991). However, other authors have suggested that medium-crystalline

dolomites can occur during shallow burial from compactional fluids (e.g., QING & MOUNTJOY 1994), or that they may simply be a result of the recrystallization of an early-formed dolomite (e.g., NOKHBATOL-FOGHAAEI *et al.* 2019). Medium-crystalline dolomites commonly form at elevated temperatures during burial and/or result from the recrystallization of precursor finer dolomites in burial environments or near-surface meteoric to mixed meteoric-marine environments (GREGG & SIBLEY 1984; GREGG & SHELTON 1990; KUPCZ & LAND 1991). Medium-crystalline dolomites have also been described as having been precipitated from mixed evaporative-meteoric waters (e.g., AZMY *et al.* 2009; AZOMANI *et al.* 2013; OLANIPEKUN *et al.* 2014). Thus, a model of dolomitization by evaporative brine reflux could possibly be invoked to interpret these dolomites in the Sargelu Formation. The presence of an anhydrite cement within these dolomites also supports the idea of evaporation being a related process in the diagenetic environment.

In comparison to the Sargelu Formation dolomites which, as noted above, are planar (euhedral to subhedral), the dolomites of the Naokelekan Formation are non-planar (anhedral). These dolomites are represented by densely packed dolomite aggregates formed of very fine individual dolomite crystals (4 to 14 µm in size). The Naokelekan Formation dolomite is equivalent to the xenotopic mosaic texture of SIBLEY & GREGG (1987).

According to MACHEL (2004), dolomites can theoretically form in three different ways, namely: the replacement of CaCO_3 by $\text{CaMg}(\text{CO}_3)_2$; cementation; and precipitation from aqueous solutions to form primary dolomite. Primary dolomite appears to be rare and restricted to some evaporitic lagoonal and/or lacustrine settings (FOLK & LAND 1975; BOGGS 2009). The dolomites of the Naokelekan Formation overlie the organic-rich shales and limestones, and are very fine. Such finely crystalline dolomites can form as a result of slow crystallization, under evaporative conditions, within highly concentrated Mg-enriched brines (FOLK & LAND 1975). A recent study by PRETO *et al.* (2015) revealed that mosaic dolomites consisting of aggregates of nanometer-scale ‘growth units’ could be considered as indicative of a primary origin. The dolomites described from the Naokelekan Formation clearly formed in a near-surface setting (see above). In addition, the lack of any evidence of direct replacement of precursor grains or minerals would suggest that the dolomites of the Naokelekan Formation may have been directly precipitated (cf. EL-SAYED 2001).

9.3. Geochemical proxies for evaporitic conditions

As noted earlier, the lower part of the Sargelu Formation comprises dolomite, while the upper part consists of dolomite beds alternating with shales, as well as rare cherts and one single limestone bed. When the shale has a high carbonate content, this is indicative of slow sedimentation, with the carbonate depositing continuously with the shale (cf. [ORHAN et al. 2019](#)). In contrast, the base of the Naokelekan Formation comprises just shale (basal 5 m), moving upward into limestone, with a single bed of dolomite at the top. As with the Sargelu Formation, the high carbonate content within the shale beds is indicative of slow sedimentation.

As noted above, twelve mudstone samples were analysed. Values of Sr, Ca and Al were interpreted in terms of salinity and/or aridity. There is an overall increase in Ca content (e.g., 12.51, 21.55, 31.98 %) within the shale samples from the Sargelu and Naokelekan formations with a corresponding decrease in Al content (e.g., 0.44, 1.30, 2.17 %), except for one shale sample at the base of the upper part of the Sargelu Formation which has a considerably lower value of Ca (3.92 %) and a higher value of Al (9.99 %) (see Table 4; Fig. 10).

This inverse relationship between the Ca and Al contents is indicative of low detrital input with carbonate sedimentation being predominant (cf. [ORHAN et al. 2019](#)). In addition, these elemental variations would indicate that deposition occurred under arid conditions (cf. [ORHAN et al. 2019](#)) with the exception of the basal sediments of the upper part of the Sargelu Formation.

The trace element Sr can be used to provide some indication of the degree of salinity within the depositional setting. In the shales of both the Sargelu and Naokelekan formations, Sr shows particularly high values (81, 124, and 298 ppm) (Table 4). A number of authors (e.g., [READ et al. 1995](#); [PRICE 1999](#); [VINCENT et al. 2006](#)) suggested that such high values can be interpreted as being indicative of saline conditions within the area of deposition. Together, these various proxies would suggest that deposition occurred in an area of slow sedimentation, with little detrital input and under arid conditions. The ambient waters had elevated salinity values. The fact that fossils have been recorded in the sediments of the Sargelu Formation but not in the overlying Naokelekan Formation (see above) might suggest that salinity values increased from base to top in the profile, resulting in an environment in Naokelekan Formation times which was

particularly inhospitable. However, there are fossils present within the Naokelekan Formation elsewhere in Northern Iraq, which may suggest that conditions were variable across the depositional setting – possibly as a result of the subdivision of the basinal setting due to ongoing tectonic activity.

In summary, the geochemical proxy results would support the idea of higher salinities and evaporation rates (as a result of the aridity) within the depositional area of the Sargelu and Naokelekan formations. However, it would also appear that these interpretations cannot be extended across the broader extent of these formations – due largely, as noted above, to the relatively rich faunal content which have been reported from Northern Iraq (e.g., [JASSIM & BUDAY 2006b](#)). The fact that the area was tectonically active may, therefore, have resulted in the formation of smaller sub-basins within the broader Jurassic-age setting where elevated salinities may have resulted in the higher Sr values recorded.

9.4. Geochemical proxies for palaeoredox conditions

Oxygen levels in marine environments show different proportions depending on the depositional setting and the water depth (e.g., [WANG et al. 2018](#)). Determining the concentration of dissolved oxygen in seawater is of great importance when interpreting the depositional setting. The level of dissolved oxygen (i.e. the environmental redox conditions) allows settings to be classified as oxic, suboxic and anoxic with measurable quantities of H₂S representing euxinic conditions ([SAVRDA & BOTTJER 1991](#); [WIGNALL 1994](#)). A range of geochemical proxies were measured from the shales of the Sargelu and Naokelekan formations to provide information about the redox state of the depositional environments of both formations in the area of the Banik section from northernmost Iraq (e.g., [JONES & MANNING 1994](#); [RIMMER 2004](#); [DEEPULAL et al. 2012](#); [RAMOS-VÁZQUEZ et al. 2017](#)). These include authigenic U, U/Th, V/Cr, Ni/Co, and V/Sc redox sensitive elements (e.g., U, Th, V, Cr, Ni, and Cu) which are moderately enriched in anoxic sediments ([YARINCIK et al. 2000](#); [YANG et al. 2004](#); [GUO et al. 2007](#)) (see Table 3; Fig. 11).

Within the shales of the study area, high U contents (>4 ppm) have been recorded, suggesting that sea water conditions during the time of deposition in the Sarge-

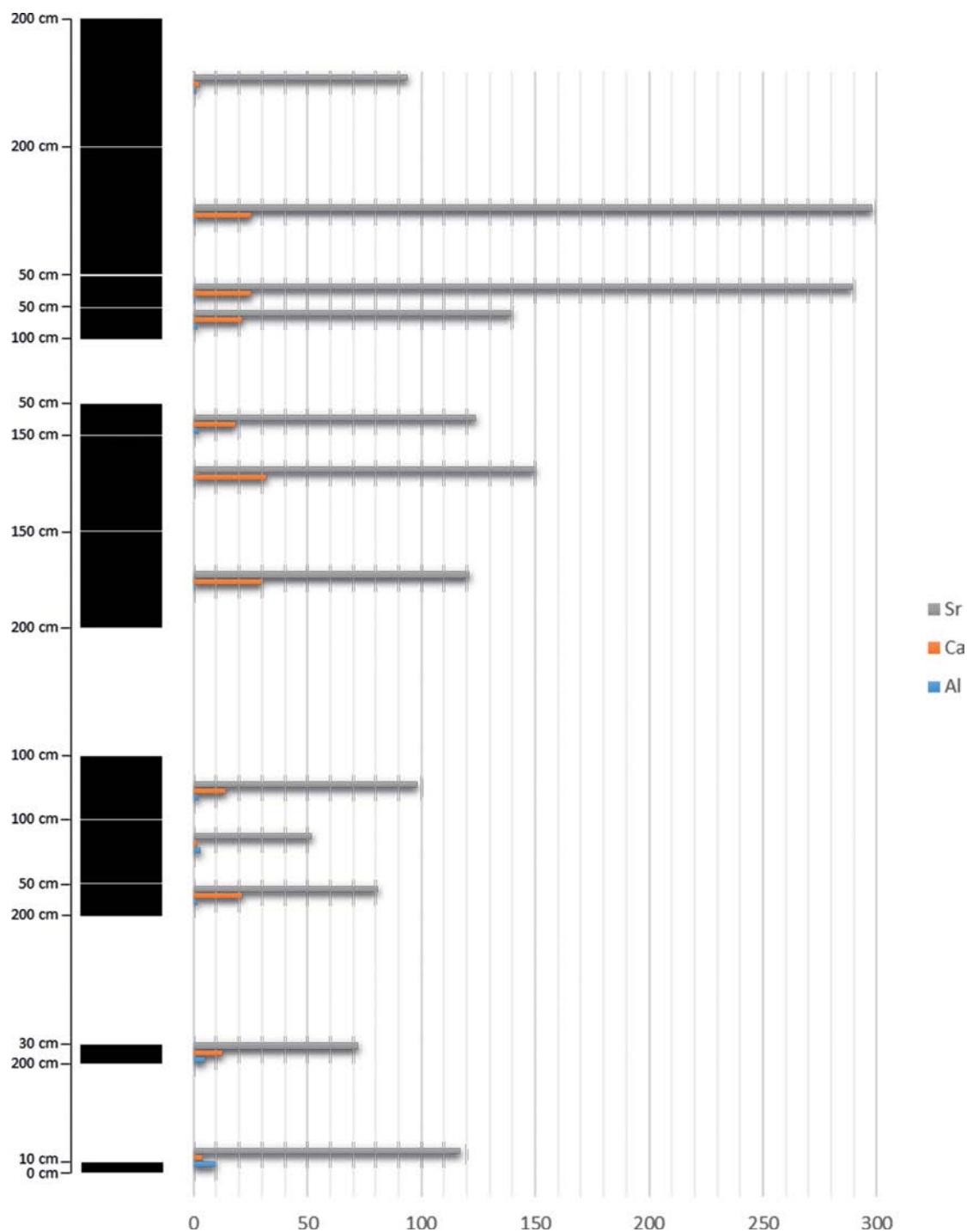


Fig. 10. Shale beds from the upper part of the Sargelu Formation and the lower part of the Naokelekan Formation, from the measured log of the Banik section, northernmost Iraq, showing geochemical proxies for evaporitic conditions.

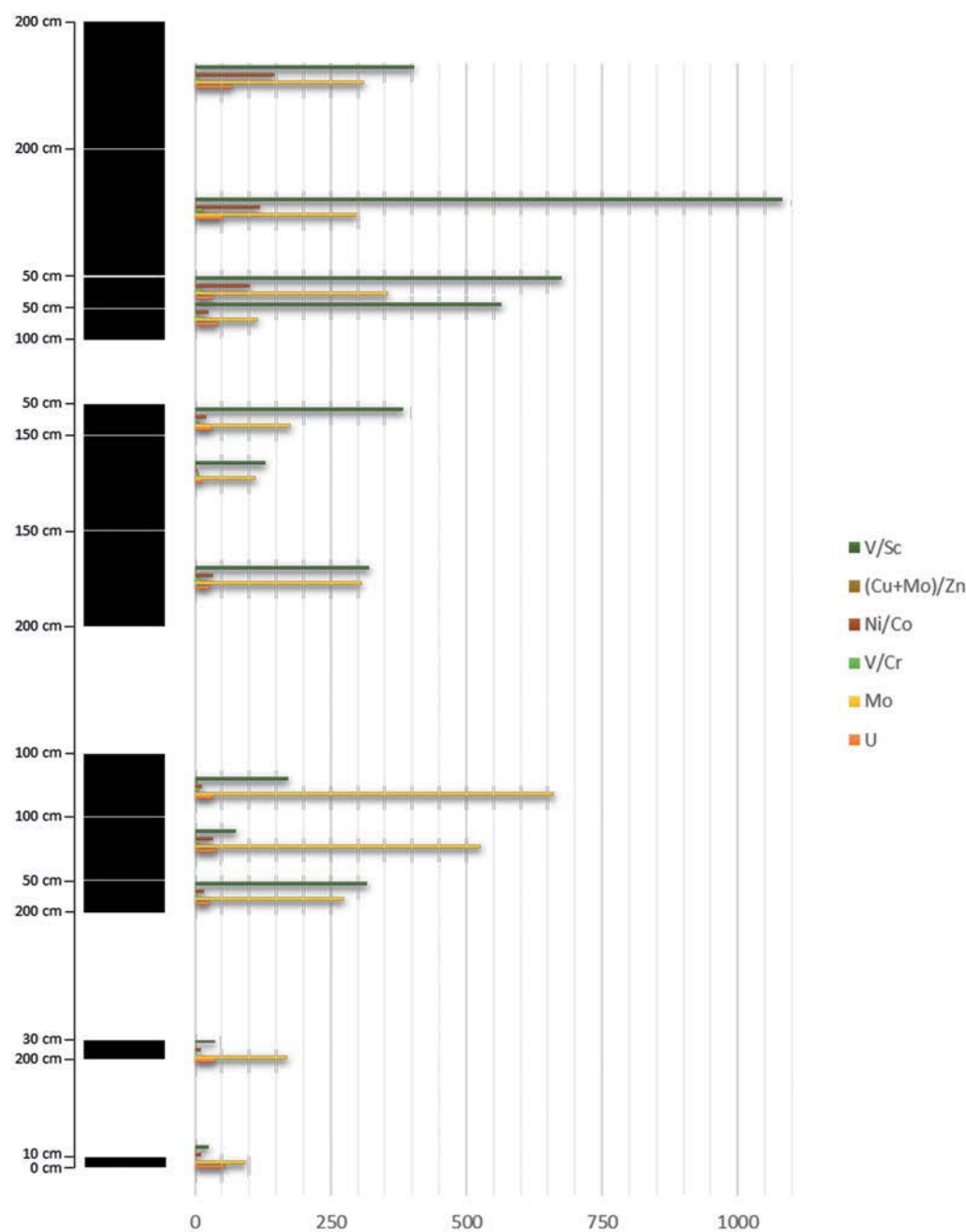


Fig. 11. Shale beds from the upper part of the Sargelu Formation and the lower part of the Naokelekan Formation, from the measured log of the Banik section, northernmost Iraq, showing geochemical proxies for palaeoredox conditions.

lu and Naokelekan formations were euxinic (cf. VERMA & KUMAR 2018). Indeed, the measured U values were particularly high, ranging from 13.5–54.6 ppm in the Sargelu Formation and increasing from 33.8 ppm up to 68.3 ppm in the overlying Naokelekan Formation (Table 3).

Cr is associated with the clay fraction of the sediment and is unaffected by redox conditions. In contrast V, as V⁴⁺ is bound to organic matter and, therefore, tends to be concentrated in sediment deposited under anoxic conditions (JONES & MANNING 1994). Therefore, the V/Cr ratio of the sediment could be regarded as

providing evidence of anoxic conditions. Ratio values of >4.5 suggest anoxic conditions, while values which are <2 suggest that oxic conditions prevailed (JONES & MANNING 1994). The V/Cr values at the base of the upper part of the Sargelu Formation (i.e. 1.92, 2.01) would both possibly suggest that the sediments were deposited under oxic conditions. However, moving up section, the values increase markedly into the zone of anoxic conditions (i.e. values >4.5). Moving from the Sargelu Formation into the overlying Naokelekan Formation, the V/Cr values increase markedly once again. Indeed, the basal value for the Naokelekan Formation is 9.13, increasing rapidly to 11.98 and even to 14.99. Such values are more than double some of the Sargelu Formation values. This would suggest that anoxia became more prevalent within the period during which the Naokelekan Formation sediments were deposited.

A number of authors, including KREJCI-GRAF (1966), ERNST (1970), DILL (1986), JONES and MANNING (1994), and DEEPULAL *et al.* (2012) have suggested that the Ni/Co ratio can be used as an indicator of palaeoredox conditions. According to KREJCI-GRAF (1966) and ERNST (1970), the ratio values of Ni/Co which are <1 indicate that the sediments were deposited within the oxic zone, whilst values >1 indicate that they were deposited within the anoxic zone. Commonly, Ni is enriched in sediments containing large amounts of organic matter while Co is typically associated with the clay fraction. High Ni/Co values are, therefore, typical of reducing conditions in which organic matter accumulates in the sediment (e.g., RAISWELL & PLANT 1980; PATTERSON *et al.* 1986). This was observed from the high Ni/Co values of the shales of the Naokelekan Formation as compared to those of the Sargelu Formation. The Ni/Co values of the Naokelekan Formation (c. 24–45) are noticeably higher than those recorded from the underlying Sargelu Formation (c. 5–33) (see Table 3).

HALLBERG (1976) has suggested that Cu/Zn ratios would increase in a strongly reducing environment, where under euxinic conditions more Cu is precipitated than Zn due to the solubility of their sulphides. The (Cu+Mo)/Zn ratio has been calculated for the shale samples in this study. Table 3 illustrates these high values for some samples from the Sargelu Formation (e.g., 1.84, 3.23, and 4.39). In contrast, the samples from the Naokelekan Formation show considerably lower values than those recorded from the underlying Sargelu Formation (e.g., 0.29–1.09).

Mo is considered to be indicative of sediment deposition under sulphate-reducing conditions (RIMMER

2004). Relatively high values of Mo are recorded within the shale samples in this study, which may indicate the reducing conditions during the time of their deposition. The Mo values at the base of the upper part of the Sargelu Formation are 94 and 170 ppm, increasing rapidly to 307 ppm and even to 662 ppm. However, the Mo values into the overlying Naokelekan Formation are considerably high (c. 116–356 ppm) (see Table 3).

KIMURA & WATANABE (2001) suggested that the V/Sc ratio can be used as a proxy indicator for redox conditions, where ratios of <9 indicate oxidizing conditions and values of >9 suggest that conditions were suboxic (KIMURA & WATANABE 2001). The calculated values of V/Sc of the shale samples from both formations are >9 which indicate the suboxic field. However, there is a rapid increase of V/Sc values from the basal sediments (i.e. 25–37.86) into the upper sediments (i.e. up to 383) within the upper part of the Sargelu Formation and moving into the overlying Naokelekan Formation, these values increase markedly to 675 and even to 1082 (see Table 3).

These geochemical proxies would suggest that while both formations were deposited under broadly anoxic (or low oxygen) conditions, there were clear differences moving up section. The basal sediments of the upper part of the Sargelu Formation suggest that redox conditions were less prevalent while these sediments were deposited, but on moving into the middle and upper sediments of the upper part of the same formation there is evidence of a rapid increase in anoxia. In the Naokelekan Formation, conditions were clearly anoxic. This could be interpreted as resulting from the palaeogeographic situation in the Late Mesozoic and Early Cenozoic, where tectonic activity, eustatic sea-level changes, and climate variations were controlling sedimentation. Deposition of the Middle to Upper Jurassic successions coincided with a broad eustatic transgression (BUDAY 1980; HAQ 2018), resulting in higher global sea levels over time (HALLAM 1982; ALSHARHAN & NAIRN 2003). Despite the eustatic rise, the depositional setting for the Middle to Late Jurassic-age Sargelu and Naokelekan formations, is interpreted to have been broadly shallow marine (shelf), in contrast to the deeper-water setting suggested by JASSIM & BUDAY (2006a). This disparity in terms of the rising sea level and the shallow-marine deposition would suggest that tectonic activity (i.e. Cimmerian-related uplift, see also BUDAY 1980) would have negated, or modified, the sea-level rise. This contrasts also with, for example, Sargelu Formation sediments elsewhere in Kurdistan which have been interpreted as having

been deposited in deeper waters (e.g., ABDULA *et al.* 2015). The aridity of the depositional setting correlates well with the suggested Jurassic climate being dominated by tropical-subtropical conditions (HALLAM 1982). As noted above, the inferred higher salinity values may have been related to tectonic control on the broader basin, with the formation of subbasins. If this was, indeed, the case, it would also explain the variations in oxygen levels – with periods of lower oxygen being possibly related to sill formation and the resultant basin restriction (e.g., SLATT *et al.* 2015). Indeed, the presence of the nannofossil *Cyclagelosphaera margerelii* sp. in the Naokelekan Formation is indicative of higher salinities (e.g., TREMOLADA *et al.* 2006), as noted by ABDULA (2016).

10. Summary and conclusions

The Middle to Upper Jurassic succession of the Banik section from northernmost Iraq were deposited in the Iraqi Zagros Basin/Zagros Fold belt. Sedimentation took place within the northeastern boundary of the Arabian Plate. A range of analyses – sedimentological, petrographical and microfacies – have been carried out on the carbonate sediments, whilst the clastic sediments were analysed in terms of their geochemistry. The succession is dominated by dolomites, limestones, mudstones and rare cherts. Deposition of the Sargelu and Naokelekan formations is interpreted to have occurred, possibly in a shallow-marine and restricted shallow lagoon environment, respectively. This interpretation is supported by the detailed study of the microfacies and the fossil content in the area of deposition, and related/adjacent areas.

The results of the palaeoredox indicators in this study would suggest that the sedimentary successions, which are characterized by the deposition of the Middle–Late Jurassic-age Sargelu and Naokelekan formations, were accumulated under anoxic conditions. In the palaeogeographic context, as noted earlier, the region of northernmost Iraqi Kurdistan was subjected to tectonic activity. The ongoing tectonic activity might have resulted in the formation of barred subbasins in which the water circulation is topographically restricted and, therefore, generally is oxygen-depleted. Together, the evaporation processes (controlled by arid climate) would suggest that the permanently anoxic conditions were developed within those semi-enclosed subbasins.

Acknowledgements

We would like to thank BETTINA SCHULTE-VAN BERKUM, RAINER SCHWARZ and STEVE SONNTAG for their help in the laboratory work. EFFI-LAURA DREWS and HEIKE KOCH both helped with earlier versions of the diagrams. In particular we would like to thank HANS-JÜRGEN ENSIKAT for initiating and supporting the scanning electron microscopy (SEM) and energy-dispersive X-ray microanalysis (EDX). This study is supported by the Arab-German Young Academy of Sciences and Humanities (AGYA) grants (AGYA_2018_TP_13 and AGYA_2019_TP_11). Finally, we thank our reviewers (NISAN SARIASLAN and MARTIN LANGER) for their thorough reviews of the manuscript.

References

- ABDULA, R. (2010): Petroleum source rock analysis of the Jurassic Sargelu Formation, Northern Iraq. – Master's thesis, Colorado School of Mines: 125 pp.
- ABDULA, R. (2017): Source rock assessment of Naokelekan formation in Iraqi Kurdistan. – *Journal of Zankoi Sulaimani (Part-A)*, **19**: 103–124.
- ABDULA, R.A. (2016): Stratigraphy and lithology of Naokelekan Formation in Iraqi Kurdistan-Review. – *The International Journal of Engineering and Sciences*, **5**: 7–17.
- ABDULA, R.A., BALAKY, S.M., NOURMOHAMADI, M.S. & PIR-OUI, M. (2015): Microfacies Analysis and Depositional Environment of the Sargelu Formation (Middle Jurassic) from Kurdistan Region, Northern Iraq. – *Donnish Journal of Geology and Mining Research*, **1**: 001–026. <http://www.donnishjournals.org/djgmr>.
- AL-AHMED, A.A.N. (2006): Organic geochemistry, palynofacies and hydrocarbon potential of Sargelu Formation (Middle Jurassic) northern Iraq. – PhD thesis, University of Baghdad.
- AL-AMERI, T.K. & ZUMBERGE, J. (2012): Middle and Upper Jurassic hydrocarbon potential of the Zagros Fold Belt, North Iraq. – *Marine and Petroleum Geology*, **36**: 13–34. doi: [10.1016/j.marpetgeo.2012.04.004](https://doi.org/10.1016/j.marpetgeo.2012.04.004)
- AL-AMERI, T.K., AL-JUBOURI, N.M., ISA, M.J. & AL-AZZAWI, R.E. (2012): Hydrocarbons generation potential of the Jurassic-Lower Cretaceous Formation, Ajeel field, Iraq. – *Arabian Journal of Geosciences*, **6**: 3725–3735. doi: [10.1007/s12517-012-0636-0](https://doi.org/10.1007/s12517-012-0636-0)
- AL-AMERI, T.K., NAJAF, A.A., AL-KHAFAJI, A.S., ZUMBERGE, J. & PITMAN, J. (2013): Hydrocarbon potential of the Sargelu Formation, North Iraq. – *Arabian Journal of Geosciences*, **7**: 987–1000. doi: [10.1007/s12517-013-0875-8](https://doi.org/10.1007/s12517-013-0875-8)
- AL-DUJAILY, L.S. (1994): Stratigraphy section of Middle–Upper Jurassic system and Lower Cretaceous, northern Iraq. – Master's thesis, Science College, University of Baghdad, Baghdad, Iraq: 98 pp. (in Arabic, unpublished).

- AL-OMARI, F.S. & SADIQ, A. (1977): Geology of northern Iraq. – 198 pp.; Mosul (Mosul University Press) (in Arabic).
- AL-SAYYAB, A., AL-ANSARI, N., AL-RAWI, D., AL-JASSIM, J., AL-OMARI, F. & AL-SHAIKH, Z. (1982): Geology of Iraq. – 280 pp.; Mosul (Mosul University Press) (in Arabic).
- ALSHARHAN, A.S. & NAIRN, A.E.M. (2003): Sedimentary basins and petroleum geology of the Middle East. – 843 pp.; Amsterdam (Elsevier).
- ALTINLI, I.E. (1966): Geology of eastern and southeastern Anatolia, Turkey. – Bulletin of Mineral Research Exploration Institute of Turkey, Foreign Edition, Ankara, **60**: 35–76.
- AL-ZUBAIDI, A.A. & AL-ZEBARI, A.Y. (1998): Prospects for production and marketing of Iraq's heavy oil. – 221 + 10 pp.; Baghdad (Ministry of Oil, State Oil Marketing).
- AMTHOR, J.E. & FRIEDMAN, G.E. (1991): Dolomite-rock texture and secondary porosity development in Ellenburger Carbonate Group (Lower Ordovician), West Texas and Southeastern New Mexico. – Sedimentology, **38**: 343–362. doi: [10.1111/j.1365-3091.1991.tb01264.x](https://doi.org/10.1111/j.1365-3091.1991.tb01264.x)
- ANTEZANA, T., BENASSI, G., COSTANZO, G., CRESCENTI, N., FERRARI, I., GHIRARDELLI, E., GRANATA, A., GUGLIELMO, L. & MCKENZIE, K.G. (1997): Atlas of Marine Zooplankton Straits of Magellan Amphipods, Euphausiids, Mysids, Ostracods, and Chaetognaths. – 290 pp.; Heidelberg & Berlin (Springer).
- AZMY, K., KNIGHT, I., LAVOIE, D. & CHI, G. (2009): Origin of the Boat Harbour dolomites of St. George Group in western Newfoundland, Canada: implications for porosity controls. – Bulletin of Canadian Petroleum Geology, **57**: 81–104. doi: [10.2113/gscpgbull.57.1.81](https://doi.org/10.2113/gscpgbull.57.1.81)
- AZOMANI, E., AZMY, K., BLAMEY, N., BRAND, U. & AL-AASM, I. (2013): Origin of Lower Ordovician dolomites in eastern Laurentia: controls on porosity and implications from geochemistry. – Marine and Petroleum Geology, **40**: 99–114. doi: [10.1016/j.marpetgeo.2012.10.007](https://doi.org/10.1016/j.marpetgeo.2012.10.007)
- BALAKY, S.M.H. (2004): Stratigraphy and sedimentology of Sargelu Formation (Middle Jurassic) in selected sections in Erbil and Duhuk Governorates – Iraqi Kurdistan. – Master's thesis, Science College, University of Salahaddin, Erbil, Iraq: 109 pp. (unpublished).
- BATHURST, R.G.C. (1975): Carbonate sediments and their diagenesis (2nd edition). – 658 pp.; Amsterdam (Elsevier).
- BEYDOUN, Z.R. (1991): Arabian plate hydrocarbon geology and potential – A plate tectonic approach. – AAPG Studies in Geology, **33**: 1–77. doi: [10.1306/St33533](https://doi.org/10.1306/St33533)
- BEYDOUN, Z.R., CLARKE, M.W.H. & STONELEY, R. (1992): Petroleum in the Zagros Basin—a Late Tertiary foreland basin overprinted onto the outer edge of a vast hydrocarbon-rich Paleozoic-Mesozoic passive-margin shelf. – In: MACQUEEN, R.W. & LECKIE, D.A. (eds.): Foreland basins and fold belts. – American Association of Petroleum Geologists Memoir, **55**: 309–339.
- BOGGS, S.J. (2009): Principles of Sedimentology and Stratigraphy. – 688 pp.; Upper Saddle river (Pearson Prentice-Hall).
- BOLTOVSKOY, D., KOGAN, M., ALDER, V.A. & MIANZAN, H. (2003): First record of a brackish radiolarian (Polycystina): *Lophophaena rioplatensis* n.sp. in the Rio de la Plata estuary. – Journal of Plankton Research, **25**: 1551–1559. doi: [10.1093/plankt/fbg107](https://doi.org/10.1093/plankt/fbg107)
- BUCHHEIM, H.P., BRAND, L.R. & GOODWIN, H.T. (2000): Lacustrine to fluvial floodplain deposition in the Eocene Bridger Formation. – Palaeogeography, Palaeoclimatology, Palaeoecology, **162**: 191–209. doi: [10.1016/S0031-0182\(00\)00112-7](https://doi.org/10.1016/S0031-0182(00)00112-7)
- BUDAY, T. (1980): The Regional Geology of Iraq. – Stratigraphy and Palaeogeography, Publication of GEOSURV, Baghdad, **1**: 445 pp.
- CASWELL, B.A. & COE, A.L. (2013): Primary productivity controls on opportunistic bivalves during Early Jurassic oceanic deoxygenation. – Geology, **41**: 1163–1166. doi: [10.1130/G34819.1](https://doi.org/10.1130/G34819.1)
- DEEPULAL, P.M., GIREESH KUMAR, T.R., SUJATHA, C.H. & REJOMON, G. (2012): Chemometric study on the trace metal accumulation in the sediments of the Cochin Estuary-Southwest coast of India. – Environmental Monitoring and Assessment, **184**: 6261–6279. doi: [10.1007/s10661-011-2418-7](https://doi.org/10.1007/s10661-011-2418-7) PMID: 22083399
- DEFFEYES, K.S., LUCIA, F.J. & WEYL, P.K. (1965): Dolomitization of Recent and Plio-Pleistocene sediments by marine evaporite waters on Bonaire, Netherlands Antilles. – In: Pray, L.C. & Murray, R.C. (eds.): Dolomitization and Limestone Diagenesis, A Symposium. – Society of Economic Paleontologists and Mineralogists, Special Publications, **13**: 89–111.
- DILL, H. (1986): Metallogenesis of early Paleozoic graptolite shales from the Grafenthal Horst (northern Bavaria, Federal Republic of Germany). – Economic Geology, **81**: 889–903. doi: [10.2113/gsecongeo.81.4.889](https://doi.org/10.2113/gsecongeo.81.4.889)
- DUBERTRET, L. (1966): Liban, Syrie et bordure des pays voisins. Tableau stratigraphique avec carte géologique au millionième. – Notes et Memoires sur le Moyen Orient, **8**: 251–358.
- DUNHAM, R.L. (1962): Classification of carbonate rocks according to depositional texture. – American Association of Petroleum Geologists Memoir, **1**: 108–121.
- EDILBI, A.N.F. & SHERWANI, G.H. (2019): Petrography and source rock potential of Chia Gara Formation (Late Jurassic–Early Cretaceous) in Northern Iraq and Kurdistan Region. – Journal of Petroleum Exploration and Production Technology, **9**: 1801–1818. doi: [10.1007/s13202-019-0661-6](https://doi.org/10.1007/s13202-019-0661-6)
- EL-SAYED, M.I. (2001): The nature and possible origin of dolomite in Ar Rub' Al Khali, the UAE. – Carbonates and Evaporites, **16**: 210–223. doi: [10.1007/BF03175837](https://doi.org/10.1007/BF03175837)
- ERNST, W. (1970): Geochemical Facies Analysis. Methods in Geochemistry and Geophysics. – 11 + 151 pp.; Amsterdam (Elsevier).
- ETTER, W. (1996): Pseudoplanktonic and benthic invertebrates in the Middle Jurassic Opalinum Clay, northern Switzerland. – Palaeogeography, Palaeoclimatology, Palaeoecology, **126**: 325–341. doi: [10.1016/S0031-0182\(96\)00036-3](https://doi.org/10.1016/S0031-0182(96)00036-3)
- FLÜGEL, E. (2004): Microfacies of Carbonate Rocks. Analysis, Interpretation and Application. – 976 pp.; Heidelberg & Berlin (Springer).
- FOLK, R.L. & LAND, L.S. (1975): Mg/Ca ratio and salinity: two controls over crystallization of dolomite. – AAPG Bulletin, **59**: 60–68.

- FRIEDMAN, G.M. (1959): Identification of carbonate minerals by staining methods. – *Journal of Sedimentary Research*, **29**: 87–97. doi: [10.1306/74D70894-2B21-11D7-8648000102C1865D](https://doi.org/10.1306/74D70894-2B21-11D7-8648000102C1865D)
- GREGG, J.M. & SHELTON, K.L. (1990): Dolomitization and dolomite neomorphism in the back reef facies of the Bonnetterre and Davis formations Cambrian, Southeastern Missouri. – *Journal of Sedimentary Petrology*, **60**: 549–562.
- GREGG, J.M. & SIBLEY, D.F. (1984): Epigenetic dolomitization and the origin of xenotopic dolomite texture. – *Journal of Sedimentary Research*, **54**: 908–931.
- GUO, Q., SHIELDS, G.A., LIU, C., STRAUSS, H., ZHU, M., PI, D., GOLDBERG, T. & YANG, X. (2007): Trace element chemostratigraphy of two Ediacaran-Cambrian successions in South China: implications for organosedimentary metal enrichment and silicification in the early Cambrian. – *Palaeogeography, Palaeoclimatology, Palaeoecology*, **254**: 194–216. doi: [10.1016/j.palaeo.2007.03.016](https://doi.org/10.1016/j.palaeo.2007.03.016)
- HALLAM, A. (1982): The Jurassic climate. – In: *Climate in Earth History: Studies in Geophysics*, 159–163; The National Academies Press. doi: [10.17226/11798](https://doi.org/10.17226/11798)
- HALLBERG, R.O. (1976): A geochemical method for investigation of palaeoredox conditions in sediments. – *Ambio Special Report*, **4**: 139–147.
- HAQ, B.U. (2018): Jurassic sea-level variations: A reappraisal. – *GSA Today*, **28**.
- HILL, K.C. & SHANE, S. (2009): Bayou Bend signs agreements for three highly prospective blocks in Kurdistan: Bayou Bend Petroleum Ltd. <https://www.shamara-nepetroleum.com/news/bayou-bend-signs-agreements-for-three-highly-prosp-122630/>
- JACH, R. (2007): *Bositra* limestones – a step towards radiolarites: case study from the Tatra Mountains. – *Annales Societatis Geologorum Poloniae*, **77**: 161–170.
- JAJU, M.M., NADER, F.H., ROURE, F. & MATENCO, L. (2016): Optimal aquifers and reservoirs for CCS and EOR in the Kingdom of Saudi Arabia: an overview. – *Arabian Journal of Geosciences*, **9**: 604 pp.
- JAMES, G.A. & WYND, J.G. (1965): Stratigraphic nomenclature of Iranian oil consortium agreement area. – *AAPG Bulletin*, **49**: 2182–2245.
- JASSIM, S.Z. & AL-GAILANI, M. (2006): Hydrocarbons, chapter 18. – In: JASSIM, S.Z. & GOFF, J.C. (eds.): *Geology of Iraq* (1st edition): 232–250; Brno (Prague and Moravian Museum).
- JASSIM, S.Z. & BUDAY, T. (2006a): Units of the Unstable Shelf and the Zagros Suture, chapter 6. – In: JASSIM, S.Z. & GOFF, J.C. (eds.): *Geology of Iraq* (1st edition): 71–83; Brno Republic (Prague & Moravian Museum).
- JASSIM, S.Z. & BUDAY, T. (2006b): Late Toarcian-Early Tithonian (Mid-Late Jurassic) Megasequence AP7, chapter 10. – In: JASSIM, S.Z. & GOFF, J.C. (eds.): *Geology of Iraq* (1st edition): 117–123; Brno (Prague & Moravian Museum).
- JASSIM, S.Z. & GOFF, J.C. (2006): *Geology of Iraq*. – 352 pp.; Dolin (Prague & Moravian Museum Brno).
- JARUN, Y. & XIAOQIAO, W. (1996): Jurassic ammonite morphotypes as water-depth indicator of Tethys-Himalaya Sea. – *Acta Palaeontologica Sinica*, **35**: 734–751.
- JONES, B. & MANNING, D.A.C. (1994): Comparison of geochemical indices used for the interpretation of palaeoredox conditions in ancient mudstones. – *Chemical Geology*, **111**: 111–129. doi: [10.1016/0009-2541\(94\)90085-X](https://doi.org/10.1016/0009-2541(94)90085-X)
- KEMLE-VON MÜCKE, S. & OBERHÄNSLI, H. (1999): The Distribution of Living Planktic Foraminifera in Relation to Southeast Atlantic Oceanography: 91–115; Heidelberg & Berlin (Springer). doi: [10.1007/978-3-642-58646-0_3](https://doi.org/10.1007/978-3-642-58646-0_3)
- KIMURA, H. & WATANABE, Y. (2001): Ocean anoxia at the Precambrian–Cambrian boundary. – *Geology*, **29**: 995–998. doi: [10.1130/0091-7613\(2001\)029<0995:OAAATPC>2.0.CO;2](https://doi.org/10.1130/0091-7613(2001)029<0995:OAAATPC>2.0.CO;2)
- KONERT, G., AFIFI, A.M., AL-HAJRI, S.A. & DROST, H.J. (2001): Paleozoic stratigraphy and hydrocarbon habitat of the Arabian Plate. – *GeoArabia*, **6**: 407–442.
- KORDI, M. (2019): Sedimentary basin analysis of the Neotethys and its hydrocarbon systems in the Southern Zagros fold-thrust belt and foreland basin. – *Earth-Science Reviews*, **191**: 1–11. doi: [10.1016/j.earscirev.2019.02.005](https://doi.org/10.1016/j.earscirev.2019.02.005)
- KREJCI-GRAF, K. (1966): *Geochemische Faziesdiagnostik*. – *Freiberger Forschungshefte*, **C 224**: 80 pp.
- KUPECZ, J.A. & LAND, L.S. (1991): Late-stage dolomitization of the Lower Ordovician Ellenburger Group, West Texas. – *Journal of Sedimentary Petrology*, **61**: 551–574.
- LE GARZIC, E., VERGÉS, J., SAPIN, F., SAURA, E., MERESSE, F. & RINGENBACH, J.C. (2019): Evolution of the NW Zagros Fold-and-Thrust Belt in Kurdistan Region of Iraq from balanced and restored crustal-scale sections and forward modelling. – *Journal of Structural Geology*, **124**: 51–69. doi: [10.1016/j.jsg.2019.04.006](https://doi.org/10.1016/j.jsg.2019.04.006)
- LIU, X., WEN, Z., WANG, Z., SONG, C. & HE, Z. (2018): Structural characteristics and main controlling factors on petroleum accumulation in Zagros Basin, Middle East. – *Journal of Natural Gas Geoscience*, **3**: 273–281. doi: [10.1016/j.jnggs.2018.11.004](https://doi.org/10.1016/j.jnggs.2018.11.004)
- MACHEL, H.G. (2004): Concepts and models of dolomitization: a critical reappraisal. The geometry and petrogenesis of dolomite hydrocarbon reservoirs. – Geological Society, London, Special Publications, **235**: 7–63. doi: [10.1144/GSL.SP.2004.235.01.02](https://doi.org/10.1144/GSL.SP.2004.235.01.02)
- MAPES, R.H. & NUETZEL, A. (2009): Late Palaeozoic mollusc reproduction: cephalopod egg-laying behavior and gastropod larval palaeobiology. – *Lethaia*, **42**: 341–356. doi: [10.1111/j.1502-3931.2008.00141.x](https://doi.org/10.1111/j.1502-3931.2008.00141.x)
- MCCORMACK, J., VIEHBERG, F., AKDEMIR, D., IMMENHAUSER, A. & KWIECIEN, O. (2019): Ostracods as ecological and isotopic indicators of lake water salinity changes: the Lake Van example. – *Biogeosciences*, **16**: 2095–2114. doi: [10.5194/bg-16-2095-2019](https://doi.org/10.5194/bg-16-2095-2019)
- McKENZIE, J.A., HSUE, K.J. & SCHNEIDER, J.F. (1980): Movement of subsurface waters under the sabkha, Abu Dhabi, UAE, and its relationship to evaporative dolomite genesis. – In: ZENGER, D.H. & ETHINGTON, R.L. (eds.): *Concepts and Models of Dolomitization*. – Society of Economic Paleontologist and Mineralogists, Special Publications, **28**: 11–30.
- McQUAID, C.D. (1996): Biology of the gastropod family Littorinidae. II. Role in the ecology of intertidal and shallow marine ecosystems. – *Oceanography and Marine Biology Annual Review*, **34**: 263–302.

- MEHMOOD, M., YASEEN, M., KHAN, E.U. & KHAN, M.J. (2018): Dolomite and dolomitization model – a short review. – *International Journal of Hydrology*, **2**: 549–553. doi: [10.15406/ijh.2018.02.00124](https://doi.org/10.15406/ijh.2018.02.00124)
- MERINO, E., CANALS, A. & FLETCHER, R.C. (2006): Genesis of self-organized zebra textures in burial dolomites: Displacive veins, induced stress, and dolomitization. – *Geologica Acta*, **4**: 383–393.
- MOHIALDEEN, I.M.J., HAKIMI, M.H. & AL-BEYATI, F.M. (2013): Geochemical and petrographic characterisation of Late Jurassic–Early Cretaceous Chia Gara Formation in Northern Iraq: palaeoenvironment and oil-generation potential. – *Marine and Petroleum Geology*, **43**: 166–177. doi: [10.1016/j.marpetgeo.2013.02.010](https://doi.org/10.1016/j.marpetgeo.2013.02.010)
- MOORE, G.T., SLOAN, L.C., HAYASHIDA, D.N. & UMRIGAR, N.P. (1992): Paleoclimate of the Kimmeridgian/Tithonian (Late Jurassic) world: II. Sensitivity tests comparing three different paleotopographic settings. – *Palaeogeography, Palaeoclimatology, Palaeoecology*, **95**: 229–252. doi: [10.1016/0031-0182\(92\)90143-S](https://doi.org/10.1016/0031-0182(92)90143-S)
- MURRIS, R.J. (1980): Middle East: Stratigraphic evolution and oil habitat. – *AAPG Bulletin*, **64**: 597–618.
- MUTTONI, G., GAETANI, M., KENT, D.V., SCIUNNACH, D., ANGIOLINI, L., BERRA, F., GARZANTI, E., MATTEI, M. & ZANCHI, A. (2009): Opening of the Neo-Tethys Ocean and the Pangea B to Pangea A transformation during the Permian. – *GeoArabia*, Gulf PetroLink, Bahrain, **14**: 17–48.
- NAGY, Z.S.R., GREGG, J.M., SHELTON, K.L., BECKER, S.P., SOMERVILLE, I.D. & JOHNSON, A.W. (2004): Early dolomitization and fluid migration through the Lower Carboniferous carbonate platform in the SE Irish Midlands: implications for reservoir attributes. The Geometry and Petrogenesis of Dolomite Hydrocarbon Reservoirs. – Geological Society, London, Special Publications, **235**: 367–392. doi: [10.1144/GSL.SP.2004.235.01.16](https://doi.org/10.1144/GSL.SP.2004.235.01.16)
- NOKHBATOLFOGHAEI, A., NEZAFATI, N., GHORBANI, M. & ETERMADI ABDOLABADI, B. (2019): Evidence for origin and alteration in the dolomites of salt diapirs, Laristan, Southern Iran. – *Carbonates and Evaporites*, **34**: 389–403. doi: [10.1007/s13146-017-0399-5](https://doi.org/10.1007/s13146-017-0399-5)
- NUMAN, N.M.S. (2000): Major cretaceous tectonic events in Iraq. – *Rafidain Journal of Science*, **11**: 32–52.
- OLANIPEKUN, B., AZMY, K. & BRAND, U. (2014): Dolomites of the Boat Harbour Formation in the Northern Peninsula, western Newfoundland, Canada: implications for dolomitization history and porosity control. – *AAPG Bulletin*, **98**: 765–791. doi: [10.1306/08281312141](https://doi.org/10.1306/08281312141)
- ORHAN, H., DELIKAN, A., DEMIR, A., KAPAN, S., OLGUN, K., ÖZMEN, A., SAYIN, Ü., EKICI, G., AYDIN, H. & NAZIK, A. (2019): Geochemical evidences of paleoenvironmental changes in Late Quaternary lacustrine sediments of the Konya Closed Basin (Konya, Turkey). – In: ZHANG, Z., KHELIFI, N., MEZGHANI, A. & HEGGY, E. (eds.): *Patterns and Mechanisms of Climate, Paleoclimate and Paleoenvironmental Changes from Low-Latitude Regions*: 73–76. doi: [10.1007/978-3-030-01599-2_17](https://doi.org/10.1007/978-3-030-01599-2_17)
- PATTERSON, J.H., RAMSDEN, A.R., DALE, L.S. & FARDY, J.J. (1986): Geochemistry and mineralogical residences of trace elements in oil shales from Julia Creek, Queensland, Australia. – *Chemical Geology*, **55**: 1–16. doi: [10.1016/0009-2541\(86\)90123-3](https://doi.org/10.1016/0009-2541(86)90123-3)
- PATTERSON, R.J. & KINSMAN, D.J.J. (1982): Formation of diagenetic dolomite in coastal sabkha along Arabian (Persian) Gulf. – *AAPG Bulletin*, **66**: 28–43.
- PERRIER, V., VANNIER, J. & SIVETER, D. (2008): The Silurian pelagic myodocope ostracod *Richteria migrans*. – *Transactions of the Royal Society of Edinburgh, Earth and Environmental Science*, **98**: 151–163.
- PRETO, N., BREDI, A., CORSO, J.D., SPOETL, C., ZORZI, F. & FRISIA, S. (2015): Primary dolomite in the Late Triassic Travenanzes Formation, Dolomites, Northern Italy: Facies control and possible bacterial influence. – *Sedimentology*, **62**: 697–716. doi: [10.1111/sed.12157](https://doi.org/10.1111/sed.12157)
- PRICE, G.D. (1999): The evidence and implications of polar ice during the Mesozoic. – *Earth-Science Reviews*, **48**: 183–210. doi: [10.1016/S0012-8252\(99\)00048-3](https://doi.org/10.1016/S0012-8252(99)00048-3)
- QING, H. & MOUNTJOY, E. (1994): Rare earth element geochemistry of dolomites in the Middle Devonian Presqu'île barrier, Western Canada Sedimentary Basin: implications for fluid-rock ratios during dolomitization. – *Journal of Sedimentary Petrology*, **41**: 787–804. doi: [10.1111/j.1365-3091.1994.tb01424.x](https://doi.org/10.1111/j.1365-3091.1994.tb01424.x)
- RAHIMI, A., ADABI, M.H., AGHANABATI, A., MAJIDI-FARD, M.R. & JAMALI, A.M. (2016): Dolomitization Mechanism Based on Petrography and Geochemistry in the Shotori Formation (Middle Triassic), Central Iran. – *Open Journal of Geology*, **6**: 1149–1168. doi: [10.4236/ojg.2016.69085](https://doi.org/10.4236/ojg.2016.69085)
- RAISWELL, R. & PLANT, J. (1980): The incorporation of trace elements into pyrite during diagenesis of black shales, Yorkshire, England. – *Economic Geology*, **75**: 684–699. doi: [10.2113/gsecongeo.75.5.684](https://doi.org/10.2113/gsecongeo.75.5.684)
- RAMEIL, N. (2008): Early diagenetic dolomitization and dedolomitization of Late Jurassic and earliest Cretaceous platform carbonates: A case study from the Jura Mountains (NW Switzerland, E France). – *Sedimentary Geology*, **212**: 70–85. doi: [10.1016/j.sedgeo.2008.10.004](https://doi.org/10.1016/j.sedgeo.2008.10.004)
- RAMOS-VÁZQUEZ, M.A., ARMSTRONG-ALTRIN, J.S., ROSALES-HOZ, L., MACHAIN-CASTILLO, M.L. & CARRANZA-EDWARD, A. (2017): Geochemistry of deep-sea sediments in two cores retrieved at the mouth of the Coatzacoalcos River delta, western Gulf of Mexico, Mexico. – *Arabian Journal of Geosciences*, **10**: 148. doi: [10.1007/s12517-017-2934-z](https://doi.org/10.1007/s12517-017-2934-z)
- READ, J.F., KERANS, C., WEBER, L.J., SARG, H.F. & WRIGHT, F.M. (1995): Milankovitch sea-level changes, cycles and reservoirs on carbonate platforms in greenhouse and ice-house worlds. – *SEPM Short Course*, **35**: 1–81. doi: [10.2110/scn.95.35](https://doi.org/10.2110/scn.95.35)
- REBOTIM, A., VOELKER, A.H.L., JONKERS, L., WANIEK, J.J., MEGGERS, H., SCHIEBEL, R., FRAILE, I., SCHULZ, M. & KUCERA, M. (2017): Factors controlling the depth habitat of planktonic foraminifera in the subtropical eastern North Atlantic. – *Biogeosciences*, **14**: 827–859. doi: [10.5194/bg-14-827-2017](https://doi.org/10.5194/bg-14-827-2017)
- REHMAN, S.U., MAHMOOD, K., AHSAN, N. & SHAH, M.M. (2016): Microfacies and depositional environments of upper cretaceous Kawagarh Formation from Chinali and Thoba sections Northeastern Hazara Basin, lesser Hima-

- layas, Pakistan. – *Journal of Himalayan Earth Sciences*, **49**: 1–16.
- RIMMER, S.M. (2004): Geochemical paleoredox indicators in Devonian-Mississippian black shales, Central Appalachian Basin (USA). – *Chemical Geology*, **206**: 373–391. doi: [10.1016/j.chemgeo.2003.12.029](https://doi.org/10.1016/j.chemgeo.2003.12.029)
- SADOONI, F.N. & ALSHARHAN, A.S. (2004): Stratigraphy, lithofacies distribution, and petroleum potential of the Triassic strata of the northern Arabian plate. – *AAPG Bulletin*, **88**: 515–538. doi: [10.1306/12030303067](https://doi.org/10.1306/12030303067)
- SALAE, A.T.S. (2001): Stratigraphy and sedimentology of the Upper Jurassic succession northeastern Iraq. – Master's thesis, University of Baghdad: 95 pp. (in Arabic).
- SAMANKASSOU, E., TRESCH, J. & STRASSER, A. (2005): Origin of peloids in Early Cretaceous deposits, Dorset, South England. – *Facies*, **51**: 264–274. doi: [10.1007/s10347-005-0002-8](https://doi.org/10.1007/s10347-005-0002-8)
- SAVRDA, C.E. & BOTTIER, D.J. (1991): Oxygen-related biofacies in marine strata: an overview and update. – In: TYSON, R.V. & PEARSON, T.H. (eds.): *Modern and Ancient Continental Shelf Anoxia*. – Geological Society, London, Special Publications, **58**: 201–219. doi: [10.1144/GSL.SP.1991.058.01.14](https://doi.org/10.1144/GSL.SP.1991.058.01.14)
- SHAREZWRI, A.O.H. (2015): Stratigraphy, microfacies analysis and depositional environment of the Upper Jurassic Naoketlekan Formation from selected sections in Kurdistan region, NE Iraq. – BSc thesis, Soran University.
- SHARLAND, P.R., ARCHER, R., CASEY, D.M., DAVIES, R.B., HALL, S.H., HEWARD, A.P., HORBURY, A.D. & SIMMONS, M.D. (2001): Arabian Plate Sequence Stratigraphy. – *GeoArabia*, Special Publication, **2**: 371 pp.
- SIBLEY, D.F. & GREGG, J.M. (1987): Classification of dolomite rock texture. – *Journal of Sedimentary Petrology*, **57**: 967–975.
- SLATT, R.M., MCCULLOUGH, B.J., MOLINARES-BLANCO, C.E. & BARUCH, E.T. (2015): Paleotopographic and Depositional Environment Control on 'Sweet Spot' Locations in Some Unconventional Resource Shales. – International Conference and Exhibition, Melbourne, Australia, 13–16. doi: [10.1190/ice2015-2197869](https://doi.org/10.1190/ice2015-2197869)
- SORKHABI, R. (2010): Why so much oil in the Middle East? – *GeoExpro*, **7**: 20–26.
- SPÖTL, C. & PITMAN, J.K. (1998): Saddle dolomite in carbonates and sandstones: a reappraisal of a burial-diagenetic concept. – In: MORAD, S. (ed.): *Carbonate Cementation in Sandstones*. – International Association of Sedimentologists, Special Publication, **26**: 437–460. doi: [10.1002/9781444304893.ch19](https://doi.org/10.1002/9781444304893.ch19)
- STAMPFLI, G.M. & BOREL, G.D. (2002): A plate tectonic model for the Paleozoic and Mesozoic constrained by dynamic plate boundaries and restored synthetic oceanic isochrons. – *Earth and Planetary Science Letters*, **196**: 17–33. doi: [10.1016/S0012-821X\(01\)00588-X](https://doi.org/10.1016/S0012-821X(01)00588-X)
- TALBOT, C.J. & ALAVI, M. (1996): The past of a future syntaxis across the Zagros. – In: ALSOP, G.I., BLUNDELL, D.J. & DAVISON, I. (eds.): *Salt Tectonics*. – Geological Society, London, Special Publication, **100**: 89–109.
- TOBIA, F.H., AL-JALEEL, H.S. & AHMAD, I.N. (2019): Provenance and depositional environment of the Middle-Late Jurassic shales, northern Iraq. – *Geosciences Journal*, **23**: 747–765. doi: [10.1007/s12303-018-0072-6](https://doi.org/10.1007/s12303-018-0072-6)
- TREMOLADA, F., BORNEMANN, A., BRALOWER, T.J., KOEBERL, C. & VAN DE SCHOOTBRUGGE, B. (2006): Paleooceanographic changes across the Jurassic/Cretaceous boundary – the calcareous phytoplankton response. – *Earth and Planetary Science Letters*, **241**: 361–371. doi: [10.1016/j.epsl.2005.11.047](https://doi.org/10.1016/j.epsl.2005.11.047)
- VAN BELLEN, R.C.V., DUNNINGTON, H.V., WETZEL, R. & MORTON, D.M. (1959): *Lexique stratigraphique international*. Paris, III, Asie, Fascicule 10a Iraq, 333.
- VERMA, R. & KUMAR, S. (2018): Uranium mineralization in Mizoram: inferences from geochemistry. – *International Journal of Research in Applied Science, Engineering and Technology*, **6**: 617–628. doi: [10.22214/ijraset.2018.4107](https://doi.org/10.22214/ijraset.2018.4107)
- VINCENT, B., RAMBEAU, C., EMMANUEL, L. & LOREAUE, J.P. (2006): Sedimentology and trace element geochemistry of shallow-marine carbonates: an approach to paleoenvironmental analysis along the Pagny-sur-Meuse section (Upper Jurassic, France). – *Facies*, **52**: 69–84. doi: [10.1007/s10347-005-0026-0](https://doi.org/10.1007/s10347-005-0026-0)
- WANG, X., ZHAO, W., ZHANG, SH., WANG, H., SU, J., CANFIELD, D.E. & HAMMARLUND, E.U. (2018): The aerobic diagenesis of Mesoproterozoic organic matter. – *Scientific Reports*, **8**: 13324. doi: [10.1038/s41598-018-31378-6](https://doi.org/10.1038/s41598-018-31378-6). PMID: 30190572
- WARREN, J. (2000): Dolomite: occurrence, evolution and economically important Associations. – *Earth-Science Reviews*, **52**: 1–81. doi: [10.1016/S0012-8252\(00\)00022-2](https://doi.org/10.1016/S0012-8252(00)00022-2)
- WETZEL, R. (1948): Sargelu Formation. – In: VAN BELLEN, R.C., DUNNINGTON, H.V., WETZEL, R. & MORTON, D.M. (eds.): *Lexique stratigraphique international*, Paris, III, Asie, Fascicule 10a Iraq: 250–253.
- WETZEL, R. & MORTON, D.M. (1950): Sargelu Formation. – In: VAN BELLEN, R.C., DUNNINGTON, H.V., WETZEL, R. & MORTON, D.M. (eds.): *Lexique stratigraphique international*, Paris, III, Asie, Fascicule 10a Iraq: 211–215.
- WIGNALL, P.B. (1994): *Black Shales*. – 127 pp.; Oxford (Clarendon Press).
- YANG, J.H., JIANG, S.Y., LING, H.F., FENG, H.Z., CHEN, Y.Q. & CHEN, J.H. (2004): Paleooceanographic significance of redox-sensitive metals of black shales in the basal Lower Cambrian Niutitang Formation in Guizhou Province, South China. – *Progress in Natural Science*, **14**: 152–157. doi: [10.1080/10020070412331343291](https://doi.org/10.1080/10020070412331343291)
- YARINCIK, K.M., MURRAY, R.W., LYONS, T.W., PETERSON, L.C. & HAUG, G.H. (2000): Oxygenation history of bottom waters in the Cariaco Basin, Venezuela, over the past 578,000 years: results from redox-sensitive metals (Mo, V, Mn, and Fe). – *Paleoceanography*, **15**: 593–604. doi: [10.1029/1999PA000401](https://doi.org/10.1029/1999PA000401)
- ZADEH, P.G., ADABI, M.H. & SADEGHI, A. (2019): Microfacies, geochemistry and sequence stratigraphy of the Sarvak Formation (Mid Cretaceous) in the Kuh-e Siah and Kuh-e Mond, Fars area, southern Iran. – *Journal of African Earth Sciences*, **160**: 1–19.
- ZAINY, M.T., AL-ANSARI, N., BAUER, T.E. & ASK, M. (2017): The tectonic and structural classifications of the Western part of the Zagros Fold and Thrust Belt, North Iraq, review and discussion. – *Journal of Earth Sciences and Geotechnical Engineering*, **7**: 71–89.

Manuscript received: May 6th, 2020.

Revised version accepted by the Bonn editor: May 15th, 2020.

Addresses of the authors:

NAGHAM OMAR, TOM McCANN, SVEN OLIVER FRANZ,
Institut für Geowissenschaften, Geologie, University
of Bonn, Nussallee 8, 53115 Bonn, Germany;
e-mail: s6naomar@uni-bonn.de

ALI I. AL-JUBOURY, Geology Department, College of
Sciences, University of Mosul, Mosul, Iraq

Table 1. Distribution of clay and non-clay minerals (in wt%) in the shales of the Middle–Late Jurassic-age Sargelu and Naokelekan formations.

Sample No.	Quartz (%)	K-feldspar (%)	Calcite (%)	Dolomite/Ankerite (%)	Illite/Muscovite (%)	Kaolinite (%)	Gypsum (%)	Pyrite (%)	Goethite (%)
S 16	–	8.32	–	11.10	64.77	12.61	–	–	3.20
S 19	–	11.28	–	60.95	25.56	–	–	–	2.21
S 21	2.15	5.94	1.31	90.60	–	–	–	–	–
S 22	57.10	21.25	1.85	0.70	14.96	–	–	–	4.14
S 23	17.63	15.03	4.20	63.14	–	–	–	–	–
S 25	8.34	5.09	72.91	13.66	–	–	–	–	–
S 26	45.26	2.60	48.65	3.49	–	–	–	–	–
S 27	13.19	17.38	38.11	31.32	–	–	–	–	–
N 1	2.68	15.35	45.37	36.60	–	–	–	–	–
N 2	2.70	6.05	87.94	2.00	–	–	1.31	–	–
N 3	3.61	6.88	85.73	1.84	–	–	0.78	1.16	–
N 4	21.40	51.30	–	–	27.30	–	–	–	–

Table 2. Major (in wt%) element concentrations for the shales of the Middle–Late Jurassic-age Sargelu and Naokelekan formations.

Component (%)	Sargelu								Naokelekan			
	16	19	21	22	23	25	26	27	1	2	3	4
SiO ₂	38.81	23.21	8.82	36.97	23.05	7.94	22.76	16.59	8.91	3.15	3.99	8.67
TiO ₂	1.22	0.69	0.32	0.57	0.43	0.21	0.06	0.47	0.36	0.14	0.19	0.31
Al ₂ O ₃	18.89	9.63	2.99	5.90	4.11	1.41	0.91	3.58	2.63	0.83	1.10	2.45
Fe ₂ O ₃	9.96	6.24	3.69	6.36	5.06	2.21	1.18	5.23	4.74	1.46	1.42	3.03
MnO	0.01	0.02	0.01	<DL	0.01	0.01	<DL	<DL	<DL	<DL	<DL	<DL
MgO	2.42	5.50	8.88	0.74	5.50	1.08	0.86	2.10	2.59	0.22	0.19	0.33
CaO	5.48	17.50	29.63	2.25	19.75	42.26	44.75	25.53	30.15	35.19	35.28	3.39
Na ₂ O	0.07	0.03	0.01	0.09	0.06	0.04	0.04	0.10	0.09	0.06	0.07	0.04
K ₂ O	5.87	4.25	1.36	3.33	2.08	0.67	0.37	1.57	1.16	0.41	0.56	1.81
P ₂ O ₅	0.95	0.40	0.24	0.35	0.37	0.06	0.07	0.24	0.38	0.19	0.14	0.41
SO ₃	0.57	1.00	1.92	7.14	2.55	2.16	1.59	4.03	4.93	6.28	6.46	10.26
Sum	84.26	68.48	57.89	63.70	63.00	58.04	72.59	59.45	55.94	47.94	49.41	30.71
L.O.I.	14.77	30.85	41.65	35.47	36.25	41.53	27.13	40.12	43.52	51.40	49.60	68.09
Total	99.03	99.33	99.54	99.17	99.25	99.57	99.72	99.57	99.46	99.34	99.01	98.80

Table 3. Trace (in ppm) element concentrations with palaeoredox proxies: Mo, U, V/Cr, Ni/Co, (Cu+Mo)/Zn, V/Sc for the shales of the Middle–Late Jurassic-age Sargelu and Naokelekan formations.

Element (ppm)	Sargelu								Naokelekan			
	16	19	21	22	23	25	26	27	1	2	3	4
Sc	15	7	<DL	11	3	<DL	<DL	<DL	<DL	<DL	<DL	7
V	375	265	316	827	519	322	130	383	564	675	1082	2823
Cr	195	132	59	117	83	28	18	55	62	56	72	303
Mn	95	97	61	52	70	45	21	60	58	23	26	20
Co	34	28	13	19	36	7	22	15	11	3	5	4
Ni	349	305	218	617	448	222	125	313	273	332	590	597
Cu	287	217	90	115	134	29	15	60	55	35	35	87
Zn	524	311	198	418	181	380	152	74	157	518	1165	524
Ga	43	17	4	9	4	2	<DL	3	2	4	3	6
As	66.2	70	47	62	68.1	25.1	13.8	41.3	36.3	25.7	27.2	77
Rb	93	58	21	53	35	16	6	38	27	11	16	37
Sr	117	72	81	52	98	121	150	124	140	289	298	94
Y	47	18	16	33	29	28	11	36	42	26	29	85
Zr	277	144	37	72	54	17	8	44	27	15	19	55
Nb	23	11	4	7	5	2	<DL	4	4	2	3	6
Cs	8	8	5	<DL	7	2	5	7	9	5	8	4
Ba	1000	121	104	141	113	32	22	82	124	230	158	366
La	91	38	9	32	16	14	6	20	33	10	16	43
Ce	84	27	23	16	26	15	13	19	12	18	1	20
Nd	42	17	10	16	16	10	5	12	14	10	12	27
Sm	6	6	<DL	5	2	2	4	7	2	3	<DL	7
Hf	3	2	<DL	<DL	<DL	<DL	<DL	<DL	<DL	<DL	<DL	<DL
W	27	23	25	32	43	17	144	25	29	9	10	15
Pb	119	24	16	20	18	15	14	19	15	14	14	22
Th	10	4	<DL	<DL	<DL	<DL	<DL	2	<DL	<DL	<DL	<DL
Mo	94	170	275	526	662	307	111	177	116	356	299	311
U	54.6	36.8	26.4	41.4	33.8	29.3	13.5	30.9	43.6	33.8	51.6	68.3
V/Cr	1.92	2.01	5.39	7.07	6.23	11.60	7.43	7.02	9.13	11.98	14.99	9.33
Ni/Co	10.22	11.02	16.52	32.97	12.37	33.09	5.71	21.15	24.19	100.61	120.33	145.71
(Cu+Mo)/Zn	0.73	1.24	1.84	1.53	4.39	0.88	0.83	3.23	1.09	0.75	0.29	0.76
V/Sc	25	37.86	316	75.18	173	322	130	383	564	675	1082	403.29

Table 4. Evaporation proxies: Al, Ca (in wt%), Sr (in ppm) for the shales of the Middle–Late Jurassic-age Sargelu and Naokelekan formations.

Sample No.	Al	Ca	Sr
S 16	9.99	3.92	117
S 19	5.09	12.51	72
S 21	2.17	14.12	98
S 22	1.58	21.18	81
S 23	0.75	30.20	121
S 25	3.12	1.61	52
S 26	0.48	31.98	150
S 27	1.89	18.25	124
N 1	1.39	21.55	140
N 2	0.44	25.15	289
N 3	0.58	25.21	298
N 4	1.30	2.42	94

Appendix D



Solid bitumen in shales from the Middle to Upper Jurassic Sargelu and Naokelekan Formations of northernmost Iraq: implication for reservoir characterization

Nagham Omar¹ · Tom McCann¹ · Ali I. Al-Juboury² · Isabel Suárez-Ruiz³

Received: 25 December 2020 / Accepted: 29 March 2021
© The Author(s) 2021

Abstract

Petrographic, organic, and inorganic geochemical analysis of the solid bitumen and host shales from the Middle and Late Jurassic-age Sargelu and Naokelekan Formations of the Banik section, northernmost Iraq, was undertaken. The aim was to understand their derivation and preservation, as well as examine the carbon and oxygen isotopes, and paleoredox proxies under which the solid bitumen and host sediments were deposited. Petrographic analysis of both formations revealed the presence of solid bitumen high reflectance (first phase) and solid bitumen low reflectance (second phase). The equivalent vitrinite reflectance indicates that the solid bitumen of the two formations probably accumulated within the shale reservoirs following oil migration from source rocks located within the same formations. Mineralogical study (XRD and SEM - EDX) revealed that the shales hosting the solid bitumen also contain clay minerals (illite, rectorite, chlorite, montmorillonite, and kaolinite) as well as carbonate minerals, quartz, alkali feldspar, and pyrite. Carbon and oxygen isotope data along with paleoredox indicators suggest that both the solid bitumen sources and host shales in both formations formed within a shallow-marine setting, most probably under anoxic conditions where water circulation was restricted.

Keywords Solid bitumen · Stable isotopes · Paleoredox · Migration · Shale · Jurassic · Iraq

Introduction

Iraq is the sixth largest oil reserve in the world (Al-Zubaidi and Al-Zebari 1998; Jassim and Al-Gailani 2006), with current proven reserves of 115 billion barrels of oil (BBO) and 110 trillion cubic feet (TCF) of gas. This hydrocarbon reserve presents in three petroleum systems, namely Palaeozoic, Jurassic, and Cretaceous-Tertiary (Fig. 1) (Ahlbrandt et al. 2000; Verma et al. 2004). Most of the petroleum that has been

discovered in Iraq is reported to have been sourced from the Jurassic-age rocks and trapped in the Cretaceous- and Tertiary-age reservoirs of the Mesopotamian Basin and the Zagros Basin/Zagros Fold Belt (Pitman et al. 2004) (Fig. 1).

The study area is situated within the Kurdistan Region of Iraq which is estimated to contain about 39% of Iraq's total barrels of oil reserves. Recent studies have indicated that most of the discovered oil in the Kurdistan Region of Iraq was sourced from the Sargelu (Middle Jurassic), Naokelekan (Upper Jurassic), and Chia Gara (Late Jurassic-Early Cretaceous) Formations (Al-Ameri and Zumberge 2012; Mohialdeen et al. 2013; Tobia et al. 2019).

Because of the geological and economic importance of the Jurassic successions in Iraq, they have been described in numerous studies, the majority of which have focused on the lithology and depositional environments of the successions and their economic significance (e.g., Daoud and Karim 2010; Al-Ameri and Zumberge 2012; Al-Juboury and McCann 2013; Jasim 2013; Abdula 2017).

The Middle Jurassic-age Sargelu Formation was first described by Wetzel (1948) from the Surdash Anticline in the High Folded Zone, NE of Iraq (Bellen et al. 1959; Jassim and

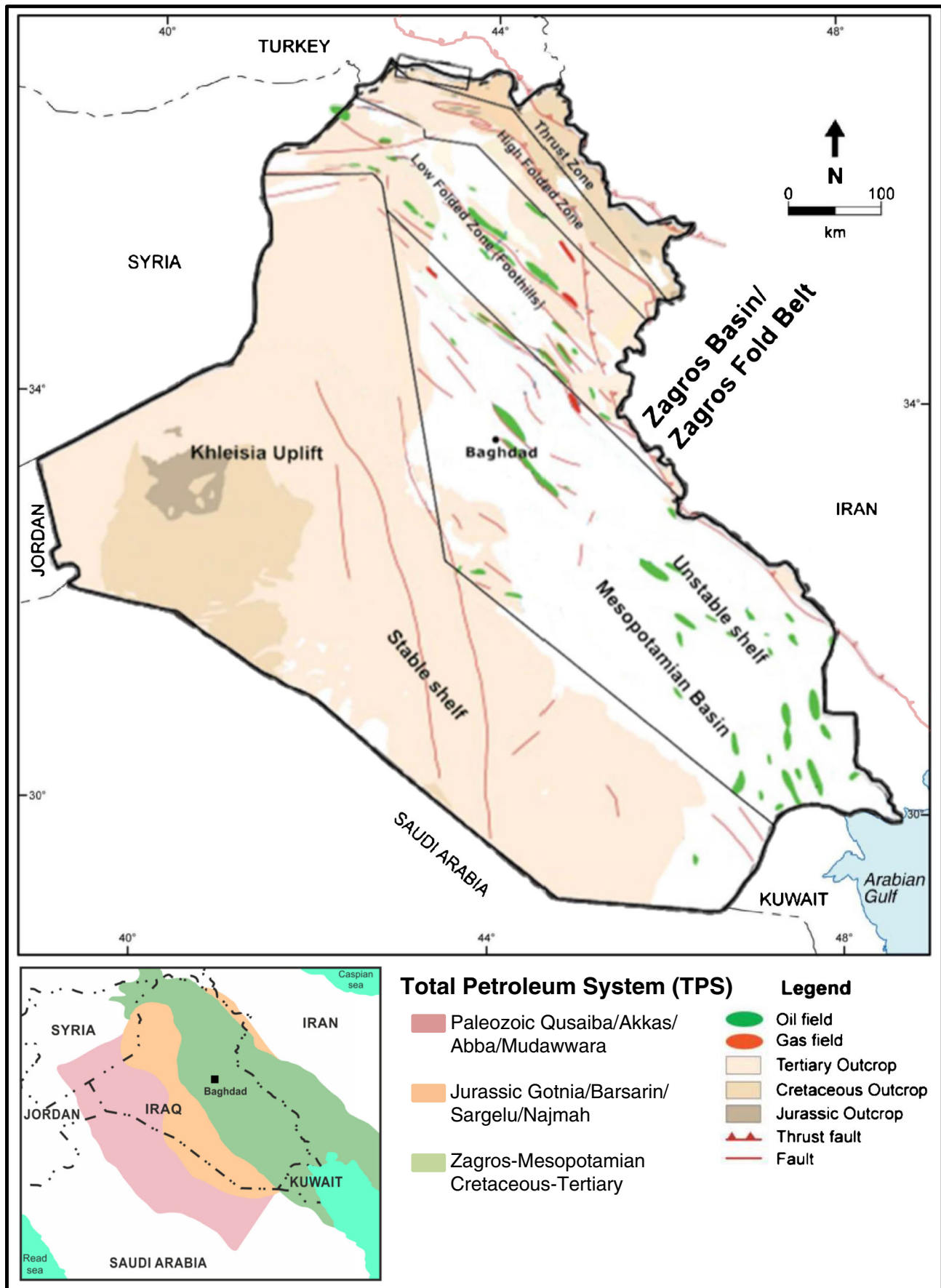
Responsible Editor: Domenico M. Doronzo

✉ Nagham Omar
s6naomar@uni-bonn.de

¹ Institut für Geowissenschaften - Geologie, University of Bonn, Nussallee 8, 53115 Bonn, Germany

² Geology Department, College of Sciences, University of Mosul, Mosul, Iraq

³ Instituto de Ciencia y Tecnología del Carbono (INCAR-CSIC), Oviedo, Spain



◀ **Fig. 1** Map showing major oil and gas fields in the regions of Mesopotamian Basin and Zagros Basin/Zagros Fold Belt (after Aqrabi 1998). Inset map depicts three total petroleum systems (TPS) that have contributed to the petroleum accumulations in Iraq (Ahlbrandt et al. 2000)

Goff 2006). Subsequently, the formation was correlated with successions in Iran (James and Wynd 1965), Turkey, and Syria (Altinli 1966; Dubertret 1966). On the contrary, the Late Jurassic-age Naokelekan Formation was first described by Wetzel and Morton (1950) from the Balambo-Tanjero Zone near Rowanduz.

The redox-sensitive trace metals have been used widely as geochemical proxies to determine the redox status of marine sediments at the time of their deposition as well as their provenance (Ramos-Vázquez and Armstrong-Altrin 2019; Bennett and Canfield 2020), and thus provide direct information on the depositional environment. Similarly, the carbon isotope geochemistry is used as a good indicator of the depositional setting waters (Bowman and Bralower 2005; Jarvis et al. 2006). On the other hand, the oxygen isotope geochemistry is considered to be an important indicator of the dominated climate conditions during the period of deposition (Bartolini et al. 2003; Ruf et al. 2005; Weissert and Erba 2004).

Future work on the organic geochemistry of the Sargelu and Naokelekan Formations has been published (Al-Ahmed 2006; Aqrabi and Badics 2015; El Diasty et al. 2018; Abdula et al. 2020). However, detailed studies of the solid bitumen from these two Jurassic-age formations were not, to date, attempted. Bellen et al. (1959) studied the presence of solid bitumens in the Naokelekan Formation, but misinterpreted them as coal horizons. To fulfill this gap, in this study, we examined the detailed petrographic, organic, and inorganic geochemistry of the solid bitumen as well as the host shales of the Sargelu and Naokelekan Formations from the Banik section in northernmost Iraq, including the carbon and oxygen isotopes and paleoredox proxies. Therefore, the objectives of this study are to (1) suggest possible depositional environment of the solid bitumen and host sediments provided by the carbon and oxygen isotopes, and paleoredox proxies, and (2) reconstruct the accumulation process for the solid bitumen present within the formations and decipher its origin by integrating the geochemical data with the equivalent vitrinite reflectance.

Geological setting

The study area is situated within the region of northernmost Iraqi Kurdistan within the Zagros Basin/Zagros Fold Belt on the northeastern boundary of the Arabian Plate (Abdula 2017; Liu et al. 2018). The Zagros Basin is one of the most hydrocarbon-rich basins in the world (Sarfi et al. 2015) with these being mainly sourced from Jurassic marine carbonates (Al-Ahmed

2006). Middle to Upper Jurassic Sargelu and Naokelekan Formations in Iraq are organic rich and comprise intercalated shallow-marine carbonates and highly porous and permeable shales/sandstones forming the main reservoir unit (Murriss 1980; Beydoun 1991; Sharland et al. 2001). The two formations are subsequently overlain by a seal of evaporites forming a closed petroleum system. The lateral extent of these formations, and related units, from Iraq to Saudi Arabia and the Gulf States is the reason for the hydrocarbon-rich productivity across the region (Murriss 1980; Beydoun 1991; Sharland et al. 2001).

The Banik section is located near the boundary between the High Folded Zone and the Thrust Zone (i.e., the Northern (Ora) Thrust Subzone) (Fig. 2a). The Sargelu and Naokelekan Formations crop out in Northern Iraq within the eroded cores and limbs of anticlines in structural zones of the Zagros Basin/Zagros Fold Belt area (Numan 2000). These zones include, from SW to NE, the Low Folded Zone (or Foothills), the High Folded Zone, and the Imbricated Zone (Fig. 2a) (Jassim and Goff 2006). According to Zainy et al. (2017), the Imbricated Zone can be further subdivided into two zones, namely the Balambo-Tanjero Subzone and the Northern (Ora) Thrust Subzone. This latter subzone is approximately 15 km wide and trends E-W in the border area of Northern Iraq and Turkey (Balaky et al. 2016; Edilbi et al. 2017; Zainy et al. 2017).

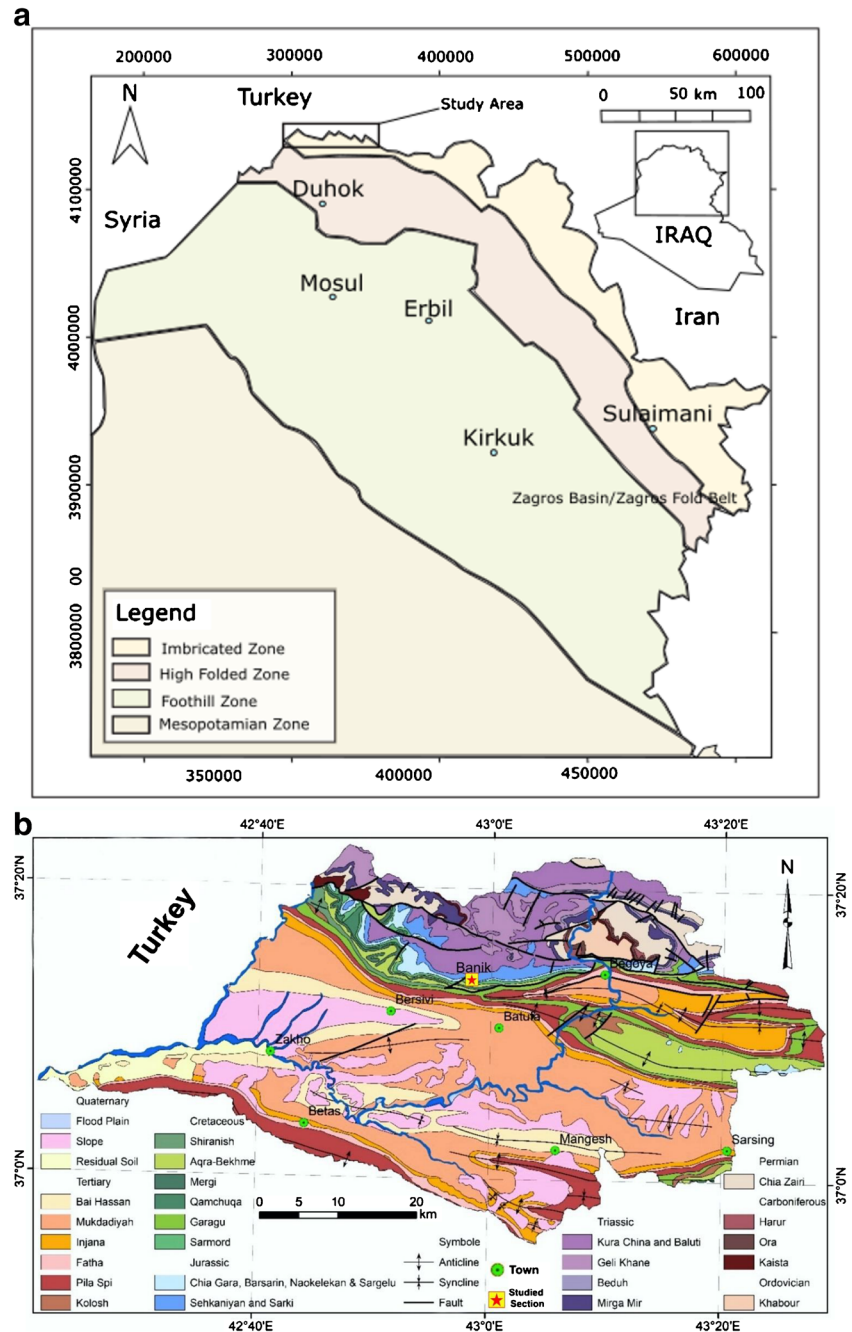
The thickness of the Sargelu Formation varies from 74 to 447 m (Jassim and Buday 2006). In its type section, the Sargelu Formation is about 115 m thick, and consists of bituminous dolomitic limestones and black shales with thin chert towards the tops (Wetzel 1948; Jassim and Buday 2006). In the subsurface, higher proportions of shale as well as rare fine-grained sandstones have also been noted (Jassim and Buday 2006).

The age of the Sargelu Formation has been determined based on the presence of the pelecypods (e.g., *Bositra buchii*), and is considered to be Bajocian-Bathonian (Bellen et al. 1959; Jassim and Goff 2006). In addition to the presence of the pelecypods in the Sargelu Formation, gastropods, radiolaria, ostracods, calcispheres, and algal filaments (e.g., Abdula et al. 2015) have been recorded within the same formation in some areas of Northern Iraq.

Al-Ameri et al. (2012) suggested a Bajocian-Bathonian, and possibly Lower Callovian, age based on palynomorph index. Thus, while a Middle Jurassic age for the Sargelu Formation has been confirmed, there is still a lack of precision with regard to the age boundaries. The contact between the Sargelu Formation and the underlying Sehkanian Formation in the type area is usually conformable and gradational (Bellen et al. 1959; Jassim and Goff 2006).

In the subsurface, the boundary is defined by the final occurrence of anhydrite (Jassim and Buday 2006). The contact with the overlying Naokelekan Formation appears to be conformable and gradational (Bellen et al. 1959; Jassim and Goff 2006). The Sargelu Formation was deposited in a basinal euxinic marine environment (Bellen et al. 1959; Jassim and Goff 2006).

Fig. 2 (a) Geological map of Northern Iraq showing the study area and the structural zones of the Zagros Basin/Zagros Fold Belt (after Awdal et al. 2016). (b) Geological map of northernmost Iraq including Banik section and the two formations (Sargelu and Naokelekan) (after Al-Mousawi et al. 2008)



The type section of the overlying Naokelekan Formation comprises 20 m and can be subdivided into three units (Wetzel and Morton 1950). From base to top, these are as follows: (a) thinly bedded, bituminous limestones with intercalated bituminous black shales and limestones, (b) thinly bedded, fossiliferous dolomitic limestones, and (c) thinly bedded, highly bituminous dolomites and limestones interbedded with black shales in the lower part (Jassim and Buday 2006). An Early Callovian-Kimmeridgian age was proposed for the Naokelekan Formation based on the recorded fauna, including belemnites, stromatoporoids, foraminifera, and algae (Jassim and Buday 2006).

The lower and upper contacts of the formation with the Sargelu and Barsarin Formations, respectively, appear to be conformable (Bellen et al. 1959; Jassim and Goff 2006). However, the recognition of the lower contact in northernmost Iraq is difficult although it is generally assumed to be gradational (Buday 1980). The lack of chert and the presence of abundant *Posidonia* and other ammonites distinguish the Sargelu Formation from the Naokelekan Formation (Wetzel 1948). Additionally, the latter contains solid bitumen (Wetzel 1948), although solid bitumen was also recorded from the Sargelu Formation as part of this study. The sediments of the Naokelekan Formation were deposited in an euxinic

environment, in a subsiding, or possibly starved, basin (Bellen et al. 1959; Jassim and Goff 2006).

The current study focused on the solid bitumen present within the host shale successions of the Sargelu and Naokelekan Formations of the Banik section (Fig. 2b). This section crops out in a region where access is now forbidden. Thus, due to recent political upheavals, this work will remain unique for the foreseeable future. The sedimentary succession from the Banik section comprises interbedded shales and carbonates (dolomites, limestones) and is considered to be of great importance given its singularity in northernmost Iraq, as well as the fact that it is the only location from which solid bitumen from the Sargelu Formation has been recorded. As noted above, the studied shale beds hosting the bitumen, particularly those from the Naokelekan Formation in the Banik area, were originally misinterpreted by Bellen et al. (1959) who described them as a 4-m-thick coal horizon, while those from the Sargelu Formation, i.e., the shale beds hosting bitumen, were recorded for the first time as part of this study. A detailed sedimentary log is shown in Fig. 3.

Materials and methods

A total of eight shale samples hosting bitumen (four from the Sargelu Formation and four from the Naokelekan Formation) were collected from the Banik section. The samples were collected for detailed petrographic, mineralogy, organic, and inorganic (trace and carbon and oxygen stable isotopic geochemistry) analyses.

Petrographic investigation of the solid bitumen was conducted using optical microscopy at the Instituto de Ciencia y Tecnología del Carbono (INCAR-CSIC) Oviedo, Spain. Organic petrography characterization was carried out on all the samples using reflected white light and blue light excitation (fluorescence mode). These analyses were mainly focused on the identification of the organic populations present in the samples, their characterization, and the reflectance measurement in the case of solid bitumen. The optical microscopy measurements were performed on particulate pellets (whole rock) with randomly orientated particles using a MPV-Combi (Leitz) microscope, reflected light, and $\times 50$ oil immersion objectives following the ASTM D 2798-09 (2010) and ISO 7404/5 (2009) norms. The pellets were prepared following a modified procedure of the ISO 7404/02 (2009) standard that does not employ a press and temperature. Fluorescence, white light observations, and optical photomicrographs were taken on a DM 4500P Leica microscope using a DFC 420C Leica camera with the corresponding software to capture and analyze the images.

The solid bitumen and host shale samples from both the Sargelu and Naokelekan Formations were examined using Cambridge S 200 Stereoscan (Cambridge, UK) and a LEO

1450 (Cambridge, UK) scanning electron microscopes, which were used for imaging, and energy dispersive X-ray (EDX) analyses. These were equipped with secondary electron (SE) and backscattered electron (BSE) detectors and an EDX analysis system (Oxford Instruments, Oxford, UK) using the Link ISIS Software at the Nees Institute Laboratory, Bonn University.

The mineralogical constituents of the host shales were determined using the XRD. Sampling material for XRD measurements was analyzed as powder preparation in a D8 Advance from the company Bruker AXS GmbH and the acquired data was analyzed using the software MacDiff 4.2.6 and Rietveld method.

The total organic carbon (TOC) measurement of the solid bitumen and host shale samples was conducted using a Vario EL cube from the company Elementar Analysensysteme GmbH.

Furthermore, stable isotopic data for carbon and oxygen were conducted at the Ruhr-Universität Bochum, with a mass spectrometer MAT253 (Thermo Fisher Scientific) equipped with a ConFlo IV and a GasBench II (both Thermo Fisher Scientific), while the inorganic trace elements of the same samples were analyzed (XRF) in the Institut für Geowissenschaften-Geologie, Bonn University. Measurements were performed with an AXIOS from the company PANalytical GmbH.

Results

Organic petrography

Petrographic analysis of the samples collected from the shale beds hosting the bitumen from the Sargelu and Naokelekan Formations revealed that the host shale is rich in solid bitumen which is interbedded with mineral matter (Fig. 4a, b). Two bitumen phases were recognized: solid bitumen with high reflectance and solid bitumen with low reflectance (Table 1). The bitumen with high reflectance can be classified as Grahamite, while the bitumen with low reflectance would correspond to a Glance Pitch (Jacob 1989). In general, the solid bitumen with high reflectance is dominant as seen by the number of nitrogen measurements (48–180) with the exception for samples 3 and 4 from the Sargelu Formation which have values of c. 25 and 32 (Table 1). The solid bitumen samples were also analyzed under a microscope for their fluorescence, as well as using UV excitation. There was no evidence of any fluorescence.

Mineralogy

The mineralogy of the solid bitumen and host shales from the Sargelu and Naokelekan Formations was carried out by means of X-ray diffraction (XRD) and SEM - EDX analysis.

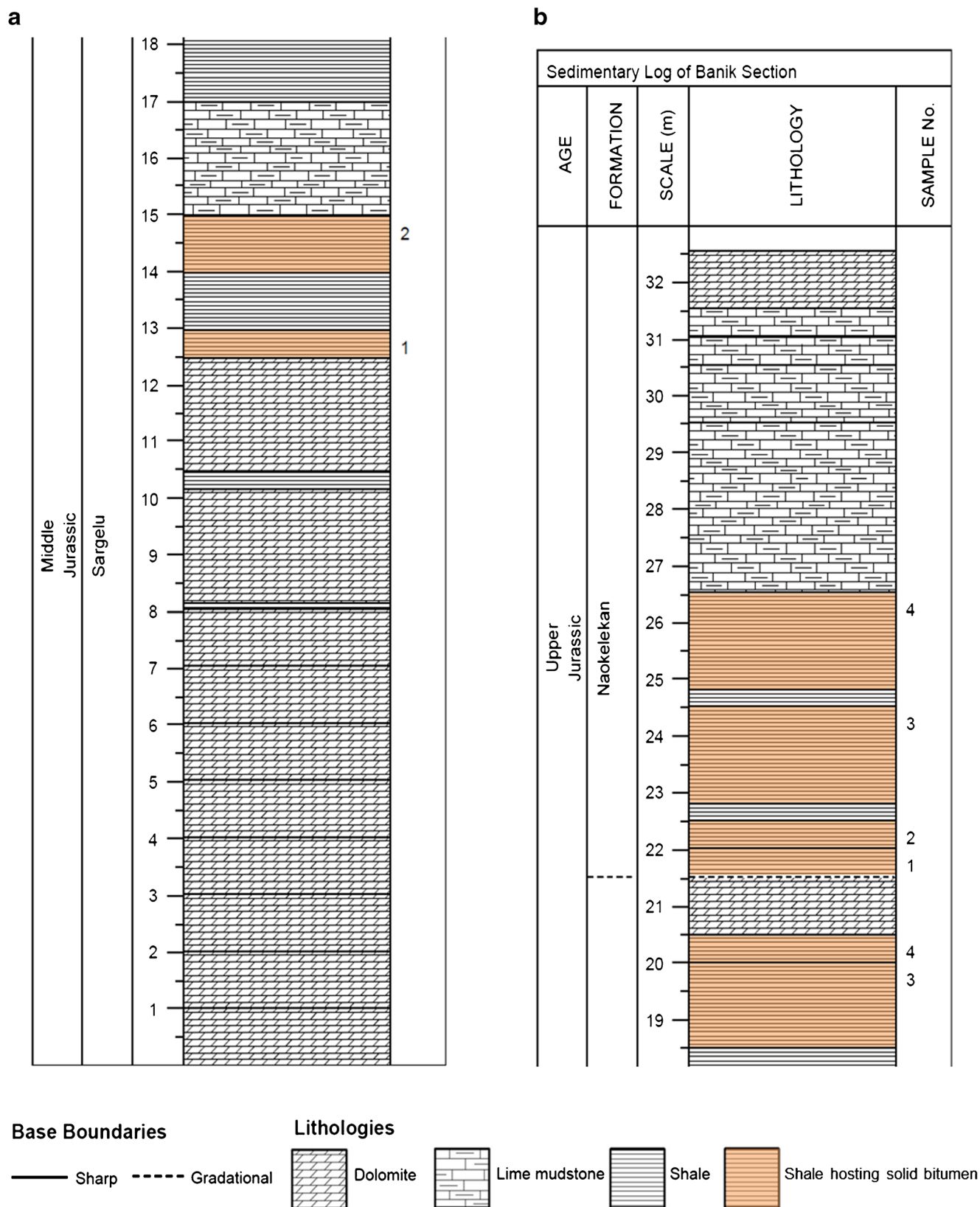


Fig. 3 Lithological section of the studied formations at Banik area of northernmost Iraq with sample locations

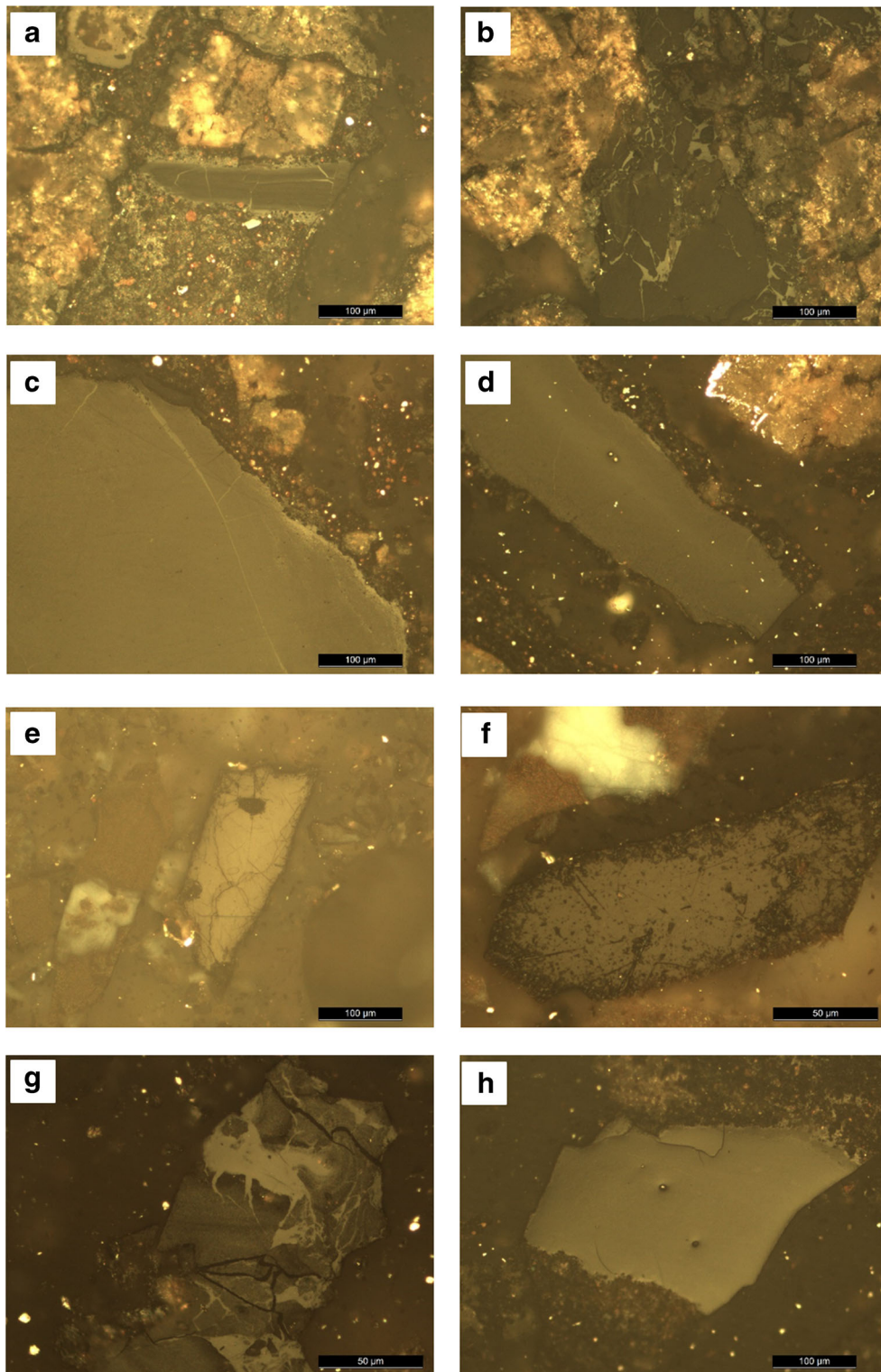


Fig. 4 (a) Optical microscopy (reflected white light) photomicrographs of the Sargelu Formation. (a)–(h) Grahamite (light chrysolite color), glance pitch (dark chrysolite color), scattered crystals of mineral matter (shiny color). (b) Optical microscopy (reflected white light) photomicrographs

of the Naokelekan Formation. (a), (b) Grahamite (light green color), glance pitch (dark green color), scattered crystals of mineral matter (shiny color). (c)–(h) Grahamite (light chrysolite color), glance pitch (dark chrysolite color), scattered crystals of mineral matter (shiny color)

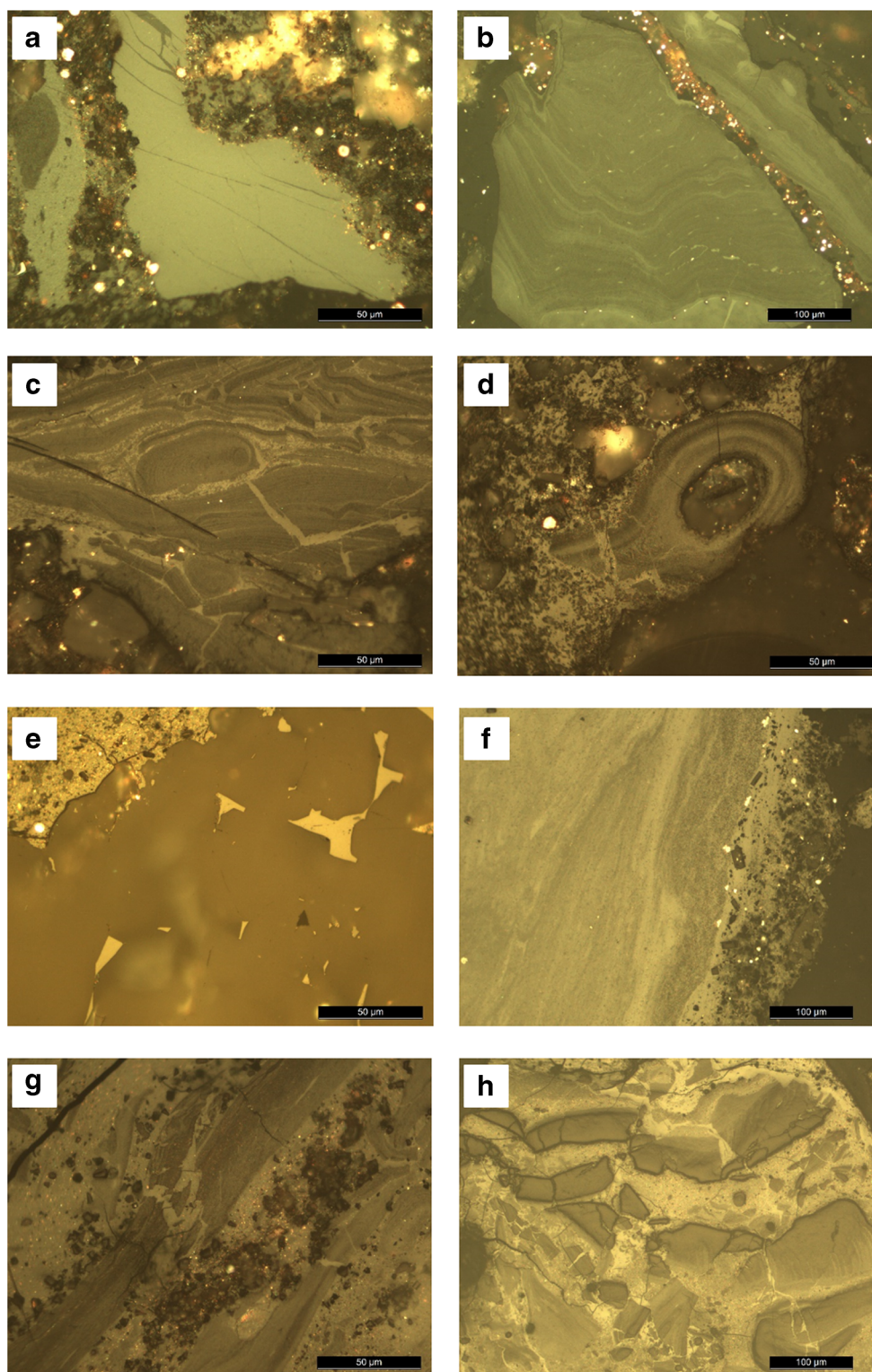


Fig. 4 (continued)

XRD analysis showed the following results averaged for minerals in the studied samples (Fig. 5a, b; Table 2). Likewise, Akkoca and Işık (2018) found these minerals in Dadaş shales, rich in organic matter, in southeastern Turkey.

Based on these results, it is concluded that the two formations differ in terms of their mineralogical compositions. The SEM and EDX analyses confirmed the presence of illite in the Naokelekan Formation (Fig. 6h;

Table 1 Solid bitumen reflectance values identified in the shale reservoirs from the Sargelu (S) and Naokelekan (N) Formations

Sample no.	Formation	Solid bitumen first phase			Solid bitumen second phase		
		Reflectance (%)	S	N	Reflectance (%)	S	N
1	Sargelu	0.45	0.08	48	0.19	0.06	12
2	Sargelu	0.54	0.07	109	0.27	0.05	50
3	Sargelu	0.52	0.04	25	0.30	0.05	65
4	Sargelu	0.66	0.06	32	0.38	0.08	68
1	Naokelekan	0.59	0.06	102	0.34	0.05	23
2	Naokelekan	0.54	0.04	69	0.36	0.07	31
3	Naokelekan	0.54	0.05	180	—	—	—
4	Naokelekan	0.51	0.04	177	0.27	0.06	23

Supplementary Fig. 1y), as well as the presence of montmorillonite and chlorite (Fig. 6h; Supplementary Fig. 1w, x), while rectorite (dioctahedral mica/montmorillonite) and kaolinite were observed from the underlying Sargelu Formation (Fig. 6d; Supplementary Fig. 1f, l).

Geochemistry

Organic geochemistry

Total carbon, organic carbon, and total sulfur The organic carbon (TOC) content (Table 3) varies from 4.3 to 14.5% in the samples from the Sargelu Formation with a mean value of 9.15%, while the total carbon (TC) content for the same samples ranges from 10.0 to 19.56% with a mean value of 15.34% (Table 3). In contrast, the samples from the Naokelekan Formation have the highest measured TOC contents (up to 48.1%; Table 3) with a mean value of 29.43%. The TC content for the same samples ranges from 24.73 to 48.9% with a mean value of 34.24% (Table 3).

The total sulfur (TS) content in the Sargelu Formation samples varies from 0.54 to 1.60%, while the samples from the Naokelekan Formation have higher TS contents ranging from 2.06 to 5.44% (Table 4).

Carbon and oxygen isotopes Table 5 lists the carbon isotope ($\delta^{13}\text{C}$) and oxygen isotope ($\delta^{18}\text{O}$) values of the solid bitumen and host shale samples from the two formations. The $\delta^{13}\text{C}$ values of the samples from the Sargelu Formation range from -2.58 to -7.10‰ , while the $\delta^{18}\text{O}$ values from the same formation range from -3.75 to -7.19‰ . In contrast, the $\delta^{13}\text{C}$ values of the samples from the Naokelekan Formation vary from -5.38 to -6.60‰ , while the $\delta^{18}\text{O}$ values range from -6.34 to -6.71‰ . One sample (sample 4) from the latter formation did not contain any carbonate (or only trace amounts; Table 2) and so no values could be calculated.

Inorganic geochemistry

X-ray fluorescence (XRF) analysis was used to determine the trace element compositions of the two formations (Table 6). The solid bitumen and host shales of the Sargelu Formation have high amounts of Ba, V, Mo, Cu, Zr, W, Zn, Sr, Cr, and Rb. The Ba values for samples 1 and 2 from the Sargelu Formation are 104 and 113 ppm, which are higher than the values of samples 3 and 4 (22–82 ppm). The V value for sample 3 from the same formation is 130 ppm, which is lower than the general values of c. 300–500 ppm. The Mo value for sample 2 from the same formation is 662 ppm, which is higher than the general values of c. 100–275 ppm. The Cu values for samples 1 and 2 of the Sargelu Formation are 90 ppm and 134 ppm, which are higher than the values of samples 3 and 4 (15–60 ppm). The Zr value of 8 ppm for sample 3 from the Sargelu Formation is lower than the general values of c. 37–54 ppm. The W value for sample 3 from the same formation is 144 ppm, which is higher than the general values of c. 20–40 ppm. The Zn value for sample 4 from the same formation is 74 ppm, which is lower than the general range of values (c. 152–200 ppm). The Sr values for samples 1 and 2 from the same formation are 81 and 98 ppm, which are lower than the values of samples 3 and 4 (c. 124–150 ppm). The Cr value for sample 3 from the same formation is 18 ppm, which is lower than the general values of c. 55–83 ppm. The Rb value for sample 3 from the same formation is 6 ppm, which is also lower than the general values of c. 21–38 ppm.

Samples from the Sargelu Formation also showed varied ranges for Ni (200–448 ppm), Mn (21–70 ppm), Pb (14–19 ppm), As (13–68 ppm), U (13–34 ppm), Ce (13–26 ppm), Y (11–36 ppm), Co (10–30 ppm), La (6–20 ppm), and Nd (5–16 ppm), while Th, Hf, Sm, Cs, Nb, Sc, and Ga have considerably lower ranges of 1–9 ppm (see Table 6).

The trace element distributions of the Naokelekan Formation are generally higher than those of the Sargelu Formation, for example, Ba (150–300 ppm), V (800–2000

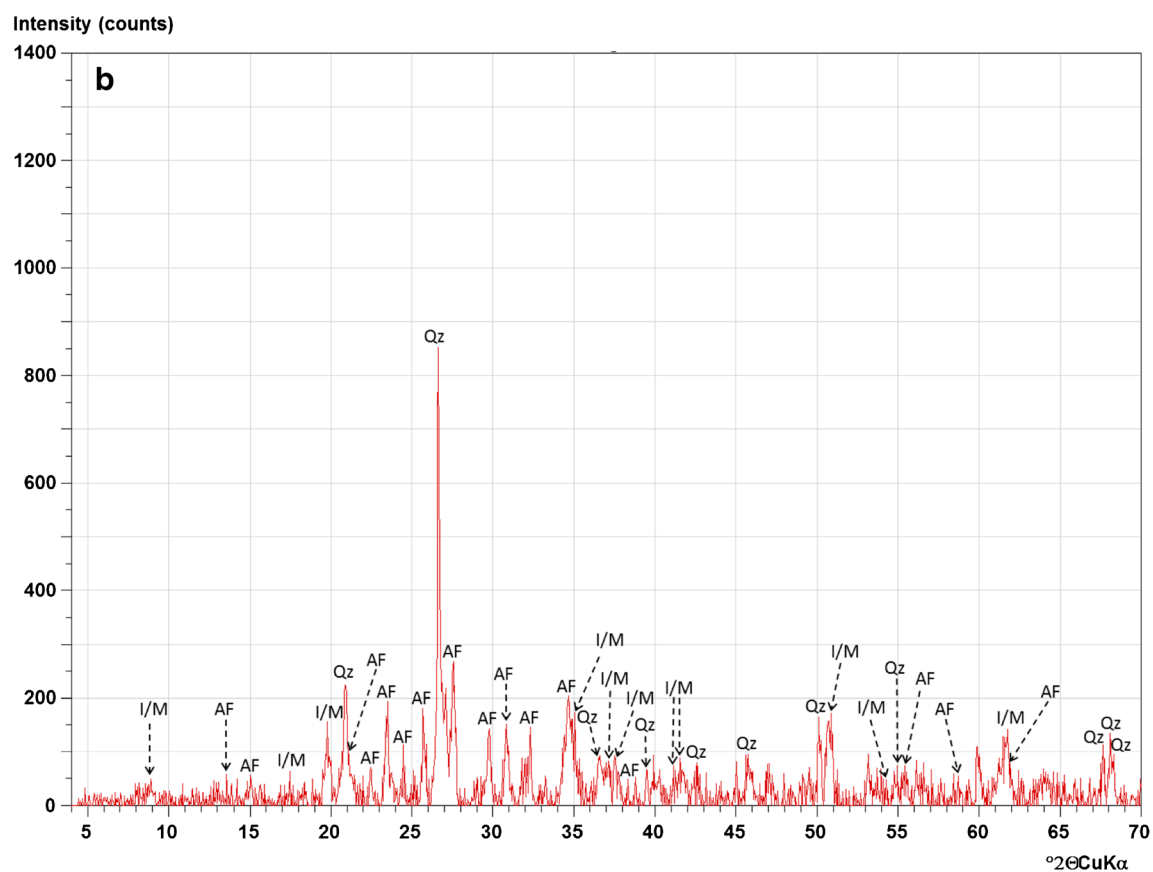
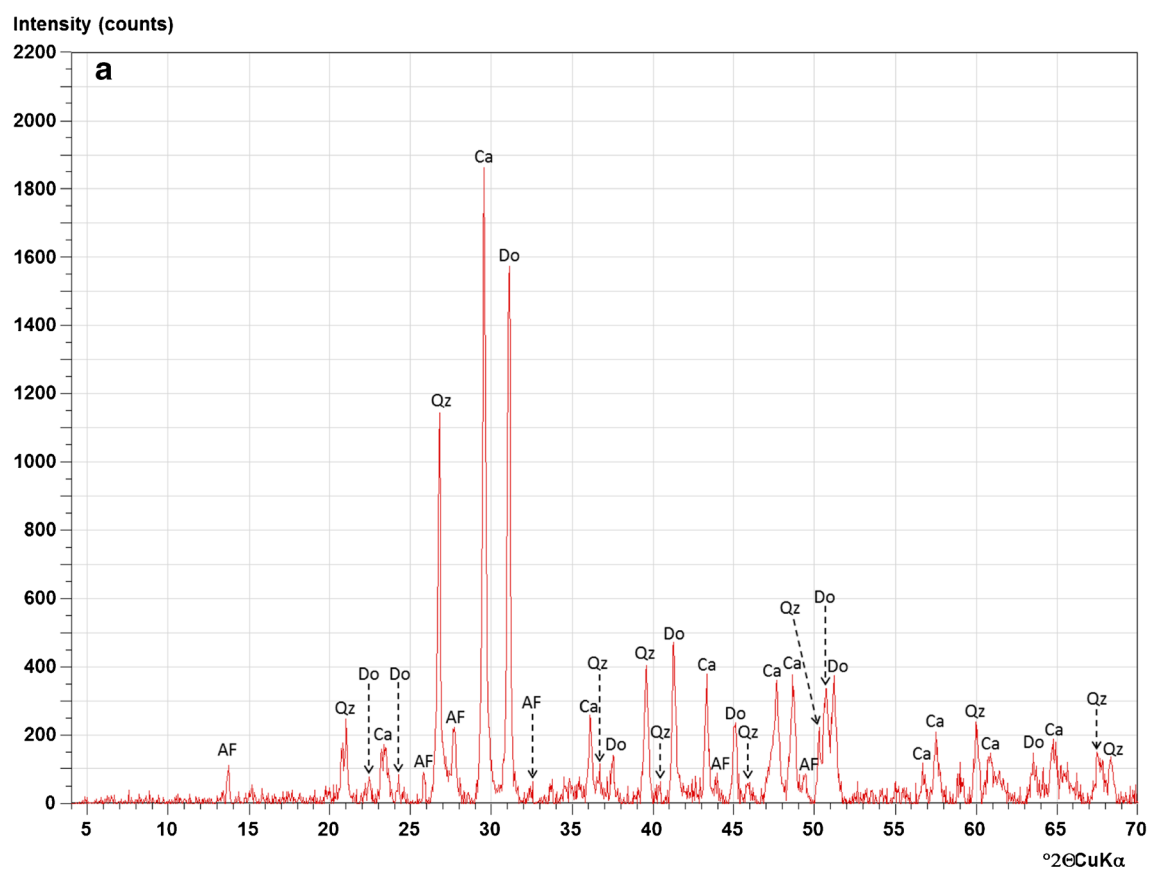


Fig. 5 X-ray diffractograms of selected samples from the Sargelu and Naokelekan Formations illustrating the clay and non-clay minerals in the host shales and solid bitumen. (a) Sample 4, Sargelu Formation. (b) Sample 4, Naokelekan Formation (see Fig. 3 for sample location)

ppm), Zn (200–1000 ppm), Cr (70–300 ppm), As (25–77 ppm), U (33–68 ppm), Y (26–85 ppm), and Nd (10–27 ppm). The values for Mn (20–58 ppm) and Co (3–11 ppm), however, are slightly lower than those from the underlying Sargelu Formation. The Th, Hf, Sm, Cs, Nb, Sc, and Ga values are very low (i.e., < 1–9 ppm), and thus very similar to those from the underlying Sargelu Formation (see Table 6).

The general range of the trace element values is similar for both formations (Table 6).

Discussion

Petrographic, organic, and inorganic geochemical analyses were undertaken on 8 samples of solid bitumen and the corresponding host shales from the Middle and Late Jurassic-age Sargelu and Naokelekan Formations from the Banik section, northernmost Iraq. While the solid bitumen is a secondary organic product resulting from the transformation of oils generated from the organic matter of primary origin (mainly highly hydrogenated organic matter), the precise origin of the solid bitumen present within the formations is unclear although the vitrinite reflectance and mineral contents provide important information in this regard. The following discussion, will review, in detail, the main aspects of the analyses, commencing with those which provide direct information on the depositional environment (i.e., isotopes, paleoredox proxies) before examining the aspects which are of more local significance (i.e., vitrinite reflectance, mineral content).

Carbon and oxygen isotope data

The carbon isotope ($\delta^{13}\text{C}$) values of the solid bitumen and host shale samples from the Sargelu and Naokelekan

Formations are all negative. Negative values are generally considered to be indicative of marine regression, while positive values have been related to periods of marine transgression (Bowman and Bralower 2005; Jarvis et al. 2006). Thus, deposition of the solid bitumen and host shales from the Sargelu and Naokelekan Formations of northernmost Iraq probably occurred during a period of marine regression and the establishment of a shallow-water depositional setting.

According to Buday (1980) and Haq (2018), the deposition of the Middle to Upper Jurassic successions coincided with a broad eustatic transgression, resulting in higher global sea level (Hallam 1982; Alsharhan and Naim 2003). Despite this eustatic rise, the carbon isotope values of the solid bitumen and host shale samples from the Middle and Late Jurassic-age Sargelu and Naokelekan Formations are interpreted as having been deposited in a shallow-marine setting. This disparity in terms of the rising eustatic sea level versus the shallow-marine setting in the area of Northern Iraq requires an explanation. Given that the region is located within the Zagros Basin/Zagros Fold Belt, an area which was tectonically active, it is possible that regional deformation due to Cimmerian-related uplift (Buday 1980) would have negated, or modified, the eustatic sea level rise.

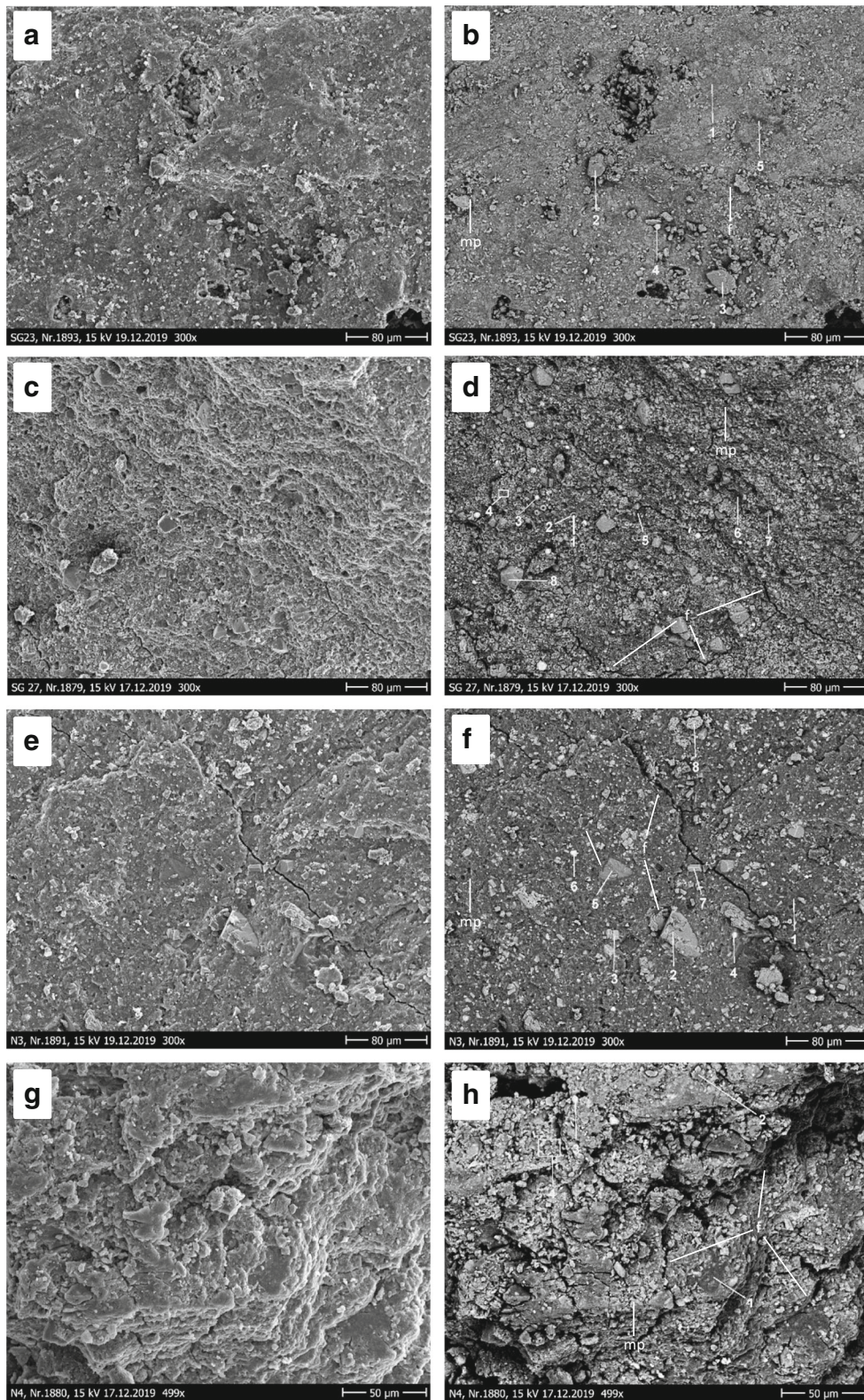
Analysis of the oxygen isotope values from the solid bitumen and host shale samples from the formations also shows negative values, indicative of warmer waters. Thus, deposition of the formations correlates well with the suggested Jurassic climate being dominated by tropical-subtropical conditions (Hallam 1982).

Paleoredox proxies

A selection of redox proxies, including Mo, U/Th, V/Cr, Ni/Co, and V/(V + Ni) (Hatch and Leventhal 1992; Rimmer 2004; Deepulal et al. 2012; Ramos-Vázquez et al. 2017; Anaya-Gregorio et al. 2018; Armstrong-Altrin 2020; Armstrong-Altrin et al. 2019; Armstrong et al. 2020; Ayala-Pérez et al. 2021), as well as the TS-TOC relationship (Pearce

Table 2 Distribution of clay and non-clay minerals (in wt%) in the solid bitumen and host shales of the Sargelu and Naokelekan Formations

Sample no.	Formation	Quartz (%)	Dolomite/ankerite (%)	Calcite (%)	Alkali feldspar (%)	Illite/muscovite (%)	Pyrite (%)
1	Sargelu	2.15	90.60	1.31	5.94	—	—
2	Sargelu	17.63	63.14	4.20	15.03	—	—
3	Sargelu	45.26	3.49	48.65	2.60	—	—
4	Sargelu	13.19	31.32	38.11	17.38	—	—
1	Naokelekan	2.68	36.60	45.37	15.35	—	—
2	Naokelekan	2.70	2.00	87.94	6.05	—	—
3	Naokelekan	3.61	1.84	85.73	6.88	—	1.16
4	Naokelekan	21.40	—	—	51.30	27.30	—



et al. 2010), were calculated from the solid bitumen and host shale samples (Fig. 7; Table 6).

The measured Mo values of the solid bitumen and host shale samples from the studied formations were very high,

ranging from 111 to 662 ppm in the Sargelu Formation and from 116 to 356 ppm in the overlying Naokelekan Formation (Fig. 7; Table 6), strongly suggesting that deposition occurred under anoxic conditions, with conditions during the

◀ **Fig. 6** SEM images of the Sargelu and Naokelekan Formations. (a) Topographic image of image (b). (b) Compositional contrast image with spotted areas. Spot 1: illite; spot 2: dolomite; spot 3: plagioclase feldspar; spot 4: illite; spot 5: pyrite framboid. (c) Topographic image of image (d). (d) Compositional contrast image with spotted areas. Spot 1: rectorite with organic matter (solid bitumen); spot 2: calcite with organic matter (solid bitumen); spot 3: pyrite framboid; spot 4: calcite with organic matter (solid bitumen); spot 5: organic matter (solid bitumen); spot 6: organic matter (solid bitumen); spot 7: kaolinite; spot 8: calcite with organic matter (solid bitumen). (e) Topographic image of image (f). (f) Compositional contrast image with spotted areas. Spot 1: organic matter (solid bitumen); spot 2: dolomite; spot 3: calcite; spot 4: pyrite framboid; spot 5: calcium phosphate with organic matter (solid bitumen); spot 6: pyrite framboid; spot 7: K-feldspar; spot 8: calcite. (g) Topographic image of image (h). (h) Compositional contrast image with spotted areas. Spot 1: pyrite framboid; spot 2: montmorillonite; spot 3: chlorite; spot 4: illite. f, fractures; mp, micropores within all samples from both formations (Sargelu and Naokelekan); topographic image, secondary electron signal (low energy); compositional contrast image, back scattered electron signal (high energy) that shows bright and dark areas. The darker areas contain lighter elements, while the brighter areas contain heavier elements

deposition of the lowermost formation possibly being more anoxic (Francois 1988; Dean et al. 1997).

Jones and Manning (1994) suggested that the U/Th ratio can be used as a proxy indicator for redox conditions, where ratios of > 1.25 are typical of anoxic deposition. Values of up to 67.6 were measured from the solid bitumen and host shale samples from the Sargelu Formation, while values up to 136.6 were measured from the solid bitumen and host shale samples from the Naokelekan Formation (Fig. 7; Table 6). These values suggest that both formations were deposited under anoxic conditions.

According to Hatch and Leventhal (1992) and Jones and Manning (1994), the ratio values of V/Cr which are < 2 indicate that the sediments were deposited within the oxic zone, while values > 4.25 indicate that they were deposited within the suboxic to anoxic zone (Hatch and Leventhal 1992; Jones

Table 4 TS and TOC relationship for the samples of the Sargelu and Naokelekan Formations

Sample no.	Formation	%TOC	%TS
1	Sargelu	7.5	0.85
2	Sargelu	10.3	1.04
3	Sargelu	4.3	0.54
4	Sargelu	14.5	1.60
1	Naokelekan	18.8	2.06
2	Naokelekan	25.9	2.99
3	Naokelekan	24.9	3.36
4	Naokelekan	48.1	5.44

and Manning 1994). The calculated V/Cr ratio values of the solid bitumen and host shale samples from the Sargelu Formation (5.39–7.43) fall within the suboxic to anoxic range. In comparison, the V/Cr ratio values from the overlying Naokelekan Formation show a marked increase, ranging from 9.13 up to 14.99. Such values are double some of those from the solid bitumen and host shale samples of the underlying Sargelu Formation. This might suggest that anoxia became more prevalent within the period during which the solid bitumen and host shales from the Naokelekan Formation were deposited (Fig. 7; Table 6).

Jones and Manning (1994) suggested that Ni/Co ratio values of < 5 indicate oxic conditions, while values of > 7 would indicate suboxic to anoxic conditions. Indeed, high Ni/Co ratio values are typical of reducing conditions where organic matter accumulates in the sediment (e.g., Raiswell and Plant 1980; Patterson et al. 1986). The Ni/Co values of the Naokelekan Formation (24.19–145.71) are noticeably higher than those recorded from the underlying Sargelu Formation (5.71–21.15), indicating that anoxia is considerably more prevalent within the Naokelekan Formation comparable to the Sargelu Formation, thus correlating well with the results obtained above (Fig. 7; Table 6).

Table 3 Total carbon, total inorganic carbon, and total organic carbon data for the samples of the Sargelu and Naokelekan Formations

Sample no.	Formation	%TC	%TIC	%TOC
1	Sargelu	15.97	8.5	7.5
2	Sargelu	15.84	5.6	10.3
3	Sargelu	10.00	5.7	4.3
4	Sargelu	19.56	5.1	14.5
Mean value	Sargelu	15.34	6.23	9.15
1	Naokelekan	24.73	5.9	18.8
2	Naokelekan	32.30	6.4	25.9
3	Naokelekan	31.04	6.1	24.9
4	Naokelekan	48.09	< 0.2	48.1
Mean value	Naokelekan	34.24	4.65	29.43

Table 5 Carbon and oxygen isotope data for the solid bitumen and host shales from the Sargelu and Naokelekan Formations

Sample no.	Formation	$\delta^{13}\text{C}$	$\delta^{18}\text{O}$
1	Sargelu	-2.58	-3.75
2	Sargelu	-5.54	-4.96
3	Sargelu	-7.10	-5.24
4	Sargelu	-5.66	-7.19
1	Naokelekan	-6.60	-6.34
2	Naokelekan	-6.53	-6.70
3	Naokelekan	-6.53	-6.71
4	Naokelekan	—	—

Table 6 Trace (in ppm) element concentrations with paleoredox proxies: Mo, U/Th, V/Cr, Ni/Co, V/(V + Ni) for the solid bitumen and host shales of the Middle–Late Jurassic-age Sargelu and Naokelekan Formations

Element (ppm)	Sargelu				Naokelekan			
	1	2	3	4	1	2	3	4
Sc	<DL	3	<DL	<DL	<DL	<DL	<DL	7
V	316	519	130	383	564	675	1082	2823
Cr	59	83	18	55	62	56	72	303
Mn	61	70	21	60	58	23	26	20
Co	13	36	22	15	11	3	5	4
Ni	218	448	125	313	273	332	590	597
Cu	90	134	15	60	55	35	35	87
Zn	198	181	152	74	157	518	1165	524
Ga	4	4	<DL	3	2	4	3	6
As	47	68.1	13.8	41.3	36.3	25.7	27.2	77
Rb	21	35	6	38	27	11	16	37
Sr	81	98	150	124	140	289	298	94
Y	16	29	11	36	42	26	29	85
Zr	37	54	8	44	27	15	19	55
Nb	4	5	<DL	4	4	2	3	6
Cs	5	7	5	7	9	5	8	4
Ba	104	113	22	82	124	230	158	366
La	9	16	6	20	33	10	16	43
Ce	23	26	13	19	12	18	1	20
Nd	10	16	5	12	14	10	12	27
Sm	<DL	2	4	7	2	3	<DL	7
Hf	<DL	<DL	<DL	<DL	<DL	<DL	<DL	<DL
W	25	43	144	25	29	9	10	15
Pb	16	18	14	19	15	14	14	22
Th	<DL	<DL	<DL	2	<DL	<DL	<DL	<DL
Mo	275	662	111	177	116	356	299	311
U	26.4	33.8	13.5	30.9	43.6	33.8	51.6	68.3
U/Th	52.8	67.6	27	15.45	87.2	67.6	103.2	136.6
V/Cr	5.39	6.23	7.43	7.02	9.13	11.98	14.99	9.33
Ni/Co	16.52	12.37	5.71	21.15	24.19	100.61	120.33	145.71
V/(V + Ni)	0.59	0.54	0.51	0.55	0.67	0.67	0.65	0.83

The V/(V + Ni) ratio is usually considered to be indicative of sediment deposition under euxinic conditions. According to Hatch and Leventhal (1992), V/(V + Ni) ratio values between 0.54 and 0.84 indicate anoxic conditions, while values greater than 0.84 would suggest euxinic conditions. The V/(V + Ni) values of the solid bitumen and host shale samples from the Sargelu Formation (i.e., 0.54–0.59) would possibly suggest that the solid bitumen and host shales of the Sargelu Formation were deposited under anoxic conditions (with the exception for one sample which has a value of c. 0.51). The V/(V + Ni) values of the solid bitumen and host shales from the overlying Naokelekan Formation increase from 0.65 to 0.83. Such values would suggest that anoxia became more prevalent within the period of deposition of the solid bitumen and host shales of the Naokelekan Formation, again

confirming the results obtained from the above analyses (Fig. 7; Table 6).

The TS-TOC relationship could be also indicative of reducing conditions (cf. Pearce et al. 2010). There is an overall increase in TS content (e.g., 1.04, 1.60, 2.06, 2.99) within the samples from the Sargelu and Naokelekan Formations with a corresponding increase in TOC content (e.g., 10.3, 14.5, 18.8, 25.9), except for one sample from the Naokelekan Formation which has a considerably higher value of TS (5.44) and a higher value of TOC (48.1) (see Table 4). This positive relationship between the TS and TOC contents is indicative of syngenetic pyrite formation under reducing conditions (Pearce et al. 2010).

According to Liu et al. (2019), pyrites can be subdivided, based on the formation mechanism, into syngenetic pyrites,

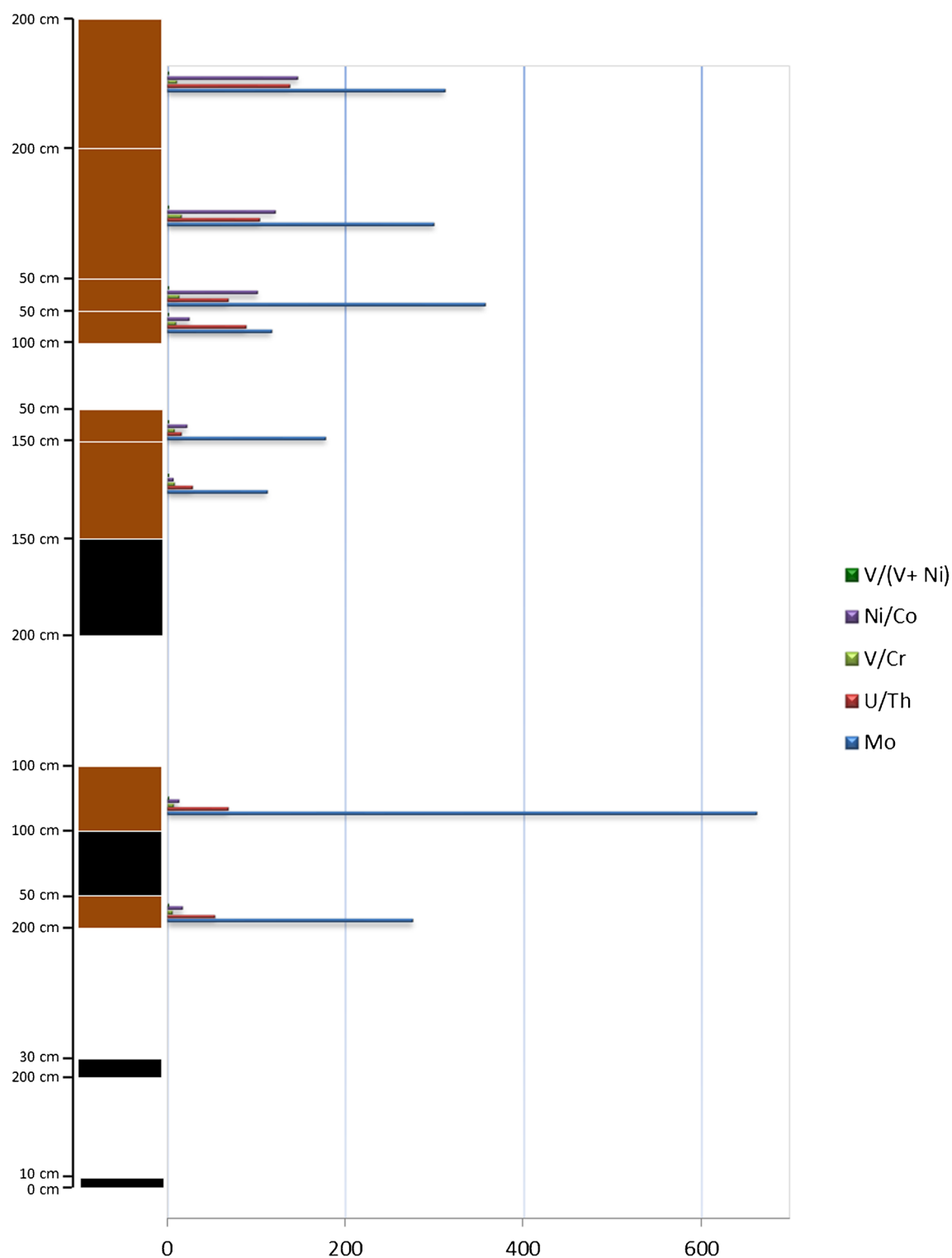


Fig. 7 The host shales and solid bitumen of the Sargelu and Naokelekan Formations, from the measured log of the Banik section, northernmost Iraq, showing geochemical proxies for paleoredox conditions. White-

colored beds, carbonate; black-colored beds, shale; dark brown-colored beds, shale hosting solid bitumen

early diagenetic pyrites, and late diagenetic pyrites. SEM and EDX analysis revealed the presence of syngenetic pyrites within all of the solid bitumen and host shale samples from the Sargelu and Naokelekan Formations (Fig. 6b, d, f, h;

Supplementary Fig. 1e, h, q, s, v). The observed syngenetic pyrites are mostly small framboids composed of microcrystals. According to Wilkin et al. (1996) and Gallego-Torres et al. (2015), the size distribution of pyrite framboids is

indicative of anoxic–euxinic environments in ancient marine sediments. As noted, the majority of the syngenetic pyrites from the Banik area are small framboids (i.e., smaller than 5 μm) suggesting that euxinic conditions were predominant during the time of deposition of the Sargelu and Naokelekan Formations (cf. Liu et al. 2019). Interestingly, a recent study (Abdula et al. 2020) on Rock-Eval analysis and organic petrographical characterization of the Upper Jurassic Naokelekan Formation from the Northern Mesopotamian Basin in Iraqi Kurdistan suggests that the co-occurrence of bituminite with pyrite framboids is indicative of reducing (anoxic to euxinic) conditions during the time of the deposition of the Naokelekan Formation sediments.

The various geochemical proxies discussed above would all suggest that the solid bitumen and host shale from both the Sargelu and Naokelekan Formations were deposited under reducing (anoxic to euxinic) conditions. Furthermore, it appears that the Naokelekan Formation was deposited during a period of more marked anoxia. Given that both formations were deposited in a shallow-marine shelf setting which would most likely be oxic, we need to explain the very clear anoxia signal which has been revealed from the geochemical proxies. Tyson (1989) and Tyson and Pearson (1991) have outlined a number of factors which can be used to determine the occurrence of dysoxic/anoxic facies in shelf settings, including high TOC contents (3–60%), absence (or low diversity) of benthos, general absence of coarse clastics, and association with warmer paleoclimates. These factors can be related to basin stratification, impingement and penetration of the expanded Oxygen Minimum Zone, and upwelling models and models related to changes in sea level and/or sea bottom topography as well as fluvial influence (e.g., Van der Zwaan and Jorissen 1991). It is difficult to determine the precise importance of the first three of these, so we will concentrate on the latter controls.

As noted above, the TOC contents of the Sargelu and Naokelekan Formations range from 4.3 to 48.1%. Additionally, the benthos, as reported by Omar et al. (2020), comprise only rare ostracods (*Loricoecia loricata*). Furthermore, the formations are dominated by mudstones, and a marked absence of coarser clastics, with deposition occurring during a warm period. These observations support the fact that the deposition of the Sargelu and Naokelekan Formations possibly occurred under low oxygen conditions (Tyson 1989). Many authors noted that rising sea level can lead to an increase in anoxia in shelf settings (Gertsch et al. 2010; Danise et al. 2013). While, the period of deposition of the Middle and Upper Jurassic formations corresponded to that of a broad eustatic transgression (Buday 1980; Haq 2018), resulting in higher global sea levels (Hallam 1982; Alsharhan and Nairn 2003). The situation, however, in Northern Iraq in Jurassic times was very different, since the environment was a shallow-marine setting at the time of deposition.

Omar et al. (2020) have interpreted the disparity in terms of the rising sea level and the shallow-marine depositional environment of the Sargelu and Naokelekan Formations in northernmost Iraq as being related to Cimmerian-related uplift tectonic activity (see also Buday 1980) which may have modified the sea level rise due to the formation of small restricted subbasins. Tobia et al. (2019) have examined the sediments of the Sargelu and Naokelekan Formations from Iraqi Kurdistan and determined that they were deposited in an anoxic deep-marine setting (with the exception of the lowermost Sargelu Formation sediments which show evidence of oxic shallow-marine setting). These results do not agree with the findings from the current study, apart from the clear anoxic signature which is present within the bulk of the Sargelu and Naokelekan Formations' sediments. The unequivocal shallow-marine signature derived from the isotopes clearly does not allow a deep-marine setting for the anoxia to be determined. Based on the factors outlined above by Tyson (1989) and Tyson and Pearson (1991), it is clear that the sediments of the Sargelu and Naokelekan Formations show a definitive anoxic signature. As noted above, the depositional setting was shallow marine; the region was also one which was tectonically active with the NE (which includes the Banik area) and N boundaries of the Arabian Plate representing the area of collision with the Cimmerian plates (Jassim and Goff 2006). Subsequent to this collision, a period of uplift (i.e., Cimmerian uplift; Buday 1980) occurred, possibly resulting in the subdivision of the depositional setting as a result of tectonic deformation (i.e., subbasin formation, basin compartmentalization; Omar et al. 2020). This tectonic fragmentation of the marine shelf into areas of higher and lower relief was similar, in some ways, to the Cretaceous-age Northern Calcareous Alps (Austria), where the depositional setting was compartmentalized as a result of deformation (Sanders 1998). Such compartmentalization (Pratt et al. 2008) would have resulted in marked differences between various subbasins, and—we would herein suggest—the development of anoxic facies within some of these subbasins. Thus, our explanation, invoking tectonic deformation resulting in the formation of subbasins with restricted circulation, would appear to be the best current explanation for this dilemma.

Vitrinite reflectance

The equivalent vitrinite reflectance value was determined for the eight samples from the Sargelu and Naokelekan Formations using three standard equations, which are as follows: Jacob (1989) equation: $\text{Ro eq. vitrinite} = 0.618 \text{ RB} + 0.40$, Riediger (1993) equation: $\text{Ro eq. vitrinite} = 0.277 \text{ RB} + 0.57$, Schoenherr et al. (2007) equation: $\text{Ro eq. vitrinite} = (\text{RB} + 0.2443) / 1.0495$. The equivalent vitrinite reflectance value is used to decipher the origin of the solid bitumen accumulated within the studied shale beds, determining whether the solid bitumen was initially oil, generated from the same shale beds,

or if it was generated elsewhere and subsequently migrated. The equivalent vitrinite reflectance values obtained from the Sargelu and Naokelekan samples are all broadly similar (Table 7). The shale containing the solid bitumen has very low equivalent vitrinite reflectance values, suggesting that the shale is not the source rocks for the solid bitumen.

Integrating the geochemical data with the equivalent vitrinite reflectance values from the studied shale allow us to reconstruct the accumulation process for the solid bitumen. During Middle and Late Jurassic times, oil migrated into the Sargelu and Naokelekan Formations. The reservoir rocks provided ideal conditions for trapping the petroleum, which was subsequently transformed into solid bitumen. Thus, the bitumen is a secondary product, and not related to the primary depositional conditions. The source of the petroleum, however, is unclear—but one possible source would be the carbonates which are interbedded with the studied shale, since the Jurassic marine carbonates are the major sources of hydrocarbons produced in the Zagros Basin (Al-Ahmed 2006) which include the Middle to Upper Jurassic Sargelu and Naokelekan Formations in Iraq.

Mineral content

As noted above, the shales within the two studied formations are the host rock for the solid bitumen which formed elsewhere and migrated into that shale where it crystallized. Examining the mineral content of the shales allows us to determine the degree to which these shale rocks provide good reservoir quality. The studied carbonate-rich shale has a heterogeneous composition as recorded in their mineralogy (Figs. 5 and 6; Table 2).

In the present work, the shale is commonly carbonate-rich including calcite and Fe-rich dolomite (ankerite); the amount of calcite ranges from 45.3 to 87.9% in the Naokelekan Formation while the amount of ankerite can be up to 90% in the Sargelu Formation (Table 2). The generation of micropores and fractures as a result of the presence of highly soluble carbonate

minerals such as calcite and dolomite, in addition to tectonically related fracturing, enhanced the storage capacity of the studied shale. Indeed, the presence of dissolution-related micropores was confirmed by SEM analysis which also revealed the presence of fractures in the studied shales (Fig. 6b, d, f, h). These micropores and fractures, acting as migration or flow conduits, would have enhanced the ability of the studied shales to act as a reservoir for the migrating bitumen.

The carbonates are, in general, better reservoir rocks. Additionally, as noted above, the carbonates which are interbedded with the shale have been regarded as one possible source of hydrocarbons for the Middle to Upper Jurassic Sargelu and Naokelekan Formations. However, the carbonate rocks of the two studied formations are not considered to be of reservoir quality. Aqrabi et al. (2010) have noted that porous Middle to Late Jurassic-age limestone reservoirs, analogous to the Arab Formation of Saudi Arabia, have not yet been described from Iraq. The Middle to Upper Jurassic source rocks in Iraq are typically condensed carbonate-rich intervals containing high-quality, organic-rich hydrocarbons and deposited under deep marine, restricted basinal conditions (Aqrabi et al. 2010).

Omar et al. (2020) have noted that the precursor limestones of the Sargelu Formation were wholly or partly converted to dolomite rock. The presence of extensive and pervasive dolomite has resulted in the formation of tight carbonate rocks so less dissolution may have occurred. The secondary porosity, which formed as a result of the dissolution of fossils, was thus filled with later calcite and dolomite cements effectively reducing porosity. The matrix permeability is similar to the porosity filled by calcite and dolomite cements, which limited any enhancement of the fluid flow by fractures, resulting in a situation where the only pathways or conduits for fluid flow were the partially filled calcite fractures and intercrystalline pores. Consequently, both the porosity and the permeability were extremely restricted, and the only available porosity was in the shales.

Table 7 The equivalent vitrinite reflectance values using different equations

Sample no.	Formation	*Ro eq. vitrinite (%)	**Ro eq. vitrinite (%)	***Ro eq. vitrinite (%)
1	Sargelu	0.68	0.69	0.66
2	Sargelu	0.73	0.72	0.75
3	Sargelu	0.72	0.71	0.73
4	Sargelu	0.81	0.75	0.86
1	Naokelekan	0.76	0.73	0.79
2	Naokelekan	0.73	0.72	0.75
3	Naokelekan	0.73	0.72	0.75
4	Naokelekan	0.72	0.71	0.72

*Jacob (1989) equation: Ro eq. vitrinite = 0.618 RB + 0.40

**Riediger (1993) equation: Ro eq. vitrinite = 0.277 RB + 0.57

***Schoenherr et al. (2007) equation: Ro eq. vitrinite = (RB + 0.2443) / 1.0495

Conclusions

The solid bitumen preserved within the shales of the Middle and Upper Jurassic succession of the Banik section from northernmost Iraq was accumulated in the Sargelu and Naokelekan Formations. The accumulation process took place within the host shale. Petrographical, mineralogical, organic, and inorganic geochemical studies have been carried out on the reservoir rocks and solid bitumen. The Banik section is dominated by dolomites, limestones, and shales. Accumulation of the solid bitumen in the host shales of the area is interpreted to have occurred, probably as a result of oil migration from other source rocks within the same formations. In terms of the geological setting, the Jurassic succession was dominated by organic-rich source rocks and highly porous and permeable reservoir rocks. Together, the results in this study would suggest that source rocks, during the Jurassic time, reached a peak for petroleum generation. Meanwhile, under the influence of the ongoing tectonic activity in the region of northernmost Iraqi Kurdistan, the occurrence of fractures and faults provided effective pathways for oil migration from the source rocks through the porous and permeable reservoir rocks (i.e., host shales) in the stratigraphic succession of the Banik section.

Additionally, the results from the carbon and oxygen isotope data and the paleoredox proxies in this study would suggest that the host shale and solid bitumen sources within the Middle–Late Jurassic-age Sargelu and Naokelekan Formations were deposited in a shallow-marine setting and under anoxic conditions.

Supplementary Information The online version contains supplementary material available at <https://doi.org/10.1007/s12517-021-07048-9>.

Acknowledgements We would like to thank, particularly, Hans-Jürgen Ensikat for initiating and supporting the scanning electron microscopy (SEM) and energy-dispersive X-ray microanalysis (EDX). Finally, we thank our reviewers for their thorough reviews of the manuscript.

Funding Open Access funding enabled and organized by Projekt DEAL. This study is supported by the Arab-German Young Academy of Sciences and Humanities (AGYA) grants (AGYA_2020_AP_01).

Declarations

Conflict of interest The authors declare that they have no competing interests.

Open Access This article is licensed under a Creative Commons Attribution 4.0 International License, which permits use, sharing, adaptation, distribution and reproduction in any medium or format, as long as you give appropriate credit to the original author(s) and the source, provide a link to the Creative Commons licence, and indicate if changes were made. The images or other third party material in this article are included in the article's Creative Commons licence, unless indicated otherwise in a

credit line to the material. If material is not included in the article's Creative Commons licence and your intended use is not permitted by statutory regulation or exceeds the permitted use, you will need to obtain permission directly from the copyright holder. To view a copy of this licence, visit <http://creativecommons.org/licenses/by/4.0/>.

References

- Abdula R (2017) Source rock assessment of Naokelekan formation in Iraqi Kurdistan. *JZS-A* 19:103–124
- Abdula RA, Balaky SM, Nourmohamadi MS, Piroui M (2015) Microfacies analysis and depositional environment of the Sargelu Formation (Middle Jurassic) from Kurdistan Region, Northern Iraq. *Donnish J Geol Min Res* 1:1–26
- Abdula RA, Kolo K, Damoulianou M, Raftopoulou V, Khanaqa P, Kalaitzidis S (2020) Rock-Eval analysis and organic petrographical characterization of the Upper Jurassic Naokelekan Formation, Northern Mesopotamian Basin, Kurdistan Region-Iraq. *BGS* 187–203
- Ahlbrandt TS, Pollastro RM, Klett TR, Schenk CJ, Lindquist SJ, Fox JE (2000) Region 2 assessment summary—Middle East and North Africa. In *USGS World Petroleum Assessment 2000—Description and Results*, Chapter R2: DDS-60, pp 46
- Akkoca DB, Işık Ü (2018) Geochemistry of Paleozoic Dadaş shales from the foreland of southeastern Turkey, Bismil, Diyarbakır. *Period di Mineral* 87:199–217
- Al-Ahmed AAN (2006) Organic geochemistry, palynofacies and hydrocarbon potential of Sargelu Formation (Middle Jurassic) northern Iraq. PhD thesis, University of Baghdad, Iraq
- Al-Ameri TK, Zumberge J (2012) Middle and Upper Jurassic hydrocarbon potential of the Zagros Fold Belt, North Iraq. *Mar Pet Geol* 36: 13–34
- Al-Ameri TK, Al-Jubouri NM, Isa MJ, Al-Azzawi RE (2012) Hydrocarbons generation potential of the Jurassic-Lower Cretaceous Formation, Ajeel field, Iraq. *Arab J Geosci* 6:3725–3735
- Al-Jubouri AI, McCann T (2013) Petrological and geochemical interpretation of Triassic-Jurassic boundary sections from North Iraq. *Geol J* 50:157–172
- Al-Mousawi HA, Sissakian VK, Fouad SF, Survey IG (2008) The geology of Zakho Quadrangle, Scale 1:250000. Baghdad, Iraq, Iraq Geological Survey
- Alsharhan AS, Naim AEM (2003) Sedimentary basins and petroleum geology of the Middle East. Netherlands, Elsevier Science, Amsterdam, 843 pp
- Altinli IE (1966) Geology of eastern and southeastern Anatolia, Turkey, pp. 35–76. Bulletin of Mineral Research Exploration Institute of Turkey, Foreign Edition, Ankara no. 60.
- Al-Zubaidi AA, Al-Zebari AY (1998) Prospects for production and marketing of Iraq's heavy oil: ministry of oil. State Oil Marketing, Baghdad, Iraq, 221, pp 10
- Anaya-Gregorio A, Armstrong-Altrin JS, Machain-Castillo ML, Montiel-Garcia PC, Ramos-Vazquez MA (2018) Textural and geochemical characteristics of late Pleistocene to Holocene fine-grained deep-sea sediment cores (GM6 and GM7), recovered from the southwestern Gulf of Mexico. *J Paleogeol* 7:1–19
- Aqrabi AAM (1998) Paleozoic stratigraphy and petroleum systems of the western and southwestern Deserts of Iraq. *GeoArabia* 3:229–247
- Aqrabi AAM, Badics B (2015) Geochemical characterisation, volumetric assessment and shale-oil/gas potential of the Middle Jurassic–Lower Cretaceous source rocks of NE Arabian Plate. *GeoArabia* 20: 99–140
- Aqrabi AAM, Goff JC, Horbury AD, Sadooni FN (2010) The petroleum geology of Iraq. Scientific Press, pp 424

- Armstrong-Altrin JS, Ramos-Vázquez MA, Hermenegildo-Ruiz NY, Madhavaraju J (2020) Microtexture and U-Pb geochronology of detrital zircon grains in the Chachalacas Beach, Veracruz State, Gulf of Mexico. *Geol J* 3:1–12. <https://doi.org/10.1002/gj.3984>
- Armstrong-Altrin JS (2020) Detrital zircon U-Pb geochronology and geochemistry of the Riachuelos and Palma Sola beach sediments, Veracruz State, Gulf of Mexico: a new insight on palaeoenvironment. *J Palaeogeogr* 9:28. <https://doi.org/10.1186/s42501-020-00075-9>
- Armstrong-Altrin JS, Botello AV, Villanueva SF, Soto LA (2019) Geochemistry of surface sediments from the northwestern Gulf of Mexico: implications for provenance and heavy metal contamination. *Geol Quart* 63(3):522–538
- Awdal A, Healy D, Alsop GI (2016) Fracture patterns and petrophysical properties of carbonates undergoing regional folding: a case study from Kurdistan, N Iraq. *Mar Pet Geol* 71:149–167
- Ayala-Pérez MP, Armstrong-Altrin JS, Machain-Castillo ML (2021) Heavy metal contamination and provenance of sediments recovered at the Grijalva River delta, southern Gulf of Mexico. *J Earth Syst Sci*. <https://doi.org/10.1007/s12040-021-01570-w>
- Balaky SM, Swrdashy AM, Mamaseni WJ (2016) Permian-Triassic lithostratigraphic study in the Northern Thrust Zone (Ora), Iraqi Kurdistan region. *Arab J Geosci* 9:343
- Bartolini A, Pittet B, Mattioli E, Hanziker JC (2003) Shallow-platform palaeoenvironmental conditions recorded in deep-shelf sediments: C and O stable isotopes in Upper Jurassic sections of southern Germany (Oxfordian – Kimmeridgian). *Sediment Geol* 160:107–130
- Bellen RCV, Dunnington HV, Wetzel R, Morton DM (1959) *Lexique Stratigraphique International*, vol III. Paris: Asie, Fascicule 10a Iraq, pp 333
- Bennett WW, Canfield DE (2020) Redox-sensitive trace metals as paleoredox proxies: a review and analysis of data from modern sediments. *Earth-Sci Rev* 204:103175
- Beydoun ZR (1991) Arabian plate hydrocarbon geology and potential. A plate tectonic approach AAPG 33:1–77
- Bowman AR, Bralower TJ (2005) Paleooceanographic significance of high-resolution carbon isotope records across the Cenomanian–Turonian boundary in the Western Interior and New Jersey coastal plain, USA. *Mar Geol* 217:305–321
- Buday T (1980) The regional geology of Iraq. *Stratigraphy and palaeogeography*. Publication of GEOSURV, vol. 1. Baghdad, p 445
- Danise S, Twitchett RJ, Little CTS, Clémence ME (2013) The impact of global warming and anoxia on marine benthic community dynamics: an example from the Toarcian (Early Jurassic). *PLoS One* 8: e56255
- Daoud HS, Karim KH (2010) Types of stromatolites in the Barsarin Formation (late Jurassic), Barzinja area, NE Iraq. *Iraqi Bull Geol Mining* 6:47–57
- Dean WE, Gardner JV, Piper DZ (1997) Inorganic geochemical indicators of glacial – interglacial changes in productivity and anoxia on the California continental margin. *Geochim Cosmochim Acta* 61: 4507–4518
- Deepulal PM, Gireesh Kumar TR, Sujatha CH, George R (2012) Chemometric study on the trace metal accumulation in the sediments of the Cochin Estuary-Southwest coast of India. *Environ Monit Assess* 184:6261–6279
- Dubertret B (1966) Liban, Syrie et bordure des pays voisins: Notes and Memoires Meyen Orient, vol. VIII. Paris.
- Edilbi ANF, Maleko MA, Mohamed AY (2017) Evaluating the Baluti Formation at Sararu village, Ora Anticline, Iraqi Kurdistan: a stratigraphic and geochemical approach. *Arab J Geosci* 10:73
- El Diasty WS, El Beialy SY, Peters KE, Batten DJ, Al-Beyati FM, Mahdi AQ, Hasseb MT (2018) Organic geochemistry of the Middle-Late Jurassic Naokelekan Formation in the Ajil and Balad oil fields, northern Iraq. *J Pet Sci Eng* 166:350–362
- Francois R (1988) A study on the regulation of the concentrations of some trace elements (Rb, Sr, Zn, Pb, Cu, V, Cr, Ni, Mn and Mo) in Saanich Inlet sediments, British Columbia, Canada. *Mar Geol* 83: 285–308
- Gallego-Torres D, Reolid M, Nieto-Moreno V, Martínez-Casado FJ (2015) Pyrite framboid size distribution as a record for relative variations in sedimentation rate: an example on the Toarcian oceanic anoxic event in South Iberian palaeomargin. *Sediment Geol* 330:59–73
- Gertsch B, Adatte T, Keller G, Tantawy AAAM, Berner Z, Mort HP, Fleitmann D (2010) Middle and late Cenomanian oceanic anoxic events in shallow and deeper shelf environments of western Morocco. *Sedimentology* 57:1430–1462
- Hallam A (1982) The Jurassic climate. In *Climate in Earth history: studies in geophysics*, pp. 159–163. The National Academies Press. <https://doi.org/10.17226/11798>
- Haq BU (2018) Jurassic sea-level variations: a reappraisal. *GSA Today* 28:4–10
- Hatch JR, Leventhal JS (1992) Relationship between inferred redox potential of the depositional environment and geochemistry of the Upper Pennsylvanian (Missourian) Stark Shale Member of the Dennis Limestone, Wabaunsee County, Kansas, USA. *Chem Geol* 99:65–82
- Jacob H (1989) Classification, structure, genesis and practical importance of natural solid oil bitumen (“migrabitumen”). *Int J Coal Geol* 11: 65–79
- James GA, Wynd JG (1965) Stratigraphic nomenclature of Iranian oil consortium agreement area. AAPG Bull 49:2182–2245
- Jarvis I, Gale AS, Jenkyns HC, Pearce MA (2006) Secular variation in Late Cretaceous carbon isotopes: a new $\delta^{13}\text{C}$ carbonate reference curve for the Cenomanian–Campanian (99.670.6 Ma). *Geol Mag* 143:561–608
- Jasim SY (2013) The potential of hydrocarbons generation in the Chia Gara Formation at Amadia area, north of Iraq. *Arab J Geosci* 6: 3313–3318
- Jassim SZ, Al-Gailani M (2006) Hydrocarbons. In: Jassim SZ, Goff JC (eds) *Geology of Iraq*. Dolin; Brno: Moravian Museum, Prague, pp 232–250
- Jassim SZ, Buday T (2006) Late Toarcian-Early Tithonian (Mid-Late Jurassic) megasequence AP7. In: Jassim SZ, Goff JC (eds) *Geology of Iraq*. Dolin; Brno: Moravian Museum, Prague, pp 117–123
- Jassim SZ, Goff J (2006) *Geology of Iraq*. Dolin; Brno: Moravian Museum, Prague, 318p
- Jones B, Manning DAC (1994) Comparison of geochemical indices used for the interpretation of palaeoredox conditions in ancient mudstones. *Chem Geol* 111:111–129
- Liu X, Wen Z, Wang Z, Song C, He Z (2018) Structural characteristics and main controlling factors on petroleum accumulation in Zagros Basin, Middle East. *J Nat Gas Geosci* 5:273–281
- Liu Z, Chen D, Zhang J, Lü X, Wang Z, Liao W, Shi X, Tang J, Xie G (2019) Pyrite morphology as an indicator of paleoredox conditions and shale gas content of the Longmaxi and Wufeng Shales in the Middle Yangtze Area, South China. *Minerals* 9:428
- Mohialdeen IMJ, Hakimi MH, Al-Beyati FM (2013) Geochemical and petrographic characterisation of Late Jurassic-Early Cretaceous Chia Gara Formation in Northern Iraq: palaeoenvironment and oil-generation potential. *Mar Pet Geol* 43:166–177
- Murris RJ (1980) Middle East: stratigraphic evolution and oil habitat. AAPG Bull 64:597–618
- Numan NMS (2000) Major cretaceous tectonic events in Iraq. *Raf J Sci* 11:32–52
- Omar N, McCann T, Al-Juboury AI, Franz SO (2020) Petrography and geochemistry of the Middle-Upper Jurassic Banik section,

- northernmost Iraq – implications for palaeoredox, evaporitic and diagenetic conditions. *N Jb Geol Palaeont Abh* 297:125–152
- Patterson JH, Ramsden AR, Dale LS, Fardy JJ (1986) Geochemistry and mineralogical residences of trace elements in oil shales from Julia Creek, Queens- land, Australia. *Chem Geol* 55:1–16
- Pearce CR, Coe AL, Cohen AS (2010) Seawater redox variations during the deposition of the Kimmeridge Clay Formation, United Kingdom (Upper Jurassic): evidence from molybdenum isotopes and trace metal ratios. *Paleoceanography* 25:PA4213
- Pitman JK, Steinshouer D, Lewan MD (2004) Petroleum generation and migration in the Mesopotamian Basin and Zagros Fold Belt of Iraq: results from a basin-modeling study. *GeoArabia* 9:41–72
- Pratt JR, Schoenbohm LA, Mortimer E, Schmitt A (2008) Basin Compartmentalization in the Sierra Pampeanas of Northwestern Argentina: case-study of the El Cajón Basin. Senior thesis, The Ohio State University, USA. Published thesis. <https://kb.osu.edu/handle/1811/57007>
- Raiswell R, Plant J (1980) The incorporation of trace elements into pyrite during diagenesis of black shales, Yorkshire, England. *Econ Geol* 75:684–699
- Ramos-Vázquez MA, Armstrong-Altrin JS (2019) Sediment chemistry and detrital zircon record in the Bosque and Paseo del Mar coastal areas from the southwestern Gulf of Mexico. *Mar Pet Geol* 110: 650–675
- Ramos-Vázquez MA, Armstrong-Altrin JS, Rosales-Hoz L, Machain-Castillo ML, Carranza-Edwards A (2017) Geochemistry of deep-sea sediments in two cores retrieved at the mouth of the Coatzacoalcos River delta, western Gulf of Mexico, Mexico. *Arab J Geosci* 10:1–19
- Riediger CL (1993) Solid bitumen reflectance and Rock-Eval Tmax as maturation indices: an example from the “Nordegg Member”, Western Canada Sedimentary Basin. *Int J Coal Geol* 22:295–315
- Rimmer SM (2004) Geochemical paleoredox indicators in Devonian-Mississippian black shales, Central Appalachian Basin (USA). *Chem Geol* 206:273–391
- Ruf M, Link E, Pross J, Aigner T (2005) integrated sequence stratigraphy: Facies, stable isotope, and palynofacies analysis in a deeper epicontinental carbonate ramp (Late Jurassic, SW Germany). *Sediment Geol* 175:391–414
- Sanders D (1998) Tectonically controlled Late Cretaceous terrestrial to neritic deposition (Northern Calcareous Alps, Tyrol, Austria). *Facies* 39:139–178
- Sarfi M, Ghasemi-Nejad E, Mahanipour A, Yazdi-Moghadam M, Sharifi M (2015) Integrated biostratigraphy and geochemistry of the lower Cretaceous Radiolarian Flood Zone of the base of the Garau Formation, northwest of Zagros Mountains, Iran. *Arab J Geosci* 8: 7245–7255
- Schoenherr J, Littke R, Urai JL, Kukla PA, Rawahi Z (2007) Polyphase thermal evolution in the Infra-Cambrian Ara Group (South Oman Salt Basin) as deduced by maturity of solid reservoir bitumen. *Org Geochem* 38:1293–1318
- Sharland PR, Archer R, Casey DM, Davies RB, Hall SH, Heward AP, Horbury AD, Simmons MD (2001) Arabian plate sequence stratigraphy. *GeoArabia*, Special Publication no. 2, Gulf PetroLink, Bahrain, pp 371
- Tobia FH, Al-Jaleel HS, Ahmad IN (2019) Provenance and depositional environment of the Middle-Late Jurassic shales, northern Iraq. *Geosci J* 23:747–765
- Tyson RV (1989) Source rock palaeoenvironments: principles, models, and mid-Cretaceous patterns. Unpublished Report for Masera Corporation, Tulsa
- Tyson RV, Pearson TH (1991) Modern and ancient continental shelf anoxia: an overview. In: Modern and Ancient continental shelf anoxia (eds. RV Tyson and TH Pearson). *Geol Soc Spec Publ* 58:1–24
- Van der Zwaan GJ, Jorissen FJ (1991) Biofacial patterns in river-induced shelf anoxia. In: Modern and ancient continental shelf anoxia (eds. RV Tyson and TH Pearson). *Geol Soc Spec Publ* 58:65–82
- Verma MK, Ahlbrandt TS, Al Gailani M (2004) Petroleum reserves and undiscovered resources in the total petroleum systems of Iraq: reserve growth and production implications. *GeoArabia* 9:51–74
- Weissert H, Erba E (2004) Volcanism CO₂ and paleoclimate: a late Jurassic – Early Cretaceous carbon and oxygen isotopes record. *J Geol Soc Lond* 161:695–702
- Wetzel R (1948) Sargelu Formation. In: Bellen RCV, Dunnigton HV, Wetzel R, Morton DM (eds) *Lexique stratigraphique international*, vol III. *Asie, Fascicule 10a Iraq*, Paris, pp 250–253
- Wetzel R, Morton DM (1950) Sehkanian Formation. In: Bellen RCV, Dunnigton HV, Wetzel R, Morton DM (eds) *Lexique stratigraphique international*, vol III. *Asie, Fascicule 10a Iraq*, Paris, pp 211–215
- Wilkin RT, Barnes HL, Brantley SL (1996) The size distribution of framboidal pyrite in modern sediments: an indicator of redox conditions. *Geochim Cosmochim Acta* 60:3897–3912
- Zainy MT, Al-Ansari N, Bauer TE, Ask M (2017) The tectonic and structural classifications of the Western part of the Zagros Fold and Thrust Belt, North Iraq, review and discussion. *J Earth Sci Geotech Eng* 7:71–89

1 Supplementary Material

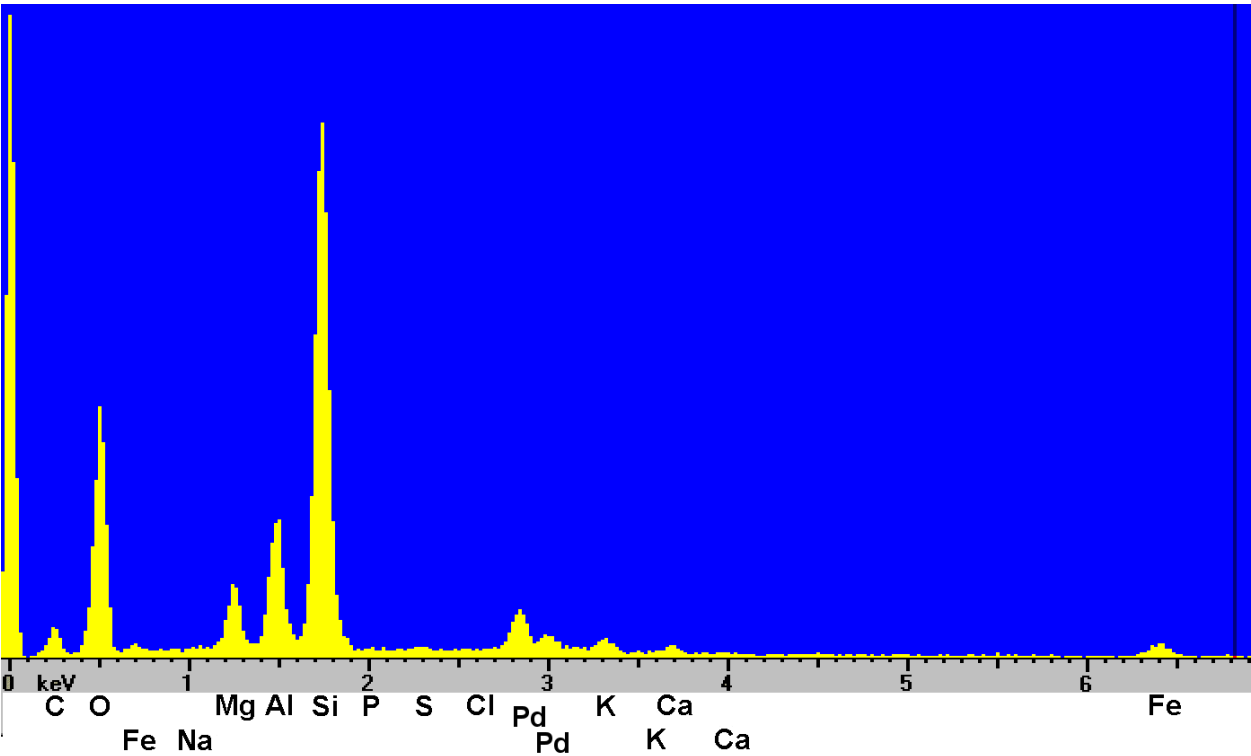
2

3 **Supplementary Figure S1.** EDX spectral analyses of spotted areas of the Sargelu and
4 Naokelekan formations, (a) Illite, (b) Dolomite, (c) Plagioclase feldspar, (d) Illite, (e) Pyrite
5 framboid, (f) Rectorite with organic matter (solid bitumen), (g) Calcite with organic matter
6 (solid bitumen), (h) Pyrite framboid, (i) Calcite with organic matter (solid bitumen), (j)
7 organic matter (solid bitumen), (k) organic matter (solid bitumen), (l) Kaolinite, (m) Calcite
8 with organic matter (solid bitumen), (n) Organic matter (solid bitumen), (o) Dolomite, (p)
9 Calcite, (q) Pyrite framboid, (r) Calcium phosphate with organic matter (solid bitumen), (s)
10 Pyrite framboid, (t) K-feldspar, (u) Calcite, (v) Pyrite framboid, (w) Montmorillonite, (x)
11 Chlorite, (y) Illite

12

13 **Supplementary Figure S1.**

14 **A.**

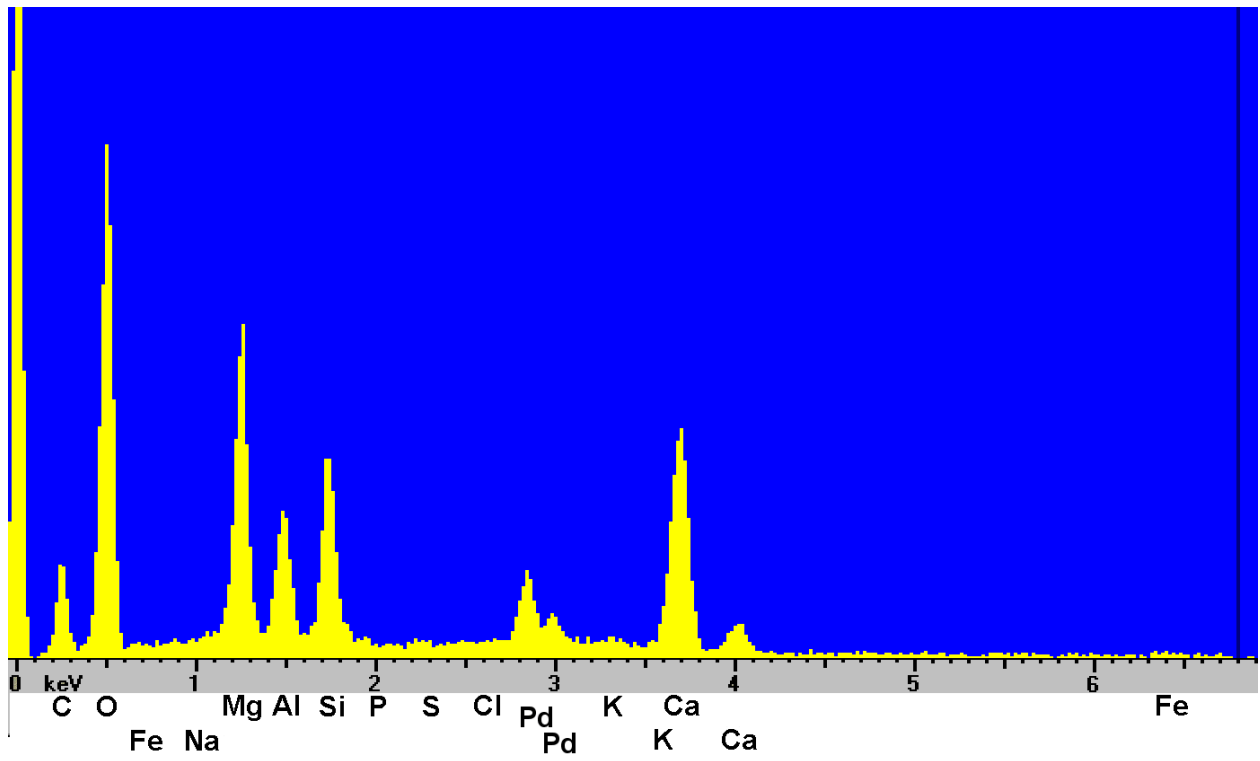


15
16
17
18
19
20
21
22
23
24
25
26
27
28
29
30

31

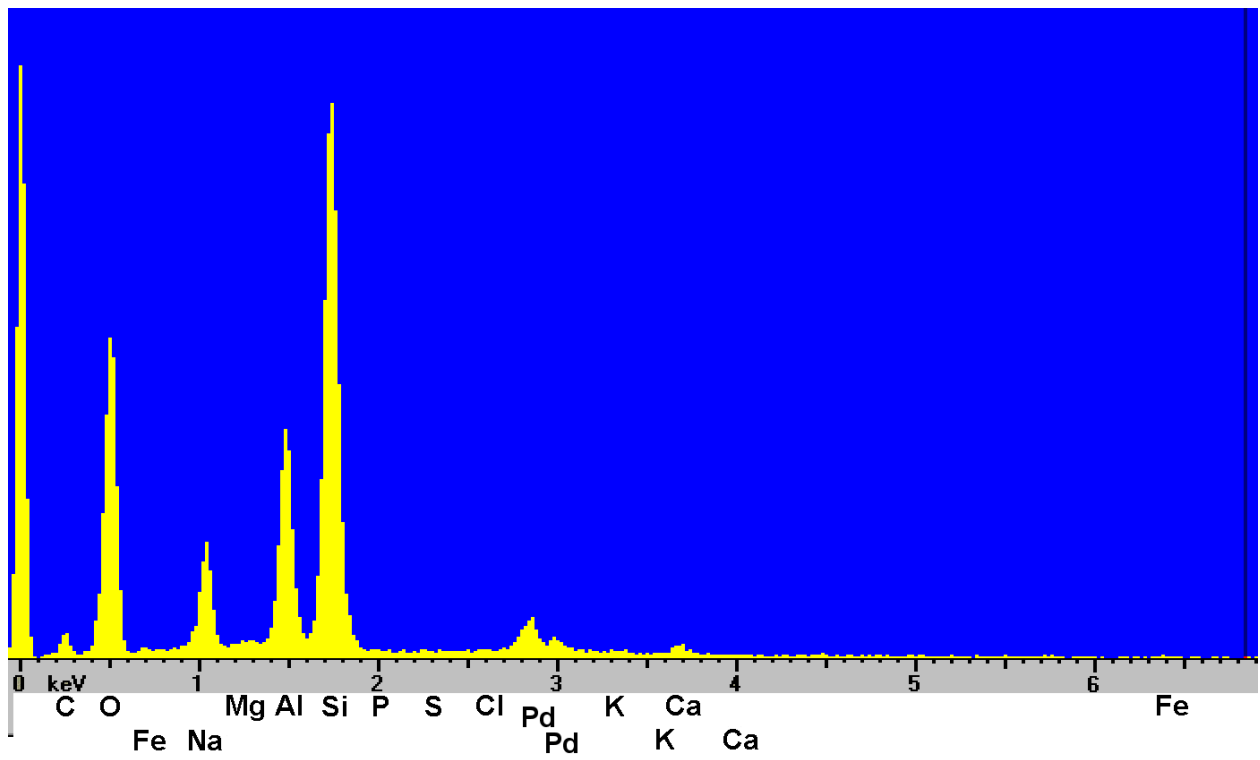
32

33 **B.**



34

35 **C.**



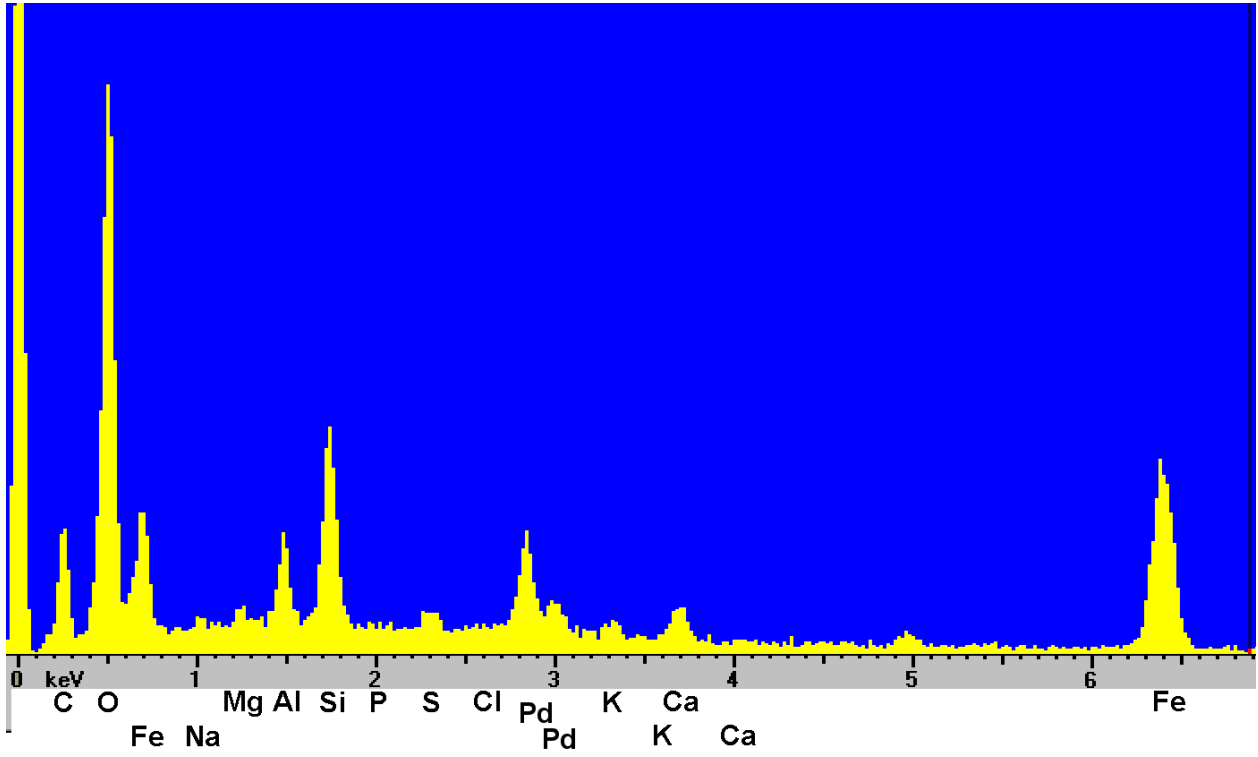
36

37

38

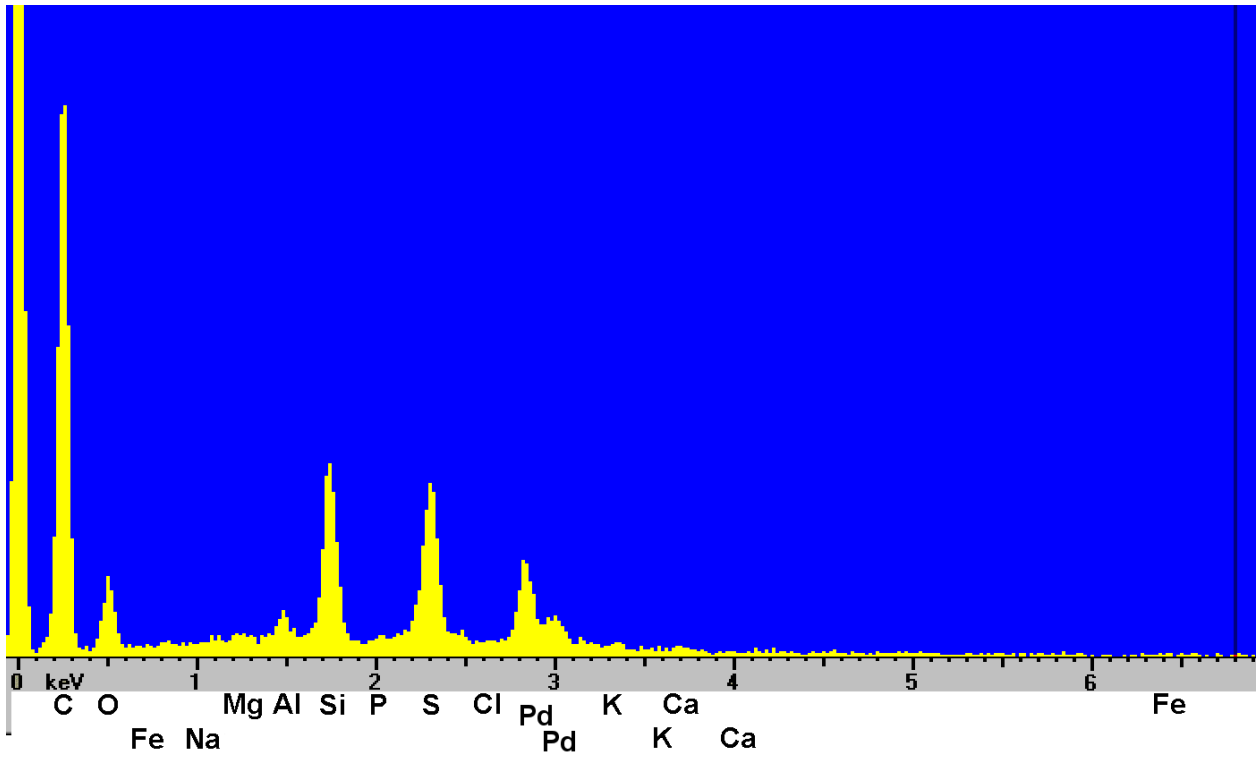
39

40 **D.**



41

42 **E.**



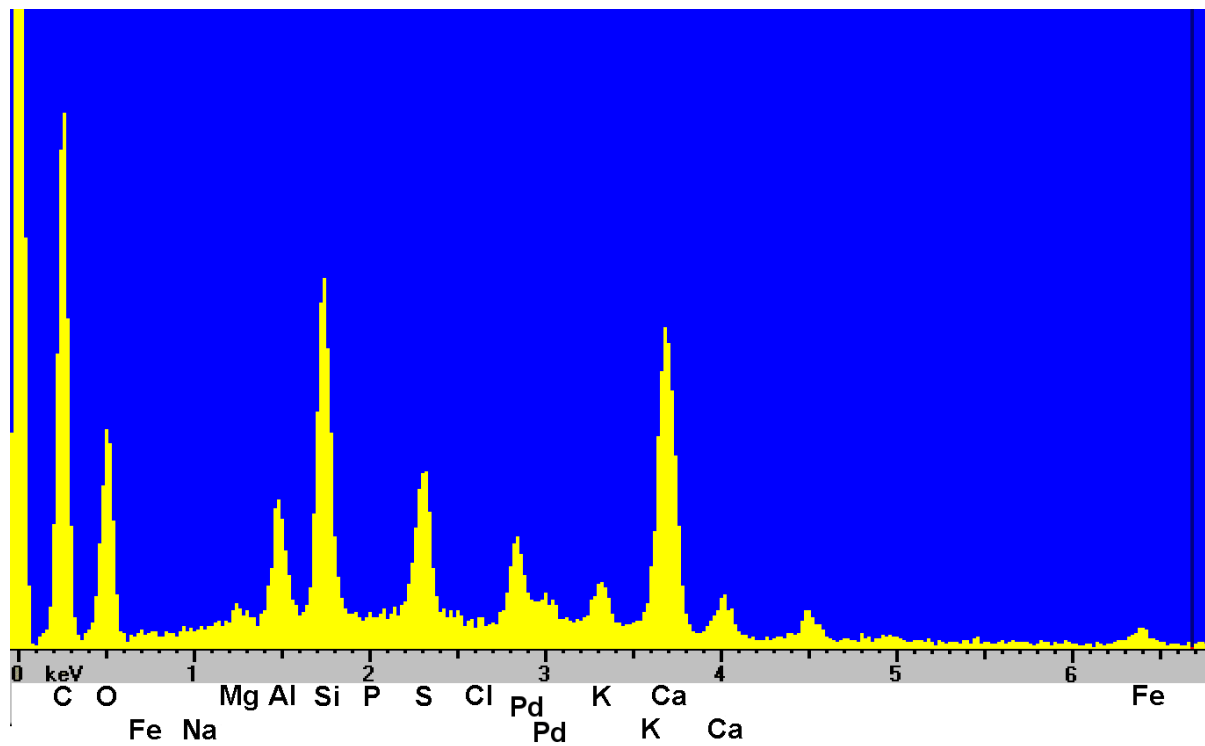
43

44

45

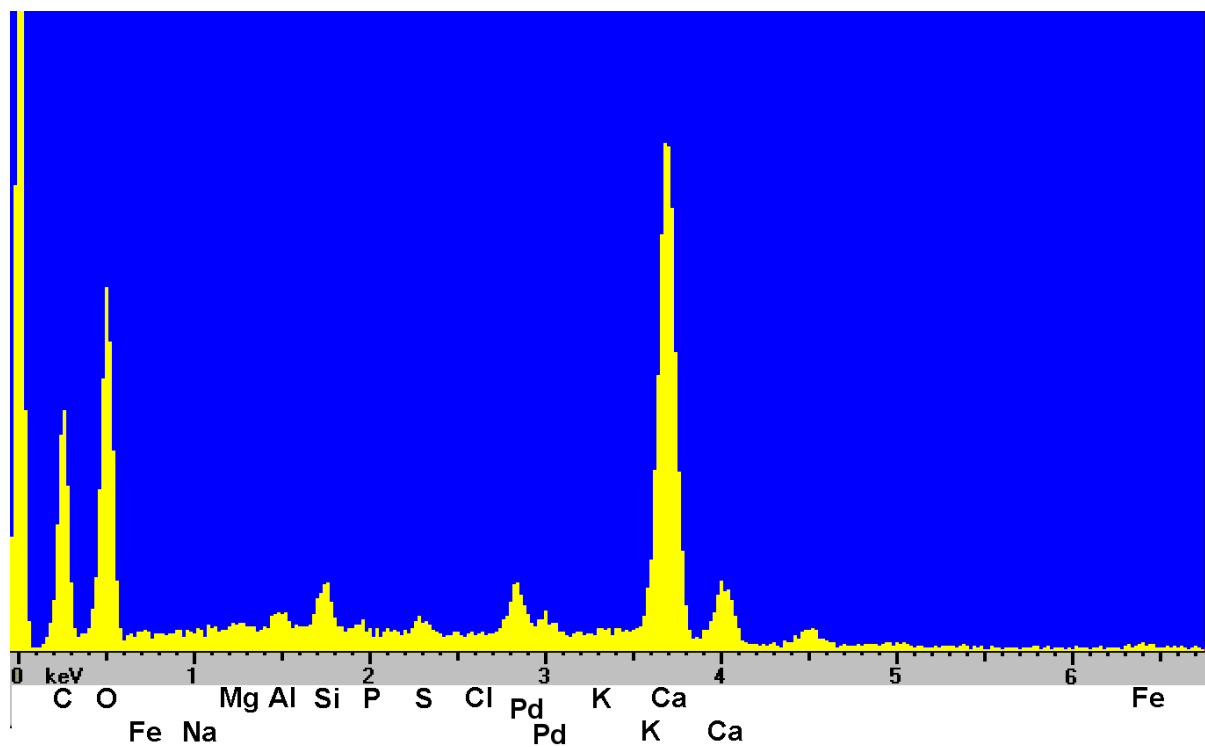
46

47 F.



48

49 G.

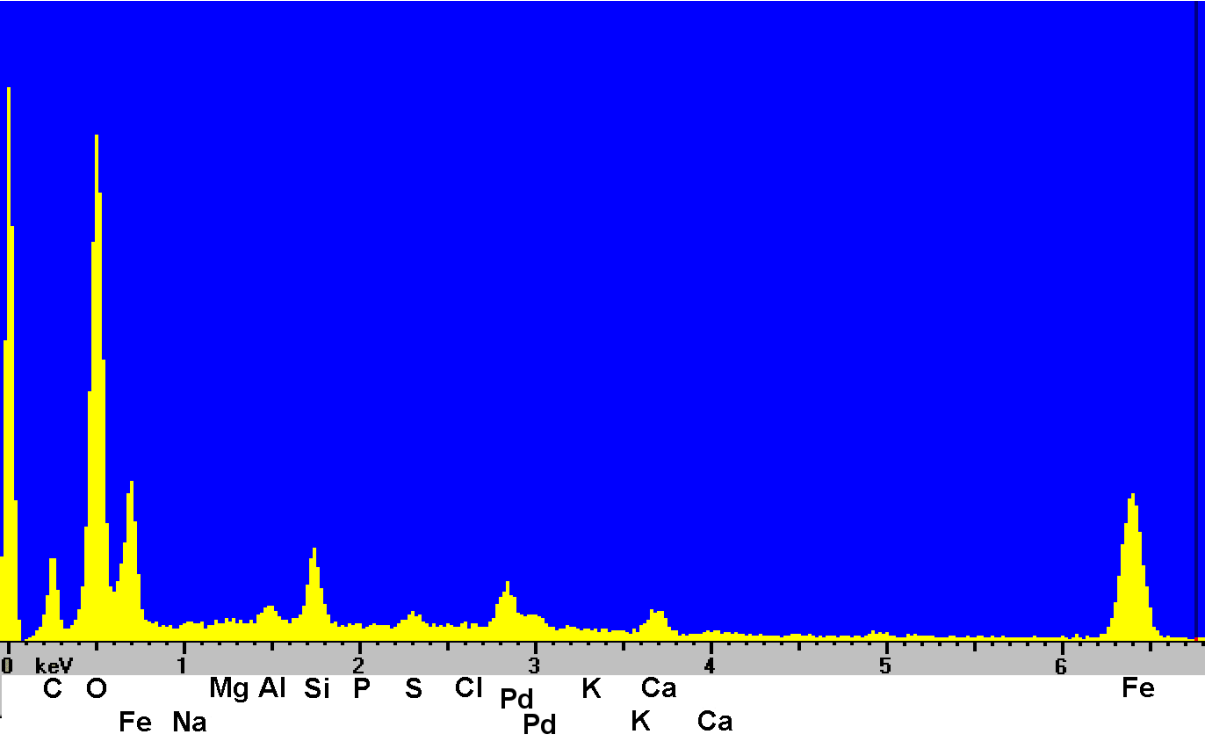


50

51

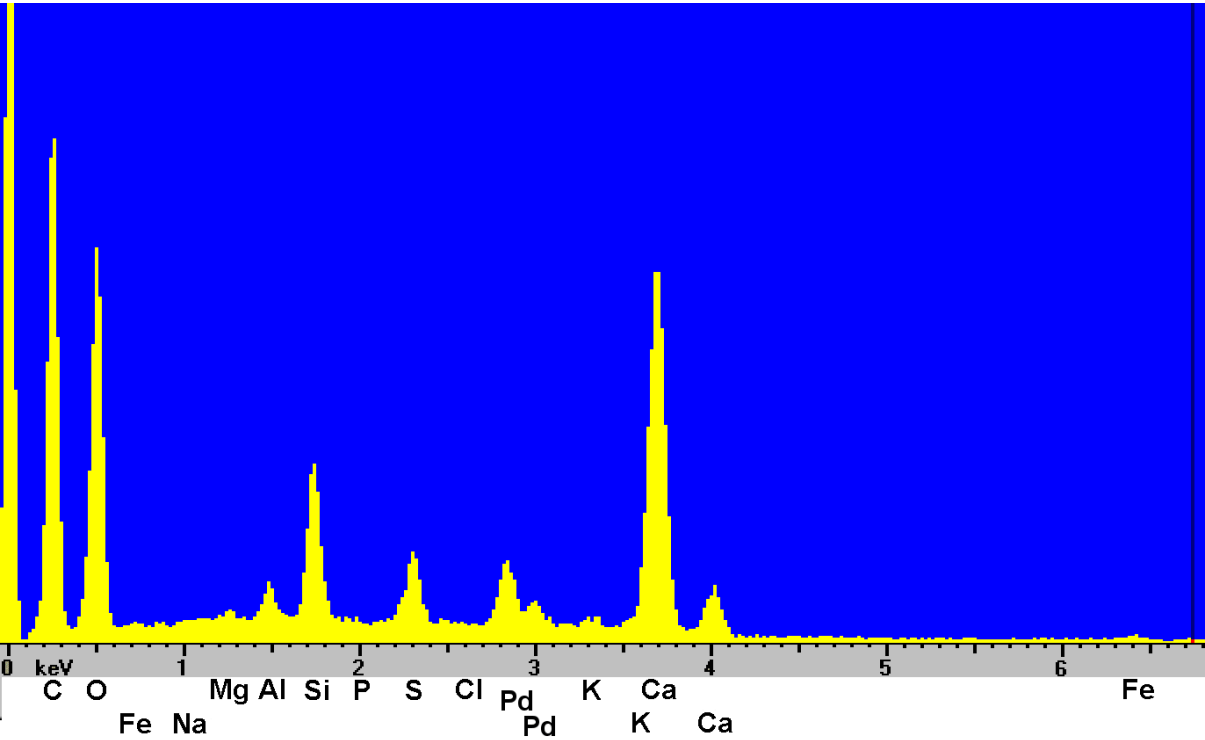
52
53
54

H.



55
56

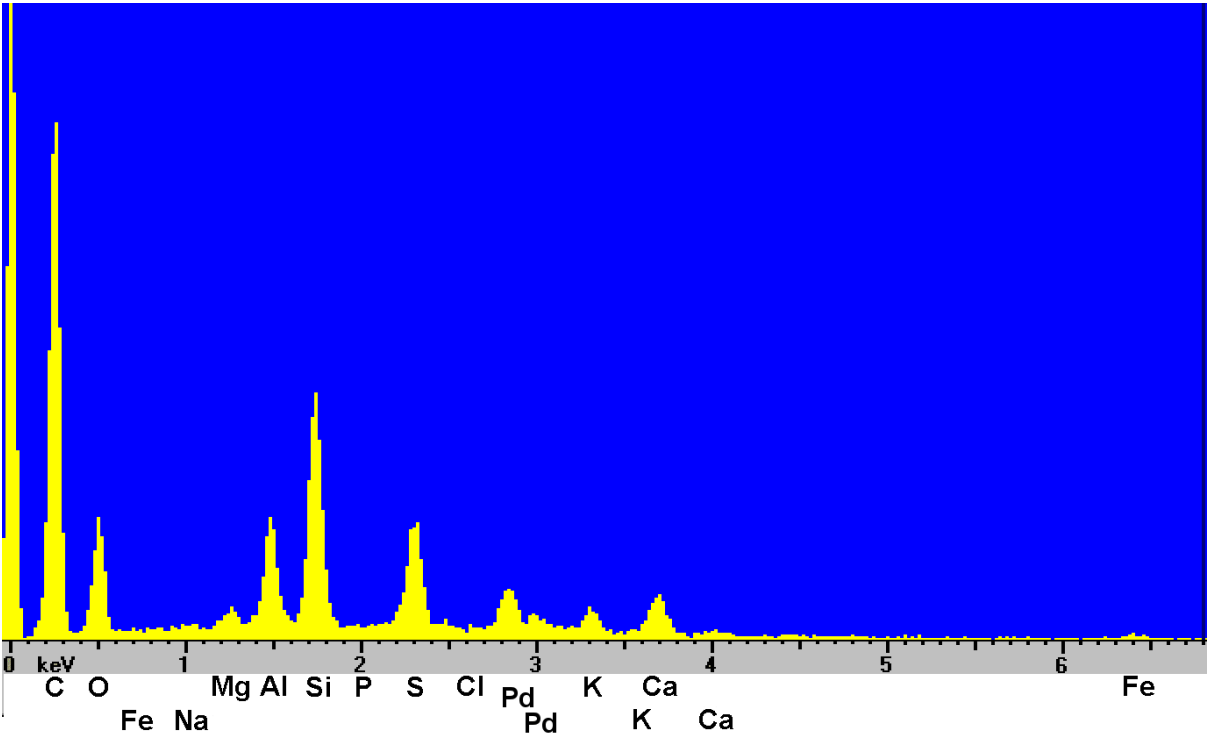
I.



57
58

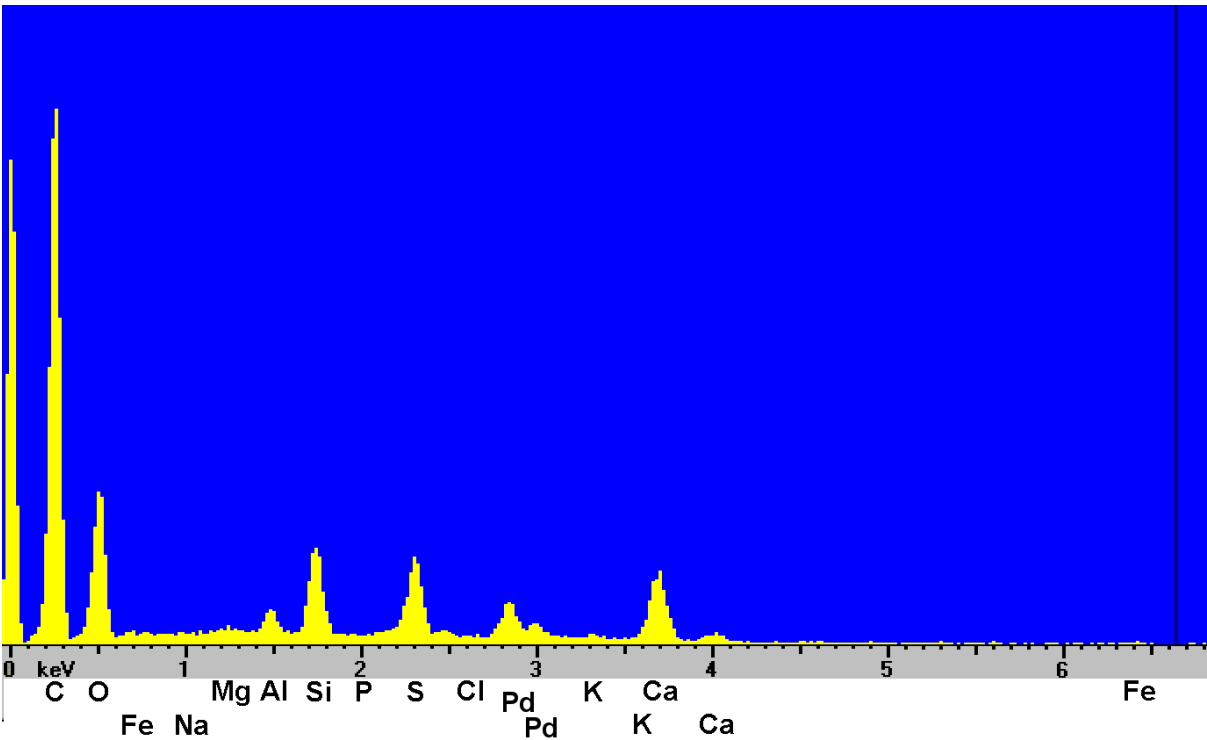
59
60
61

J.



62
63

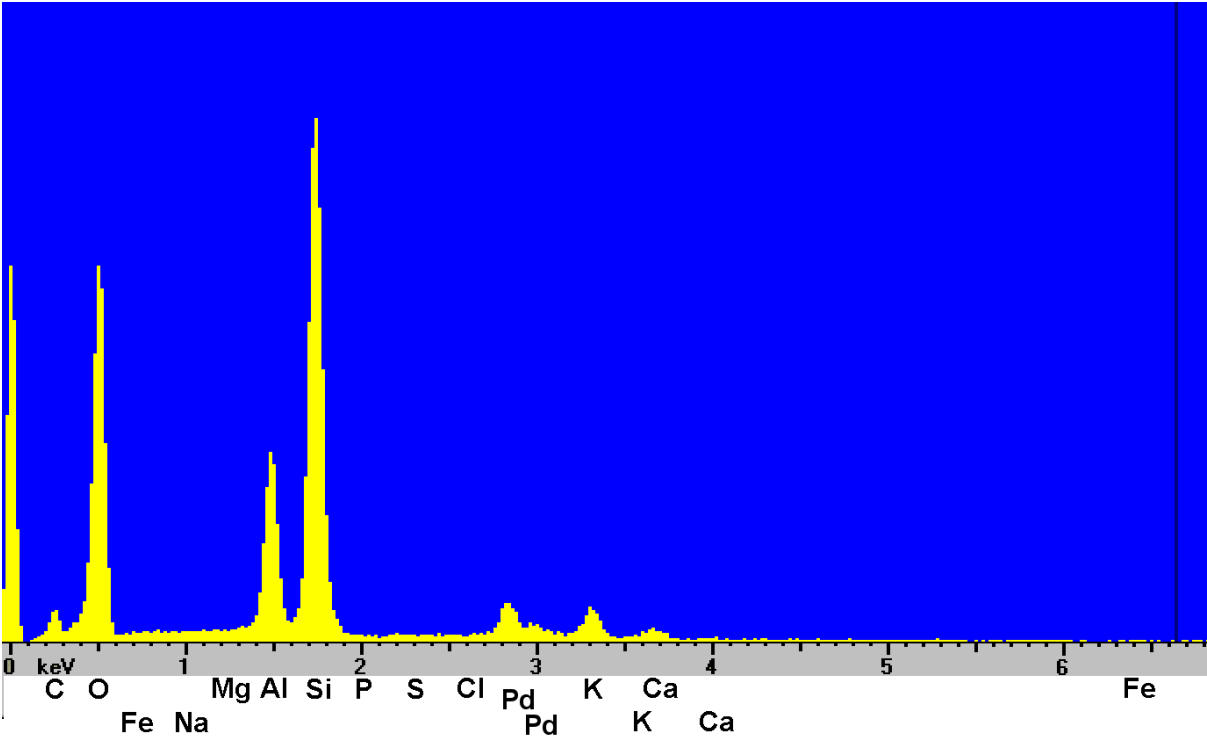
K.



64
65

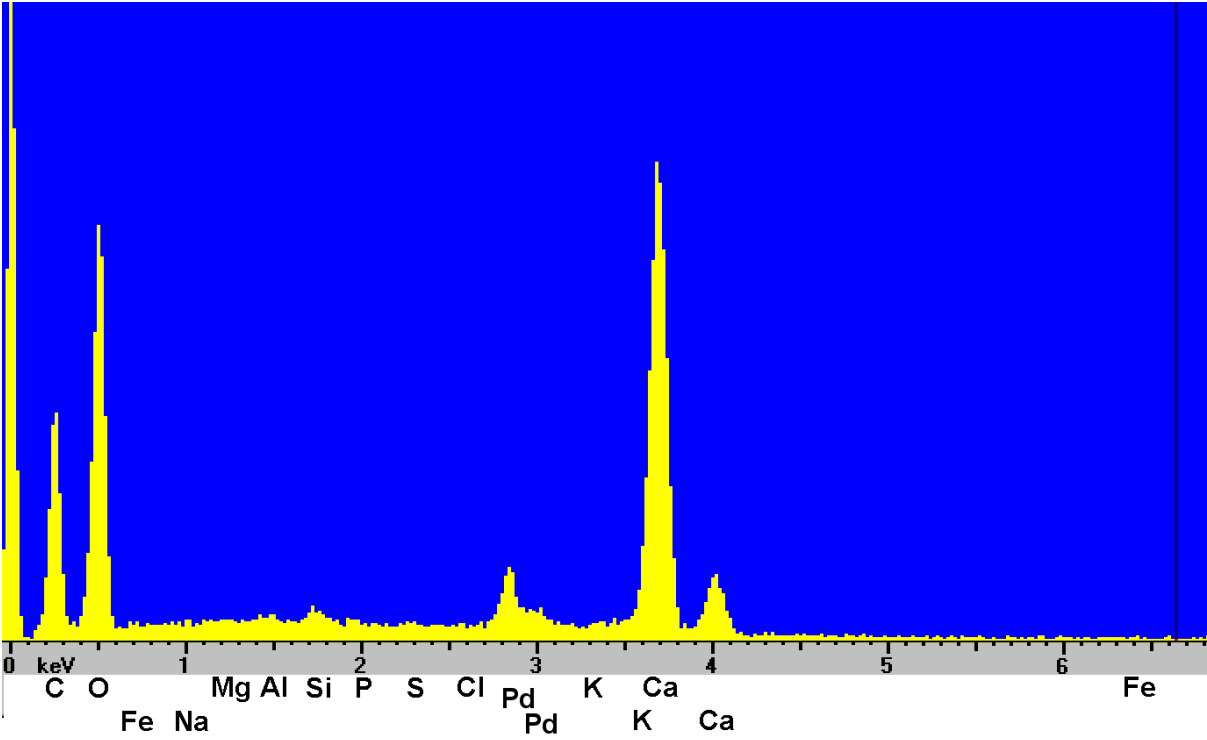
66
67
68

L.



69
70

M.

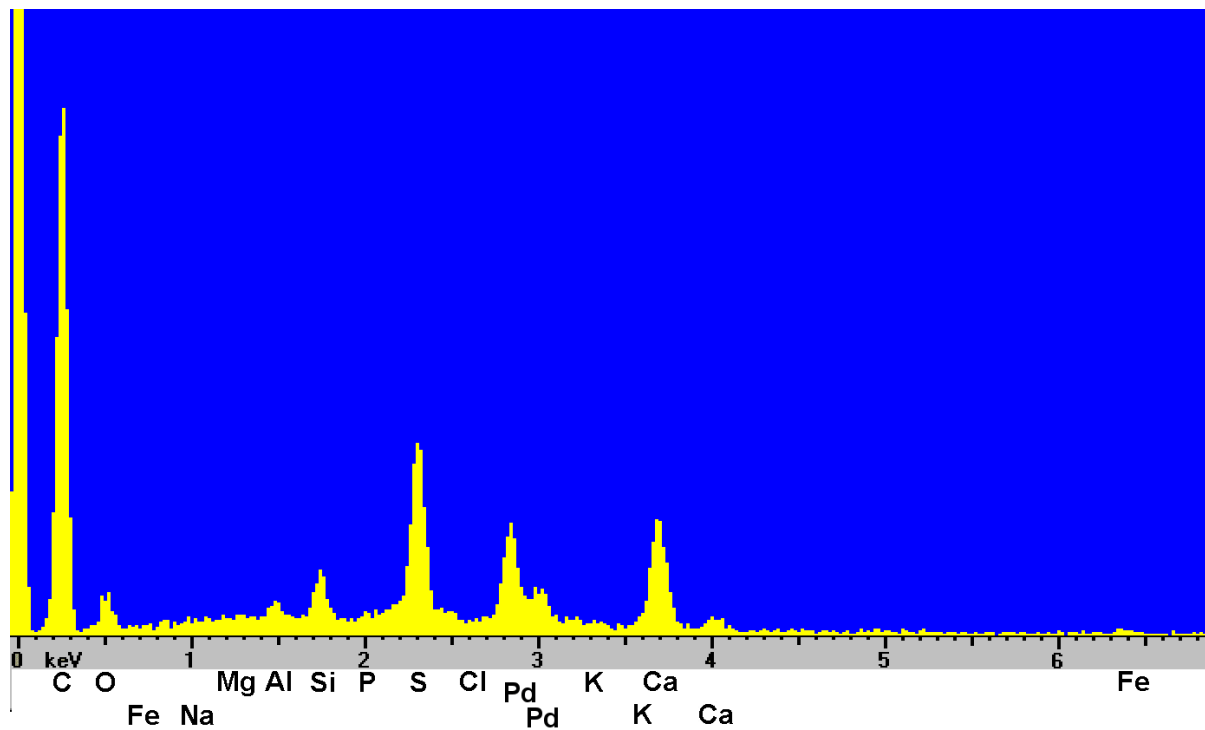


71
72

73

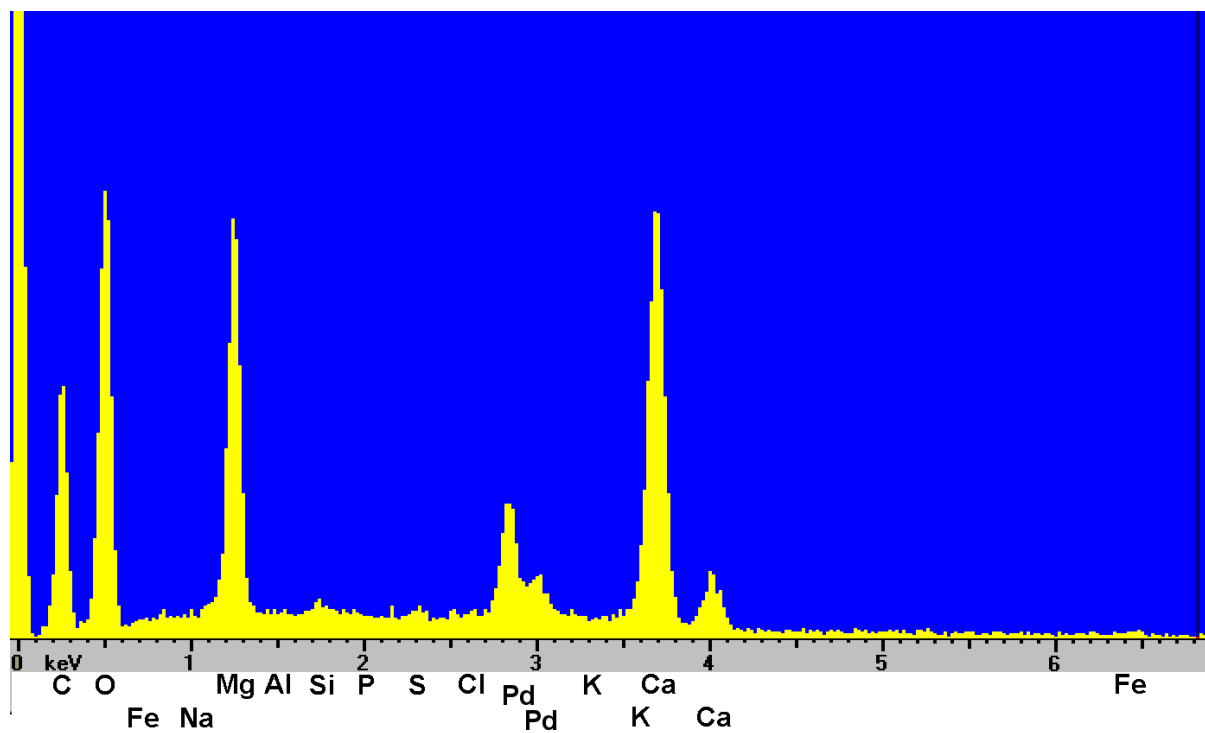
74

75 N.



76

77 O.

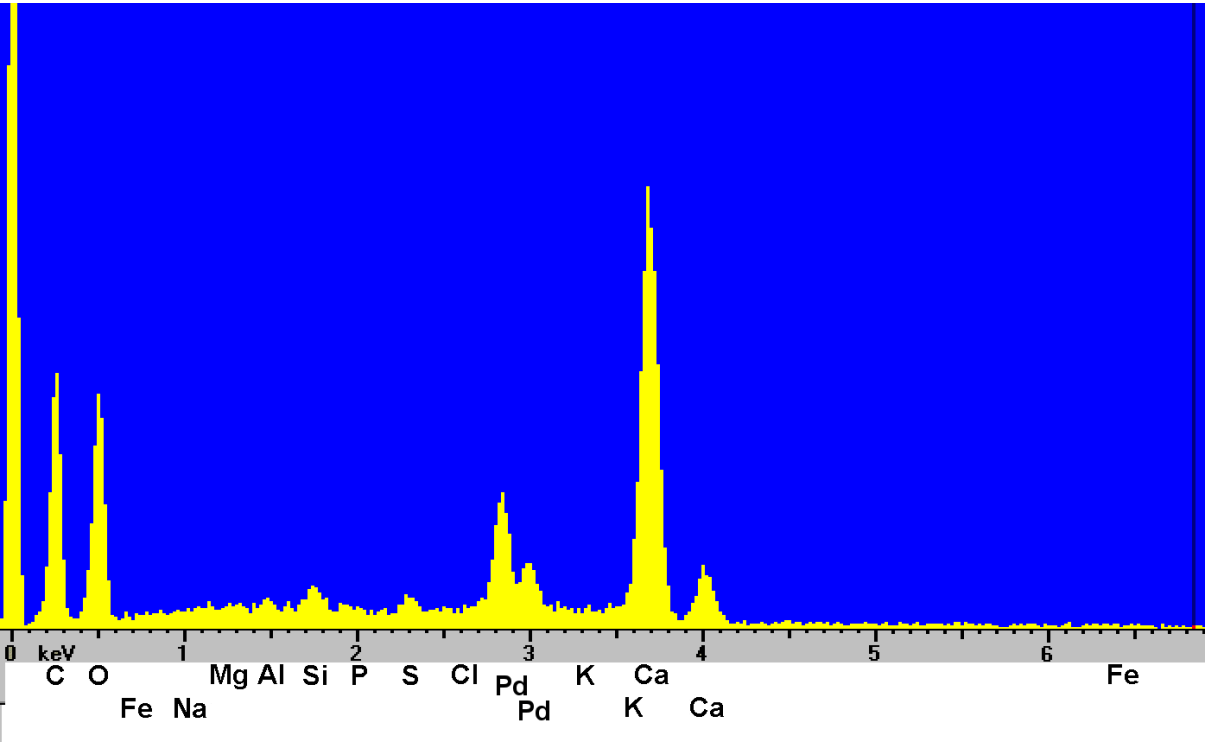


78

79

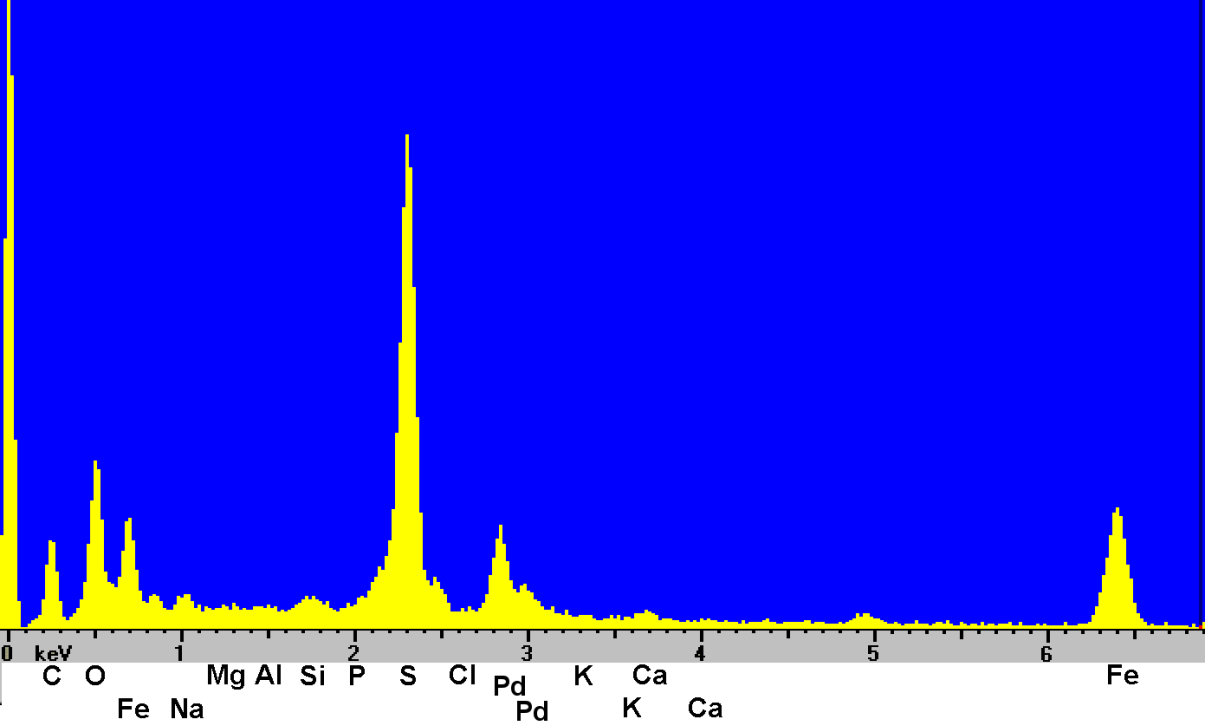
80
81
82

P.



83
84

Q.

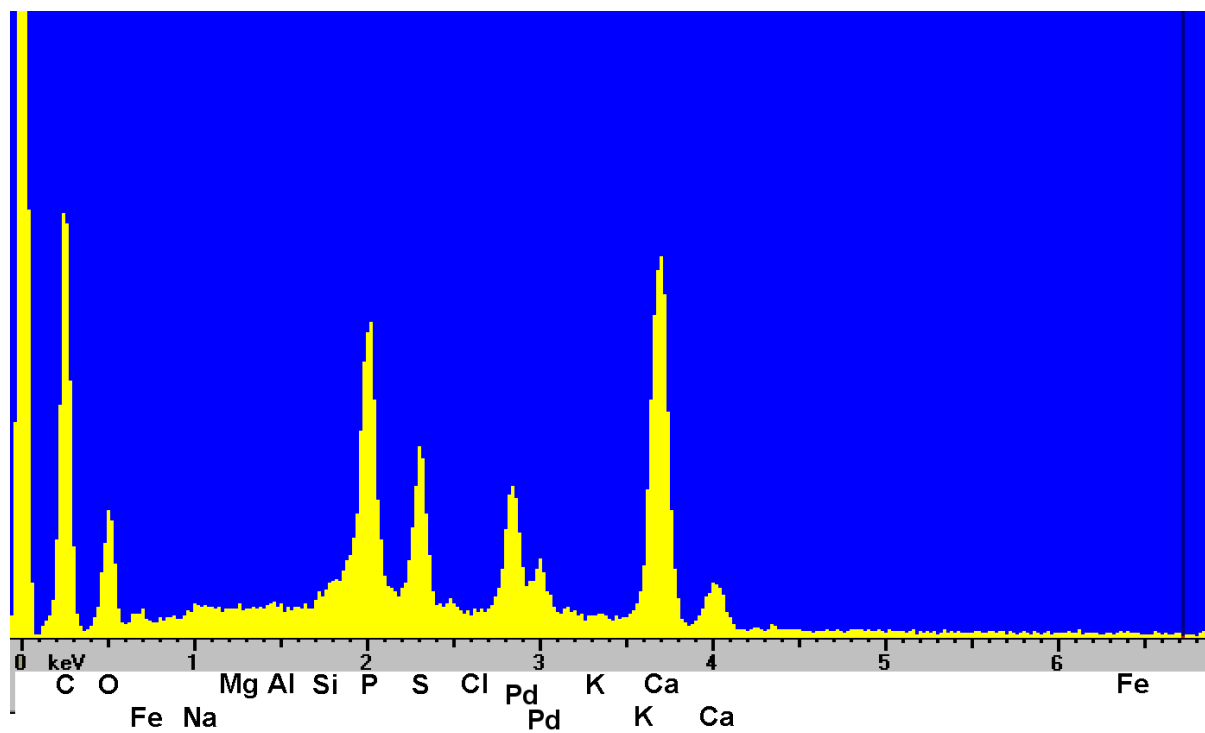


85
86

87

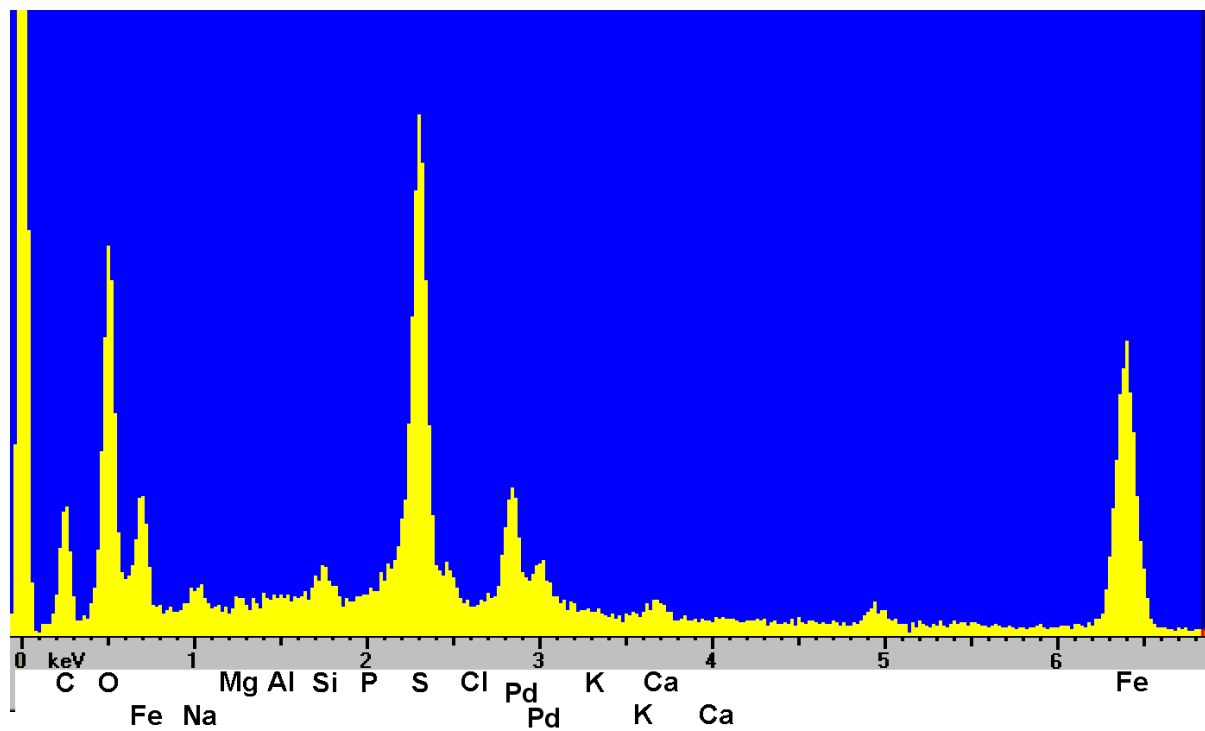
88

89 R.



90

91 S.



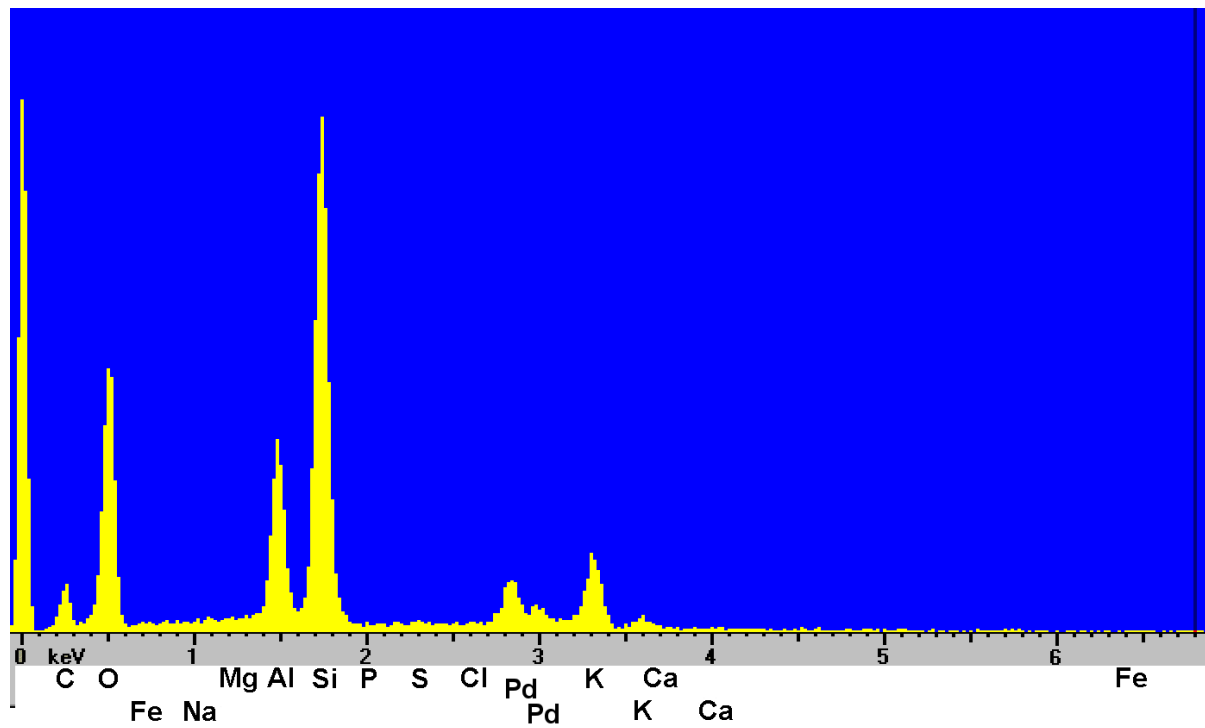
92

93

94

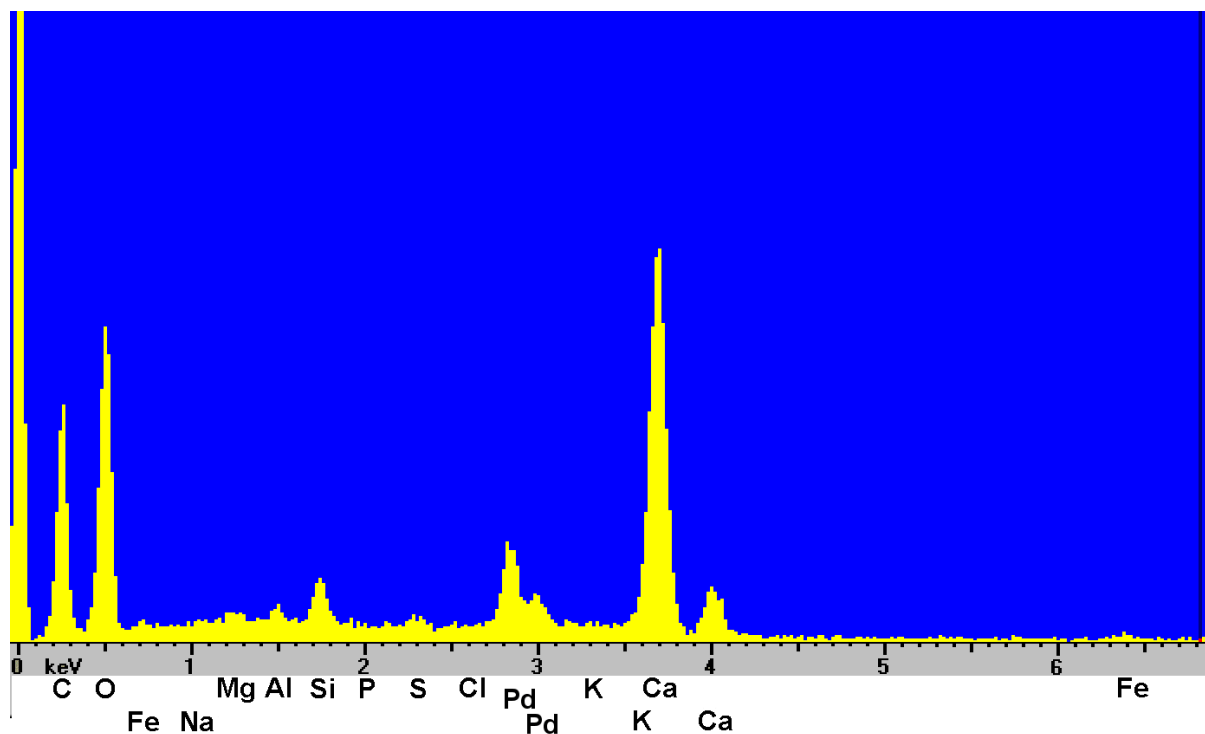
95

96 **T.**



97

98 **U.**



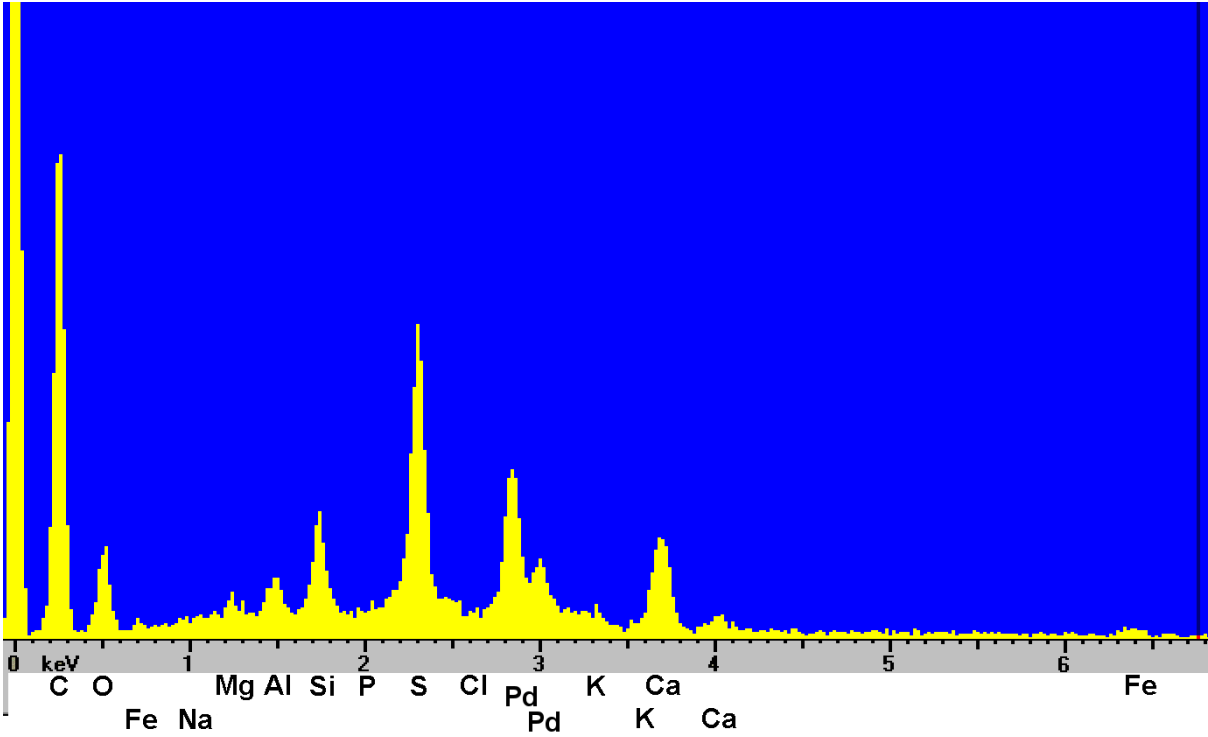
99

100

101

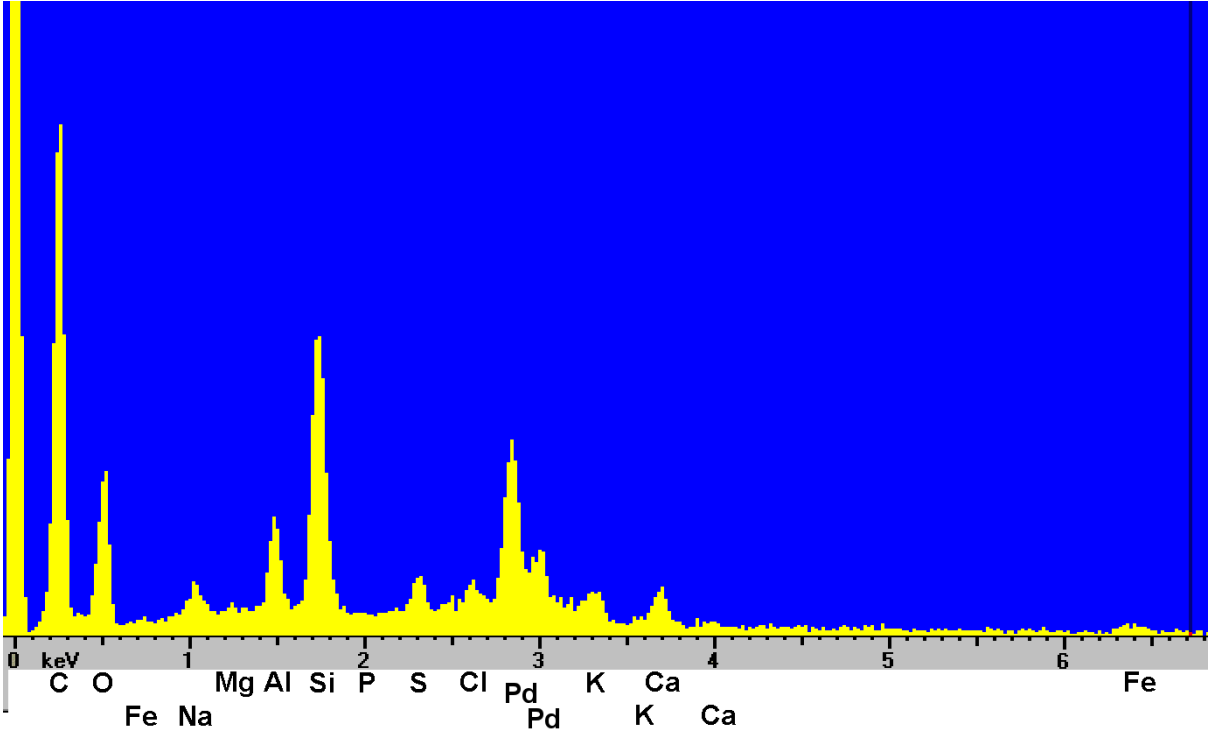
102

103 V.



104

105 W.



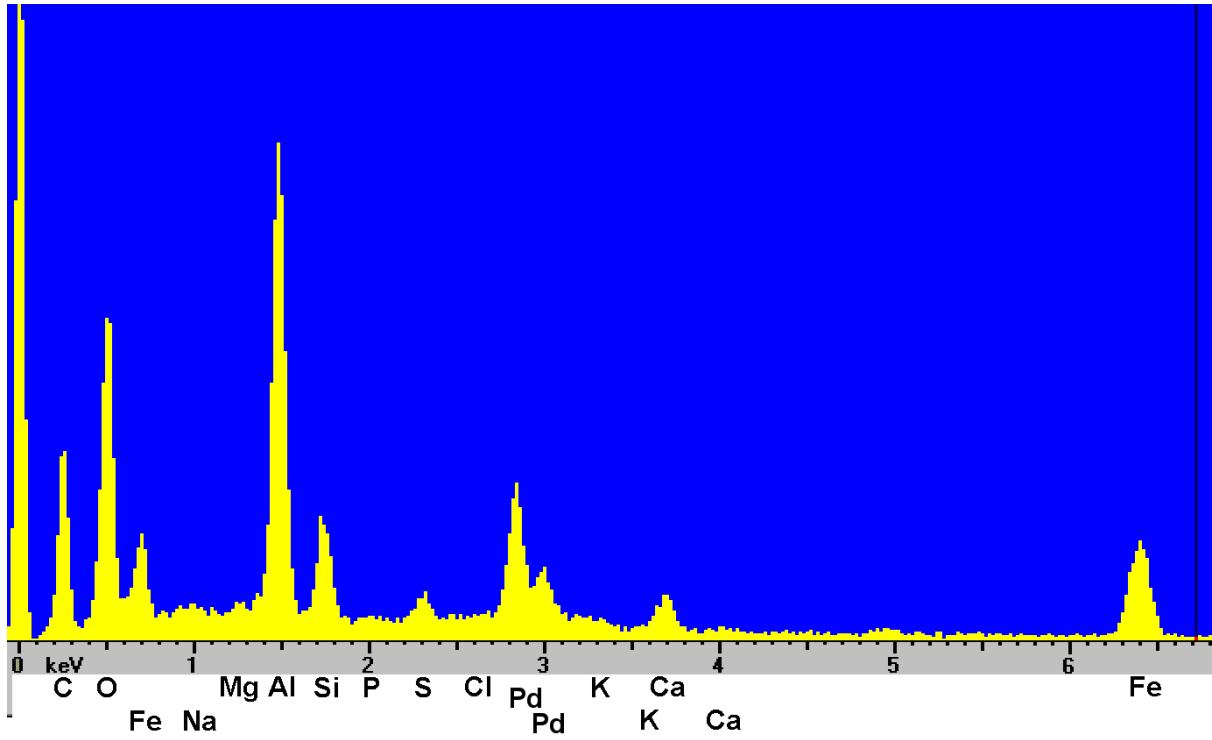
106

107

108

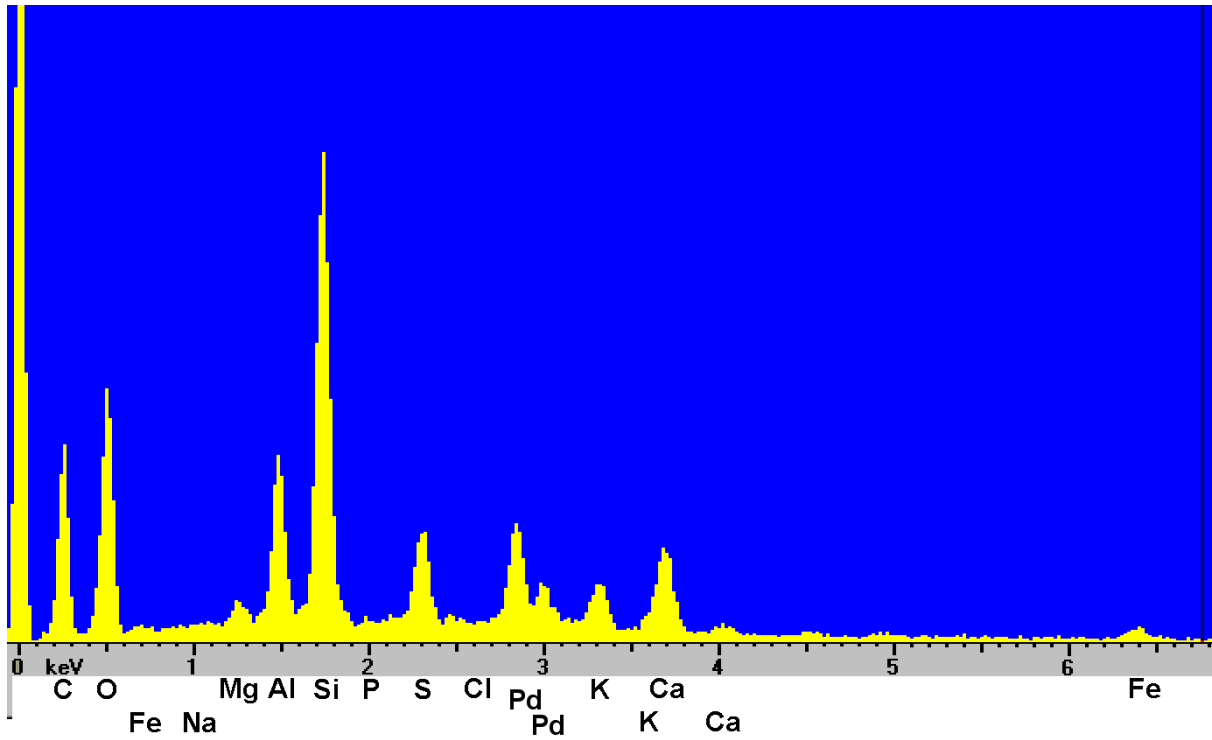
109

110 X.



111

112 Y.



113